Impact of Climatic Variability on the Fire Behaviour of Different Land Ecosystems

PhD thesis

Ana Lúcia Viegas de Barros

Supervisors:

Dr. David Stevenson and Dr. Chris Merchant

PhD in Climatology

The University of Edinburgh, 2010

Contents

Acknowledgements

This PhD research was financed by the University of Edinburgh and by the Portuguese Ministry of Science and Technology's Fundação para a Ciência e a Tecnologia.

All research studies were conducted at the University of Edinburgh's Institute of Atmospheric and Environmental Science (IAES), under the supervision of Dr. David Stevenson and Dr. Chris Merchant, whom I thank for their guidance and patient corrections of my work.

As always, Dr. Robert Kandel, senior scientist of the Centre National de Recherche Scientifique (France's National Scientific Research Agency) and member of the United States National Air and Space Administration's Earth Radiation Science Team, encouraged me in my studies, and generously sent me signed copies of his books relevant to my research.

Professor Dougal Drysdale discussed with me his thrilling bestseller, *Introduction to Fire Dynamics*, an exciting book that describes in careful and artistic detail the physical principles underlying this research.

Dr. Ruth Doherty, Professor Robert Harwood, Professor Gaby Hegerl, Professor Colin Legg, Dr. Hugh Pumphrey, Professor Simon Tett and Professor Roy Thompson attentively watched presentations of my work and made many useful comments and suggestions.

My research has also greatly benefited from discussions with Professor David Bowman, from the University of Tasmania, Dr. Michel Capderou and Dr. Andor Szantai, from the Laboratoire de Météorologie Dynamique (France's Laboratory of Dynamic Meteorology), Dr. Alexander Gershunov, from the Scripps Institution of Oceanography, Dr. George Petropoulos, from the University of Bristol, Professor Krishna Prasad Vadrevu, from the University of Maryland, and

Professor Francis Zwiers, of the Canadian Centre for Climate Modelling and Analysis.

This work would not have been done at all without my prodigious colleagues Stuart MacCallum, Owen Embury and Anthony Bloom, who expertly wrote many of the sub-routines essential for my computer programmes.

Dr. Guido van der Werf always kept me up to date with the Global Fire Emissions Database, and Professor James Randerson explained me its peculiarities.

The proficient team of Information Technology at the School of Geosciences took excellent care of Levante, my office computer, and rapidly fixed all the incoming problems.

My loyal friend Jon Dean Mountjoy, valiant defender of free thought and free speech, author of *WebLogic: the Definitive Guide*, editor-in-chief and community manager at SalesForce.com, perseveringly taught me the basis of computer science, dispelled the hazy mysteries of information technology for me, and made sure I always had the necessary up to date applications in my laptop.

Dr. John Hemming, the famous adventurer, explorer, anthropologist, witty writer, heroic champion of human rights and former director of the Royal Geographical Society, kindly showed an enthusiastic interest for my work and gave me permission to quote from his most recent literary masterpiece, *Tree of Rivers: The Story of the Amazon*.

All the prospective mistakes, inaccuracies, omissions and miscalculations in this thesis are of my entire responsibility. Each calculation achieved, each diagram accomplished, followed from the brilliant and tenacious work of my supervisors and colleagues.

"1997 was a year of devastating fires, all of them man-made. Satellites picked up 45000 conflagrations in Brazil and neighbouring countries. Then came an El Niño phenomenon (when change in currents across the Pacific Ocean causes freak warming along the coasts of the Americas) and the resulting drought meant that the annual burning of savannah in Brazil's northernmost state Roraima raged into the forests. 3 or 4 million hectares of trees went up in flames: fire-fighters were powerless to control the disaster, and it was ended only by miraculous and unexpected rains in early 1998. (…) In 2003, a record 25000 km² of forests were destroyed — which was 55% more than the average for the previous 5 years. The pace of deforestation continued to grow in successive years. (…) During the year 2004, the rate of deforestation in Mato Grosso doubled. (…) Throughout Amazonia, 640000 km² of rain forests — 13% of the total — vanished in the 4 decades since chains and bulldozers started to make devastation so easy. (…) This is just in Brazil: deforestation is also accelerating in other Amazonian nations, particularly in Peru and Bolivia."

JONH HEMMING, *Tree of Rivers: The Story of the Amazon*

Abstract

Wildfires are a natural phenomenon that strongly impacts the environment. Many terrestrial ecosystems depend on fire to maintain their ecological equilibrium and biodiversity, but new destructive fire patterns, often associated with land management practices and rapid climate change, have been degrading soil and water resources, increasing erosion by wind, precipitation and floods, decreasing biodiversity and contributing to desertification. Furthermore, pyrogenic emissions from biomass burning are an important source of atmospheric pollution and they impact the radiative balance of the troposphere, strongly contributing to the greenhouse effect. The objective of this research was to investigate the impact of climate variability on geographic, ecological, seasonal and inter-annual distributions of fires and correspondent pyrogenic emissions, across a variety of ecosystems. With this purpose, 10 years of world, monthly, 1°x1° gridded data, from the Global Fire Emissions Database, were compared with land-cover data, from the Goddard Institute of Space Studies, and with weather data, from the European Centre for Medium Range Weather Forecasting, the Global Precipitation Climatology Centre and the Global Hydrology Resource Centre. Overall, the climate parameters significantly correlated with carbon emissions were air and soil temperature, air and soil humidity, rainfall, wind speed and lightning density during the fire season, and also precipitation and snow cover up to 6 months before the fire season. Good statistical quantitative models of carbon emissions (correlations above 70%, and up to 95%, between estimated and predicted values, with residuals normally distributed) using humidity, temperature or lagged rainfall as predictors, were found almost exclusively in tropical grasslands, shrublands and woodlands, especially in Africa, where fire behaviour was more regular. In boreal and temperate forests and woodlands, where fire patterns were irregular and fire returning periods were larger, there were not enough fires, in 10 years of data, to obtain useful predictive statistical models. The fire models presented here, together with the quantitative statistical relationships found between climate and fire patterns, in different land ecosystems, are apt to be used in predictive climate models, land management, fire risk assessment and mitigation of climate change.

Chapter I Introduction

Summary and Objectives

Wildfires, in the context of this research, refer to open-air conflagrations in non-urban areas, resulting in biomass burning, i.e., combustion of natural bio-fuel, such as trees, shrubs, grass, wood, leaves, stems, litter and peat [GFED, 2006].

Biomass burning and the consequent pyrogenic emissions of gases and aerosols have a deep impact on climate and on the environment. A better knowledge about the spatial and temporal distribution of wildfires and the relationships between weather, land cover and biomass burning is essential to the improvement of land-use management techniques, fire risk assessment and predictive models of future climate, atmospheric chemistry and land ecosystem dynamics [IPCC AR4 WG1, 2007].

The objective of this research was to quantify the spatial and temporal distribution of biomass burning around the world, and to find statistical relationships between climate and wildfire regimes, lagged or simultaneous, across different geographical regions and land ecosystems.

With this purpose, spatio-temporal distributions of biomass burning and pyrogenic emissions, from 1997 to 2006, were investigated, with special attention to spatial clusters of frequent fire activity and their seasonal and inter-annual variability.

In regions where biomass burning was more frequent and regular, fire models were developed with one weather variable as predictor.

The results of this research can be used on their own, to help land management, assess fire risk and predict pyrogenic emissions, or can be implemented in models of climate, environment and atmospheric chemistry. Fire modelling is essential to predict fire events and the quantity and composition of pyrogenic emissions from biomass burning.

This introductory chapter is divided into 11 sections, which briefly present the basic notions about wildfire science and the layout of the thesis:

1) Wildfires in the geological record

2) Wildfire dynamics

3) Causes of wildfires

4) Spatial and temporal distribution of wildfires

5) Characteristics of wildfire patterns

6) Effects of wildfires on ecosystems

7) Effects of land management on wildfire behaviour

8) Effects of climate on wildfires

9) Effects of wildfires on climate

10) Detection of wildfires and estimation of pyrogenic emissions

11) Layout of the thesis

1.1 Wildfires in the Geological Record

Wildfires started having a significant impact on ecosystems during the Early Carboniferous (360:345 Ma ago). At this time, the first tall woody trees appeared and began spreading through temperate and tropical lands. Wood-decomposing bacteria were still scarce or inexistent, so fallen and buried trees just contributed to accumulate carbon in the soil, without consuming oxygen by getting decomposed; eventually, heating and compression turned those buried trees into coal. Hence, oxygen in the atmosphere was always increasing during the Carboniferous, reaching its highest concentration in Earth's history. Even during the Carboniferous Ice Age, lightning strikes and volcanic eruptions easily ignited wildfires, which propagated quickly, because of the high oxygen

concentration in the atmosphere and of the dense bio-fuel land-cover [BGS, 2009].

From the Permian on (300:251 Ma ago), plants evolved fire resistance traits -- adaptations in morphology, structure, texture and composition, like thicker bark, deeply imbedded vascular tissue, fibrous roots, protected stems and higher moisture content [USGS, 2009].

During the Cretaceous (145:65 Ma ago), flowering trees began to spread, covering many land ecosystems. Plants with seeds quickly reproduced, even if they had been consumed in a fire, and this favoured rapid evolution and speciation, resulting in many diverse vegetation types. Even after oxygen levels started decreasing, lightning, pyroclastic clouds and asteroid impacts easily ignited this biomass rich in fuel load, so wildfires continued to be frequent [USGS, 2009].

In the Holocene (from 12000 years ago until present), biomass burning became a frequent anthropogenic tool in clearing land for agriculture, pasture and sedentary settlements, with more and more fires being ignited by humans [BGS, 2009].

Presently, there is a great variety of wildfire behaviour, corresponding to a wide diversity of terrestrial ecosystems, topographical features, climate types and human land management.

1.2 Wildfire Dynamics

Fire is a manifestation of chemical reactions between combustible species and oxygen. Under appropriate circumstances, all biomass can burn. There are basically two types of combustion: flaming and smouldering. Flaming combustion releases more energy per unit time, and results in the conversion of bio-fuel into gaseous products, with abundant production of CO_2. In smouldering, less energy is released, the fuel is consumed slowly, producing more CO than in flaming, while liquid boiling products and tars condense into aerosol smoke. CO_2 is always produced in more abundance than CO, but

the ratio CO_2/CO during flaming combustions is much higher. Fire behaviour involves complex processes of heat transfer, thermodynamics, fluid dynamics and fire chemistry [Drysdale, 1998].

1.2.1 Fire Ignition

The initiation of flaming combustion is the process by which a rapid exothermic reaction is initiated, through reactions of volatiles in air, and causes the biomass to undergo change (pyrolysis), at temperatures greatly in excess of ambient. The bio-fuel is thermally decomposed and transformed into volatile species, like aerosols, trace gases and water, the products of pyrolysis [Drysdale, 1998].

The rate of pyrolysis ($\Delta m/\Delta t$), or thermal decomposition, approximately follows an Arrhenius-type dependence on temperature (equation 1.2.1.1).

$$\Delta m/ \Delta t = - k\, m = A \exp(-E_a/ RT) \qquad \text{(equation 1.2.1.1)}$$

Δm = mass of bio-fuel lost (kg)

Δt = duration of pyrolysis, or interval of measurement (s)

k = coefficient for the rate of pyrolysis (s^{-1})

m = initial mass

A = pre-exponential factor (kg/s)

E_a = activation energy (J/mol)

R = universal gas constant = 8.314 J/K/mol

T = temperature (K)

The rate of burning, i.e., the rate of mass loss from an element of surface ($\Delta m/ \Delta x\Delta y\Delta t$), depends on a balance between heat received and lost by the fuel during combustion (equation 1.2.1.2):

$$\Delta m/(\Delta x\Delta y\Delta t) = (\Delta Q_{flame}-\Delta Q_{lost})/ (Lv\ \Delta x\Delta y\Delta t) \qquad \text{(equation 1.2.1.2)}$$

$\Delta m/(\Delta x \Delta y \Delta t)$ = rate of mass loss from the surface ($kg/m^2/s$)

$\Delta x\ \Delta y$ = area of fuel surface (m^2)

Δt = duration of process (s)

ΔQ_{flame} = heat supplied by the flame back to the fuel (J)

ΔQ_{loss} = loss of heat through the fuel surface (J)

Lv = heat required to produce volatiles (corresponding to the latent heat of evaporation for liquids)

The heat flux is the rate of net heat gained through a surface, i.e., the difference between heat gained and lost divided by the duration of the process and by the effective surface area $[(\Delta Q_{flame} - \Delta Q_{lost})/(\Delta x \Delta y \Delta t)]$.

The rate of heat loss ($\Delta Qc/\ \Delta t$) during the combustion determines whether or not the reaction will be self-sustaining and propagate as a flame (equation 1.2.1.3).

$$\Delta Qc/\Delta t = \Delta Hc * vol * Cn * A * \exp (- Ea/RT) \quad \text{(equation 1.2.1.3)}$$

$\Delta Qc/\ \Delta t$ = rate of heat loss during the combustion (J/s)

ΔQc = heat of combustion released (J)

ΔHc = enthalpy or heat of combustion (J)

vol = volume (m^3)

C = concentration (mol/m^3)

n = order of the reaction: determines the units of A

A = pre-exponential factor ($mol^{-1}\ s^{-1}$)

Under suitable environmental conditions, burning is established [Drysdale, 1998].

1.2.2 Fire Spread

Fire spreads through an advanced ignition front, where the leading edge of the flame acts both as the source of pilot ignition and as the source of heat, which raises the fuel temperature in front of the flame to its fire point. The rate of fire spread depends on how rapidly the flames can spread from the point of ignition to involve an increasingly large area of combustible material, which varies with the density and type of vegetation and with the slope of the terrain [Drysdale, 1998].

Extremely intense wildfires behave erratically and unpredictably, with quick spread, abundant crowning and/or spotting, fire whirls and strong convection columns, destroying much vegetation. Smouldering fire, on the contrary, is a slow combustion of surface biomass without generating flame. However, smouldering may spread slowly and steadily during days or weeks after flaming has ceased (in rare cases, for years), so it can also damage much ground-level and underground vegetation (e.g., roots, seeds and plant stems), and emit high quantities of trace gases to the atmosphere, with a higher proportion of CO/ CO_2 than flaming fires [USDA, 2000].

The rate of energy released by biomass burning ($\Delta Qc/\Delta t$) is the most important single factor to characterise fire behaviour (equation 1.2.2.1):

$$\Delta Qc/\Delta t = \chi\ (\Delta m/\Delta x \Delta y \Delta t)\ A_{fuel}\ \Delta Hc \qquad \text{(equation 1.2.2.1)}$$

$\Delta Qc/\Delta t$ = rate of heat released during combustion

χ = factor of combustion completeness (unitless), $0 \leq \chi \leq 1$

Δm = loss of mass during combustion (kg)

$\Delta x\ \Delta y$ = element of area (m^2)

Δt = duration of combustion, or time interval of measurement (s)

A_{fuel} = fuel surface area (m^2)

ΔHc = specific enthalpy, or heat of combustion of volatiles per unit mass (J/kg)

$\Delta Qc/ \Delta t$ = rate of heat loss by combustion (J/s)

Heat transfer, from flames and combustion products to the environment, increases the surrounding temperature in an element of area $\Delta x\ \Delta y$; the higher the ambient temperature, the quicker the fire point can be attained (equation 1.2.2.2):

$$\Delta Q/ (\Delta x \Delta y \Delta t) = h\ \Delta T \qquad \text{(equation 1.2.2.2)}$$

$\Delta Q/ (\Delta x \Delta y \Delta t)$ = flux of heat loss ($J/m^2/s$)

h = heat transfer coefficient ($J\ m^{-2}s^{-1}K^{-1}$)

$\Delta x\ \Delta y$ = area element (m^2)

ΔT = variation of temperature (K)

The fundamental equation of fire spread (equation 1.2.2.3) shows the influence of fuel density, thermal conductivity and heat capacity on the propagation of ignition:

$$\Delta Q/ (\Delta x \Delta y \Delta t) = \rho\ V\ \Delta H \qquad \text{(equation 1.2.2.3)}$$

$\Delta Q/ (\Delta x \Delta y \Delta t)$ = flux of heat, i.e., rate of heat transfer across an element of surface ($J/m^2/s$)

ρ = fuel density (kg/m^3)

V = rate of spread (m/s) = $1/ (k\ \rho\ c)$

ΔH = change in enthalpy as a unit mass of fuel raises it temperature until fire point (J/kg)

k = thermal conductivity

c = heat capacity

Heat transfer depends on the ambient temperature and on the characteristics of the bio-fuel - thick and heavy fuel transfers heat slowly, so it takes more time to ignite, and its thermal capacity and conductivity vary quickly with humidity [Drysdale, 1998].

Therefore, it is expected that fuel type, air humidity and temperature strongly influence fire behaviour, which suggested the choice of predictors for the fire models in this research (table 2.1.3).

1.2.3 Fire Extinction

Wildfires end (equation 1.2.3) if there is no more fuel to burn - which often occurs in grasslands or other ecosystems with limited fuel available - or if weather conditions make heat transfer insufficient – often in the case of forests or woodlands, where fuel is abundant [Drysdale, 1998].

The cooling of fuel by water is the most effective extinction method, because water has a very high latent heat of evaporation. Intense flaming fires, however, may persist in light rainfall, since the total downward momentum of the water must overcome the total upward momentum of the fire plume, otherwise the droplets of rain cannot reach the burning fuel surface. The evaporative loss of small water droplets, as they pass through the fire plume, diminishes the amount of water that may reach the fuel bed [Drysdale, 1998].

$$S = $$

$$=(\phi\ \Delta Hc - Lv)\ \Delta m_{burnt}/\ \Delta x\Delta y\Delta t + \Delta Q_E/\ \Delta x\Delta y\Delta t - \Delta Q_L/\ \Delta x\Delta y\Delta t - \Delta Q_W/\ \Delta x\Delta y\Delta t$$

(equation 1.2.3)

S = flux of sensible heat: if negative, leads to flame extinction ($J/m^2/s$)

ϕ = fraction of the heat of combustion transferred back to the surface (unitless)

ΔHc = specific enthalpy of combustion, or heat released by complete combustion per unit mass (J/kg)

Lv = heat required to produce volatiles

$\Delta m/ \Delta t$ = rate of burning (kg/s)

$\Delta Q_E/ (\Delta x \Delta y \Delta t)$ = flux of external heating ($J/s/m^2$)

$\Delta Q_L/ (\Delta x \Delta y \Delta t)$ = flux of heat loss without water ($J/s/m^2$)

$\Delta Q_W/ (\Delta x \Delta y \Delta t)$ = flux of heat loss on account of water ($J/s/m^2$)

If the flames are extinct without reducing the supply of flammable vapours to below a critical level, there is the risk of re-ignition, until the fuel cools to below its fire point [Drysdale, 1998].

As it was verified during this research, rainfall causes an abrupt decrease in burnt area during the fire season, with the scatterplots of burnt area versus precipitation showing an accentuated curve of the type 1/x (e.g. figure 2.2.6).

1.3 Causes of Wildfires

The most significant factors in determining the rate of flame spread in biomass burning depend on the chemical composition of the bio-fuel (which can vary monthly) and on its physical properties: initial temperature, surface geometry, orientation relatively to the direction of propagation, thickness, heat capacity, thermal conductivity, density and continuity; environmental factors that directly affect biomass burning are atmospheric composition and pressure, temperature, humidity, lightning density and wind speed [Drysdale, 1998].

Nowadays, many wildfires are directly ignited by humans, accidentally or on purpose, or are an indirect consequence of human activities. In many circumstances, it is unclear whether fires can be attributed exclusively to natural or to anthropogenic causes [FAO, 2005].

At a local scale, wildfires caused directly by humans, besides arson and accidental ignitions, are usually land management prescribed fires, with the purpose of clearing lands, for pasture or agriculture, or to reduce fuel load in order to avoid unpredictable, intense and destructive conflagrations [FAO, 2005].

At a regional and mid-term scale, many human activities indirectly influence wildfire behaviour, such as [GEO-4, 2007]:

-- fracturing of the frozen surface layer in arctic areas (permafrost), leaving tundra grasslands exposed to fire, when water evaporates;

-- lowered albedo of grasslands in melted arctic or alpine ice cover, flooded by the water rising from the subsoil, preventing the top water layer from freezing again, even when temperatures drop below 0ºC;

-- conversion of forests and woodlands into shrublands or grasslands, with shorter fire return periods, for agricultural or pastoral land use;

-- replacement of native vegetation for another, with more economic interest, but less adapted to the regional climate and with different fire resistance;

-- spontaneous combustion from heat generated by the decomposing activity of bacteria associated with livestock;

-- combustion in abandoned coal mines and underground smouldering fire in peat bogs, which can last for years, igniting wildfires at the surface during the dry season;

-- accumulation of large quantities of bio-fuel caused by fire suppression, leading, sooner or later, to extremely intense, destructive and uncontrollable wildfires.

At a global scale, climate change of anthropogenic origin is increasing the frequency of wildfires in places experiencing higher temperatures, lower humidity, reduced precipitation, prolonged droughts, more frequent heat waves and El Niño episodes in the tropics, earlier snowmelts in temperate and polar regions, and stronger convective systems, with higher density of lightning strikes [IPCC AR4 WG1, chapter 9, 2007].

Examples of natural occurring wildfires, without human intervention, are those ignited by lava and pyroclastic clouds, from volcanic

eruptions, and the regular biomass burning in fire-dependent ecosystems, ignited by lightning [GEO-4, 2007].

1.4 Spatial and Temporal Distribution of Wildfires

Wildfires can occur anywhere where vegetation is available to burn, but they are rare in ecosystems with extreme weather conditions [Olson, 1983; Houghton, 1987]:

-- Equatorial rainforests, where rainfall is frequent and intense, and where biomass decomposes rapidly, not needing to burn to become part of the soil;

-- Deserts, where vegetation is too sparse to develop a fire of considerable dimensions: even if some desert plants grow with reserves of liquid water below the barren surface, they are usually too sparse to sustain prolonged biomass burning;

-- Taiga ecosystems (e.g., black fir in permafrost), where the weather is too cold for fire to ignite and/ or spread: water is permanently frozen, such as in tundra and permafrost.

Wildfires occur mostly in the ecosystems with a moderate climate [FAO, 2006]:

-- Temperate forests and woodlands, where the climate is sufficiently moist to allow the growth of trees, but features extended dry, hot periods, when fallen branches, leaves and other material can dry out and become highly flammable.

-- Tropical dry forests and woodlands, where fires spread most widely during drought years;

-- Tropical shrublands and grasslands, especially following a rainy growing season that gives abundant fuel load to burn during the fire season.

In tropical grasslands and temperate forests, regular, low intensity wildfires are useful to destroy dead plants that could otherwise accumulate and hinder the living ones. Some of these woodlands and

forests are fire-dependent, inhabited by pyrophylous animals and plants that need burned wood to survive [FAO, 2006].

Topography may also create a local climate, with different wildfire patterns than the surrounding areas. Mountains can have a dry climate, and regular fire occurrences, in one side and a rainy climate in the other, with rare fire events. Some lower elevations may have more frequent fire return intervals, whereas higher and wetter elevations may have less frequent natural fires [USDA, 2000]. Fires tend to propagate upwards and are more severe on upper slopes [Rothermel, 1985; Viegas, 1993; Butler & al., 2007], so a forest uphill, where ignition is difficult because of relatively high humidity, can catch fire on account of grassland in a valley or low land.

Fire seasons occur during the dry months of the year warm enough to sustain biomass burning. In temperate climates, this happens during the summer, but, in tropical zones, summer is the wet season, whereas winter is dry, but still warm enough for fire ignition and spread [GEO-4, 2007].

Until present, wildfires were rare in land ecosystems where biodiversity was either exceptionally rich or rather limited: warm and wet equatorial rainforests, the ecosystems with greater variety of fauna and flora, and sub-polar conifer forests (taiga), with a scarce number of species. However, rapid climate change and deforestation are triggering fires even in some of these ecosystems [GEO-4, 2007].

1.5 Characteristics of Wildfire Patterns

A fire regime describes the pattern that fire follows in a particular ecosystem and it consists of the following components [Bond & Keeley, 2005; Van Wagtendonk, 2006]:

-- Frequency: the fire return period (interval between fires at a given site), or the amount of time it takes to burn the equivalent

of a specified area. Fire frequency depends on the time necessary for the prevalent bio-fuel type to grow back.

-- Seasonality: the time of year during which fires are most common. Biomass burning often occurs mainly during the dry season, especially when it is concurrent with a strong lightning density.

-- Intensity: the energy released in the fire front per unit length (J/m/s).

-- Spread pattern: the level at which biomass burning occurs, viz., in the ground, at the surface and/ or on the crown of trees. Ecosystems may experience mostly one level of fire or a mix of the three. Ground fires propagate through soil rich in organic matter, surface fires through low-level vegetation (“crawling”), and crown fires through the top branches of shrubs and trees ("crowning"). Burning leaves carried by the wind ("spotting") also propagate fire and can cause great tree mortality over large areas.

-- Severity: the impact that a fire has on an ecosystem, here defined as plant mortality. The intensity of a wildfire is the energy released per unit length of fire-line (J/m/s), which can be estimated as the product of linear spread rate (m/s), heat of combustion (J/kg) and combusted fuel mass per unit area (kg/m^2), or via flame length correlation.

-- Extent: the total amount of burnt area after a wildfire. The area of vegetation affected by the fire, but not burnt, may also be considered.

These fire characteristics determine differential changes in the ecosystems, and influence what type of plant species survive and how they will be able to use burned areas.

1.6 Effects of Wildfires on Ecosystems

Fire serves many important functions within fire-adapted ecosystems, e.g., nutrient cycling, diversity maintenance, community composition and habitat structure. Natural fire regimes are important to maintain biodiversity and to avoid fuel build up [GEO-4, 2007].

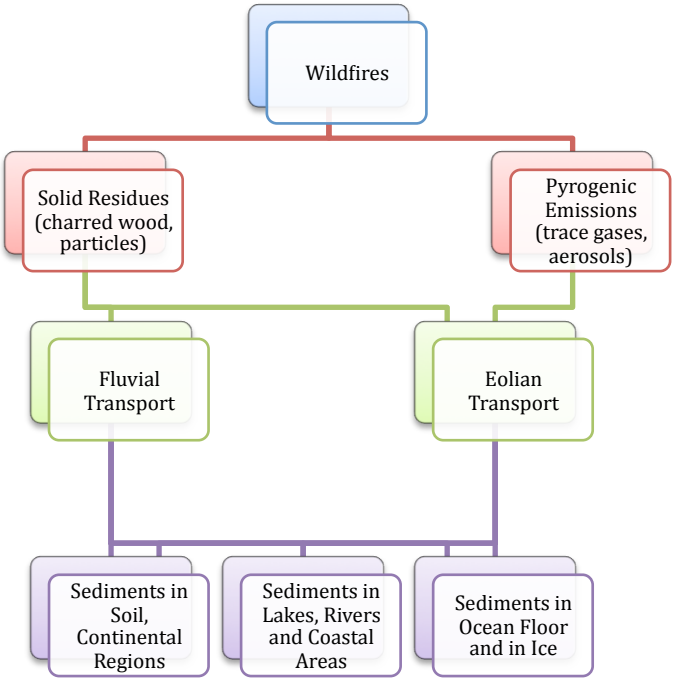

Figure 1.6 Schematic representation of types of transport and deposition of residues from wildfires.

1.6.1 Natural and Regular Biomass Burning

Wildfires are a natural phenomenon and an integral component to the functioning, regeneration and biodiversity of many ecosystems [GEO-4, 2007]:

-- Frequent fires allow a great number of species to exist within an ecosystem, by creating post-fire succession stages and habitats, beginning with downed trees and debris, then with fast-growing herbaceous plants, and finally with slowly-growing woody species, exploited by different species of plants, animals and microbes, all contributing to the accumulation of fuel load until the next fire;

-- Low-intensity fires destroy the debris of dead plants and allow the soil to receive more rain and to retain more moisture;

-- Charcoal, left as a residue of burnt wood, has considerable absorptive properties for nutrients and water;

-- Residual organic matter, left from low-intensity fires, adds nutrients to the soil;

-- Fire-dependent plants have flammable oils that can sustain ignition and fire spread, and fire or smoke-activated seeds or buds that quickly germinate and mature after a fire event, without competition from other species;

-- Some hydraulic changes caused by fire increase flooding, silt removal and deposition of habitat substrate, regenerating of aquatic habitats;

-- Shade-intolerant plants require fire to make light gaps in the vegetation canopy, so that the new seedlings can compete with other plants;

-- Low-intensity fires spare the soil microbes underground and favour the multiplication of microbial organisms on account of the post-fire increase in soil nutrients;

-- Some fauna and insects also depend on regular biomass burning to survive;

-- Smouldering or moderate flaming fires burn in the forest understory, removing small trees and herbaceous groundcover;

-- Frequent and low intensity fires in dry tropical forests remove plant litter and ground soil temperatures are not lethal to deep roots;

-- Shrublands are typically dry and prone to accumulations of highly volatile fuels, so regular low-intensity fires, that follow the path of greatest amount of dry fuel material, allow for new shrubs to grow;

-- In grasslands, fire is the primary mode of decomposition, making it essential in nutrient cycling;

-- In savannas, recently burned areas provide new nutritious forage for herbivores, and allow grazing intolerant grass species to grow in the abandoned lawns and thus persist within the ecosystem.

1.6.2 Damages Caused by Intense Wildfires

Uncharacteristic intense wildfires of large extent can cause great environmental damage [USDA RMRS-GTR-42, 2000]:

-- Soil moisture decreases, because of the ground's exposure to sunlight, evaporation and increased thermal amplitudes, with warming during the day and rapid cooling during the night;

-- Nutrients are lost by oxidation, volatilization, leeching by water, which makes the soil more vulnerable to erosion and floods;

-- Because of chemical reactions at high temperatures and combustion of acidic substances, wildfires alter the texture, composition and structure of soils, making them more alkaline (higher pH);

-- Soils become water-repellent, because fire heats organic matter on the ground into a waxy covering, which decreases their ability to form aggregates (clumps of soil that increase the porosity of the ground to water);

-- Fire frequency is typically high in grasslands and shrublands, where new fuel load grows every year, but low in forests, where trees take a much longer time to grow;

-- The increased fire frequency in ecosystems not adapted to frequent fires may completely eliminate native plant communities, specially very flammable fire-intolerant plants, which are then replaced with non-native plants, more fire adapted, providing fuel load for a next fire and preventing the return of the native plants;

-- High-severity fires damage aquifers, hydric resources and aquatic habitats.

1.7 Effects of Land Management on Wildfire Behaviour

Fire behaviour greatly depends on land cover. In the last centuries, human intervention in the landscape deeply changed many fire

regimes, through land management techniques such as logging, mining, fire suppression, prescribed fires, clearing, silviculture, agriculture, pasture and farming methods [FAO, 1995].

1.7.1 Land Use

Presently, anthropogenic conversion of forests or woodlands into shrublands or grasslands, for agricultural and pastoral land use (e.g., grazing and slash-and-burn agriculture), together with the replacement of native species, adapted to the environment, for others, economically more profitable, but misfit to the local climate, are increasing the frequency of fire events in many regions. Land use and, in particular, deforestation, has a substantial effect on regional climate, vegetation dynamics and fire risk [GEO-4, 2007].

Fire suppression is useful to reduce ecological damage during dry periods, especially in ecosystems where wildfire patterns depend mainly on strong winds and low humidity. However, if the density of fuel load impacts the intensity of wildfires, then reduction of fuel through prescribed burning will be more adequate [USDA, 2000; Fernandes & Botelho, 2003].

Plants in an ecosystem are adapted to their particular historical fire regime, so altered fire patterns may change the selective pressures on plants and benefit invasive and non-native species that are better able to colonize burned areas quickly and exploit the new post fire conditions [GEO-4, 2007].

1.7.2 Fire Suppression

Anthropogenic suppression of normal wildfires alters ecosystem dynamics, structure and species composition. It allows for damaging fire-intolerant invasive plant and animal species populations to grow uncontrolled by fire, so pyrophilous plants and animal species are negatively affected. Fire suppression modifies the natural fire

regime, especially in areas with naturally short fire return intervals; the accumulation of dead plant material for several years results in an unusual density of fuel loads, and the longer bio-fuel accumulates, the greater the damage when an unexpected fire burns out of control. This abundance of bio-fuel can lead to uncharacteristic fires, with more complete combustion, quicker fire spread and larger burnt areas than in the historical fire regime [USDA RMRS-GTR-42, 2000].

1.7.3 Prescribed Fires

Prescribed fires are a useful land management tool and can be more effective than natural fires to maintain the diversity and integrity of ecosystems, since they can be adapted with precision to plant life cycles. In semi-arid ecosystems, like dry tropical and boreal forests and woodlands, decomposition is slow, so fire is crucial to return nutrients to the soil and to eliminate debris and sustain productivity. Prescribed fires during the dormant season in grasslands clear debris and helps the control of invasive seeds, without resorting to herbicides or pesticides, increasing biodiversity and plant nutrient uptake [Keeley, 2001; Fernandes & Botelho, 2003].

1.8 Effects of Climate on Wildfires

Wildfire patterns respond to climate changes, directly and indirectly, and may reinforce or attenuate them, through various positive and/or negative feedback mechanisms. Fires are affected by climate, which varies in time because of external solar forcings (cycles in Earth's orbit eccentricity, position and inclination of the tilt, cycles of Sun spots), of internal geophysical forcings (cycle of strengthening, weakening and direction reversing of the magnetic field) and of atmosphere/ocean dynamics [IPCC AR4 WG1,

chapter 6, 2007]. Atmosphere and ocean dynamics are the only forcings that may change significantly over short periods of time, so they are the only type of climatic variability relevant to this research.

Weather varies regularly throughout the year, because of changes in the distance between the Earth and the Sun, and of the varying angle of incoming solar radiation. Seasonal variations outside the equatorial zone usually far exceed the smaller inter-annual variability in homonymous months of different years [IPCC AR4 WG1, chapter 2, 2007].

Atmosphere and ocean dynamics are greatly influenced by human activity and rapid climate change is disrupting fire patterns in many ecosystems. In regions where episodes of drought and/or high temperatures are now more frequent, fires are becoming increasingly more intensive and spreading more quickly and over larger areas, causing great damage to land ecosystems and water resources and even changing the regional climate [IPCC AR4 WG1, chapter 7, 2007].

1.8.1 Climate change effects favouring wildfires

Greenhouse gases are good absorbers of the long-wave infra-red terrestrial radiation, thus contributing to raise the average temperature of the Earth's surface.

The most common greenhouse gases in the atmosphere are water vapour (H_2O), carbon dioxide (CO_2), methane (CH_4), nitrous oxide (N_2O), chloro-fluoro-carbons (CFCs) and tropospheric ozone (O_3). Some chemically active gases, like carbon monoxide (CO), nitrogen oxides (NO_x) and non-methane hydro-carbons (NMHCs) are precursors of tropospheric O_3, thus also contributing, albeit indirectly, to the greenhouse effect. Increasing concentrations of greenhouse gases are contributing to global warming [IPCC AR4 WG1, chapters 2 and 9, 2007].

More energy available in the climatic system is likely to increase the frequency, intensity and spatial extent of extreme weather events, such as floods, droughts, hurricanes, thunderstorms and

heat-waves; some of these climatic changes are favourable to wildfires [IPCC AR4 WG1, chapter 10, 2007]:

-- More frequent heat waves dry the soil, worsening the effects of erosion; when water evaporates from the ground-surface, the level of ground water sinks, draining nearby lakes, rivers and irrigation systems, which contributes to droughts [GEO-4, 2007];

-- The tree line in some mountains is rising uphill, so fires can ignite and spread at higher altitudes, where steeper slopes benefit fire spread [GEO-4, 2007];

-- Earlier snowmelt is increasing the length of the fire season in certain forests [Westerling, 2001; IPCC AR4 WG1, chapter 7, 2007];

-- Some cold conifer forests (taiga) are migrating to where alpine shrublands and grasslands (tundra) used to be, increasing fire risk in those areas [GEO-4, 2007];

-- Prolonged drought in some areas is causing the evaporation of water in plants to exceed that absorbed from the soil, so those plants are drying out and releasing flammable essences, making ignition easy [GEO-4, 2007];

-- Mountain glaciers (rivers of ice) are retreating uphill and flowing faster to the sea, turning to streams and lakes of melting ice before they reach the coast, exposing mountain vegetation to wildfires [IPCC AR4 WG1, chapter 4, 2007];

-- Growing seasons and dry periods are getting longer in boreal forests [CCSC, 2009];

-- Permafrost is melting, exposing arctic shrublands and grasslands to fire, and allowing for swamps filled with decaying vegetation to release methane [GEO-4, 2007];

-- Some vegetation species (mainly grass) are becoming more abundant with longer summers and increased CO_2 levels, thus increasing the fuel load available to burn [GEO-4, 2007];

-- In the abundance of CO_2, plants close part of their stomata, thus absorbing less ground level O_3 and other pollutants [Kürshner & al., 1997; Sanderson & al., 2007];

-- In some regions, the dry season is becoming drier and warmer [IPCC AR4 WG1, chapter 10, 2007; CCSC, 2009];

-- Some forests, where fires were usually moderate, leaving most of the trees alive, are now suffering crown fires that cause extensive mortality [GEO-4, 2007]

-- There is an increased frequency of lighting strikes in some areas, igniting fire before the rainy season [IPCC AR4 WG1, chapter 7, 2007];

-- Higher frequencies of climatic oscillations are causing quick successions of extreme weather conditions advantageous to fires (e.g., the El Niño Southern Oscillation, a pattern of extreme weather in the tropical Pacific) [IPCC AR4 WG1, chapter 10, 2007; CCSC, 2009].

1.8.2 Climate change effects reducing wildfires

Some climatic changes in several ecosystems can also contribute to reduce biomass burning, either by altering weather conditions or by reducing the quantity of fuel loads available to burn:

-- Melted water from continental ice sheets (e.g. in North West Antarctica and Greenland) pouring into the ocean, together with thermal expansion of ocean waters, are contributing to a rise in sea levels, and the inundation of coastal areas [CCSC, 2009];

-- Land contamination with salty water will destroy much of littoral vegetation in areas that will become nearer the sea [GEO-4, 2007];

-- Overflowing rivers will wash off much vegetation in fluvial ecosystems [GEO-4, 2007];

-- Cooling of littoral areas where warm ocean currents are weakened may lead to lower temperatures during the fire season [CCSC, 2009];

-- Acidification of soils and acid rain diminish plant growth [FAO, 1995];

-- Deforestation and conversion of forests and woodlands into shrublands and grasslands usually decrease fuel load [GEO-4, 2007];

-- Desertification caused by droughts and/ or soil damage removes the fuel load necessary for biomass burning [GEO-4, 2007];

-- Warmer water and moist air enhance convective storms, tornadoes and hurricanes, increasing rainfall in some areas, thus diminishing the opportunities for fire ignition and spread. If conditions become rarely dry enough for ignition, some fire dependent ecosystems may disappear [GEO-4, 2007; CCSC, 2009].

1.9 Effect of Wildfires on Climate

Aerosols and chemically active gases released to the atmosphere during biomass burning can be spread around the globe by tropospheric currents, changing the atmospheric composition. Some pyrogenic emissions (viz. direct and indirect greenhouse gases and aerosols) alter the Earth's radiation balance. Changes in ecosystems and land cover caused by intense wildfires over large areas can also impact regional climates [IPCC AR4 WG1, 2007].

1.9.1 Warming Effects of Wildfires on Climate

Wildfires have a net warming effect in the climatic system [IPCC AR4 WG1, chapter 10, 2007]:

-- Biomass burning emits greenhouse gases and quickly releases all the carbon stored in the burnt vegetation during its lifetime, so the burned areas become a carbon source instead of a carbon sink;

-- Forests and woodlands are progressively transformed into grasslands and shrublands, which absorb little carbon and quickly release it after being consumed by animals;

-- Burnt landscapes often experience decreased humidity, cloudiness and rainfall.

Positive feedbacks enhance the initial imbalance, leading to an even greater temperature change [IPCC AR4 WG1, 2007].

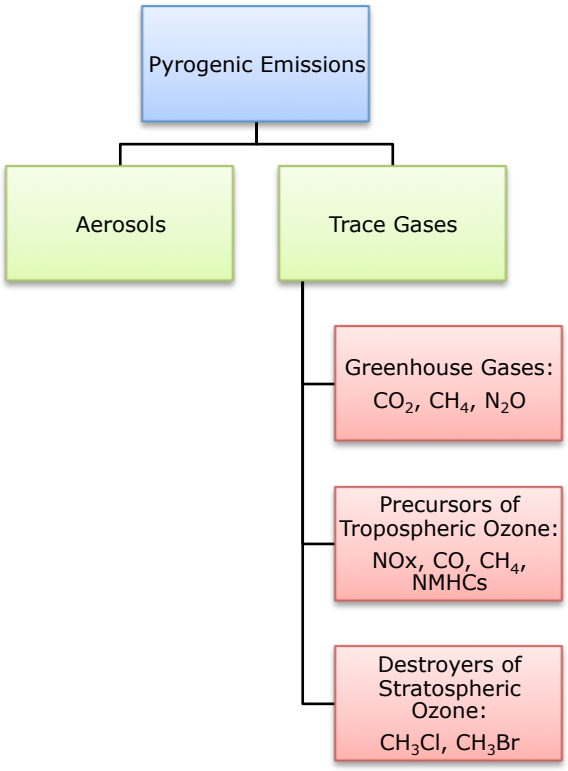

Figure 1.9.1 Schematic representation of types of pyrogenic emissions from biomass burning.

1.9.2 Cooling Effects of Wildfires on Climate

Wildfires have also some cooling effects in the Earth's climatic system, albeit surpassed by the warming effects [IPCC AR4 WG1, chapter 7, 2007; CCSC, 2009]:

-- Dust storms triggered by fires and pyrogenic aerosols can scatter sunlight, reducing the amount of solar radiation that reaches the Earth's surface, thus lowering temperature at the surface;

-- Pyrogenic aerosols and dust provide nucleation points for condensation, increasing the formation of clouds, which cool the atmosphere by reflecting sunlight back into space;

-- After a wildfire, the albedo of some ecosystems may increase, reflecting more sunlight and losing heat more rapidly at night, cooling the surface;

-- Burned land is more exposed to erosion by wind, rain and flowing water, and removes more CO_2 from the air.

The warming impact of fires far surpasses the cooling effects, however: for instance, greenhouse gases persist in the atmosphere for much longer than aerosols, thus counteracting their effect; the carbon-sinking effect of CO_2 dissolved in the rain, streams or groundwater, eroding rocks and forming bicarbonates, is very slow; and the exposed soils also release greenhouse gases, especially decaying peat, very rich in carbon [IPCC AR4 WG1, chapter 7, 2007; GEO-4, 2007].

1.10 Detection of Wildfires

For a global study of wildfires, it is necessary to have data about burnt areas and pyrogenic emissions in all the land ecosystems of the world. However, many wildfires occur in remote regions, far from populated areas, where there is no possibility of ground measurements or any local assessment of fire behaviour; therefore, information from satellite-sensors is essential, since it is the only way to monitor the whole surface of the planet.

The fire models obtained in this research were based only in statistical relationships between climate variables and fire data, without making any assumptions about the topography, orography, land cover, fuel type, vegetation structure, ecosystem dynamics or any other variables. Some of these characteristics, however, were used to plan the research and draw conclusions afterwards.

Fire data was obtained from the Global Fire Emission Database version 2.1 (GFEDv2.1), compiled with satellite-sensor data, from MODIS (Moderate Resolution Imaging Spectroradiometer), ATSR (Along Track Scanning Radiometer) and VIRS (Visible and Infrared Scanner), and complemented with the Carnegie-Ames-Stanford Approach (CASA) biogeochemical model, and with data from ground measurements and vegetation cover maps [Randerson & al., 2006].

The GFED is based mainly in burned area maps produced with Moderate Resolution Imaging Spectroradiometer (MODIS) surface reflectance imagery. When MODIS fire data were not available, burned area was estimated using local regression, regional regression trees and cross-calibration with the Tropical Rainfall Measuring Mission (TRMM)'s Visible and Infra-Red Scanner (VIRS) and with the Along-Track Scanning Radiometer (ATSR). Results were then compared with L3JRC, GLOBCARBON and MODIS MCD45A1 burned area products [Randerson & al., 2006].

Errors in these estimations do not add linearly, so the final uncertainty is difficult to quantify, and it was not conclusively established for the GFED version 2.1. The new GFED version 3, with data from 1997 to 2009, estimates a global average of 3.30 – 4.31 × 10^{12} m^2 per year in burnt area, and an average global uncertainty of 20% in the evaluations of area burned per year [Giglio & al., 2010], inferring that the uncertainty for GFED v2.1 might be even higher.

Weather and land-cover data, based on satellite-sensor and ground measurements, were downloaded from the websites of the European Centre for Medium-Range Weather Forecast (ECMWF), the Global Hydrology Research Project (GHRP), the Global Precipitation Climatology Project (GPCP) and the Goddard Institute of Space Studies (GISS).

1.11 Layout of the thesis

This thesis is divided into 4 chapters:

1) Introduction, with a brief presentation of the basis of wildfire science, necessary to plan and organize the present research;

2) Methodology, with detailed descriptions of data, and with graphic representations and explanations of all the mathematical and statistical calculations;

3) Results and Discussion, with the presentation and examination of the most important results and respective analysis and discussion;

4) Conclusions, with the summary of the most important results and correspondent interpretations.

The acronyms and symbols used in the text are listed in annex.

Chapter II Methodology

Summary

The objective of this research was to investigate global spatial and temporal distributions of biomass burning and pyrogenic emissions, with particular attention to their inter-annual variability, and to detect and quantify possible statistical relationships between climate and wildfire patterns, in different land ecosystems. With this purpose, global fire data were compared with world data of land cover and of climatic parameters.

This chapter describes the process of choosing, formatting and analysing the data considered more relevant to wildfire behaviour, and explains the statistical and graphical methods used to summarize, present and analyse these data, and then to produce fire models.

This chapter describes the methodology of this research, and it is divided into 3 sub-chapters:

1) Data Choice and Presentation: overall presentation of the data used, explaining the reasons for their choice, and detailing the sources, units and original resolution;

2) Data Analysis: explanation of the statistical methods employed to analyze the data;

3) Fire Models: description of the procedures for obtaining fire models in the regions with regular and frequent fire events.

2.1 Data Choice and Presentation

This sub-chapter presents the basic scientific principles leading to the choice of data more appropriate to the study of wildfire behaviour, and shows global maps illustrating the spatial and temporal distribution of the chosen climatic variables.

The principles of wildfire dynamics, i.e., thermodynamics applied to biomass burning in large open spaces, together with several results from laboratory experiments and observations of prescribed fires, indicate that the biomass burnt in a certain region, with a fixed topography, varies with the weather and with the quantity of fuel load available to burn (equation 2.1).

$$BB = f(FL, WP_1, \ldots, WP_n) \qquad \text{(equation 2.1)}$$

BB = biomass burnt

FL = fuel load

WP = weather parameter (e.g., temperature, humidity, etc.)

f(x) = a function of x, i.e., it varies with x

The characteristics of biomass burning over a large open area may considerably depart from what was observed in laboratory experiments (equations 1.2.1.1 to 1.2.3), because they are influenced by many uncontrollable variables and heterogeneous conditions. The composition and structure of the vegetation, the characteristics of the terrain, such as elevation and slope, and the weather conditions, such as temperature, humidity, precipitation, wind speed, snow cover, soil moisture and location of lightning strikes, are generally the most influential factors in ignition, spread, intensity and extinction of wildfires [Drysdale, 1998].

This research is made on a global scale, from 1997 to 2006, with a resolution of 1 degree by 1 degree, and uses data of land cover, geodesy, fuel load, burnt area, pyrogenic emissions and meteorological variables, given by satellite-sensor data and ground

measurements, complemented with biogeochemical models (tables 2.1.1-3).

Data	Final Units	Source and Resolution
Burnt Fraction	unitless ($m^2\_A_{burnt}$/ $m^2\_A_{total}$)	GFEDv2.1 (1°×1°)
Burnt Area	m^2	GFEDv2.1 + WGS (derived)
Fuel Load	kg_C/ m^2	GFEDv2.1 (1°×1°)
Combustion Completeness	unitless (kg_C fuel burnt/ kg_C fuel available)	GFEDv2.1 (1°×1°)
Biomass Burnt as Carbon Emissions	kg_C/ m^2	GFEDv2.1 (1°×1°)
All Pyrogenic Emissions	kg_chemicalX	GFEDv2.1 (1°×1°)

Table 2.1.1 Summary of the data on biomass burning, with the correspondent units, resolution and data sources.

Data on biomass burning (table 2.1.1) were compared to the meteorological variables considered more relevant to wildfire behaviour (table 2.1.3): temperature measured 2 metres above the ground, soil temperature in the 1st layer, lightning density, wind speed, relative humidity, specific humidity, soil wetness, rainfall and snow depth.

Data	Source
Geodesy	WGS, NGA
Land Cover	GISS, NASA
Topography (Global Digital Elevation Model)	JPL + METI
Desertification Vulnerability	NRCS, USDA

Table 2.1.2 Summary of the data on geodesy, geographic features and land cover, with the correspondent data sources.

Global monthly datasets of burnt fractions and fire emissions were provided by the Global Fire Emissions Database version 2.1 [Randerson & al., 2006]. These datasets consist of one-by-one degree gridded monthly burned area, fuel load, combustion completeness and biomass burnt (equivalent to total carbon emissions), from January 1997 to December 2006. They are based on raw data from satellite sensors -- Tropical Rainfall Measuring Mission (TRMM), Visible and Infra-Red Spectrometer (VIRS), Along Track Scanning Radiometer (ATSR), Moderate Resolution Imaging Spectrometer (MODIS), Advanced Very High Resolution Radiometer (AVHRR), ground data, regional vegetation data and the Carnegie-Ames-Stanford Approach (CASA) satellite-sensor-driven biogeochemical model [Giglio & al., 2006].

The classification of land cover is given by the Goddard Institute of Space Studies, of the United States' National Aeronautics and Space Administration [GISS, 2009], and other data about land cover are given by the Food and Agriculture Organization of the United Nations [FAO, 2005] and by the United States Department of Agriculture [USDA, 2000].

Geodetic information is given by the World Geodetic System of 1984 (WGS84), the Global Digital Elevation Model (GDEM) and by the US National Geospatial Intelligence Agency (NGA) and Japan's Ministry of Economy, Trade and Industry (METI).

Data sets about meteorological variables were downloaded from the websites of the European Centre of Medium-Range Weather Forecast

(ECMWF), the Global Precipitation Climatology Project (GPCP) and the Global Hydrology Research Project (GHRP).

Data	Final Units	Source and Original Resolution
Air Temperature (2m altitude)	Kelvin	ECMWF (2.5°×2.5°)
Soil Temperature (0.07m depth)	Kelvin	ECMWF (2.5°×2.5°)
Wind Speed	m/s	ECMWF (2.5°×2.5°)
Lightning Density	flashes/m^2/day	GHRP (1.125°×1.125°)
Relative Humidity	kg_vapour x 100%/ kg_maximum_vapour	ECMWF (2.5°×2.5°)
Surface Pressure	Pascal (N/m^2)	ECMWF (2.5°×2.5°)
Specific Humidity	kg_water/ kg_total_air	ECMWF (derived)
Soil Wetness (0.07m depth)	m^3_water/ m^3_soil	ECMWF (2.5°×2.5°)
Rainfall	m/month	GPCP (1°×1°)
Snow Depth	m	ECMWF (2.5°×2.5°)

Table 2.1.3 Summary of the chosen climatic parameters, with the correspondent units, resolution and data sources.

All data in this research were converted to SI units (Système International d'Unités), even if other units are more usual (e.g. rain is always expressed in metres, not in millimetres, and mass of carbon is expressed in kilograms, not teragrams).

Standard computer subroutines were used to transform all the raw data into the same format. Whenever data were given at a lower resolution than GFED's one degree by one degree (e.g., 1.25°×1.25°

or 2.5°×2.5°), interpolation methods were used to fit the data into a 1°×1° resolution format. Data points were ordered to form a conventional world map, from pixel number 1, with its superior "left" corner at (180°W; 90°N), until pixel number 64800 (360×180), with its inferior "right" corner at (180°E; 90°S). For the 720 pixels (360×2) adjacent to the North and South Poles, there is no distinction between left and right in the superior and inferior corners, respectively, since they are spherical triangles, with 3 corners, not spherical sectors with 4 corners, as the remaining 64080 pixels.

Therefore, all final datasets used in the analyses (sections 2.2 and 2.3) had exactly the same format, with 64800 data points corresponding to the total number of pixels in a world map divided into 360 degrees of longitude and 180 degrees of latitude, ordered from (180°W; 90°N) to (180°E; 90°S), with all values expressed in SI units.

This sub-chapter is divided into 17 sections, describing the geographical, environmental and climatic features important for this research:

1) Geodesy
2) Burnt Area
3) Fuel Loads
4) Combustion Completeness
5) Carbon Emissions
6) Direct Pyrogenic Emissions
7) Temperature
8) Wind Speed
9) Lightning Density
10) Humidity
11) Soil Moisture
12) Precipitation
13) Snow Depth
14) Land Cover Classification
15) Regions
16) Topography
17) Deforestation and Land Degradation

2.1.1 Geodesy

The mathematical model of the Earth used in all calculations is the ellipsoid of revolution (an oblate spheroid) defined by the World Geodetic System of 1984 (WGS 84), given by the United States' National Geospatial Intelligence Agency [NGA, 1997].

The area of each pixel was calculated with the standard geometrical equations for this ellipsoid. The total surface area of the ellipsoid obtained with this model (equation 2.1.1) is approximately 5.1006×10^{14} m^2.

$$S_{ellipsoid} = 2\pi a^2 + \pi(b^2/e)\ \ln[(1+e)/(1-e)] = 2\pi\ [a^2 + (b^2/e)\ \text{arctanh}(e)] \quad \text{(equation 2.1.1)}$$

$S_{ellipsoid}$ = surface area of the Earth (m^2)

a = equatorial radius = semi-major axis (m)

b = polar radius = semi-minor axis (m)

e = first eccentricity (unitless)

2.1.2 Burnt Areas

Global data of fire counts and burnt scars were given by hot spots and reflectance changes in satellite-sensor images. Fire satellite data were then implemented in regional fire models [Giglio & al., 2006], to estimate the monthly burnt fraction on each spherical sector of 1 degree of longitude by 1 degree of latitude. Monthly values of burnt fractions, given by the GFEDv2.1 [Randerson & al., 2007], were plotted in world maps (figure 2.1.2).

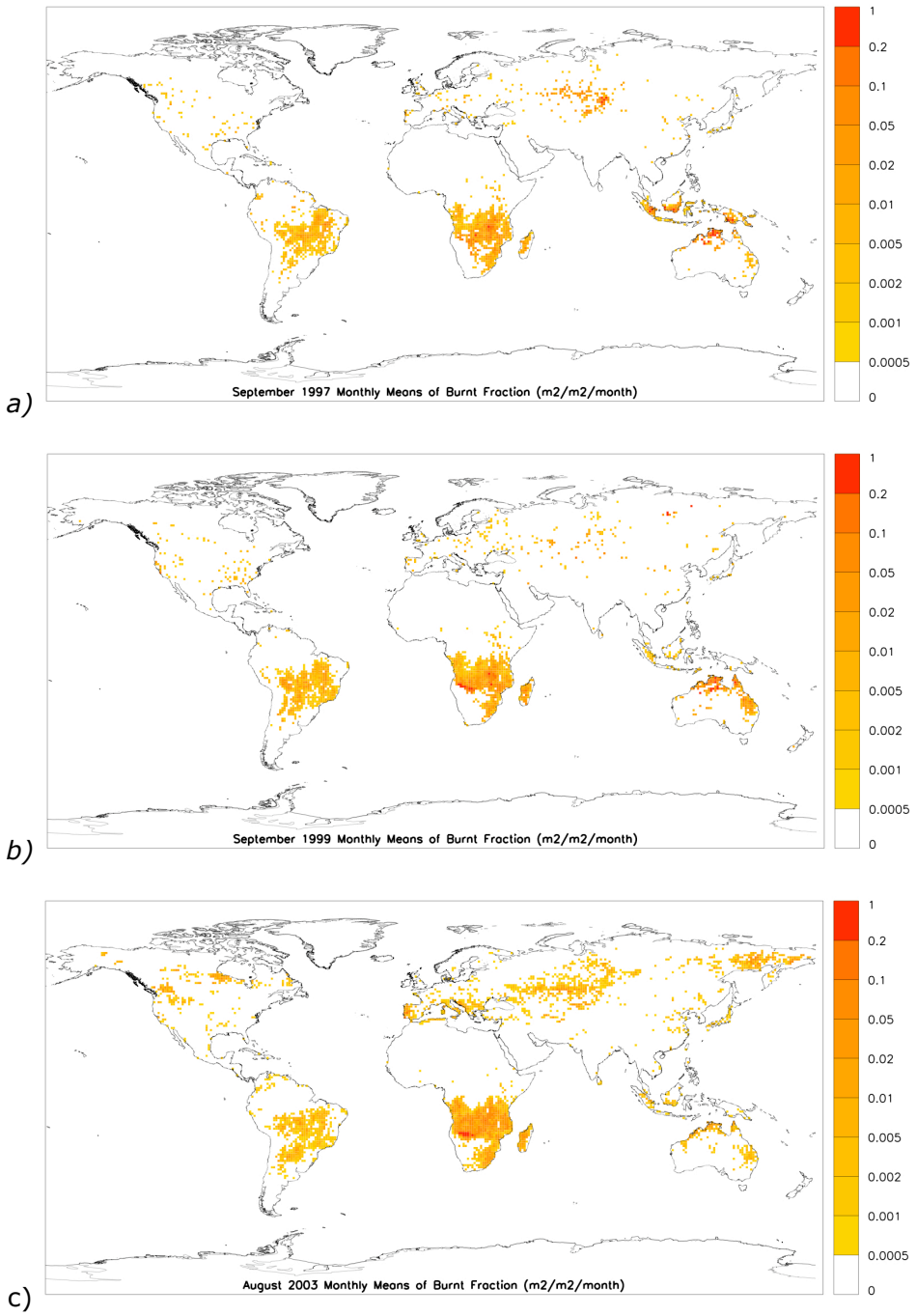

Figure 2.1.2 World maps of monthly burnt fractions in a) September 1997 (an El Niño year), b) September 1999 (a La Niña year) and c) August 2003 (during the European heat wave). There is a considerable inter-annual variability in temperate forests, which have a long fire return period, and in equatorial rainforests, which rarely burn.

Pixels of 1°×1° resolution are, geometrically, sectors of spherical surface delimited by 2 adjacent longitudes (lon1 and lon2) and

latitudes (lat1 and lat2). Pixel areas (A_{pixel}) are computed (equation 2.1.2.1) using the authalic radius ($R_{authalic}$) of the Earth, i.e., the radius of a perfect sphere, with the same surface area as the planet, taking into account a curvy equatorial zone and flattened poles [OD of Mathematics, 2005].

$$A_{pixel} = 2\,[R_{authalic}]^2\,|\sin(lat1)-\sin(lat2)|\,|lon1(^\circ)-lon2(^\circ)|/\,360^\circ \quad \text{(equation 2.1.2.1)}$$

A_{pixel} = area of the given pixel (m^2)

lon 1 and lon 2 = longitudes, in degrees, of the western and eastern extremities of the given pixel, respectively

lat 1 and lat 2 = latitudes, in degrees, of the southern and northern extremities of the pixel, respectively

$R_{authalic}$ = authalic radius (for a sphere of equal surface area as the Earth) = $\frac{1}{2}\sqrt{(S_{Ellipsoid}/\pi)} \approx 6.3710071809\times10^6$ m

The total burnt area (BA) in each pixel is the product of the burnt fraction of the pixel (BF) by its area (A_{pixel}) (equation 2.1.2.2).

$$BA = BF \times A_{pixel} \quad \text{(equation 2.1.2.2)}$$

BA = burnt area in the whole pixel (m^2)

BF = burnt fraction of the pixel (unitless)

2.1.3 Fuel Loads

The fuel load (FL) is the mass of carbon available to burn per unit area (A), in each grid cell (equation 2.1.3.1). It is expressed in kilograms of carbon per square metre, and is given by the GFED v2.1, based on land cover maps and regional vegetation models [Randerson et al., 2007]. Fuel load consists of the mass of carbon present in wood (W), living plants (L) and dead vegetation not burned (D):

$FL = (W + L + D) / A_{pixel}$ (equation 2.1.3.1)

FL = fuel load available to burn (kg_C/m^2)

W = mass of carbon in wood (kg)

L = mass of carbon in living plants (kg)

D = dead vegetation not burned (kg)

The vegetation killed by fire but not burnt (D_{fire}) consists of plants that died, on account of the heat and ashes of previous wildfires, but were not combusted (equation 2.1.3.2). It is expressed in kilograms of carbon, and can be computed multiplying a fire-induced mortality factor (MF_{fire}) by the quantity of living plants (L).

D_{fire} (kg_C) $= MF_{fire} \times L$ (equation 2.1.3.2)

D_{fire} = mass of carbon in the vegetation killed by previous fires but not burnt (kg)

MF_{fire} = fire-induced mortality factor (unitless)

The abundance of bio-fuel in conditions to be burnt greatly determines fire behaviour (equations 1.2.2.1, 1.2.2.3 and 1.2.3).

Fuel load depends on net primary production, above ground and below ground biomass and litter, herbivore consumption, fuel wood collection, combustion and fire induced mortality. It may considerably vary from season to season, in grasslands and shrublands, and from year to year, in forests and woodlands. Rainforests are the ecosystems with more abundance in fuel load, followed by temperate and boreal forests (figure 2.1.3).

a)

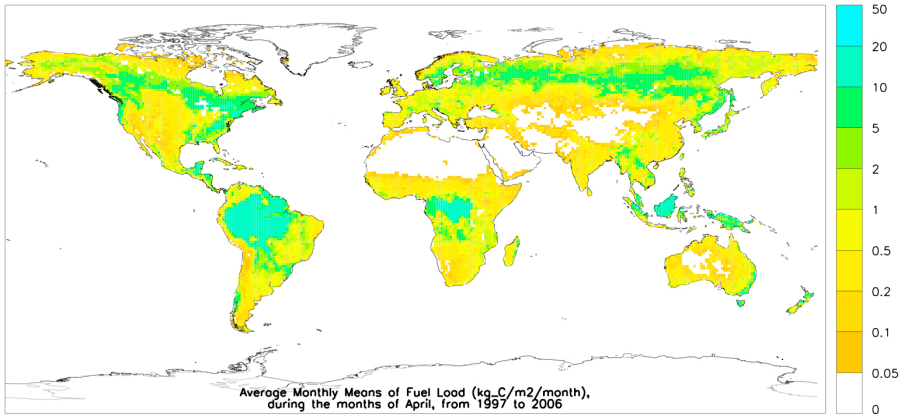

b)

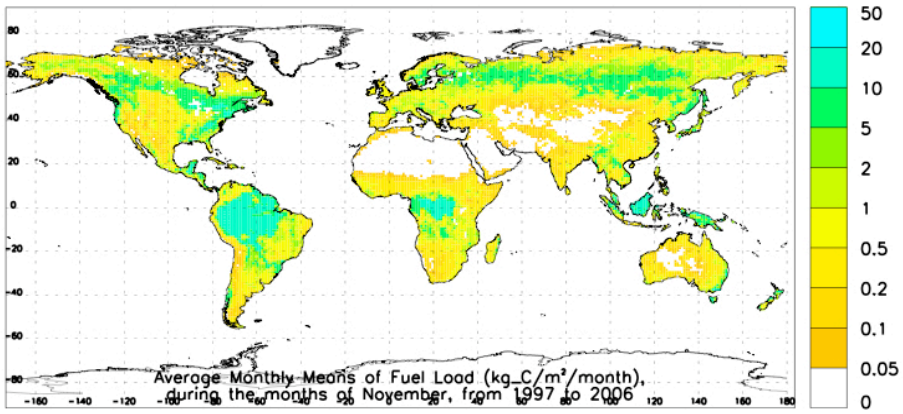

Figure 2.1.3 World map of the climatic average of monthly fuel loads (kg Carbon per square metre and per month) during the months of a) April and b) November, from 1997 to 2006.

2.1.4 Combustion Completeness

Combustion completeness (CC) is a measure of how much biomass is burnt relatively to the total available, expressed as the ratio of the bio-fuel actually combusted (FL_{burnt}) to the total bio-fuel in the area affected by the fire ($FL_{available}$). Combustion completeness is unitless and it varies from 0 to 1 (equation 2.1.4).

$$CC = FL_{burnt} / FL_{available} \qquad \text{(equation 2.1.4)}$$

CC = combustion completeness (unitless)

FL_{burnt} = mass of carbon in the bio-fuel burnt (kg)

$FL_{available}$ = mass of carbon in the total bio-fuel available to burn (kg)

The amount of material burned in a region exposed to fire will depend on the fuel type (leaf, stem, fine litter, coarse litter, peat), on the organic content of the soil and on the moisture of both the fuel and the soil. The same fuel will have a higher combustion completeness if it is dry on a dry soil exposed to a flaming fire than if it is wet on a moist soil and in contact with a smouldering fire [Drysdale, 1998; USDA, 2000].

Complete combustion would result in production of CO_2 and H_2O alone, but, in wildfires, combustion is usually incomplete. The ratio CO_2/CO gives information about the type of fire, flaming or smouldering. Proportionately, flaming fires give much more CO_2 than smouldering fires. Combustion completeness determines the relative proportions of substances emitted during biomass burning [Andreae & Merlet, 2001].

Data about combustion completeness were given by the GFEDv2.1 [Randerson & al., 2008], based on land cover data and on results from laboratory experiments [Andreae & Merlet, 2001]. In this case, combustion completeness was not measured directly, it was estimated from vegetation data, based on the assumption that grasslands burn more intensively than shrublands, which burn more than woodlands, which, in turn, burn more than forests (figure 2.1.4). These estimates of combustion completeness allow the evaluation of how thoroughly, on average, the vegetation in each pixel is expected to burn during a fire. However, these values do not take into account the intensity of a particular fire that may cause a completeness of combustion higher or lower than average.

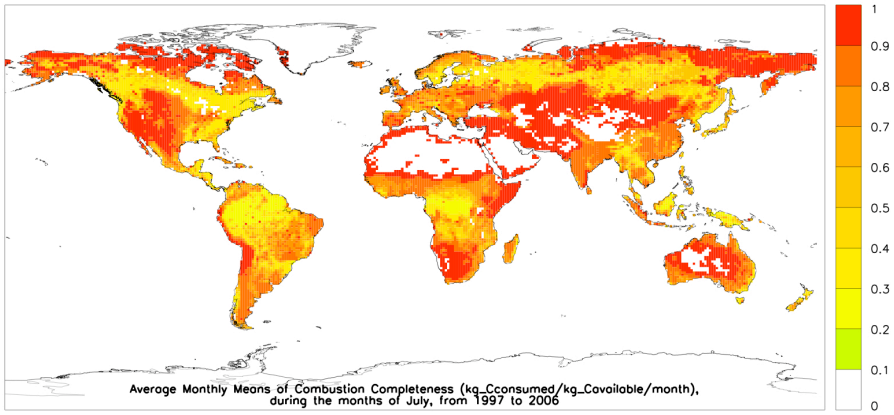

Figure 2.1.4 World map of the climatic averages of monthly combustion completeness (kg of carbon consumed per kg of carbon available and per month) during the months of July, from 1997 to 2006, in all land ecosystems covered with vegetation.

2.1.5 Biomass Burnt (Carbon Emissions)

Carbon emissions correspond to the mass of carbon in the biomass burnt. In the GFED v2.1, biomass burnt is equivalent to carbon emissions and is estimated from satellite-sensor data, ground observations and biogeochemical models (figure 2.1.5); the other pyrogenic emissions are inferred from the values of biomass burned, using laboratory emission factors and land cover data [Randerson & al., 2007].

a)

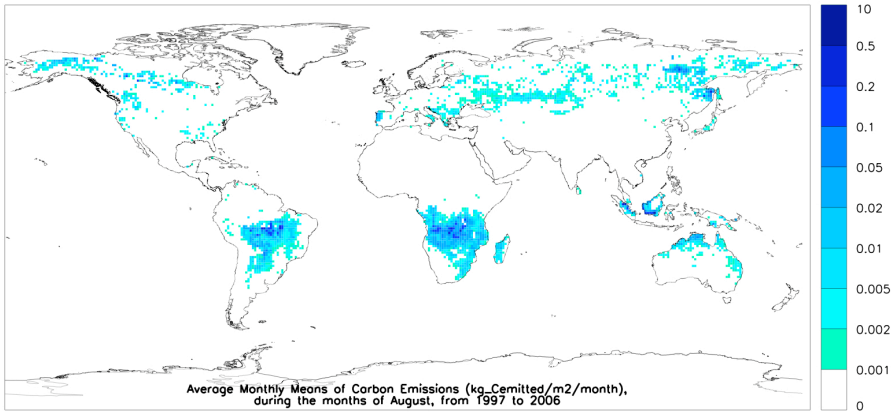

b)

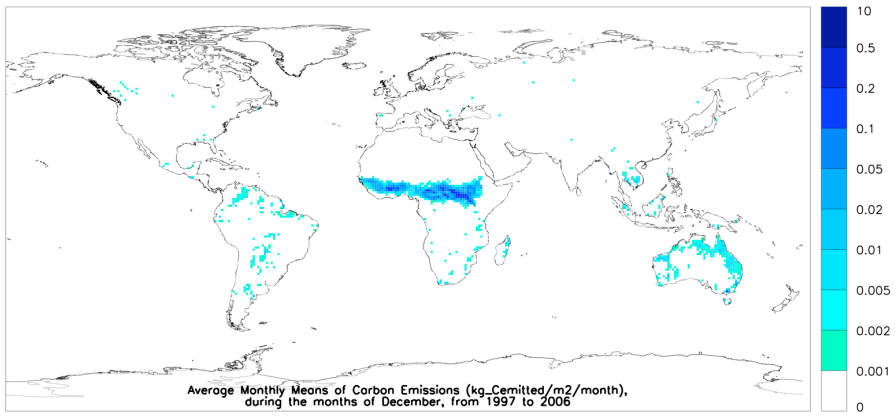

Figure 2.1.5 World maps of the climatic average of monthly carbon emissions (kg of carbon emitted per square metre and per month), during the months of a) August and b) December, from 1997 to 2006.

The quantity of biomass burnt (equation 2.1.5) was given by the GFEDv2.1, where it is calculated as the product of fuel load times burnt area times the combustion completeness [Seiler & Crutzen, 1980].

$$C\_emissions = FL \times BA \times CC \qquad \text{(equation 2.1.5)}$$

C_emissions = total mass of carbon in the biomass burned (kg_C/month)

FL = mass of carbon in the fuel load (kg_C)

BA = burnt area (m^2) = BF × area (m^2)

CC = combustion completeness (unitless, from 0 to 1)

2.1.6 Direct Pyrogenic Emissions

The stages of bio-fuel combustion are (1st) ignition, then (2nd) flaming and glowing and pyrolysis, then (3rd) glowing and pyrolysis (smouldering), then (4th) just glowing and finally (5th) extinction. Each stage involves different chemical processes that result in different pyrogenic emissions [Drysdale, 1998].

The emission factor of a chemical trace species X (EF_X) is the ratio of mass of the trace species X emitted ($m\_X_{emission}$) to the total dry biomass burnt (m_total) (equation 2.1.6.1). Emission factors vary with the fuel composition, moisture, fire severity and fire behaviour [Drysdale, 1998].

In open vegetation fires, where a moving fire front passes through bio-fuel, all combustion types can occur at any time in different places of the area burning. The combined emissions of trace gases and aerosols are released into the smoke plume. Vegetation that burns with higher intensity has a more complete combustion, which leads to a larger fraction of highly oxidised species (CO_2, NOx). Low intensity smouldering releases more reduced forms (CO, NH_3) [Drysdale, 1998].

However, in practice, pyrogenic emissions are computed as the product of two ratios, more easily obtained in laboratory experiments: the ratio of emission of the species X ($m\_X_{emission}$) to the emission of carbon ($m\_C_{emission}$), and the ratio of carbon emissions ($m\_C_{emission}$) to the total dry biomass burnt (m_total) [Andreae & Merlet, 2001].

$$EF\_X = m\_X_{emission}/m\_total = (m\_X_{emission}/m\_C_{emission})\ (m\_C_{emission}/m\_total)$$

(equation 2.1.6.1)

EF_X = emission factor of the chemical X (unitless)

$m\_X_{emission}$ = mass of chemical X ($kg\_X_{emission}$)

m_total = total dry biomass burned (kg)

$m\_C_{emission}$ = mass of carbon emissions ($kg\_C_{emission}$)

The emission of a chemical species X ($m\_X_{emission}$) is obtained by multiplying the amount of dry biomass burnt (m_total), within a grid cell, during a time interval, with the emission factors (EF) of the various smoke constituents (equation 2.1.6.2). These emission factors are determined by the composition of the fuel and by the physical and chemical processes during combustion [Randerson & al., 2001].

$$m\_X_{emission} = m\_total \times EF\_X \qquad \text{(equation 2.1.6.2)}$$

In the GFEDv2.1, pyrogenic emissions of a certain trace gas or aerosol are usually computed as the product of carbon emissions ($m\_C_{emission}$) by the ratio of emission of that trace species to carbon emissions (equation 2.1.6.3), given by laboratory experiments [Andreae & Merlet, 2001].

$$m\_X_{emission} = m\_C_{emission} \, (m\_X_{emission} / \, m\_C_{emission}) \qquad \text{(equation 2.1.6.3)}$$

Pyrogenic emissions of trace gases and aerosol species ($m\_X_{emission}$) given by the GFEDv2.1 [Randerson & al., 2008], e.g. carbon dioxide (CO_2), carbon monoxide (CO), methane (CH_4), nitrous oxide (N_2O), nitrogen oxides (NO_x) and particulate matter (TPM), were calculated with emission factors from Andreae and Merlet multiplied by carbon emissions (equation 2.1.6.4).

$$m\_C_{emission} \times EF\_X = m\_X_{emission} \qquad \text{(equation 2.1.6.4)}$$

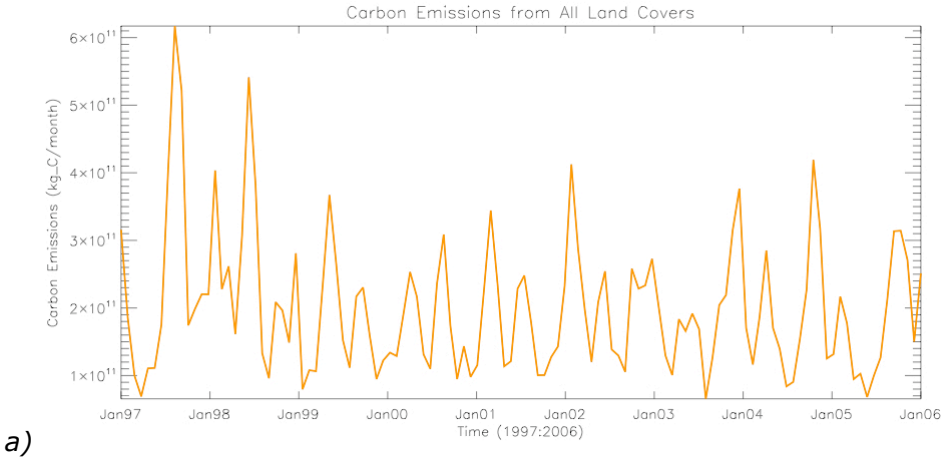

a)

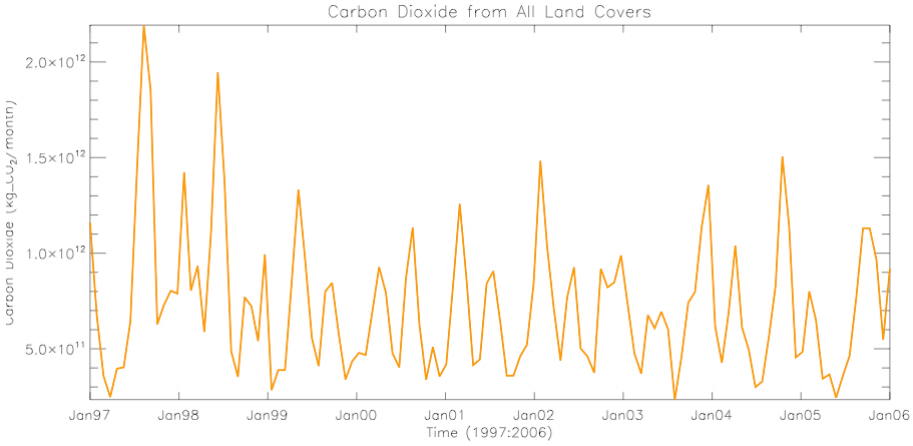

b)

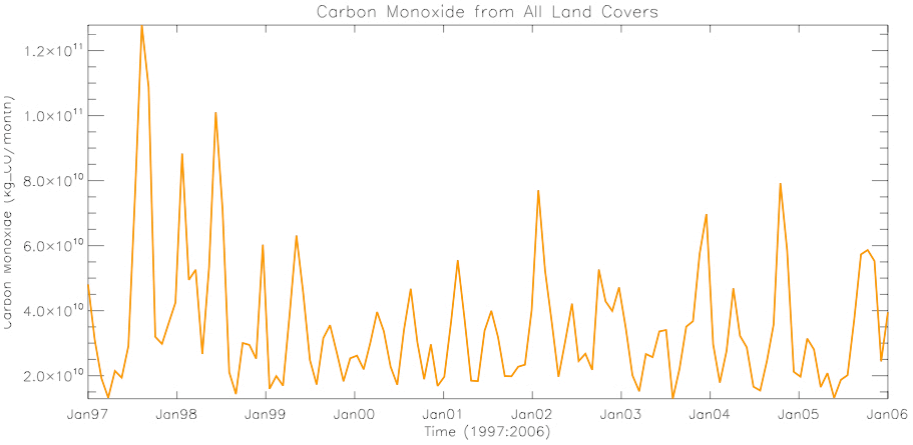

c)

Figure 2.1.6 Time series of GFED v2.1 estimated pyrogenic emissions for all wildfires in land ecosystems, from 1997 to 2006: a) carbon emissions (C), b) carbon dioxide (CO_2) and c) carbon monoxide (CO).

Carbon emissions for all land covers (figure 2.1.6 a) have high peaks between 1997 and 1998, corresponding to an El Niño event. The

time series for carbon dioxide (figure 2.1.6 b) has a similar pattern to that of the total carbon emissions, whereas the carbon monoxide time series (figure 2.1.6 c) has a rather distinct pattern: this illustrates the fact that CO_2 constitutes the bulk of pyrogenic emissions, and that different types of combustion release different proportions of CO and CO_2.

2.1.7 Air Temperature

Air temperature is a measure of the overall kinetic energy of the air molecules, measured by thermometers near the ground or by radiation in satellite-sensors [OD of Weather, 2008].

Temperature is one of the most important factors in possibility of ignition and fire spread [Drysdale, 1998], as seen in the fundamental equations of fire dynamics (equations 1.2.1.1, 1.2.1.3 and 1.2.2.2). The temperature of the soil at the surface (figure 2.1.7), down to a depth of 0.07 m (1^{st} layer of soil), is quite similar to the temperature of the air measured 2m above the ground.

Air temperature at 2 metres of height and soil temperature in the first layer are usually quite similar, so one or the other can be used for statistical calculations. Subsequent analyses with rank-correlation maps (section 2.2.2) have shown that biomass burnt is more correlated with the maximum daily value of air or soil temperature than with the average of 4 daily values, so the monthly mean of the maximum daily values [ECMWF, 2008] was chosen as the parameter to represent the influence of temperature in fire behaviour.

Because the continental masses are concentrated in the northern hemisphere, and Antarctica, in the south polar region, has no vegetation cover, the southern hemisphere land ecosystems have in average higher temperatures throughout the year. The highest and lowest average soil temperatures in vegetation areas occur near deserts in sub-tropical and sub-polar zones, respectively (figure 2.1.7).

a)

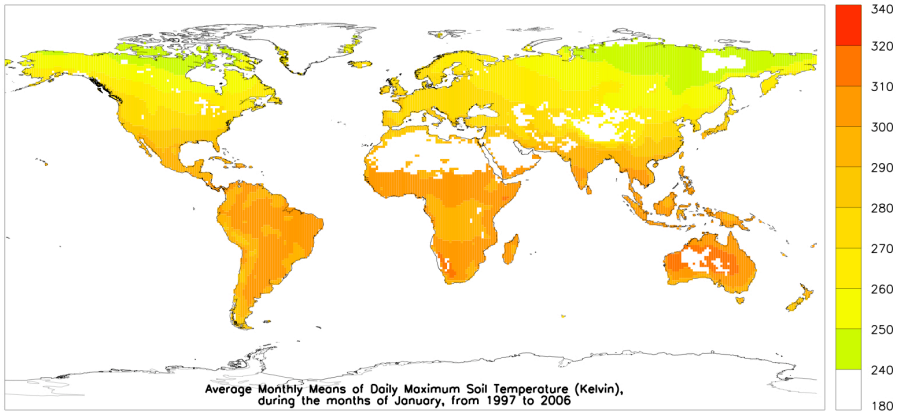

b)

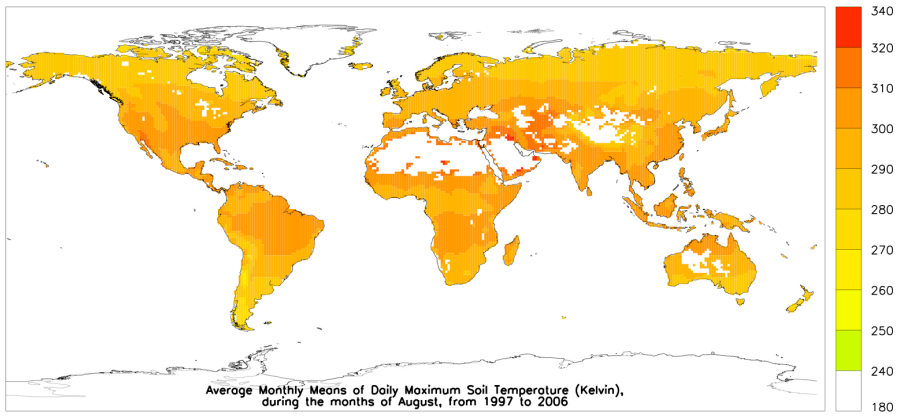

Figure 2.1.7 World maps of the climatic averages of monthly means of daily maximum soil temperature (Kelvin), during the months of a) January and b) August, from 1997 to 2006, in all land ecosystems covered by vegetation. Pixels with warmer soil are shown in red; green pixels have a cooler soil, in average, in the respective month.

2.1.8 Wind Speed

Wind speed is the horizontal motion of air relative to the Earth's surface, measured by anemometers [OD of Weather, 2008].

Different vegetation types and structures respond differently to wind speeds. Wind contributes to increase vegetation dryness, airflow into the flames and transport of flaming material over great distances [Drysdale, 1998], which favours fire spread (equations 1.2.2.1 and 1.2.2.2). Wind speed can vary considerable from season to season (figures 2.1.8).

Subsequent analyses with rank-correlation maps (section 2.2.2) have shown that the monthly average of maximum wind speed daily value was more strongly related to burnt fraction than to the average of 4 daily values, so the monthly arithmetical mean of the maximum daily wind speed [ECMWF, 2008] was chosen as the parameter to represent the impact of wind in fire behaviour.

a)

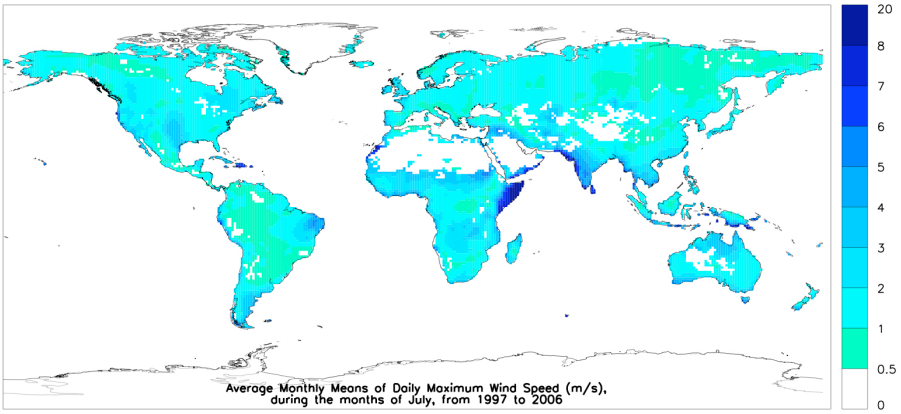

b)

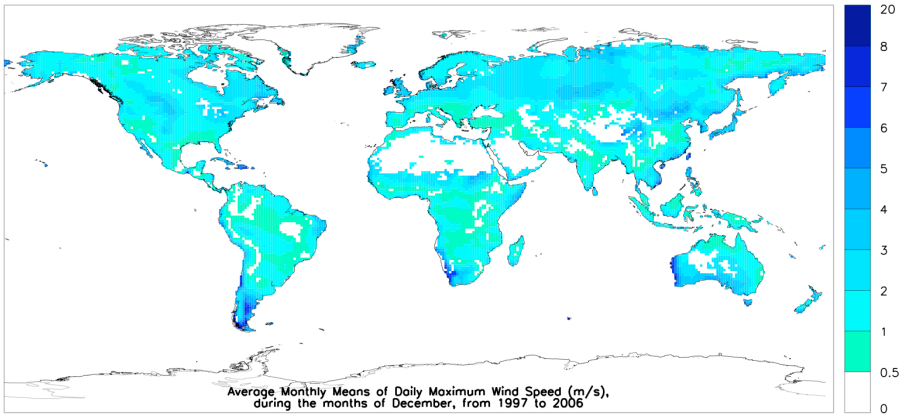

Figure 2.1.8 World maps of the climatic averages of monthly means of maximum daily wind speed, during the months of a) July and b) December, from 1997 to 2006, in all land ecosystems covered with vegetation. Pixels with the strongest winds are coloured in dark blue. Wind speed is very high in western India and eastern equatorial Africa, during the monsoon months (e.g., July), and in the west coasts of South Africa and Southern Australia, as well as in the extreme south of South America, during the summer of the Southern Hemisphere.

2.1.9 Lightning Density

Lightning is a large spark produced by an abrupt discontinuous discharge of electricity through the air during turbulent conditions of the atmosphere [Meteorology Source Book, 1988].

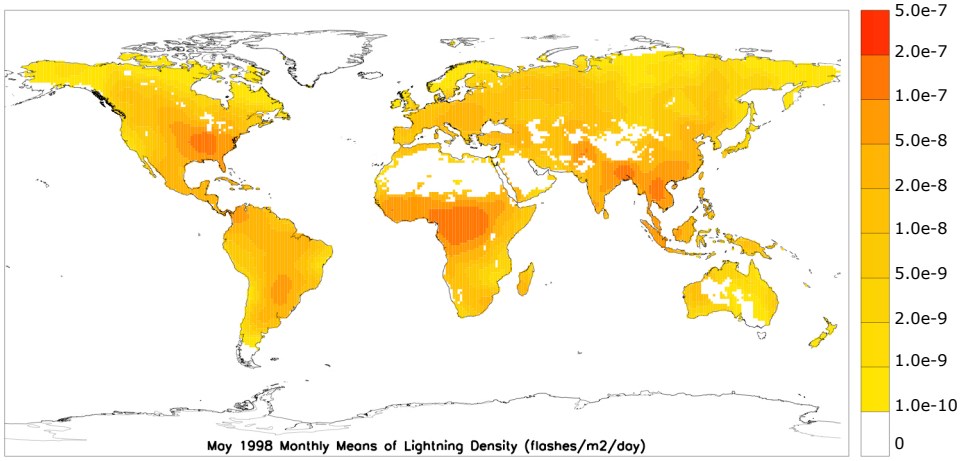

a)

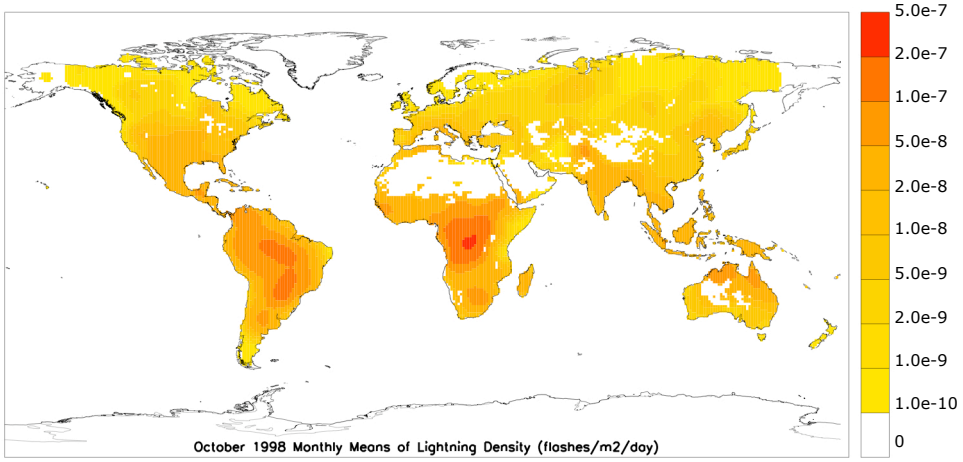

b)

Figure 2.1.9 World maps of the climatic averages of monthly means of daily lightning density (flashes/m^2/day), during the months of a) May and b) October, from 1997 to 2006, in all land ecosystems covered with vegetation. Red pixels show the areas of higher lightning density.

Lightning density data were obtained from the Global Hydrology Research Centre [GHRC, 2005]. Monthly arithmetic means of flash

counts, at 1.125° × 1.125° of resolution, were interpolated to 1°×1° pixels (figure 2.1.9). From 1997 to 2006, some months of data were missing.

Lightning density is a major contribution to fires in many land ecosystems [van Wagtendonk, 2007], providing the initial energy necessary for ignition (equations 1.2.1.1, 1.2.1.2 and 1.2.1.3).

The effects of electrical discharges near the ground are quite variable; in dry weather, sparks easily ignite fire, but, if lightning is concurrent with rain, ignitions diminish during periods of higher lightning density, as often happens in monsoon regions (figure 2.2.2.2).

2.1.10 Humidity

The specific humidity of a parcel of air is the ratio of the mass of water vapour to the total mass of air [OD of Weather, 2008], here expressed in SI units of kg of water vapour per kg of total air.

According to the principles of fire dynamics, ignition and spread are considerably hindered in conditions of wet soil and moist air (equations 1.2.1.1 to 1.2.2.3), which also favour fire extinction (equation 1.2.3), so humidity levels are an important factor in fire behaviour [Drysdale, 1998].

Specific humidity was chosen to represent air humidity (figure 2.1.10), since it is an independent physical quantity, unlike relative humidity, which varies with temperature, by definition. However, since this parameter was not directly available from ECMWF (2008), it had to be obtained through relative humidity, temperature and surface pressure.

a)

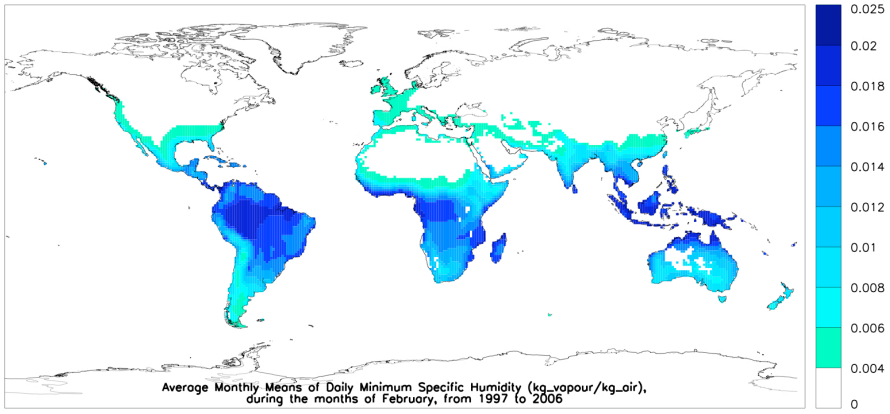

b)

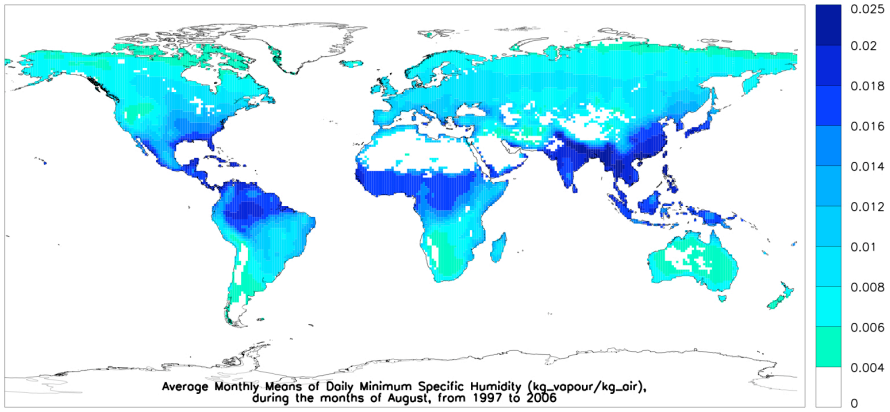

Figure 2.1.10 World maps of the climatic averages of monthly means of daily minimum specific humidity (kg_vapour/ kg_air), during the months of a) February and b) August, from 1997 to 2006, in all land ecosystems covered with vegetation. Dark blue pixels show the areas of highest humidity.

The relative humidity of air at a given temperature (equation 2.1.10.1) is the ratio of the vapour pressure to the saturation vapour pressure of water at the same temperature [OD of Weather, 2008].

$RH\ (T) = p\ H_2O\ /\ p\ sat\ H_2O\ (T)$ (equation 2.1.10.1)

The surface pressure is the force exerted by the column of air extending from the surface to the outer limit of the atmosphere and subject to the Earth's gravitational attraction, measured by barometers and expressed in Pascal ($kg/m/s^2$) [OD of Weather, 2008].

The specific humidity can be deducted from the relative humidity, temperature and surface pressure (equation 2.1.10.2).

$$SH = (\varepsilon^2 RH^2 / p\ dry) \times \exp(17.269\ (T-273.3)/ T)$$

(equation 2.1.10.2)

SH = specific humidity (unitless)

RH = relative humidity (unitless)

p dry = pressure of dry air (Pa)

T = surface air temperature (Kelvin)

ε (epsilon) = parameter for saturated SH = 0.62197 ($N^{1/2}\ m^{-1}$)

2.1.11 Soil Moisture in the 1st layer

Soil moisture is the moisture content of soil above the water table, including water vapour in the pores [OD of Weather, 2008], expressed here as the volume of water per volume of soil (m^3_water/m^3_soil).

Soil moisture data were given by the ECMWF (2008) at 2.5 by 2.5 degrees of resolution, and then interpolated to 1 by 1 degree. Only the first layer (defined as the top soil layer with 0.07 m of depth) was taken into account, because it is the one more directly related to probability of ignition, fire spread and extinction (equations 1.2.1.1 to 1.2.3). Seasonal variations of soil moisture are noticeable in many regions (figure 2.1.11).

Subsequent analyses with rank-correlation maps (section 2.2.2) suggest that the minimum daily value is often better correlated with biomass burning than the average value of 4 hourly values, so the former parameter was chosen to represent the impact of soil moisture in fire behaviour.

a)

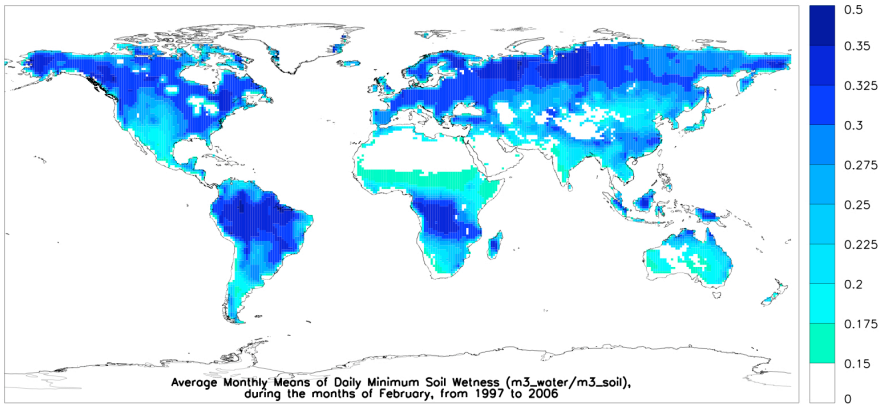

b)

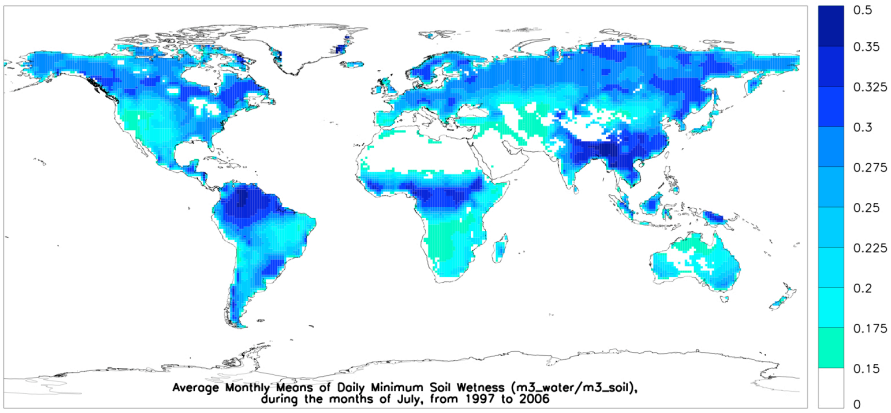

Figure 2.1.11 World maps of the climatic averages of monthly means of daily minimum soil moisture (m^3_water/ m^3_soil), during the months of a) February and b) August, from 1997 to 2006, in all land ecosystems covered with vegetation. Pixels in dark blue show the areas of highest soil wetness.

2.1.12 Precipitation

Precipitation is the fallout of water, liquid or frozen, from the atmosphere, and its values represent the total amount of liquid water equivalent of all forms of precipitation (rain, drizzle, hail, sleet, ice crystals and snow), measured by rain-gauges [Meteorology Source Book, 1988]. Precipitation greatly favours fire extinction [Drysdale, 1998], therefore it is a very important parameter in wildfire behaviour (equation 1.2.3).

Data on precipitation were given by the GPCP (2008), already in one degree by one degree of resolution, and are expressed here in SI units of metres per month (figure 2.1.12).

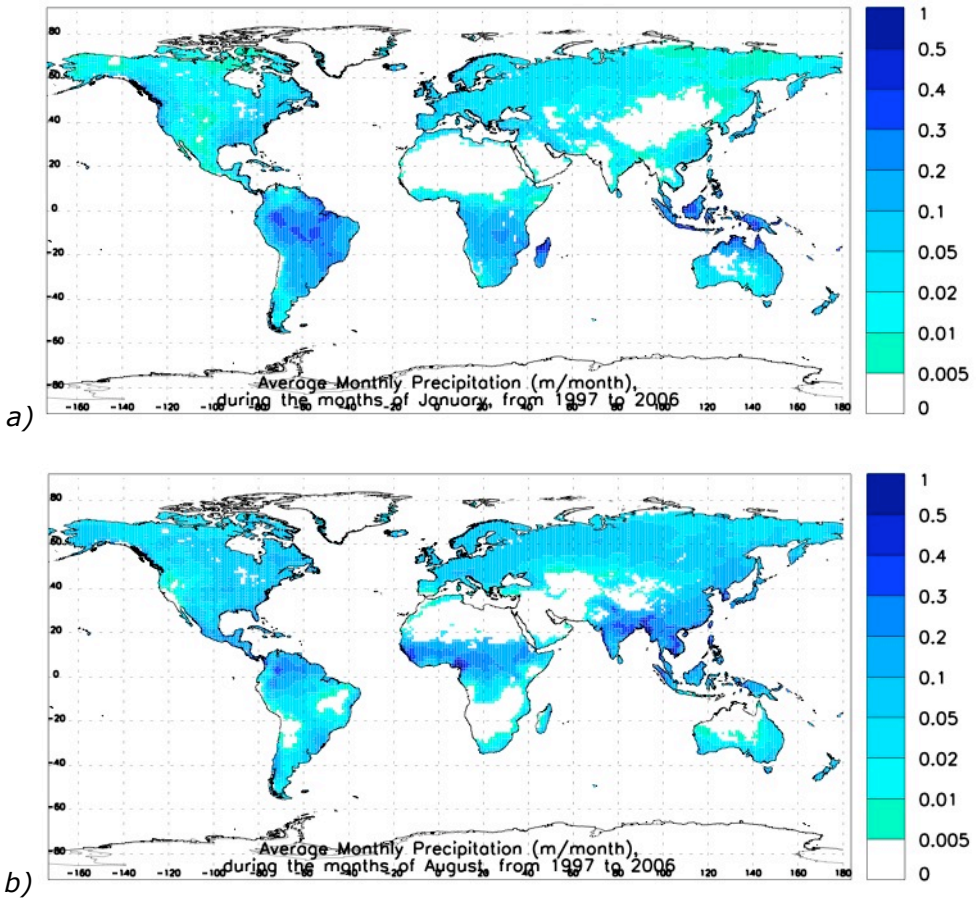

Figure 2.1.12 World maps of the climatic averages of monthly precipitation (m/ month) during the months of a) January and b) August, from 1997 to 2006, in all land ecosystems covered with vegetation. Pixels in dark blue show the areas of more intense precipitation.

2.1.13 Snow Depth

Snow depth is the depth of solid precipitation, in the form of ice crystals or snowflakes, accumulated on the ground [OD of Weather, 2008]. Values of snow depth were obtained from the ECMWF (2008),

with 2.5 by 2.5 degrees of resolution, then interpolated to 1 by 1 degree, and were expressed here in SI units of metres.

Subsequent analyses with rank-correlation maps (section 2.2.2) suggested that biomass burning was more closely related to the maximum daily value of snow depth than to the average daily value. Therefore, the monthly average of maximum daily snow depth was chosen to represent the impact of snow in fire behaviour (figure 2.2.13).

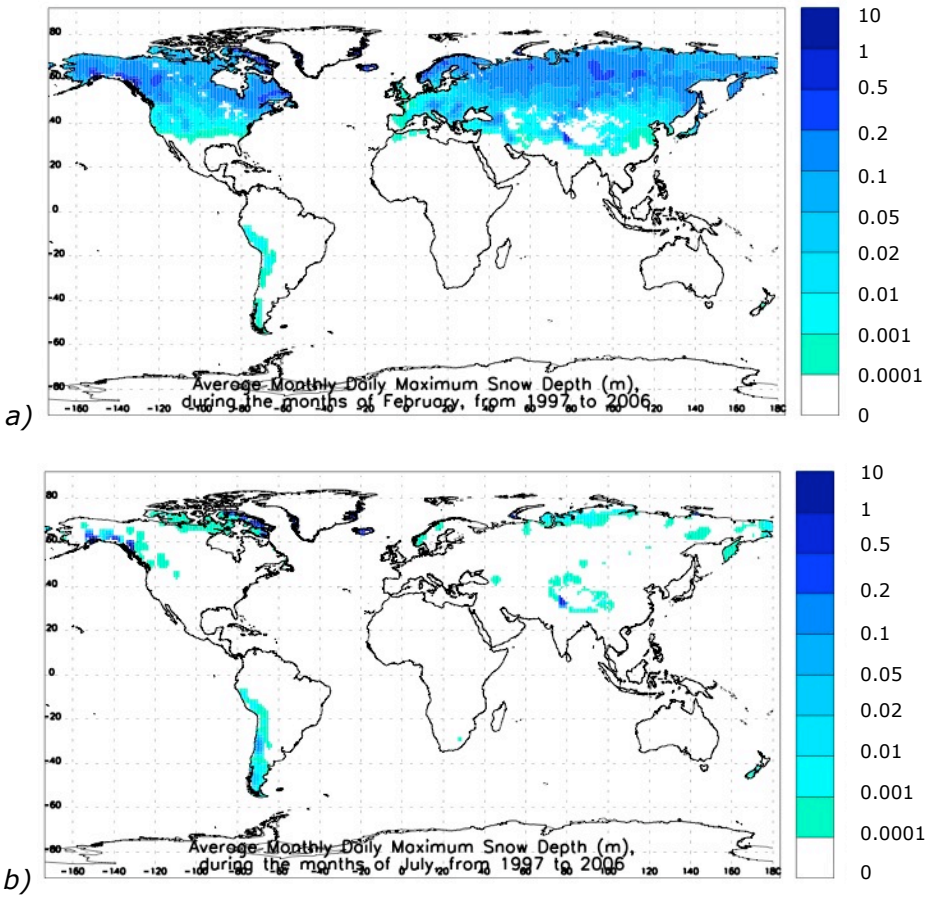

Figure 2.1.13 World maps of the climatic average of monthly means of daily maximum snow depth (metres), during the months of a) February and b) July, from 1997 to 2006, in all land ecosystems covered with vegetation.

Earlier snowmelt may cause a deficit of soil water during the following fire season (Westerling & al., 1999; Immeerzeel & al., 2009), but snow can also have a drying effect on the soil cover [Pearce, 2000]; therefore, both positive and negative anomalies of

snow can make vegetation more vulnerable to fire, depending on the ecosystem.

There is a noticeable seasonal variability in snow depth over the Northern Hemisphere (figure 2.1.13). Some mountain regions were always covered with snow.

2.1.14 Land Cover Classification

Wildfires can occur anywhere in the world where there is vegetation available to burn (figure 2.1.14), but some ecosystems are much more susceptible than others to fire occurrences.

In this research, the land cover classification [GISS, 2005] has 28 distinct terrestrial ecosystem types (tables 2.1.14). The knowledge about the ecosystem does not affect the analyses themselves, it is only used to choose eco-regions with a relative homogeneity, and then to draw interpretations and conclusions about the results.

Number	Forest Ecosystems
1	Tropical Evergreen Rainforests
2	(Sub)Tropical Evergreen Seasonal Broad-Leaved Forests
3	Subtropical Evergreen Rainforests
4	Temperate/Subpolar Evergreen Rainforests
5	Temperate Evergreen Seasonal Broad-Leaved Forests
6	Evergreen Broad-Leaved Sclerophyllous Forests
7	(Sub)Tropical Evergreen Needle-Leaved Forests
8	Temperate/Subpolar Evergreen Needle-Leaved Forests

9	(Sub)Tropical Drought-Deciduous Forests
10	Cold-Deciduous Forests with Evergreens
11	Cold-Deciduous Forests without Evergreens

Table 2.1.14 a Classification of forest ecosystems [GISS, 2005], with identification key for the land-cover map (figure 2.1.14).

Number	**Woodland Ecosystems**
12	Xeromorphic Woodlands
13	Evergreen Broad-Leaved Sclerophyllous Woodlands
14	Evergreen Needle-Leaved Woodlands
15	(Sub)Tropical Drought-Deciduous Woodlands
16	Cold-Deciduous Woodlands

Table 2.1.14 b Classification of woodland ecosystems [GISS, 2005], with identification key for the land-cover map (figure 2.1.14).

Number	**Shrubland Ecosystems**
17	Evergreen Broad-Leaved/Dwarf Shrublands
18	Evergreen Needle-Leaved/Microphyllous Shrublands
19	Drought-Deciduous Shrublands
20	Cold-Deciduous Subalpine/Subpolar Shrublands
21	Xeromorphic/Dwarf Shrublands

Table 2.1.14 c Classification of shrubland ecosystems [GISS, 2005], with identification key for the land-cover map (figure 2.1.14).

Number	Grassland Ecosystems
22	Arctic/Alpine Tundra, Mossy Bogs
23	Grassland, 10-40% Woody Cover
24	Grassland, <10% Woody Cover
25	Grassland, Shrub Cover
26	Tall Grassland, No Woody Cover
27	Medium Grassland, No Woody Cover
28	Short Grassland, No Woody Cover
29	Forb Formations (Flowers, Herbs)

Table 2.1.14 d Classification of grassland ecosystems [GISS, 2005], with identification key for the land-cover map (figure 2.1.14).

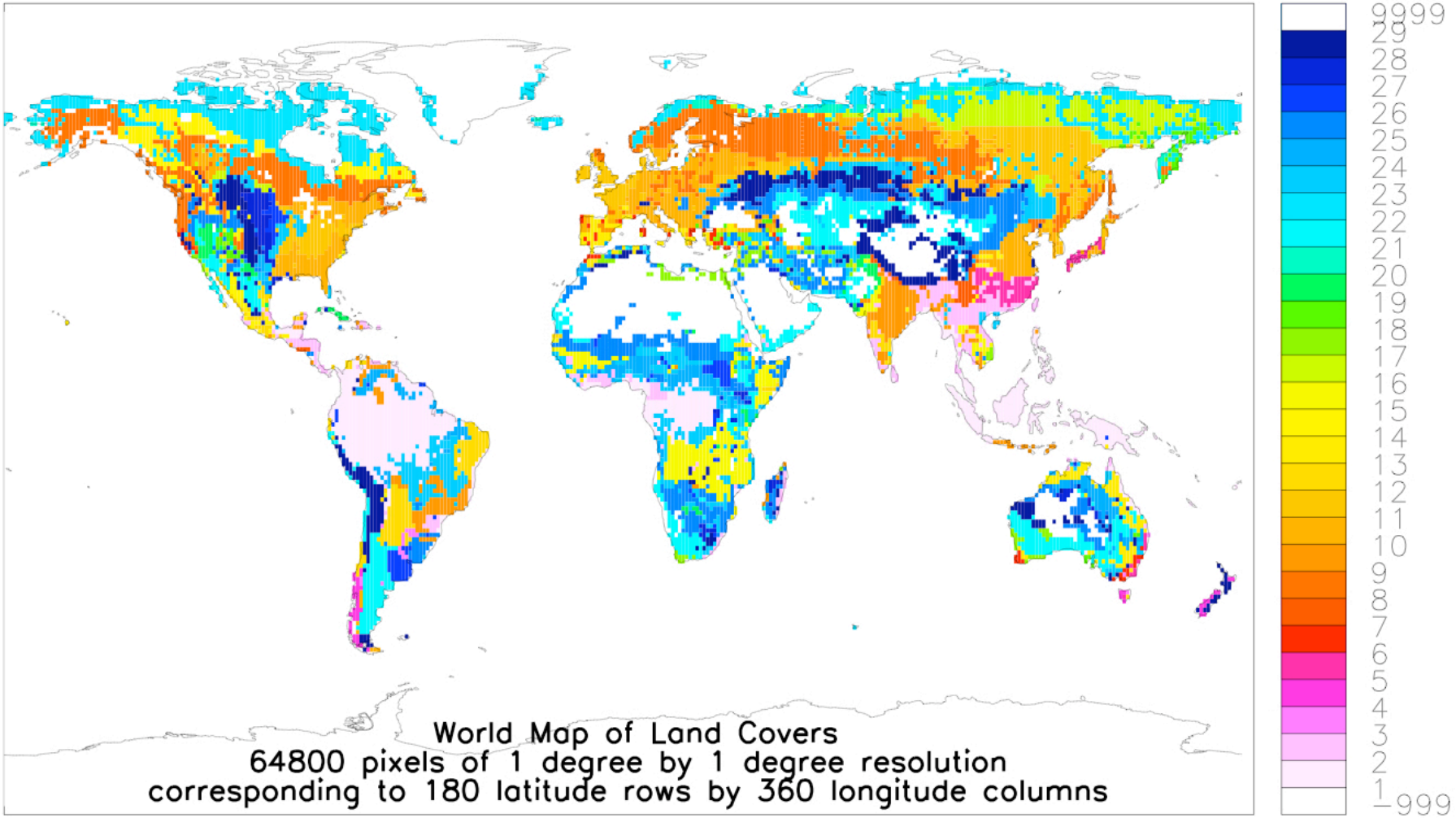

Figure 2.1.14 World map of land cover, showing the distribution of 29 different ecosystems (key in tables 2.1.14).

2.1.15 Topography

The characteristics of the terrain, such as slope and elevation, affect fire spread [Drysdale, 1998], but, since this study is focused on temporal variability, the characteristics of the region that do not significantly vary in 10 years were not included in the calculations.

A world topography map (figure 2.1.15), based on the 2009 Global Digital Elevation Model (GDEM), obtained by processing and stereo-correlating optical images from the Advanced Space-borne Thermal Emission and Reflection Radiometer (ASTER), is here used to assess possible influences of topography on the spatial distribution of fires, e.g., regional pattern clusters of similar wildfire behaviour near mountains and valleys. For example, the shape of the south of the Himalayas is often detectable in maps of burnt areas (e.g., figure 2.1.2).

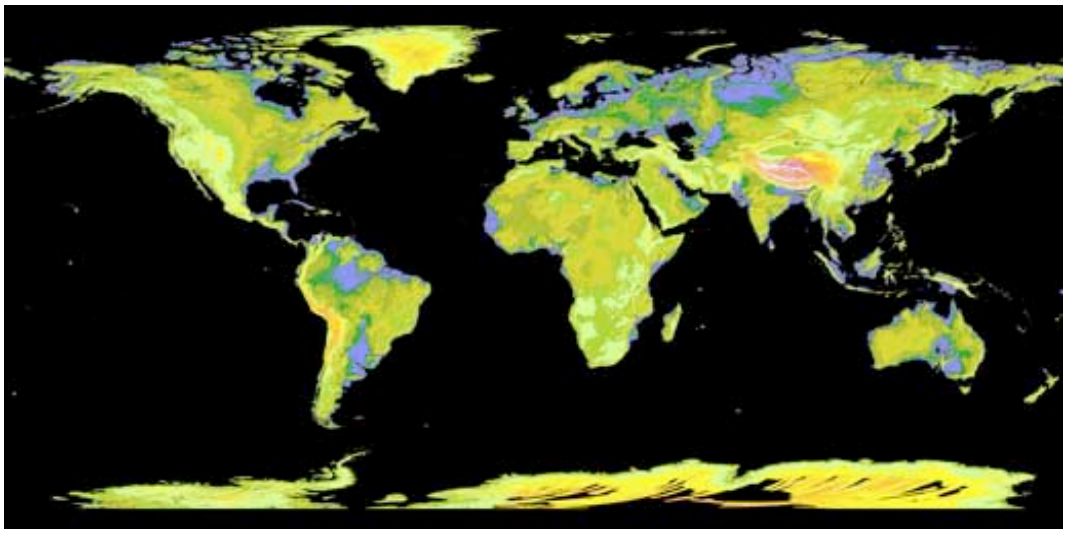

Figure 2.1.15 World map of topography, with lower elevations in purple, medium elevations in green and yellow, and higher elevations in orange, red and white [GDEM, 2009].

2.1.16 Desertification and Land Degradation

Many areas classified as forests and woodlands are rapidly being transformed into shrublands and grasslands because of deforestation and land use [FAO, 2005].

Global maps featuring areas of severest land degradation, deforestation or desertification (figure 2.1.16) were used to search for possible explanations of patterns of fire behaviour different from those of neighbouring areas within the same ecosystem and climate. From 1997 to 2006, most fires in the equatorial rainforests of Africa and South America occurred in vulnerable areas of deforestation and land conversion (compare with figure 2.1.2).

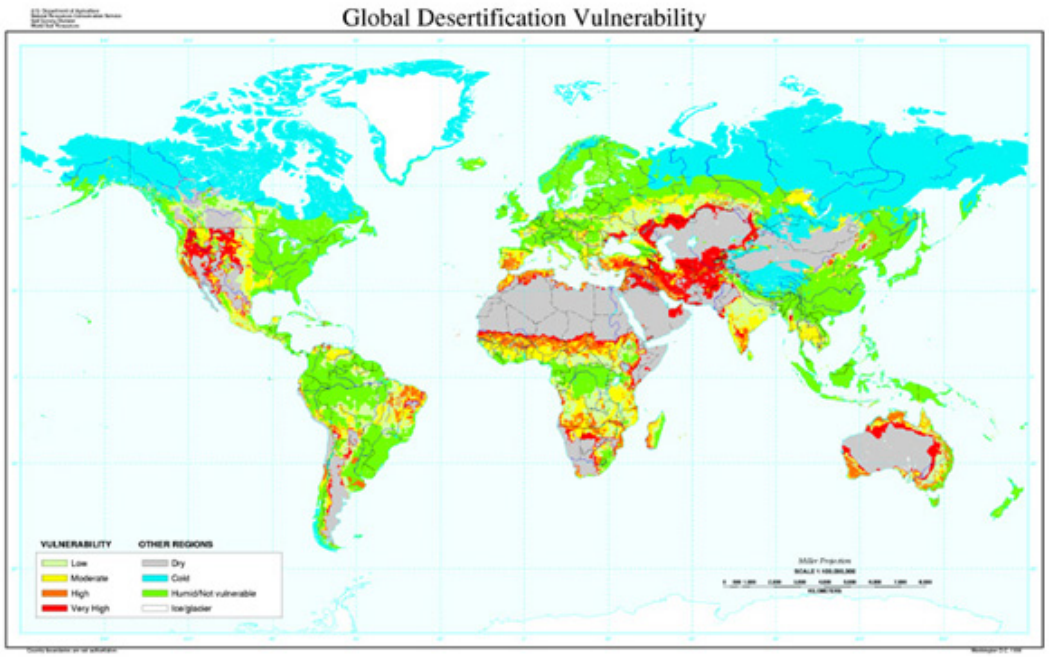

Figure 2.1.16 World Map of Desertification Vulnerability [USDA NRCS, 2008].

2.2 Data Analysis

This sub-chapter describes the analysis of global data, related to burnt areas, biomass burnt, fuel loads and weather variables, from 1997 to 2006, in all land covered with vegetation. It is divided into six sections, which describe the procedures to obtain:

1) statistical summaries of the chosen data;

2) concurrent temporal rank-correlations between biomass burnt and weather variables in individual pixels;

3) lagged temporal rank-correlations, between biomass burnt and weather variables a certain time before, in individual pixels;

4) rank-scatterplots of carbon emissions versus climatic parameters, for individual pixels, to check some of the results from 2) and 3);

5) scatterplots of carbon emissions versus climatic parameters, for whole eco-regions;

6) time-series of carbon emissions and of weather variables, for individual pixels.

2.2.1 Statistical Summaries

All data sets refer to global land data, from 1997 to 2006. Data values refer to monthly means of burnt areas, fuel loads, biomass burnt (expressed as carbon emissions) and weather variables, namely maximum daily temperature at 2m height, maximum daily soil temperature, maximum daily wind speed near the surface, lightning density, minimum daily specific humidity, minimum daily relative humidity, minimum daily soil moisture in the first layer (0.07 m of depth), daily precipitation and maximum daily snow depth.

Data values for each month were formatted to coincide with the format of the Global Fire Emissions Database. For each month, there are 64800 data points, the number of spherical sectors of the surface of the Geoid (a mathematical model of the surface of the Earth) with surface area equivalent, in each case, to 1° of longitude x 1° of latitude. In the context of this research, these

spherical sectors are designated as “pixels”, because they correspond to picture elements in satellite-sensor imagery. Therefore, all global data sets, after being formatted, have 64800 “pixels”, corresponding to a total of 360° of longitude by 180° of latitude. Each data point is centred in one spherical sector (pixel). Pixels are ordered, the first being the one with the top left corner at longitude 180ºW and latitude +90ºN (-180; 90), and the last being the one with the bottom right corner at longitude 180ºE and latitude 90ºS (180; -90). Only pixels on land covered with vegetation are considered. All other pixels, referring to sea, lakes, rivers, deserts, ice and urban areas, were masked off. All values are monthly arithmetic means, expressed in the International System of Units (SI).

For each parameter (burnt area, carbon emissions or weather variable) and for each valid point (centre of a pixel over a vegetation area), the following statistics about the distribution of measurements were calculated:

a) Climatic monthly mean:

The climatic monthly mean of a parameter, for each of the 12 months of the year, refers here to the arithmetic mean of the values of that parameter in the homonymous months (i.e., of the same name) of all the years of observations (equation 2.2.1.1).

$$\mu_X (m) = [X(m, \text{year } 1) + \ldots + X(m, \text{year } n)] / n$$

(equation 2.2.1.1)

$\mu_X(m)$ = arithmetic mean of parameter X in month m during n years

X (m, year i) = value of parameter X in month m and year i

m = month of the year, from January to December, in a total of 12

n = number of years (in this case, n=10, from 1997 to 2006)

For each pixel and for each variable, there are always 12 climatic monthly means, corresponding to the 12 months of the year, independently of the number of years of data.

b) Standard-deviation:

A standard-deviation from the climatic mean is calculated for each of the 12 months of the year (equation 2.2.1.2). The standard-deviation of a set of data is the average distance from the mean, so it takes into account the deviation of every observed monthly value from the climatic mean of all the months of the same name. Therefore, the standard-deviation is a sensitive indicator of the variability of the observed parameters.

$$\sigma(m) = \left[\left(\sum_{mm=1}^{120} [X(mm) - \mu_X(m)]^2 \right) / (n-1) \right]^{1/2}$$

(equation 2.2.1.2)

σ = standard-deviation, for each of the 12 months of the year

X = observed parameter, for each of the 120 months of data

μ_X = climatic mean of X, for each of the 12 months of the year

mm = chronological month, from January 1997 to December 2006, in a total of 120

m = month of the year, from January to December, in a total of 12

n = number of years (the factor “n-1” is related to the fact that there are only “n-1” independent pieces of information besides the mean), in a total of 10

To assess the interannual variability of a climate parameter in different ecosystems, the relative standard-deviation, or coefficient of variation, the ratio of the standard-deviation to the mean, is often more useful. For example, tropical regions with large and regular carbon emissions, but little year-to-year variations in fire behaviour, will possibly have large standard deviations just because of the large total amount of biomass burnt every month of the fire season, whereas temperate regions of strong interannual variability in biomass burning will have comparatively small standard deviations, just because the total pyrogenic emissions are much smaller.

rel σ = σ / μ_X (equation 2.2.1.3)

rel σ = relative standard-deviation for each of the 12 months of the year

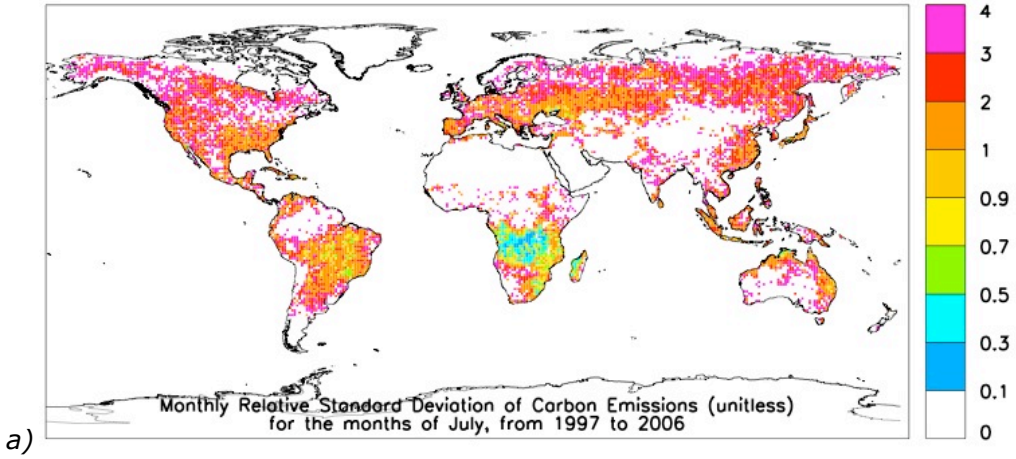

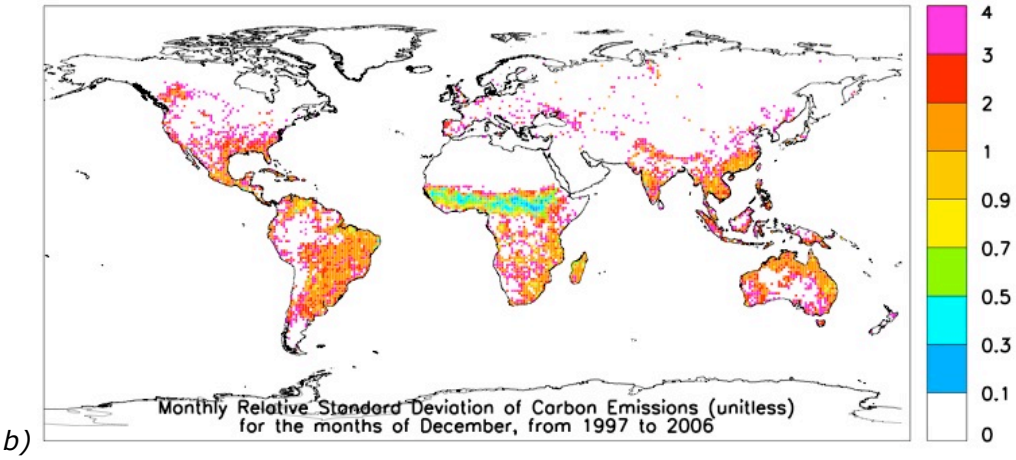

Figure 2.2.1.1 World maps of monthly relative standard deviations of carbon emissions, for the months of a) July and b) December, from 1997 to 2006. Areas of regular biomass burning, with little interannual variability, have small relative standard-deviations (blue and green pixels), whereas regions with more interannual variability have larger relative standard-deviations during the fire season (pink and red pixels).

Maps of relative standard deviation (figure 2.2.1.1), i.e., of standard deviation normalized (divided) by the mean, indicate the regions with more relative variability in carbon emissions, even if the absolute values of those variations are much inferior to those of regions with more regular and abundant fire emissions.

Carbon emissions are more regular in tropical grasslands and woodlands, with little interannual variability, and small relative standard deviation, whereas biomass burnt in temperate regions has larger relative standard-deviations during the fire season.

c) Monthly anomalies:

For each chronological month, from 1997 to 2006, the monthly anomaly is calculated, i.e., the deviation from the climatic mean in months of the same name (equation 2.2.1.3).

Monthly anomalies are used to assess how much a weather parameter deviated from the average value in a certain month.

Monthly deviations always refer to the climatic mean in months of the same name

If the deviation were taken from the annual mean, that would express mainly the seasonal cycle, related to the Earth's orbit round the sun, not the inter-annual changes connected to climate variability.

$$X\_an\ (mm) = X(mm) - \mu_x\ (m) \qquad \text{(equation 2.2.1.3)}$$

X_an (mm) = parameter anomaly for month mm, in a total of 120, from January 1997 to December 2006

X(mm) = value of parameter X for month mm, in a total of 120, from January 1997 to December 2006

$\mu_x(m)$ = climatic mean of X for homonymous months m of any year, in a total of 12, from January to December

2.2.2 Rank-Correlation Maps

The standard procedure to examine if a certain weather parameter influences the quantity of biomass burnt is to plot one against the other. If the resultant scatter-plot of biomass burnt versus the weather variable presents a visible regular pattern, there may be a relationship between both. However, in this case, it would be

impractical to produce and analyse scatter-plots of biomass burnt versus several weather variables for every vegetation-pixel (surface sector of 1° longitude × 1° latitude corresponding to land with vegetation). Instead, rank-correlations between biomass burnt and weather parameters in each vegetation-pixel were directly computed, and the relevant values plotted in a world map.

Rank-correlation is a non-parametric measure of the extent to which two parameters are related. No relationship between the data sets is assumed: the measurements are just converted to ranks. Ranking is the allocation of ranks to data items. Rank number 1 is given to the lowest data value, rank number 2 to the second lowest value and so on, until the highest data value, which receives the highest rank, n, the total number of elements in the data set. If there are q identical data values, after rank p, then all of them are given the rank equal to the average of the ranks they would be given if different: (p+1 + … + p+q)/ q. The following data value, different from those previous q values, will have rank p+q+1.

The rank-correlation coefficient is the numerical value that expresses how consistently two variables vary together, without taking into account how they vary. If the relationship between variables is unknown, then a linear correlation, the measure of the linear relationship between 2 variables, is not an adequate assessment. Although independent variables should not present a significant correlation, dependent variables, even if they strongly vary together, may have a non-linear dependency, with a small linear correlation.

The linear correlation coefficient between 2 parameters is their normalized covariance, i.e., their tendency, if any, to rise and fall together, or inversely. The covariance must be normalized, so it can be known how well a straight line would fit through a scatter-plot of both parameters and compare results with those of other scatter-plots. Then it becomes a unitless measure, between -1 and 1, of how much those 2 parameters vary together in a linear way. A linear correlation is positive if both variables increase and decrease together, and negative if one increases while the other decreases. The absolute value of the linear correlation is high if one variable varies proportionately with the other (equation 2.2.2.1).

$\rho(X, Y) = \text{cov}(X,Y) / \sigma(X)\,\sigma(Y) =$

$= E[(X - \text{mean}X)(Y - \text{mean}Y)] / \sigma(X)\,\sigma(Y) =$

$= [E(XY) - E(X)E(Y)] / \sqrt{[E(X^2) - E^2(X)]} / \sqrt{[E(Y^2) - E^2(Y)]}$

(equation 2.2.2.1)

$\rho(X, Y)$ = linear correlation between a weather parameter (X) and carbon emissions (Y)

σ = standard deviation = $\sqrt{(E[(X - E(X))^2])}$

$\sigma^2 = E[(X - E(X))^2] =$

= variance, i.e., the measure of dispersion of the probability distribution of a random variable.

$E(x) = \int x\,\varphi(x)\,dx$ = expected value, i.e., the probability-weighted average value of the random variable, analogous to the "centre-of-mass" of the distribution of probability $\varphi(X)$.

This formula was constructed specifically to force the function to give normalised results ($-1 \leq$ correlation $(X,Y) \leq +1$), by using the Cauchy-Bunyakovskii-Schwarz inequality. Its main purpose is to give a value equal to or near +1, if the parameters vary in the same sense, equal to or near -1, if one parameter increases while the other decreases, or near 0, if they do not vary with each other [OD of Statistics, 2008]. If, whenever a climatic parameter increases or decreases, there is a correspondent increase or decrease in biomass burning, compared with the dispersion in their probability distributions, then those two variables are linearly correlated.

A detailed explanation of these mathematical formulae can be found in any compendium of Advanced Statistics (e.g., Storch & Zwiers, 1999; Wilks, 2005).

Linear correlations between biomass burnt and a climate variable in each data point would only produce high values if the biomass burnt varied linearly with the climate variable; even if they both co-varied strongly, the linear correlation could still be low, because the variation was not linear. Generally, it would not be expected that the biomass burnt would vary in such a simple linear way with any climate parameters. Linear correlations are neither robust nor resilient measurements and would not be much helpful without analyzing a scatter-plot for each data-point. Even if there seemed to be a good linear correlation, it would probably be because the

computer program fitted a line through a curve, giving a relatively high linear correlation, if the curve varied slowly (figure 2.2.4 a).

To obviate these problems, it is not the values of biomass burnt and weather variables that are compared, but their ranks. If a weather parameter strongly influences the quantity of burnt biomass, then the highest and lowest values of that climate variable will probably occur simultaneously with the highest or lowest values of burnt area, even if the correlation between them is not linear. Therefore, rank-correlation coefficients are used to identify regions where a certain weather parameter strongly contributes to biomass burning (figure 2.2.4 b).

For each vegetation-pixel, the linear correlations between ranks of the monthly averages of a certain climate parameter and the correspondent ranks of monthly biomass burnt, from 1997 to 2006, were calculated. These rank-correlations were then plotted in world maps (e.g., figure 2.2.2.2), to try to detect trends in wildfire behaviour.

Pixels with low rank-correlations (inferior to 25%) between biomass burning and a weather variable were ignored in the discussions about the overall effect of that weather parameter on the fire behaviour of eco-regions, but all pixels with significant fire events were later taken into the calculations to find models for different months of the year.

From observations of these rank-correlation maps, fire behaviour seemed to be more directly dependent on ecosystems than on climate types. Several ecosystems in different latitudes and climate zones have more similar patterns of wildfire behaviour than the same climate type but with different vegetation.

Linear correlations between mathematical transformations of weather variables and carbon emissions were also plotted, to try to find out if there were any known mathematical relationships (e.g., log x, $1/x$, x^2) that conveyed the relationships between some weather parameters and carbon emissions. However, fire patterns vary from pixel to pixel and from month to month, so overall the results were much weaker than for rank-correlations.

Outside the fire season, even extreme weather anomalies usually do not influence wildfires. Therefore, to avoid correlating many zero

burnt areas with weather parameters, analyses only include months of climatic fire, i.e., months when there was at least 1 fire over the years considered. In order to have enough data to obtain reliable values, rank-correlations were only computed in pixels where, in 10 years, there were at least 10 months with monthly burnt fractions superior to 0.0001 (0.01%). With these demands, the chi-square tests for goodness-of-fit consistently had p-values smaller than 0.01, giving strong evidence against the hypothesis that these results were obtained by chance alone.

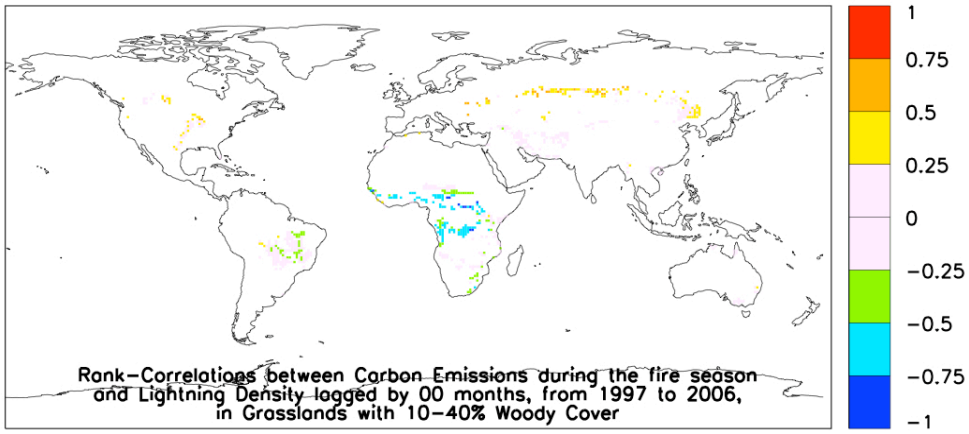

Figure 2.2.2.2 World map of rank-correlations between biomass burnt and lightning density. Pixels in yellow and orange show places where fires increase with lightning; pixels where there is a decrease of fire activity with electric atmospheric discharges (associated to convective rainfall near the equator) are shown in green and blue.

2.2.3 Lagged Rank-Correlation Maps

Weather patterns can influence wildfires months afterwards, so rank-correlations between biomass burnt and weather variables some months before were also computed. To accurately compute correlations between 2 variables, each pair of measurements should be independent from the others. This is rarely the case for weather variables separated by short periods of time, since the weather in one particular day is often well correlated to the weather in the

preceding days. However, monthly means greatly attenuate the natural auto-correlation in meteorological variables (Storch & Zwiers, 1999; Wilks, 2005), and the approach of rank-correlations by lags is based on this assumption.

Rank-correlations were often low when they were computed for all the values of biomass burnt versus a climate parameter n months before. Strong weather anomalies that occur during a cold winter or rainy season are not likely to affect the probability of concurrent fire, as they would during the hot or dry season. In eco-regions where fires only occur during the dry season, there would be correlations between wildfires during the non-fire season (zero) and weather variables during the fire season that might also be zero (e.g., precipitation). Therefore, the dry fire season was determined for each eco-region and, then, the biomass burnt was correlated with the climate parameters some time before. In following analyses, months without fires were ignored, so that only positive values of burnt area and carbon emissions were being correlated with a climate parameter, some time before.

In the cases where the fire season was limited to a well-defined dry season, the results were stronger, because all wildfires were statistically tested for connections with climate parameters in approximately the same time before.

Finally, it was decided to correlate parameters in the whole climatic fire season, i.e., in the months of the year where fire occurred during at least one of the 10 homonymous months of the 10 years analysed, from 1997 to 2006, since the strongest correlations were frequently obtained this way. Like in the case of concurrent rank-correlation maps, pixels with lagged rank-correlations plotted had at least one month of 0.01% of burnt fraction per year.

Lagged correlations, like concurrent ones, may considerably vary from region to region, even within the same ecosystem. For instance (figure 2.2.3), rainfall during the wet season in tropical zones contributes to vegetation growth, leading to abundance of fuel load available to burn during the next fire season. However, in sub-tropical and temperate regions, like in Australia, precipitation during the winter contributes to soil moisture, making vegetation less prone to fire in the following summer.

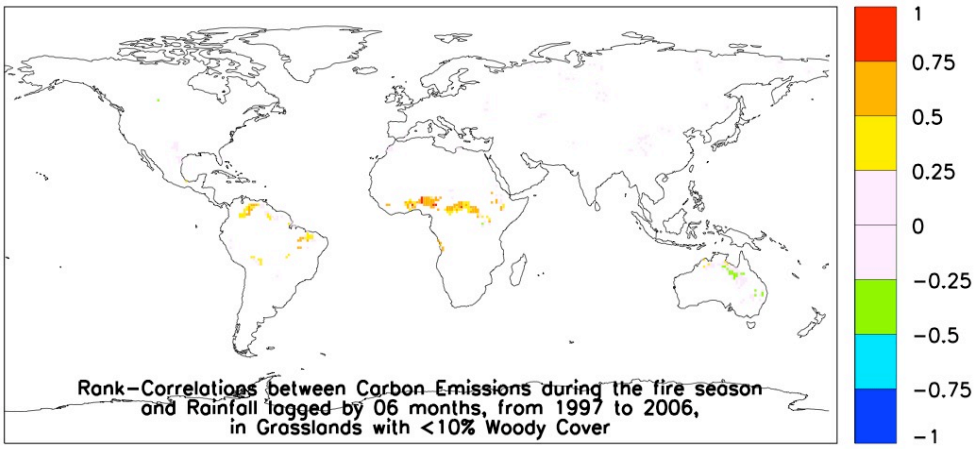

Figure 2.2.3 World map of rank-correlations between biomass burnt during the fire season and precipitation 6 months before, from 1997 to 2006, in grasslands with less than 10% of wood cover.

Some of these results were confirmed by graphical analyses of individual pixels, with rank-scatterplots, to check if the points really closely follow a line, or if they were just separated clusters of points joined together by a line.

If the rank-correlation maps show a considerable area covered with high rank-correlation (superior to 75%) pixels, than it is difficult to maintain that all these results can be ascribed to chance alone.

2.2.4 Rank-Scatterplots

Some results shown in the rank-correlations maps were checked by rank-scatterplots. There are too many points with significant correlations to produce a scatterplot for each of them, but some of the strongest correlations were checked in the ecosystems with more fires.

In a scatter-plot with lots of values, it may be difficult to discover a curve that reflects a relationship between biomass burnt and a climatic variable (figure 2.2.4 a). Plotting ranks of burnt fraction or carbon emissions against ranks of weather parameters

allow us to verify if biomass burning significantly co-vary in any way with that weather variable. If there is any kind of covariance, positive or negative, the scatterplot of the ranks will be a straight line, easier to detect. No matter how complex the relationship is, if one always increases while the other increases or decreases, then the ranked scatter-plot will tend to be linear (figure 2.2.4 b).

In rank-scatterplots, the values of a climate variable are ranked, from the lowest to the highest, and plotted against the ranks of burnt area or of carbon emissions values. The lowest value of carbon emitted, or of burnt area, gets the lowest rank, 1st, whereas the largest value gets the highest rank, nth, n being the number of data elements. If q data points have the same value, then they all get the same rank, computed as the average of all q ranks that would have been allocated to the q data points, had they been distinct. This rank is repeated q times, before the following rank, which is the same if the previous q data points had been distinct.

The ranks of burnt area and carbon emissions are compared to the ranks of weather parameters for the same month. If there is a significant relationship between wildfires and any weather variable, such as temperature, air humidity, precipitation or wind, in a certain region, then the largest fires will often occur when those climatic parameters are much higher or lower than usual.

Rank-scatterplots make it possible to easily eliminate cases where there is no detectable relationship between biomass burnt and a certain weather parameter. If there were any kind of relationship, the ranked values would vary monotonically with each other. If biomass burnt is a monotonic function of some climatic variable within some thresholds (always increasing or always decreasing), and if this trend is not hindered by the influence of other variable(s), then the scatterplots will present an increasing or decreasing curve (figure 2.2.4 a), and the rank-scatterplots will show a line (figure 2.2.4 b).

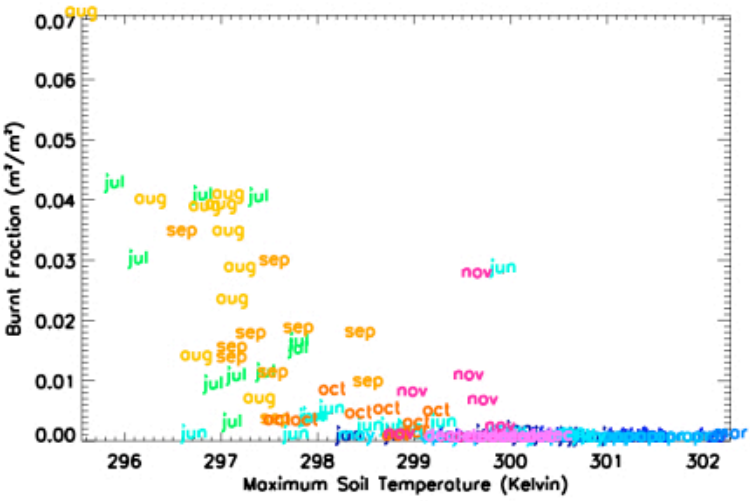

a)

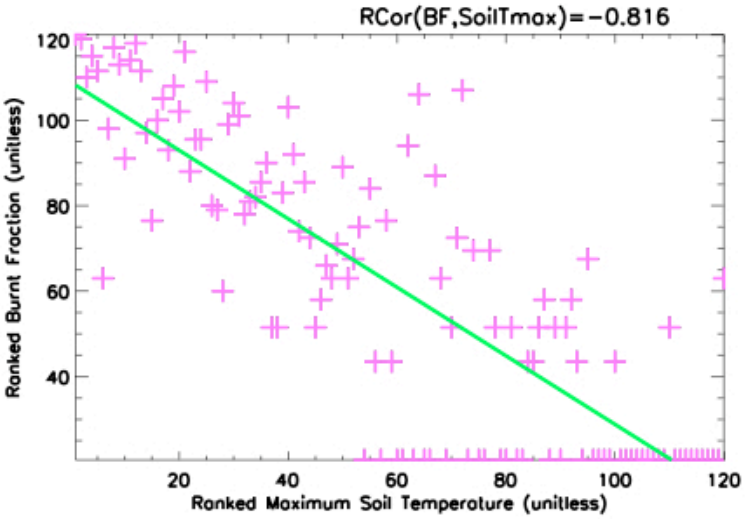

b)

Figure 2.2.4 Scatterplots of burnt areas in the savannah of South Equatorial Africa versus maximum soil temperature, in absolute values (a) and in ranks (b). If the relationship between variables is monotonic, then it will appear as a straight line in a rank-scatterplot, regardless of the shape of the original curve.

In this case, ranked scatter-plots (figure 2.2.4 b) were mainly used to confirm some of the results shown in the rank-correlation maps. Sometimes, the value of a rank-correlation may be high (r-cor > 75%), but obtained with few points (pixels) that match the data selection criteria (e.g., months of the year with at least 1 value of burnt area superior to 0.01% over 10 years), so this value is only reliable after a graphical check showing several points with a distribution approximately homogeneous along a straight line.

The rank-correlation coefficient (r-cor) measures the strength and direction of the linear relationship between the ranked data sets. For example, fires in the South Equatorial African savannah occur during the dry colder season, whereas the highest temperatures are concurrent with convective precipitation during the rainy season, which gives an unusual negative rank-correlation between temperature and biomass burning (figures 2.2.4).

2.2.5 Choice of Regions

The choice of regions was based on geographic limits and climatic zones (figure 2.2.5).

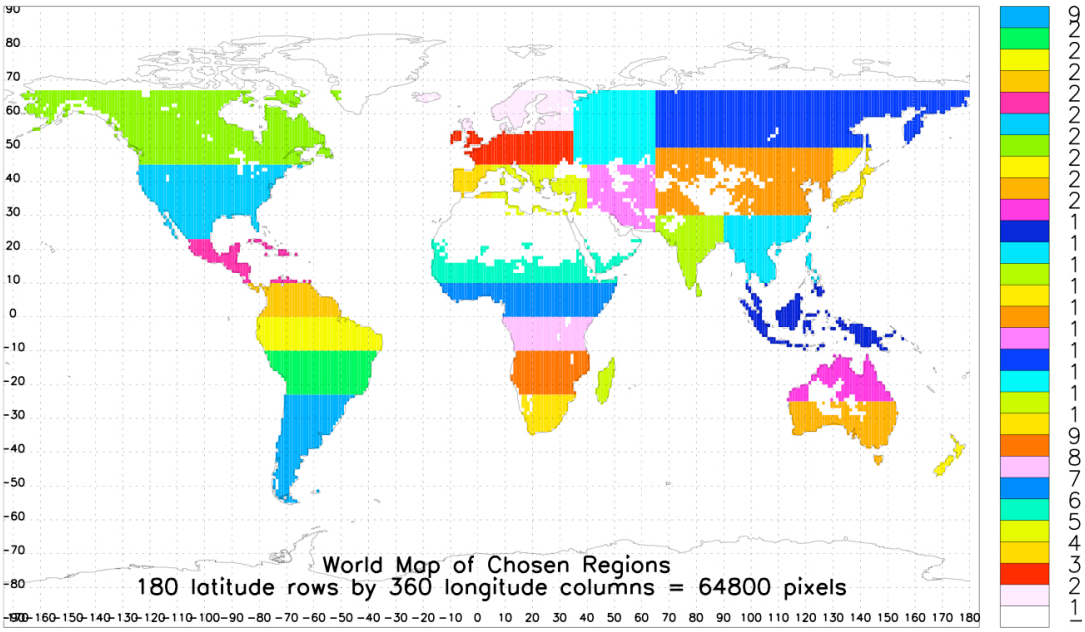

Figure 2.2.5 World map of the 28 chosen regions (key in tables 2.2.5 a-e). Each section belongs exclusively to one main climatic zone: sub-polar, temperate, subtropical or tropical. There are no fire regions within the polar circles.

Continents were subdivided into several regions (tables 2.2.5 a-e), according to the following criteria:

-- A region should preferably belong to one hemisphere only, although sections in the equatorial zone may include portions of both hemispheres;

-- A region should be exclusively sub-polar, temperate, subtropical or tropical, without mixing main climatic zones;

-- A region should not include more than one continent, sub-continent, large archipelago or island;

-- A region should not contain large areas classified as the same ecosystem separated by other ecosystem types: non-contiguous regions, even with the same type of land cover, tend to respond differently to climate variations and to have distinct fire regimes.

Number	Region (Europe)	Coordinates
1	Northern Europe	[-30:35; 55:67]
2	Central Europe	[-10:35;45:55]
3	Iberia	[-10:5; 35:45]
4	Mediterranean	[5:40; 30:45]

Table 2.2.5 a Geographical regions of Europe used in this research, with the respective geographical coordinates in the form [minimum to maximum longitude; minimum to maximum latitude], and a key for figure 2.2.5.

Number	Region (Africa)	Coordinates
5	North Africa	[-20:50; 10:23]
6	North Equatorial Africa	[-15:50; 0:10]
7	South Equatorial Africa	[5:45; -10:0]
8	Central Southern Africa	[10:40; -23:-10]
9	South Southern Africa	[10:40; -35:-23]
10	Madagascar	[40:50; -30:-10]

Table 2.2.5 b Geographical regions of Africa used in this research, with the respective geographical coordinates in the form [minimum to maximum longitude; minimum to maximum latitude], and a key for figure 2.2.5.

Number	Region (Asia)/ Pacific)	Coordinates
11	West Russia	[35:65; 45:67]
12	East Russia	[65:180; 50:67]
13	West Asia	[40:65; 25:45]
14	Central Asia	[65:130; 30:50]
15	Japan	[130:150; 30:50]
16	India	[65:90; 0:30]
17	South East Asia	[90:130; 10:30]
18	Equatorial Asia	[90:160; -10:10]

Table 2.2.5 c Geographical regions of Asia used in this research, with the respective geographical coordinates in the form [minimum to maximum longitude; minimum to maximum latitude], and a key for figure 2.2.5.

Number	Region (Pacific)	Coordinates
19	North Australia	[110:160; -25:-10]
20	South Australia	[110:160; -45:-25]
21	New Zealand	[165:180; -50:-30]

Table 2.2.5 d Geographical regions of the Pacific used in this research, with the respective geographical coordinates in the form [minimum to maximum longitude; minimum to maximum latitude], and a key for figure 2.2.5.

Number	Region (Americas)	Coordinates
22	Northern North America	[-170:-50; 45:67]
23	Southern North America	[-125:-60; 23:45]
24	Central America	[-110:-60; 10:23]
25	North Equatorial South America	[-90:-50; 0:10]
26	South Equatorial South America	[-85:-30; -10:0]
27	Central South America	[-80:-35; -23:-10]
28	Southern South America	[-80:-45; -55:-23]

Table 2.2.5 e Geographical regions of the Americas used in this research, with the respective geographical coordinates in the form [minimum to maximum longitude; minimum to maximum latitude], and a key for figure 2.2.5.

Results were separated by eco-regions, i.e., ecosystems within the chosen geographic regions, for a question of convenience, but taking into consideration that the classifications of land cover and climate are quite general, often including many different vegetation types and climate patterns under the same designations. Previous analyses with average values over large regions (e.g., more than 20 pixels) did not show clear patterns. Subsequent statistical analyses were always done in individual pixels or in pixels grouped together, never in averages for whole eco-regions. Therefore, possible inaccuracies in these classifications do not affect the conclusions for individual pixels.

2.2.6 Scatter-Plots

After analysing all the monthly maps of burnt area, carbon emissions, fire intensity and weather parameters, from 1997 to 2006, it is possible to form a general idea of how wildfire behaviour varies over the continents, from season to season and from year to year.

Relationships between biomass burnt and weather variables were looked for, in each ecosystem. However, scatter-plots of biomass burnt versus weather parameters, for the same ecosystem type, aggregating different continents and different climate zones, do not show clear relationships. Even if some of the land ecosystems seem to have a coherent pattern of fire behaviour, data in the scatter-plots were too scattered for any curve to be fit, indicating that there is not any function between biomass burnt and weather variables that can be used for a same ecosystem in the whole world.

Therefore, the world was divided into geographical regions, according to the already stated criteria, and eco-regions were investigated. Only the climatic fire eco-region was considered, disregarding pixels where burnt fractions were inferior 0.01%, since the objective of the statistical analysis itself is precisely to draw conclusions about areas affected by fire. The land-cover classification was only used as a reference: no prior knowledge of the regional characteristics was assumed.

For each eco-region, the climatic average of biomass burnt for each month of the year was plotted, so the maximum number of points for each pixel was 12, corresponding to the 12 months of the year. Each point in these scatter-plots corresponds to 1 month of the year, in 1 pixel belonging to the eco-region, where fire sometimes occurs – a "climatic-fire-pixel". Pixels where fire never occurs, and months that never have fires, were excluded. Only values relative to pixels and months where and when fire sometimes occurs were plotted (figure 2.2.6).

Data were not averaged over the eco-region -- all the data points with climatic fire were included, so the number of points in the scatter-plot has a maximum of 12 times the number of pixels in the areas of the eco-region where fire sometimes occurs. Fire seasons rarely last all year, so often there were much less than 12 months per pixel.

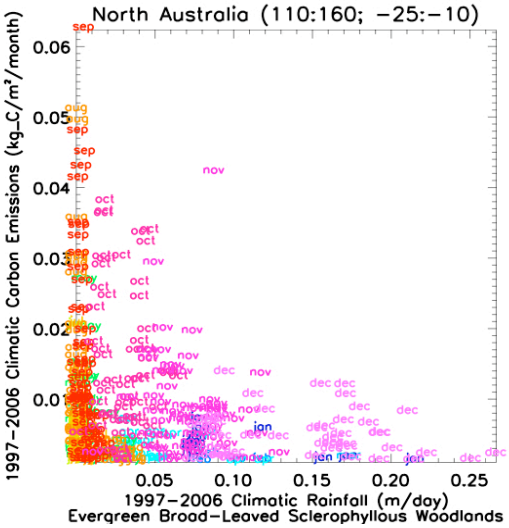

Figure 2.2.6 Scatterplot of biomass burnt (expressed as carbon emissions) versus rainfall in the evergreen broad-leaved sclerophyllous woodlands of North Australia. Points follow approximately the shape of the inverse function (y=1/x), since precipitation strongly hinders ignition and fire spread.

Several of these scatterplots present recognizable patterns, but generally the curves are not well defined. For some eco-regions, it was possible to find the threshold of temperature, humidity and rainfall below or above which fires do not usually occur.

2.2.7 Time Series

Time series refer to plots of changes in parameters over time [OD of Statistics]. Biomass burnt and weather parameters vary from season to season and from year to year, so, to follow these changes, 3 types of time series were produced for each parameter:

-- Climatic monthly mean values, from January to December;

-- Monthly values, from January 1997 to December 2006;

-- Monthly anomalies, also through those 10 years.

In each eco-region, climatic parameters (temperature, humidity, rainfall, snow depth, wind speed and lightning density) were averaged over that area and plotted in a time series, from January 1997 to December 2006, in a total of 10 years, below the graphic of burnt fraction or of carbon emissions, to try to detect patterns.

Time series were only plotted for individual pixels, because, in previous analyses, time series of weather parameters averaged over whole eco-regions did not show significant patterns. Since there are too many pixels to produce scatterplots and time series for each, only a few were selected, namely those with very high rank-correlations between biomass burnt and a climate variable and where good models were found. In some cases (e.g., figure 2.2.7), the highest temperatures were associated with convective rainfall, so fires occurred during the colder dry season. The standard deviation of the n observations (σ) and the standard deviation of the mean ($\sigma / \sqrt{n}$) were also calculated and plotted in the time series of the climatic values for each of the 12 months of the year.

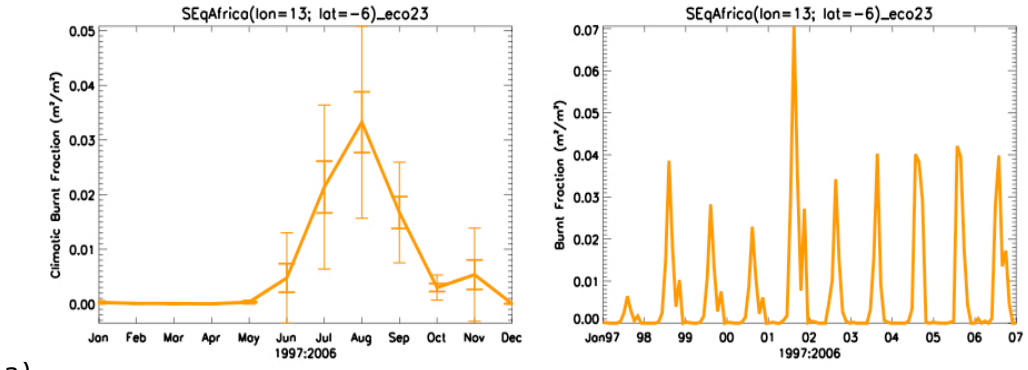

a)

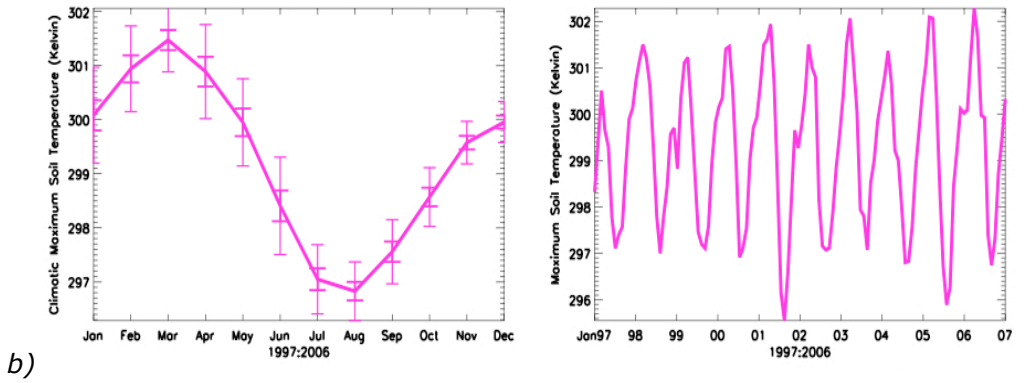

b)

Figure 2.2.7 Time series of burnt area (a) and of maximum soil temperature (b), for climatic values in the 12 months of the year (left) and for all 120 months of data (right), in an individual pixel of the South Equatorial African savannah. Climatic values are shown with standard deviations of the n observations (σ) and of the mean ($\sigma/\sqrt{n}$), for each month of the year.

2.3 Fire Models

This sub-chapter describes the construction of the statistical models for the prediction of future carbon emissions based on meteorological data. It begins with a description of the various scatterplots of carbon emissions versus meteorological variables, followed by curve and line fittings, construction of models, comparisons between models and observations, with scatterplots and with time series, and it ends with the explanation of the tests applied to choose the best models.

1) Scatterplots;

2) Models with 1 variable;

3) Time series;

4) Model versus observations;

5) Normal probability plot;

6) Residual versus fitted values;

7) Histograms;

8) Residual time series;

9) Models with 2 variables.

2.3.1 Scatterplots

Scatterplots of biomass burnt versus weather parameters, in specific eco-regions, have shown certain relationships between weather and wildfires (e.g., figure 2.3.1.1).

Because of the large quantity of pixels in many eco-regions, only monthly climatic averages were used in the plots, so each pixel was represented by a maximum of 12 months, not by 120. Each month of the year in the scatterplots represents the average of all homonymous months from 1997 to 2006. For example, a point marked “January” is the mean value of the weather parameter for all Januaries, from 1997 to 2006.

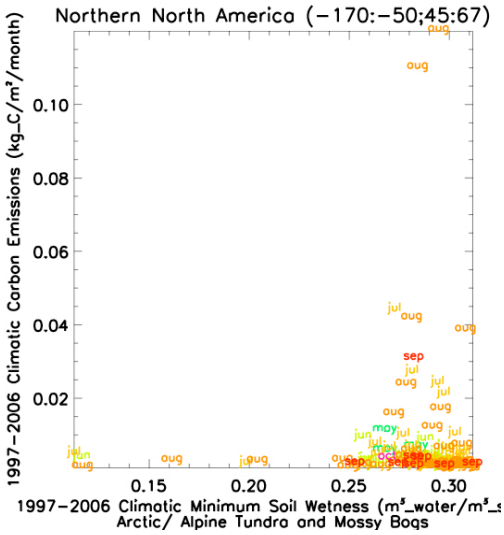

Figure 2.3.1.1 Scatterplot of monthly climatic minimum soil wetness versus monthly climatic carbon emissions, in the arctic tundra of Northern North America. Each point in the scatterplot corresponds to one pixel in the eco-region and to one month of the climatic fire season (months of the year that had at least one monthly burnt area superior to 0.01% during the 10 years analyzed). Each monthly climatic value is the average of the values of all homonymous months from 1997 to 2006.

These observations were corroborated when scatter-plots were plotted for individual pixels, this time with all individual 120 monthly values, correspondent to 10 years of data, from 1997 to 2006. Fire behaviour was found to vary from pixel to pixel, so scatterplots were made for individual pixels. These scatterplots show that, in different months, or groups of months, there are different relationships between burnt area and specific meteorological variables. Some scatterplots (figure 2.3.1.2) show an exceptional case of burnt area in a pixel decreasing with soil temperature: this happens in monsoon regions, where the warmest weather is followed by convective rainfall and consequent fire extinction.

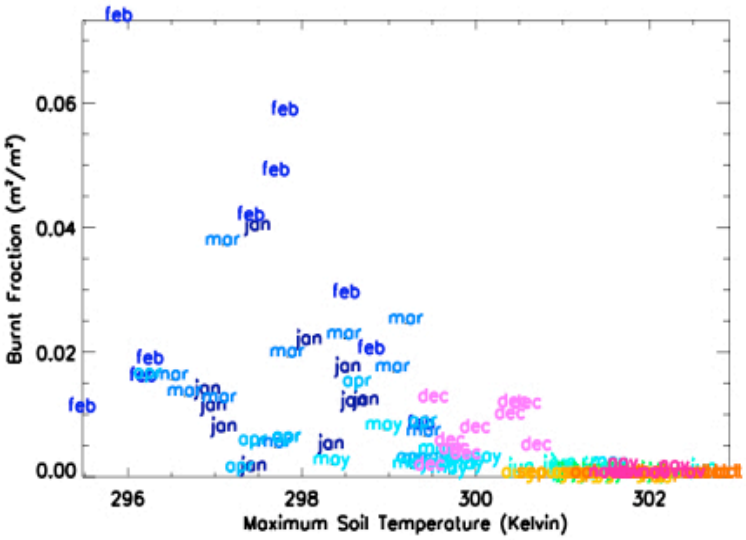

Figure 2.3.1.2 Scatterplot of burnt fraction versus maximum soil temperature for a pixel in the drought-deciduous woodlands of North Africa. Each point corresponds to the same pixel and to one of the 120 months analyzed.

Sometimes, it was possible to group a few months with similar behaviour, e.g., prior to the fire season until the maximum, then another group for the declining of the fire season; however, it was usually difficult to aggregate them, since fire behaviour did not change abruptly from one group to the other, or else there would be just one or few months markedly different from all the others. Also, the greater the separation of pixels in an eco-region, the more they tended to have different months in different "behaviour-groups": the distribution of months per behaviour-group was not the same from pixel to pixel.

Therefore, it was decided to make individual fire models for each pixel and for each month of the year. Each pixel with regular fire events can have a maximum of 12 different models, one for each group of homonymous months, though often it has less than 6, since the other months are out of the fire season.

In the first attempts to produce a fire model, strongly non-gaussian distributions of meteorological data, such as burnt areas and rainfall, were converted to near normal distributions by logarithmic, root and inverse functions. Transformations of humidity to inverse humidity (1/x), and of temperature to square temperature (x^2), with carbon emissions not transformed, gave better results

than logarithmic transforms of carbon emissions and predictors. Lines were fitted through the transformed data, with all the months included, corresponding to lines fit through all the points in scatterplots of burnt area or carbon emissions versus weather variables. Overall, the models of biomass burnt that produced the best results were those based on the inverse function of minimum relative or specific humidity. However, these results were much inferior to those obtained fitting lines through homonymous months and producing a model for each pixel and for each of the 12 months of the year with regular fires; therefore, linear fits through homonymous months, for each pixel, was the method eventually chosen to produce fire models.

2.3.2 Linear Fits

The method that gave the best results, up to a linear correlation of 0.97 between the model and the observations, was that of one linear model for each pixel and for each group of 10 homonymous months of the fire season. Linear models for each month make reasonable predictions for many pixels (correlations superior to 75% between models and observations), with just one climate variable, often the minimum specific humidity or the maximum temperature, in pixels with regular biomass burning.

Models are based on a maximum of 12 linear fits, one for each month of the year, from January to December, and they are only meaningful during the fire season.

The linear equations of the straight lines that best fitted the data were used to make predictions of biomass burnt C, based on observed values of the corresponding weather variable X:

$$C(i, j) = m(i,j)\, X + b(i, j) + \varepsilon \qquad \text{(equation 2.3.2)}$$

C = carbon emissions

i = pixel of 1 degree by 1 degree, identified by a latitude and a longitude

j = month of the year, from January to December

m = slope of the line = change in carbon emissions when the weather variable increases by one unit

X = weather variable

b = intercept (point where the line crosses the axis) = value of the predicted carbon emissions when the weather variable is zero (it may not have any practical meaning, if it falls out of the actual values of the data set, since the correspondent values of X or C may not be possible)

ε = error or residual = difference between predictions and observations

These fire models only work within an interval of values, $[x_0: x_f]$ and $[y_0: y_f]$; extrapolations were not made for values of climatic parameters superior or inferior to those observed in each pixel, from 1997 to 2006.

Months of the year without any significant fire event (burnt fraction inferior to 0.01%) from 1997 to 2006, were excluded, otherwise it would not be possible to consistently get good fits.

The chi-square test for goodness of fit was used to compare the distribution of anomalies with the chi-square distribution, to make sure that relatively large anomalies were less frequent than those closer to the standard-deviation.

When only months with significant fire events were included (burnt fraction superior to 0.01%), p-values inferior to 0.01 were often obtained in the chi-square test for goodness of fit, giving strong evidence that these results could not be ascribed to chance alone.

Weather variables change much more inter-seasonally than inter-annually, except in equatorial rainforests, so it is often possible to obtain a good linear fit through homonymous months. Some times, results were slightly better if a line was fit through an adequate transformation of a weather variable (e.g., inverse humidity).

Fitting a line through all homonymous months, regardless of the shape of the scatter-plot, provides an automatic and quick method of finding models without having to analyse each scatter-plot individually (figure 2.3.2). Geometrically, this is identical to

approximating a closed curve, similar to a circumference, by small segments of line; it is known that the true shape of the line is a curve, but, if approximated by a regular closed curve, like a circumference, it may, in many points, get farther from the real curve than the small segments adjusted for small pieces of the true curve. So, the set of all small segments may provide more useful models and accurate predictions than a continuous curve, theoretically more correct, but which may deviate from the true curve in many points. The real variation for all months is better explained by a curve, often matching the graphic of a function corresponding to a fire dynamics equation relating the weather variable to fire spread, but better predictions are obtained with a model made of small linear segments.

With this method, no matter what the shape of the scatter-plot is, as long as it approximately follows a fairly regular monotonous curve, with enough data, not too scattered, computer programmes can quickly produce reasonable models for just one variable, as long as that weather parameter considerably influences the burnt area and carbon emissions (e.g., biomass burning rank-correlated by more than 75% with a weather variable).

There were also cases where the model obtained was very good (predictions correlated by more than 90% with GFED estimates, even when the rank-correlation between biomass burnt versus the climate parameter was not too high, precisely because different months had different behaviours, and followed lines of different inclinations. Had a curve been fitted through all the points, much of the variation would have been missed. Consequently, even pixels with only moderate rank-correlations (between 50% and 75%) overall may get a good fire model with this method.

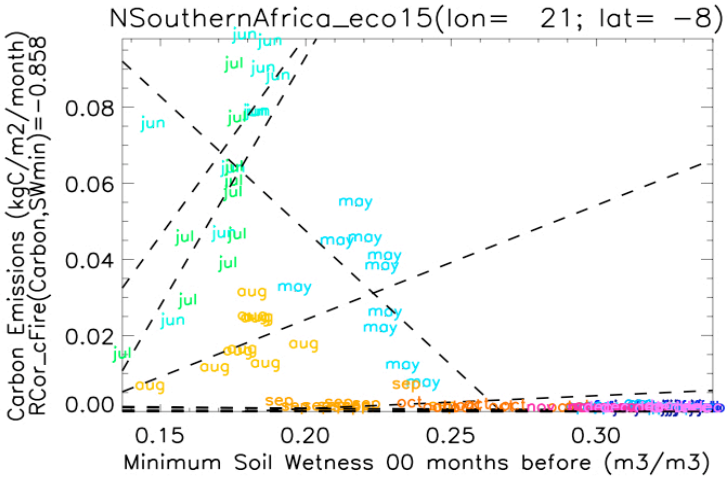
NSouthernAfrica_eco15(lon= 21; lat= −8)
Carbon Emissions (kgC/m2/month)
RCor_cFire(Carbon,SWmin)=−0.858
0.00
0.02
0.04
0.06
0.08
0.15
0.20
0.25
0.30
Minimum Soil Wetness 00 months before (m3/m3)

a)

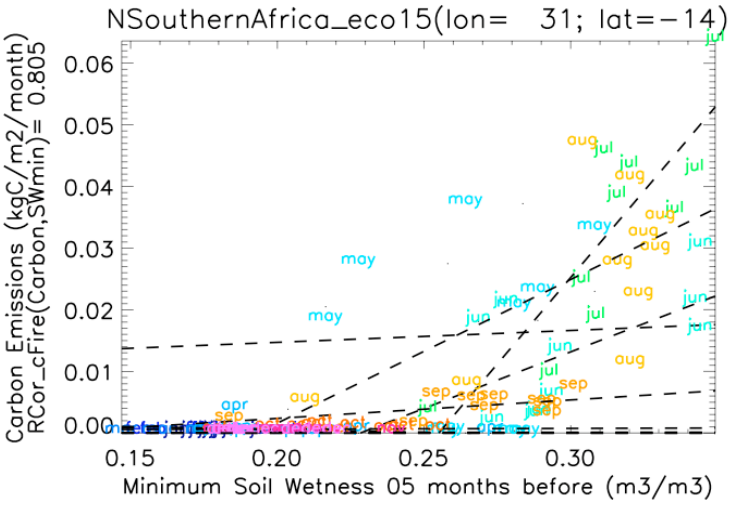
NSouthernAfrica_eco15(lon= 31; lat=−14)
Carbon Emissions (kgC/m2/month)
RCor_cFire(Carbon,SWmin)= 0.805
0.00
0.01
0.02
0.03
0.04
0.05
0.06
0.15
0.20
0.25
0.30
Minimum Soil Wetness 05 months before (m3/m3)

b)

c)

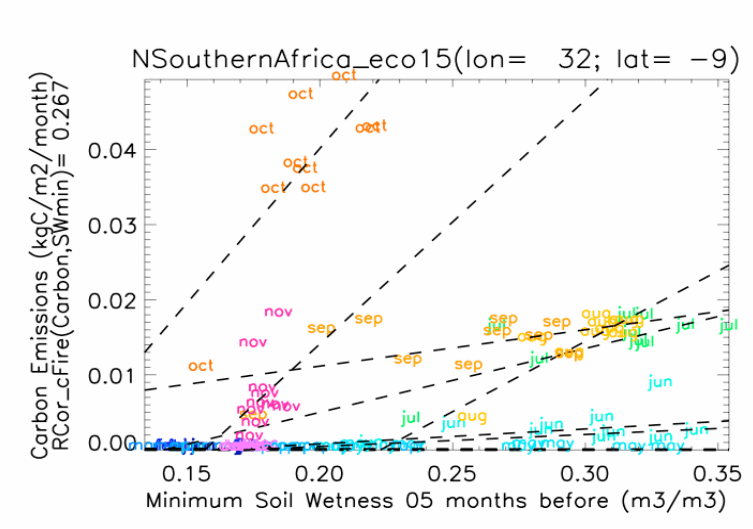

Figure 2.3.2 Scatterplots of biomass burnt, expressed as carbon emissions, versus minimum soil wetness, contemporary (a) and lagged by 5 months (b and c), in the pixels of tropical and subtropical drought-deciduous woodlands of North Southern Africa. All these cases produced good models, correlated by 90% or more with observations, even though the overall rank-correlation between variables, in case c), is rather low (less than 30%).

Good models were obtained only in pixels and months with regular, frequent and considerable biomass burning, i.e., months of the year where fires occurred every year and were easily detected by the satellite sensors. Overall high rank-correlations between fires and a weather variable, with data normally distributed, are usually a sufficient condition to obtain good models with this method (figures 2.3.2 a) and b)), but not necessary. Certain cases with low overall rank-correlations still can produce good models with this method (figure 2.3.2. c), showing the importance of using different parameters for different months of the year in each model.

2.3.3 Time Series of Models and Observations

After the models were constructed, those better correlated with the observations were plotted in time series, and these superimposed on the time series of observations, for comparison. The models

considered as the best were those that not only closely followed the observed data, but also followed the variability of the peaks and lows of the observed time series: the highest and lowest peaks of the model should preferably coincide with the highest and lowest peaks in the observations, respectively.

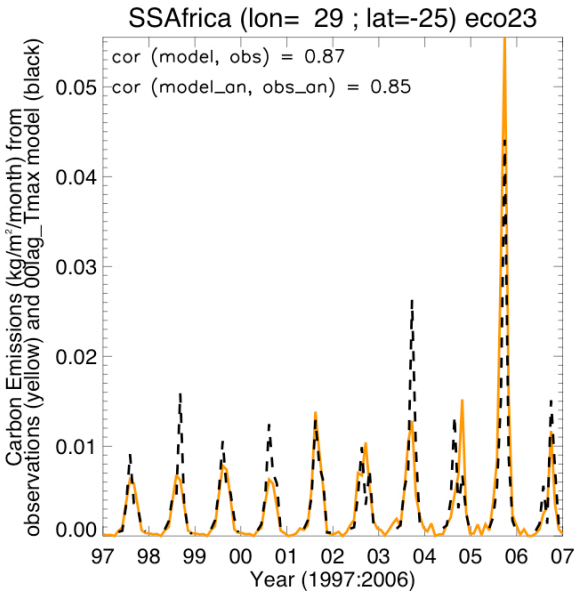

Figure 2.3.3 Time series of biomass burning (expressed as carbon emissions), from 1997 to 2006, given by GFED estimates (solid orange line), for one individual pixel in the grasslands of South Southern Africa. Over-plotted in black is a fire model, based on monthly averages of maximum air temperature, for months with burnt fractions superior to 0.01%. There is a high correlation (87%) between the predicted carbon emissions and those of GFED estimates. However, since based on average values, the model under-estimates the peak in biomass burning of 2005 and over-estimates the minimal emissions of 2000.

These time series (e.g., figures 2.3.3.1 and 2.3.3.2) show the observed values of carbon emissions and the predicted values, based on a model of the type C = m X + b (as in equation 2.3.2), with the slope (m) and the intercept (b) varying from month to month and from pixel to pixel.

Anomalies for both the observations and the model were calculated, expressing the monthly deviation from the monthly climatic value

(i.e., the average value for homonymous months during the 10 years of data).

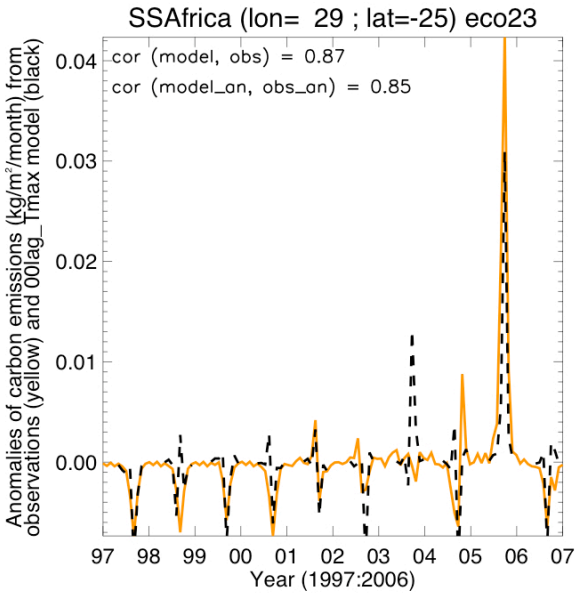

Figure 2.3.3.2 Time series of anomalies in biomass burning (expressed as the difference between monthly carbon emissions and their climatic average in 10 homonymous months), from 1997 to 2006, given by GFED estimates (solid orange line), for one individual pixel in the grasslands of South Southern Africa. Over-plotted in black are the anomalies of biomass burning predicted by a model based on monthly averages of maximum air temperature. The high correlation (above 75%) between the predicted anomalies and those of GFED estimates show that this model captures a considerable part of the interannual variability in carbon emissions. Still, there is a significant under-estimation of the largest positive anomaly and an over-estimation of the smallest negative anomalies.

Monthly anomalies predicted by the models were superimposed on time series of observed anomalies, i.e., deviations of each monthly value from the climatic average of 10 homonymous months, from 1997 to 2006 (figure 2.3.3.2). As expected, both model and observation anomalies have positive and negative values and are distributed above and below zero, with a null average value.

The best models were chosen according to the criteria of having a correlation with the observations superior to 85% and a correlation between its anomalies and those of the observations superior to 70%.

2.3.4 Scatterplots of Models versus Observations

After each fire model is obtained, the modelled carbon emissions are plotted against the observed values (figure 2.3.4). Ideally, there should be an even spread (standard deviation) in the values of carbon emissions along the axis of the weather variable – the homoskedasticity condition. This would ensure that the best-fitting line would work well for all relevant values of the weather variables. However, this rarely occurs with these models, because big fires are often much less frequent and much more irregular than smaller ones, so there is usually a visible heteroskedasticity in the scatterplots of predicted versus observed values.

For a numerical measure of model fit, the coefficient of determination, R^2, was used, computed as the square of the correlation coefficient between the observed carbon emissions and their predicted values. R^2 is the proportion of variability in carbon emissions that is explained by the statistical model based on a meteorological variable, so it provides a measure of how accurately future carbon emissions could be predicted by the model.

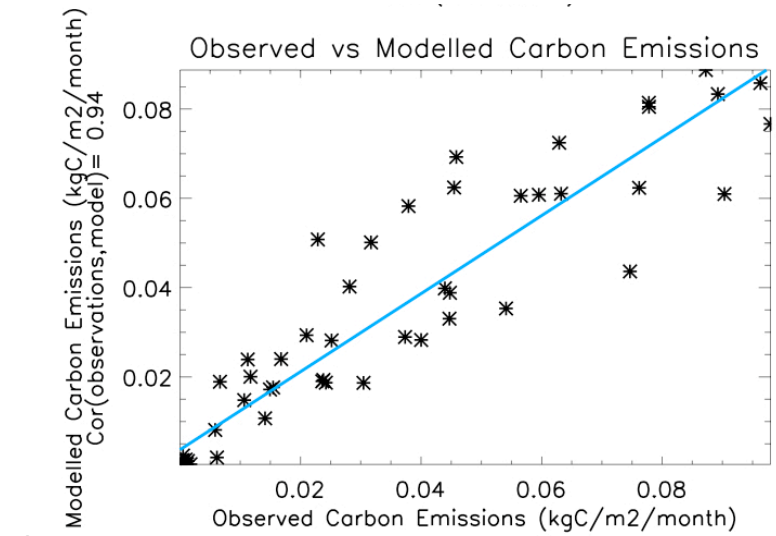

a)

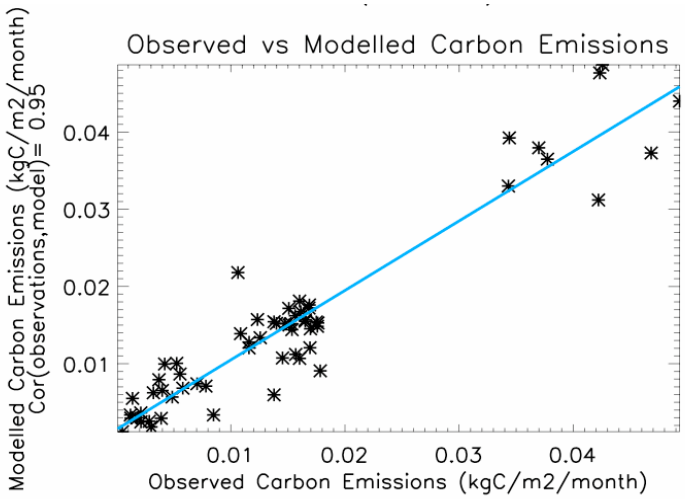

b)

Figure 2.3.4 Scatterplots of model predictions based on soil wetness lagged by 5 months, for individual pixels, a) [21°E, 8°S] and b) [32°E, 9°S], in the tropical and subtropical drought deciduous woodlands of North Southern Africa. Pixel [21°E, 8°S] has a rank correlation of 85.8% with soil wetness lagged by 5 months, predictor that gives a correlation of 94% with the observations. However, in pixel [32°E, 9°S], the correlation with observations is even higher, at 95%, although the biomass burnt is weakly correlated (26.7%) to lagged soil wetness overall. This illustrates the advantage of producing different models for different months.

In the cases where the line fits well (correlation superior to 90%), there is not much left to explain about the value of carbon emissions other than using the appropriate weather variable and its

relationship to the occurrence of wildfires and correspondent biomass burning.

However, to check how well the model fits the data, the coefficient of determination is not enough, because that does not take into account the distribution of the residuals, i.e., the difference between the observed value of carbon emissions from a data set and the predictions from the model [OD of Statistics, 2008]. For the purpose of checking the reliability of the estimates of the regression models, four types of residual plots were used, as follows.

2.3.5 Normal Probability Plot

A positive residual corresponds to an underestimation, and a negative residual to an overestimation. For the best models, the 4 standard plots of residuals were produced, to verify if their distribution allows drawing conclusions based on the results of the models.

Typical parametric tests strongly rely on the average as a measure of central tendency, but, if the data does not have a normal distribution, or at least symmetrical, then the mean is not a good measure of the centre of the data. Therefore, it is important to check if the predicted carbon emissions have a normal distribution.

Normal probability plots (figure 2.3.5) were used to compare the distribution of frequencies of occurrence of residual values with the line correspondent to the normal distribution, to check if the points are symmetric or, on the contrary, skewed to the left or to the right.

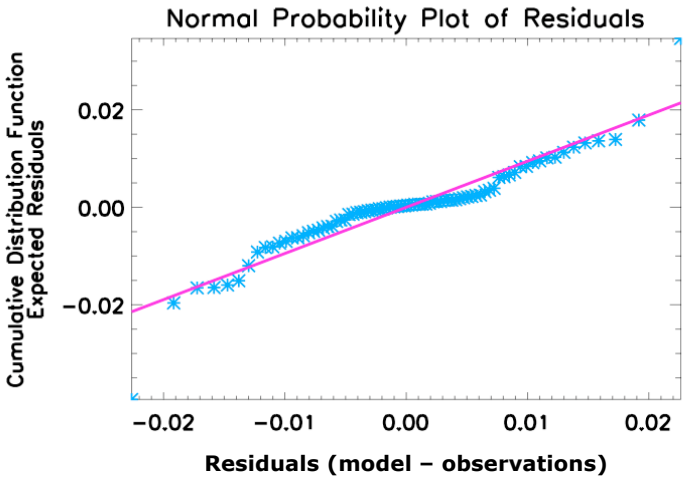

Figure 2.3.5 Normal probability plot of the residuals of burnt fraction predicted by a fire model with soil wetness lagged by 5 months as the predictor, in one individual pixel (30°E, 17°S) in the tropical and subtropical drought deciduous woodlands of North Southern Africa. Normal probability plots are scatterplots of the expected residuals versus the observed residuals, so the points (shown in blue) should follow approximately a straight line (shown in pink), as in this case.

2.3.6 Scatterplot of Residuals versus Predictions

To fit the conditions for a linear regression model, the residuals should be scattered around the best fitting line (figure 2.3.6), according to the 68-95-99.7 rule of Gaussian distributions (68% within 1 standard deviation of the line, 95% within 2 standard deviations and 99.7% within 3 standard deviations), i.e., most points close to the line, and fewer and fewer points as the distance from the line increases.

However, in the cases studied, there was a considerable heteroskedasticity: the spread in the residuals increased with the quantity of carbon emissions. Ideally, this should not occur, but it does happen here, because there are usually less big fires than small ones, and many factors contribute to the spread of wildfires.

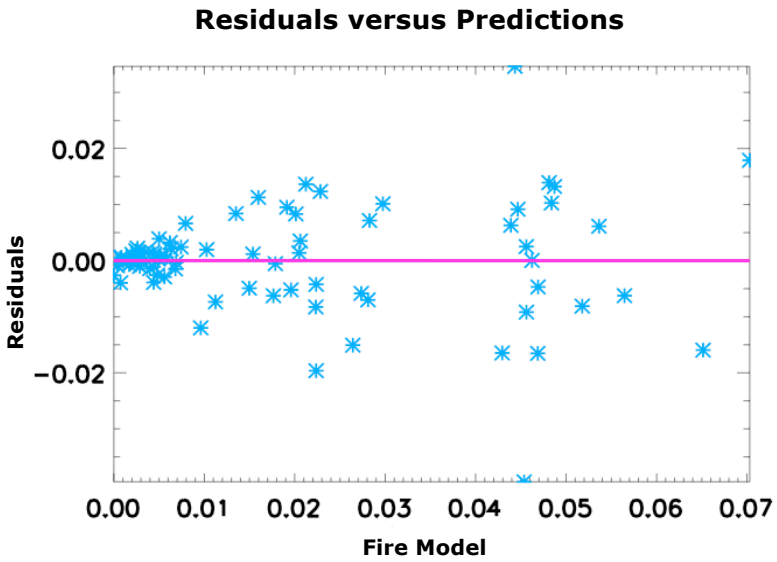

Figure 2.3.6 Scatterplot of residuals versus values of burnt fraction predicted by a fire model with soil wetness lagged by 5 months as the predictor, in one individual pixel (30, -17) in the tropical and subtropical drought deciduous woodlands of North Southern Africa. The fitted line in pink passes through zero, since the average of all residuals is zero.

2.3.7 Histogram of the Residuals

A histogram is a diagram that uses rectangles to represent frequency [OD of Statistics, 2006]. For each rectangle, the area is proportional to the frequency represented. Histograms of the residuals (figure 2.3.7) are non-parametric estimators of their underlying probability distribution, and show how frequently certain intervals of residual values occur. For the statistical analyses to be meaningful, residuals must have a normal distribution and be approximately symmetric (not much skewed), since the mean or average should be a good measure of the centre of the data. Histograms must take a bell shape, showing non-skewed residuals, i.e., not set off to one side or to the other.

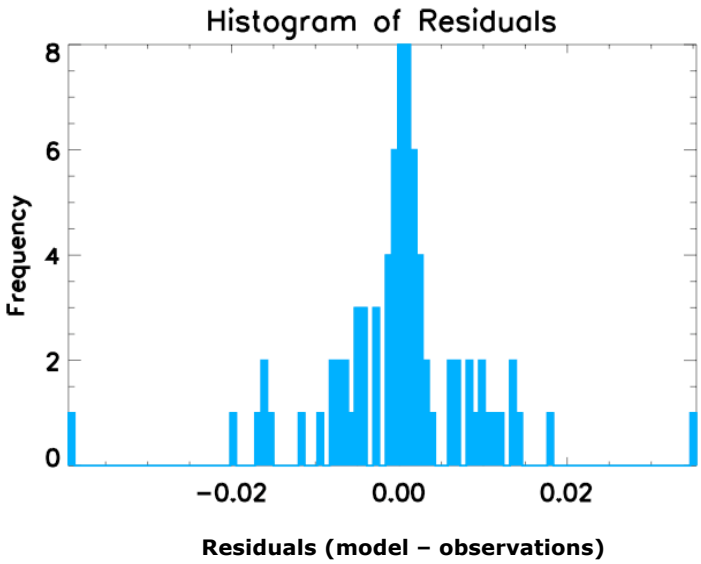

Figure 2.3.7 Histogram of the residuals of burnt fraction values predicted by a fire model with soil wetness lagged by 5 months as the predictor, in one individual pixel (30, -17), in the tropical and subtropical drought-deciduous woodlands of North Southern Africa. The residues should have a Gaussian distribution, with most residues being small, and larger residues being more infrequent.

2.3.8 Time Series of the Residuals

The residuals of the model are plotted according to the chronological order of the data (figure 2.3.8). This time series should not show a large continuous time period of residues of the same signal (positive or negative), since that would indicate a possible strong influence of the results of one year in the results of the following year. Over and underestimates should appear at random: there should not be several contiguous years with under or overestimates. If there is a visible pattern in the residuals, the model may not fit well.

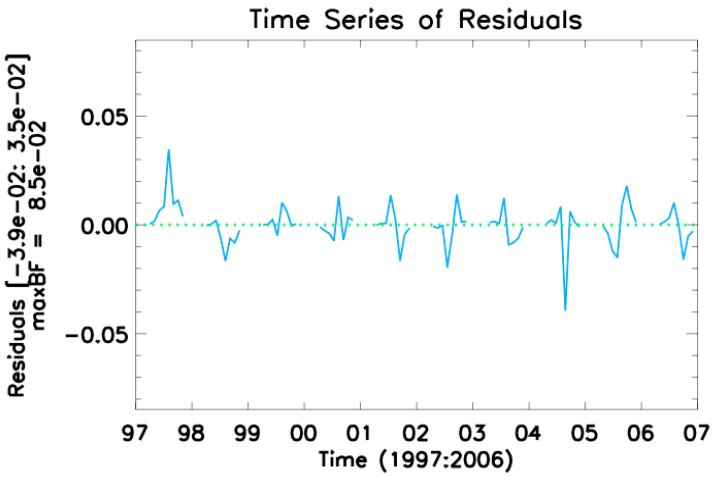

Figure 2.3.8 Time series of the residuals of burnt fraction values predicted by a fire model with soil wetness lagged by 5 months as the predictor, in one individual pixel (30°E, 17°S), in the tropical and subtropical drought-deciduous woodlands of North Southern Africa.

2.3.9 Models with 2 variables

Most of the best models were obtained using rainfall during the growing season or humidity during the fire season as a predictor. These models have just one variable (equation 2.3.9.1), and attempts have been made to improve them with another variable (equation 2.3.9.2).

$$y_1 = b_0 + b_1 x_1 \qquad \text{(equation 2.3.9.1)}$$

$$y_2 = b_0 + b_1 x_1 + b_2 x_2 \qquad \text{(equation 2.3.9.2)}$$

y = linear model, or the best fitting linear function for the data

b_0 = intercept

b_1 = slope of the first predictor

b_2 = slope of the second predictor

x_1 = first predictor

x_2 = second predictor

All weather variables were correlated with each other through rank-correlation maps and scatterplots: they tended to be correlated in many areas, which is unhelpful to add a second variable, since all variables in a model should be as independent as possible, to avoid multi-colinearity. If 2 predictors are related to each other, they should not be both in the same model, since redundancy hinders its predictability.

Correlations, however, diminished when the variables were lagged, so it was possible to obtain 2 relatively independent variables, maximum temperature, concurrent with the fire events, and lagged rainfall 5 or 6 months before.

Weather variables not strongly related to carbon emissions were eliminated.

Scatter-plots of residuals for humidity-based models versus all the other weather variables have shown that, overall, residuals correlated best with rainfall 5 or 6 months before.

Likewise, scatterplots of residuals from models based on lagged rainfall were moderately correlated with maximum temperature during the fire season.

Therefore, lagged rainfall and concurrent temperature were used to try to find better fitting models:

BB = c1 05_Rain + c2 Tmax + c3

BB = biomass burning expressed as carbon emissions (kg/ month)

c1 = slope of first predictor

c2 = slope of second predictor

05_Rain = rainfall lagged by 5 months before the fire event, as 1st predictor

Tmax = maximum temperature contemporary with the fire event, as 2nd predictor

c3 = intercept

After both predictors were introduced in the model, the goodness of fit was checked, and the new residuals were calculated.

The final models with 2 variables were not significantly better than the ones with just 1 variable, possibly on account of the coarseness of data resolution, so models with more than 1 variable were not pursued. The rest of the research only considered single variable models.

Chapter III Results & Discussion

Summary

This chapter presents and discusses the results obtained in the data analysis. The discussion is focused on the spatial and temporal distribution of wildfires and on how they are influenced by different weather parameters in different ecosystems, trying to find explanations for distinct fire behaviours.

The results consist mainly in correlations and statistical models related to fire and weather data, and they are presented in world maps, time series and scatterplots. At the appropriate spatial and temporal scales, the results are shown for land ecosystems, for geographical regions and their broad ecosystems (forests, woodlands, shrublands and grasslands), for eco-regions (i.e., specific ecosystems within geographical regions) and for individual pixels and months.

Statistical models, based on 10 years of fire and weather data, from 1997 to 2006, were obtained in individual pixels where wildfires are frequent and respond consistently to climatic variability. For the areas with best models (correlation [model, data] superior to 75%), projections of carbon emissions for the year 2007 are presented and compared to GFEDv2.1 estimates.

This chapter is divided into 29 sub-chapters, corresponding to the 28 ecosystems investigated, as defined by NASA's Goddard Institute of Space Studies, plus the 1 additional subchapter with an overview of spatial and temporal fire distribution and behaviour in the 4 broad land ecosystem types (forests, woodlands, shrublands and grasslands).

Each subchapter relative to a specific ecosystem starts with a summary of its fire behaviour followed by a discussion of its susceptibility to weather parameters and possible physical explanations. At least one world map is presented, showing the

geographical distribution of the ecosystem, and the places, if any, where good fire models were found. When relevant, there are also world maps of rank-correlations between carbon emissions from wildfires and weather parameters.

For the eco-regions with more carbon emissions and more homogeneous fire behaviour throughout a large area, scatterplots of carbon emissions versus weather parameters are shown. Additional scatterplots of rank-correlations between carbon emissions and lagged rainfall versus the lags are shown for eco-regions where rainfall during the growing season strongly contributes to larger carbon emissions during the following fire season, due to the abundance of fuel load.

For the eco-regions where most pixels have good models (correlation between model and estimates superior to 75%), projections for the year 2007 are presented, as a validation method for the statistical models obtained with GFED v2.1 data from 1997 to 2006.

3.1 Tropical Evergreen Rainforests

Fires in tropical evergreen rainforests occurred mainly in areas of deforestation. The interiors of the Amazonia, of the Equatorial African Rainforest and of the Equatorial Asian Rainforest receive abundant precipitation all year round and have no significant fire activity (figure 3.1.1). Large areas of the Amazonia and of Equatorial Africa were excluded from the analyses because they never burned during the 10 years of data.

However, the borders of these rainforests are being subject to intense deforestation and land conversion, making them more and more prone to wildfires [Le Page & al., 2008]. Fires in these ecosystems release large quantities of carbon emissions, because they are very rich in fuel loads [GFEDv2.1, 2007].

After a specially wet rainy season, there were fewer fires during the dry season in the monsoon area of West Africa, but more in South

Equatorial Africa, Equatorial Asia, Central America and Central South America.

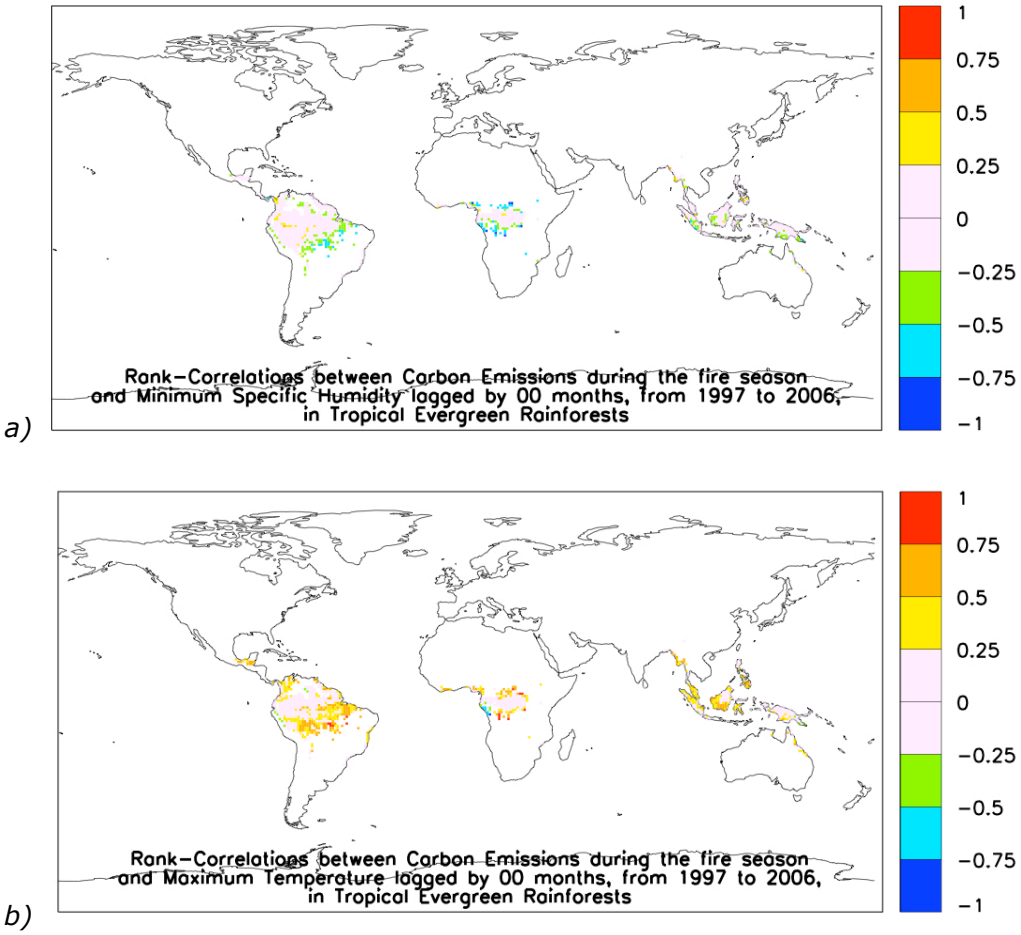

Figure 3.1.1 World maps of rank-correlations between wildfires and a) air humidity and b) air temperature, during the fire season, from 1997 to 2006, in tropical evergreen rainforests. Pixels in green and blue show areas where fires increase during a) drier or b) colder weather, whereas yellow, orange and red pixels show areas where fires are increase with a) more humid or b) warmer weather.

Humidity considerably repressed wildfires (some negative correlations superior to 75%) in the borders of tropical evergreen rainforests of Equatorial Africa, North Southern Africa, Central America, South America, South East Asia and Equatorial Asia, Northern Australia (figure 3.1.1 a). This agrees with previous research about the importance of soil wetness in preventing fire in

the rainforests of Equatorial Asia [Nieuwstadt & Sheil, 2005] and in the Amazon [Williamson & al., 2000], both by hindering ignition and by preventing tree mortality caused by drought that will increase fire risk.

The borders of the Amazon and of the Equatorial Africa rainforest undergoing rapid deforestation had a different behaviour from the interior. In equatorial rainforests, vegetation rarely burns, except near the borders of the forest, or where the population density is higher, with many roads and large agricultural fields (e.g. Manaus city, in the Amazon).

Higher temperatures during the fire season are strongly correlated (by more than 75%) with larger burnt areas (figure 3.1.1 b and 3.1.2).

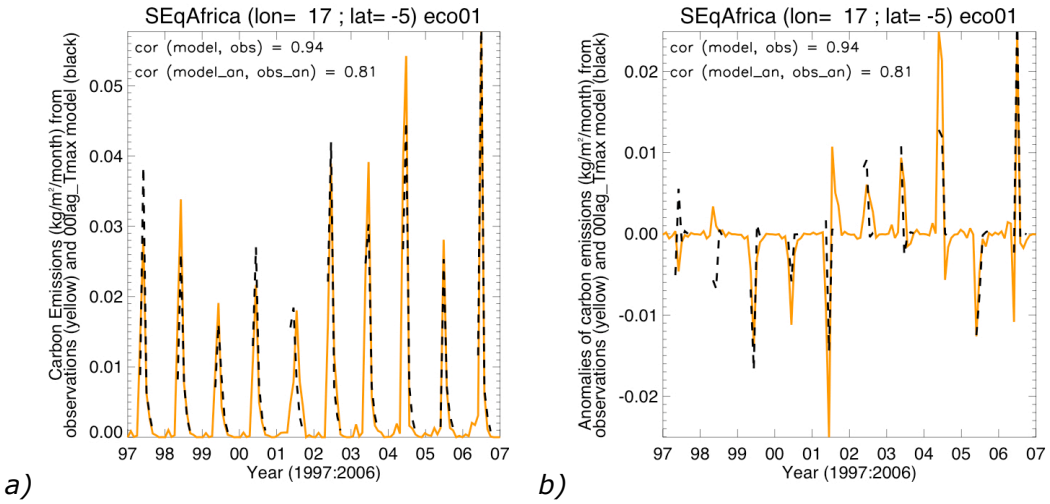

Figure 3.1.2 Time series of carbon emissions (a) and anomalies (b), given by GFED estimates, from 1997 to 2006, for an individual pixel in the rainforests of South Equatorial Africa, in yellow. A model with monthly averages of maximum daily temperature as a predictor is superposed in black.

Temperature is a good predictor of biomass burning (correlations between model and estimates superior to 75%) only in the borders of the equatorial rainforest (figure 3.1.2), where rank-correlations between temperature and carbon emissions are high (red pixels in figure 3.1.1 b).

Contemporary humidity, contemporary soil wetness and rainfall prior to the fire season, are also good predictors of biomass burning

(figures 3.1.3 and 3.1.4), as shown in scatterplots of predictions for the year 2007, based on models obtained with data from 1997 to 2006, versus the observations.

The observed deforestation areas are becoming larger and larger, so more carbon emissions are to be expected from these ecosystems.

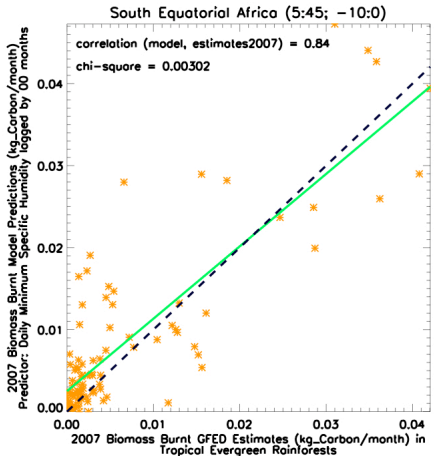

a)

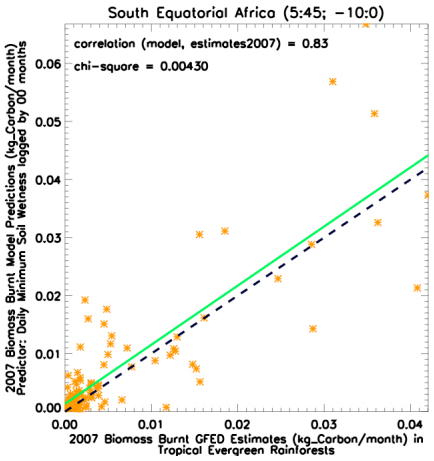

b)

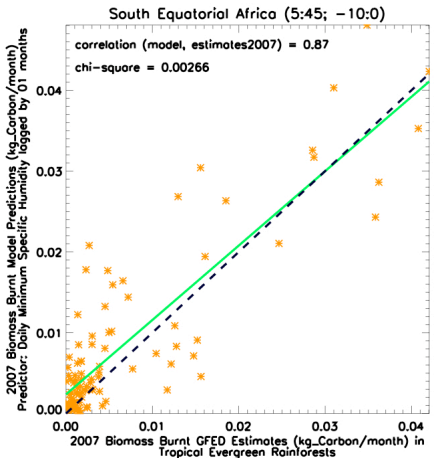
South Equatorial Africa (5:45; −10:0)
correlation (model, estimates2007) = 0.87
chi-square = 0.00266
2007 Biomass Burnt Model Predictions (kg_Carbon/month)
Predictor: Daily Minimum Specific Humidity lagged by 01 months
2007 Biomass Burnt GFED Estimates (kg_Carbon/month) in
Tropical Evergreen Rainforests

c)

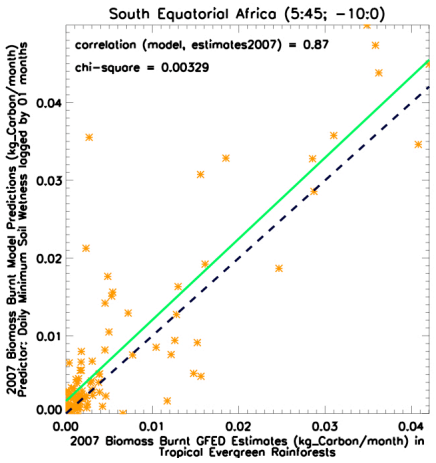
South Equatorial Africa (5:45; −10:0)
correlation (model, estimates2007) = 0.87
chi-square = 0.00329
2007 Biomass Burnt Model Predictions (kg_Carbon/month)
Predictor: Daily Minimum Soil Wetness lagged by 01 months
2007 Biomass Burnt GFED Estimates (kg_Carbon/month) in
Tropical Evergreen Rainforests

d)

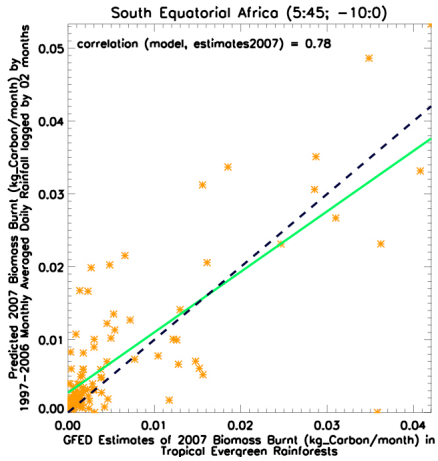
South Equatorial Africa (5:45; −10:0)
correlation (model, estimates2007) = 0.78
Predicted 2007 Biomass Burnt (kg_Carbon/month) by
1997-2006 Monthly Averaged Daily Rainfall lagged by 02 months
GFED Estimates of 2007 Biomass Burnt (kg_Carbon/month) in
Tropical Evergreen Rainforests

e)

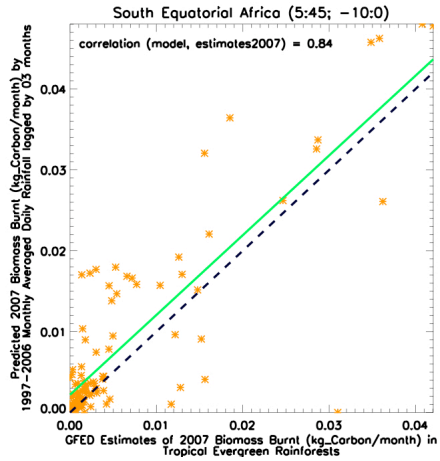
South Equatorial Africa (5:45; −10:0)
correlation (model, estimates2007) = 0.84
Predicted 2007 Biomass Burnt (kg_Carbon/month) by
1997-2006 Monthly Averaged Daily Rainfall lagged by 03 months
GFED Estimates of 2007 Biomass Burnt (kg_Carbon/month) in
Tropical Evergreen Rainforests

f)

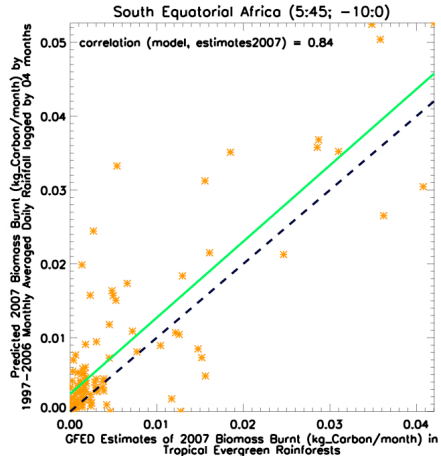
South Equatorial Africa (5:45; −10:0)
correlation (model, estimates2007) = 0.84
Predicted 2007 Biomass Burnt (kg_Carbon/month) by
1997-2006 Monthly Averaged Daily Rainfall lagged by 04 months
GFED Estimates of 2007 Biomass Burnt (kg_Carbon/month) in
Tropical Evergreen Rainforests

g)

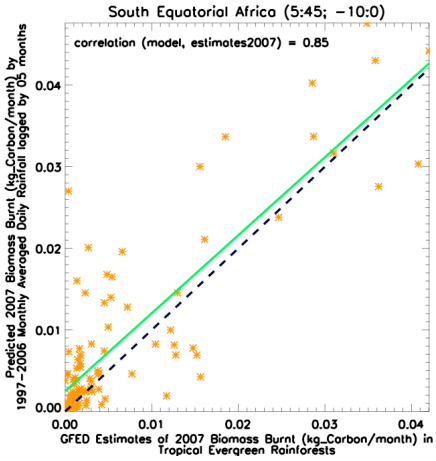
South Equatorial Africa (5:45; −10:0)
correlation (model, estimates2007) = 0.85
Predicted 2007 Biomass Burnt (kg_Carbon/month) by
1997-2006 Monthly Averaged Daily Rainfall lagged by 05 months
GFED Estimates of 2007 Biomass Burnt (kg_Carbon/month) in
Tropical Evergreen Rainforests

h)

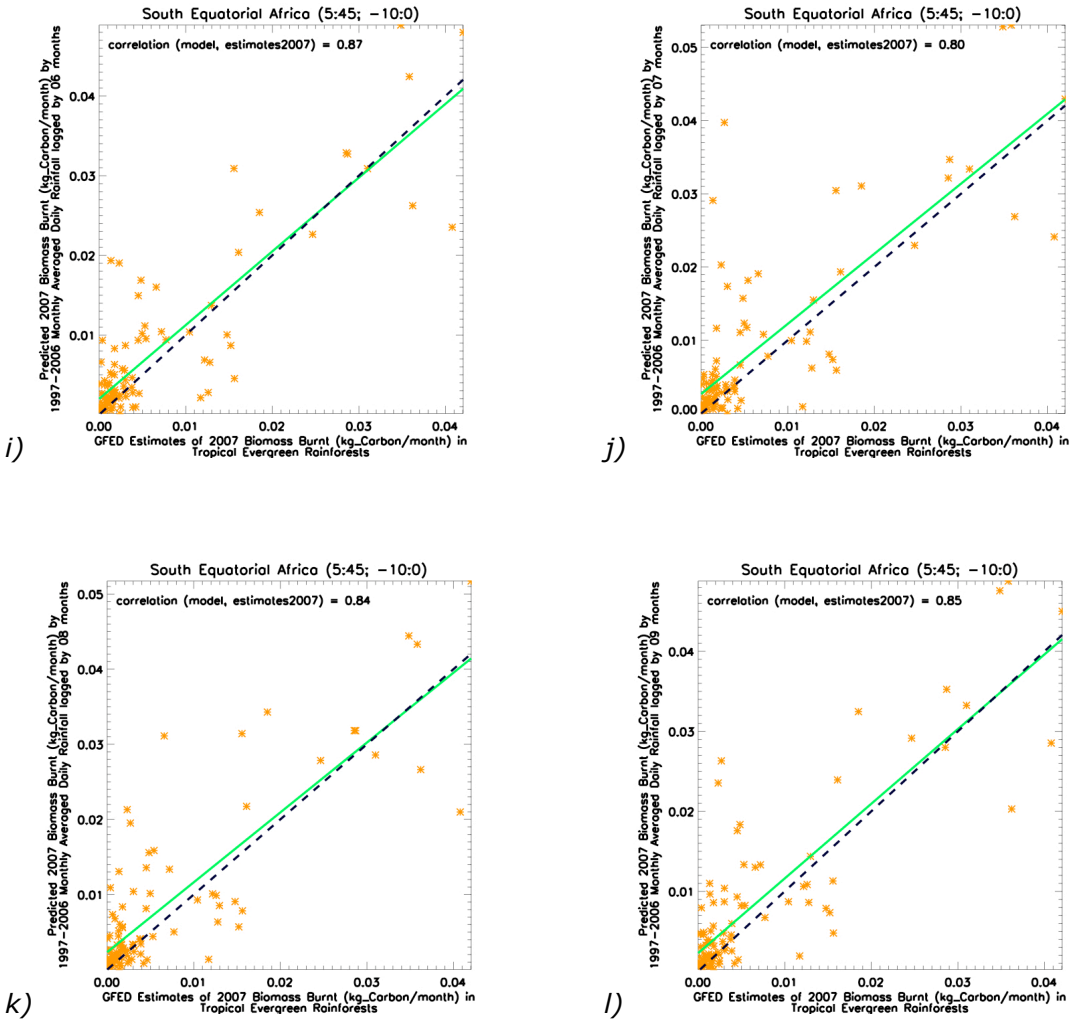

Figure 3.1.3 Scatterplots of predicted biomass burnt for the year of 2007 versus the correspondent GFED estimates, expressed in kilograms of carbon emissions per month, in the tropical evergreen rainforests of South Equatorial Africa. The green line shows the linear fit through the points, whereas the black dashed line marks where the 1:1 ideal slope would be. Fire models based on monthly averaged daily minimum specific humidity a) concurrent with the fire events and c) lagged by 1 month; on monthly averaged daily minimum soil wetness, b) contemporary and d) lagged by 1 month; and on monthly averaged daily rainfall, lagged by 2 (e), 3 (f), 4 (g), 5 (h), 6 (i), 7 (j), 8 (k) and 9 months (l). Air humidity and soil wetness during the fire season give similarly good models when used as predictors.

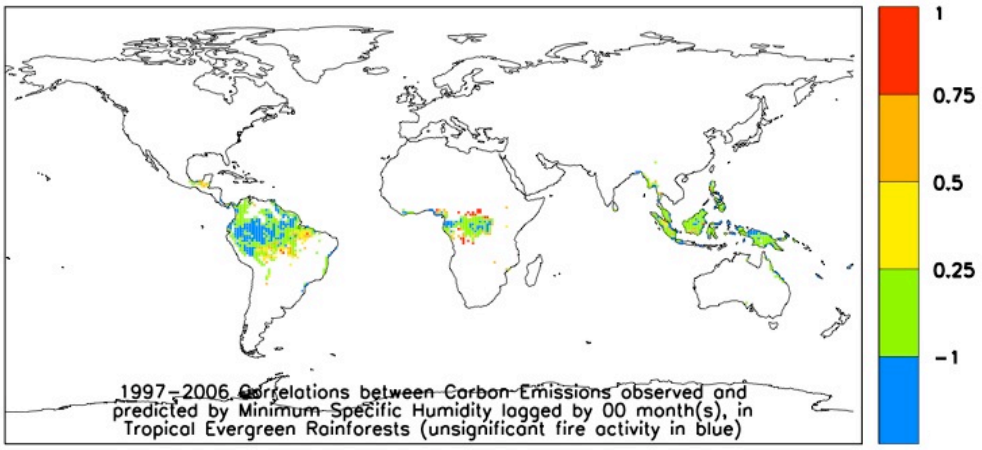

Figure 3.1.4 World map of correlations between model predictions and GFED estimations of carbon emissions from wildfires, from 1997 to 2006, in tropical evergreen rainforests, with specific humidity during the fire season as the predictor. Red pixels have the best models (correlations with observations above 75%), followed by orange and yellow pixels with correlations between 50% and 75%, and between 25% and 50%, respectively. Green pixels do not have reliable models with this predictor. Blue pixels do not show significant fire activity at 1ºx1º resolution.

3.2 (Sub-) Tropical Evergreen Seasonal Broad-Leaved Forests

Tropical and sub-tropical evergreen seasonal broad-leaved forests do not usually burn, since they receive much rainfall all year round, but logging and deforestation are making them more prone to fires, and especially vulnerable during El Niño episodes, when severe drought and hot weather greatly exacerbate fire risk [Le Page & al., 2008]. Most fires in these ecosystems occurred in land conversion areas (figure 2.2.16), especially during very warm weather (figure 3.2.1 b).

Rainfall and high humidity during the growing season in Equatorial Africa, Southern Africa, India, Sri Lanka, South East Asia and Central America were correlated with more fires in the following fire season, except in the monsoon region of West Africa, which had fewer fires after a rainy wet season (correlation maps not shown).

Rainy and humid fire seasons in Equatorial Africa, South Southern Africa, Madagascar, India, South East Asia, Central America and Southern South America had fewer fires (figure 3.2.1 a).

Deforestation rates are rapidly increasing in the subtropical forests of South East Asia, Equatorial Asia, Central America and South America [FAO report, 2005], so more carbon emissions are to be expected from these ecosystems.

Rainfall prior to the fire season and contemporary humidity, soil wetness and temperature were all good predictors of biomass burning in the monsoon region of West Africa (figures 3.2.2-3).

a)

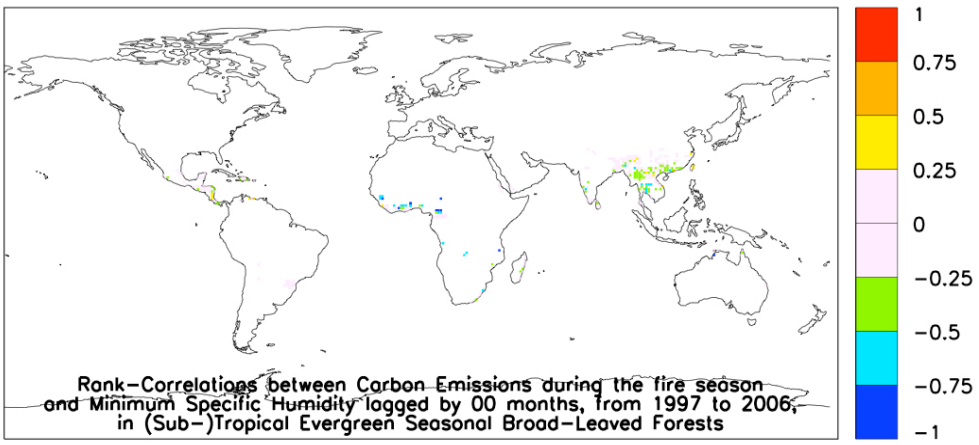

b)

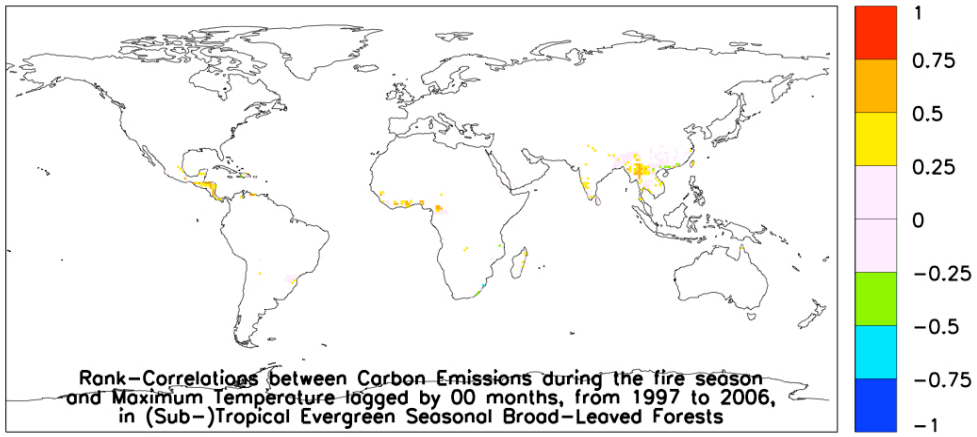

Figure 3.2.1 World maps of rank-correlations between wildfires and a) air humidity and b) air temperature, during the fire season, from 1997 to 2006, in tropical and sub-tropical evergreen seasonal broad-leaved forests. Pixels in green and blue show areas where fires increase during a) drier or b) colder weather, whereas yellow, orange and red pixels show areas where fires are increase with a) more humid or b) warmer weather.

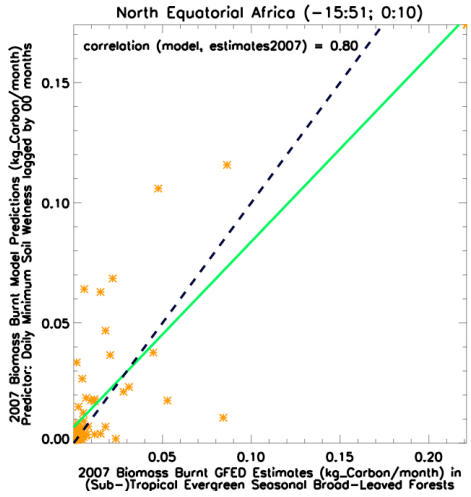

Figure 3.2.2 Scatterplot of predicted biomass burnt for the year 2007 versus GFED estimates. The green line shows the linear fit through the points, whereas the black dashed line indicates the 1:1 ideal slope. Models based on monthly averaged daily minimum soil wetness during the fire season. Carbon emissions from large fires, for which data is scarce, are under-predicted, but the model can probably improve with more data.

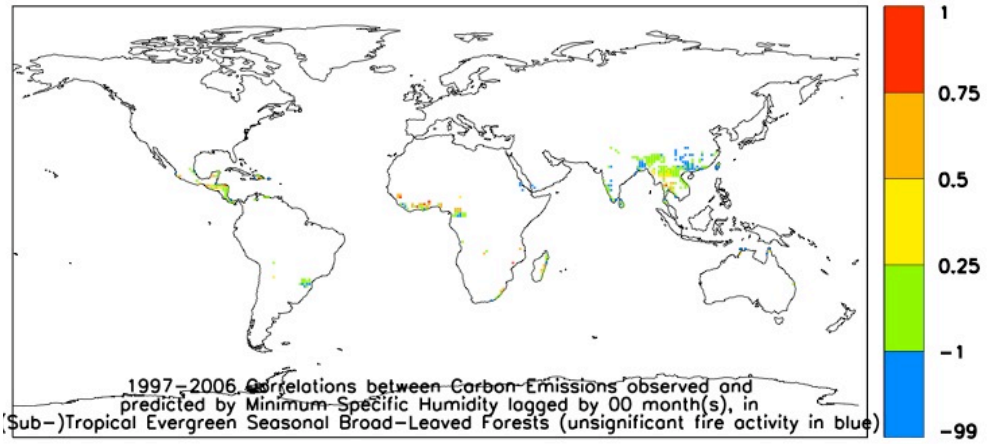

Figure 3.2.3 World map of correlations between model predictions and GFED estimations of carbon emissions from wildfires, from 1997 to 2006, in tropical and sub-tropical evergreen seasonal broad-leaved forests, with specific humidity during the fire season as the predictor. Red pixels have the best models (correlations with observations above 75%), followed by orange and yellow pixels with correlations between 50% and 75%, and between 25% and 50%, respectively. Green pixels do not have reliable models with this predictor. Blue pixels do not show significant fire activity at 1ºx1º resolution.

3.3 Sub-Tropical Evergreen Rainforests

Sub-tropical evergreen rainforests are represented mainly in Southern South America and in southern east Australia.

After a rainy and humid winter, fires slightly increased in the Andes and in Tasmania, but decreased in Southern South America. Humid summers had fewer fires in the Andes, but more in Southern South America and Tasmania. Humidity had no discernible effects after 6 months. More humid summers tended to have more fires, possibly because warmer summers tend to be more humid at sub-polar latitudes.

The total number of fires in 10 years was too small to obtain good models for individual pixels (figure 3.3.1).

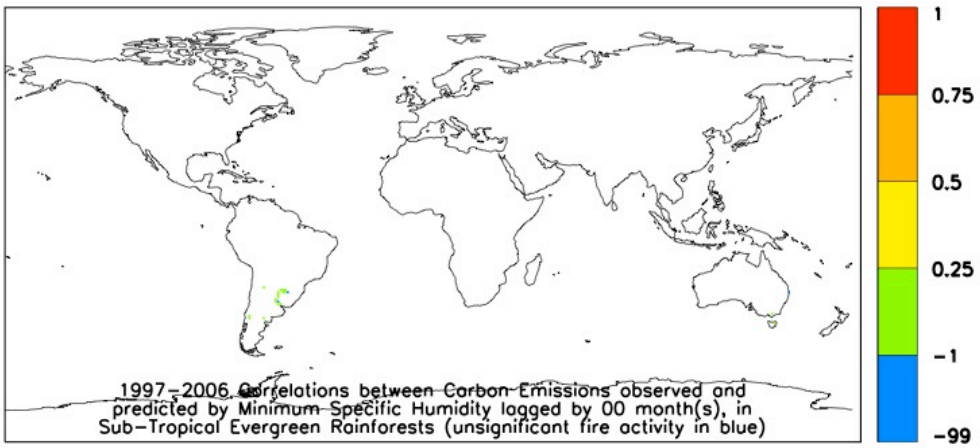

Figure 3.3.1 World map of correlations between model predictions and GFED estimations of carbon emissions from wildfires, from 1997 to 2006, in tropical and subtropical evergreen rainforests, with specific humidity during the fire season as the predictor. Red pixels have the best models (correlations with observations above 75%), followed by orange and yellow pixels with correlations between 50% and 75%, and between 25% and 50%, respectively. Green pixels do not have reliable models with this predictor. Blue pixels do not show significant fire activity at 1ºx1º resolution.

3.4 Temperate/ Sub-Polar Evergreen Rainforests

Temperate and sub-polar evergreen rainforests are represented mainly in Tasmania, New Zealand and in the mountains of Southern South America.

Humid summers in temperate and sub-polar evergreen rainforests had more fires, maybe because warmer summers are also more humid [Gentemann & al., 2008]. Warmer weather was positively correlated with fires. Fire behaviour in these forests did not show sensitivity to humidity lagged by periods superior to 3 months (correlation maps not shown).

The total number of fires in 10 years was too small for significant statistical results in individual pixels (figure 3.4.1).

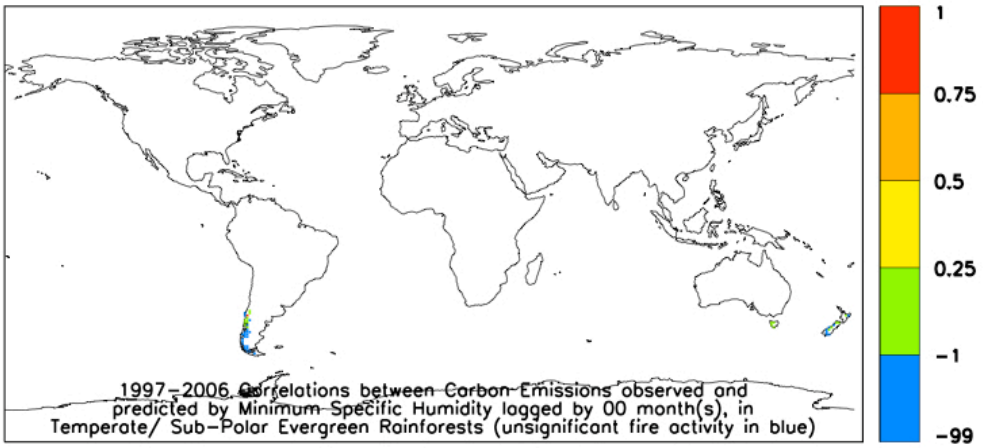

Figure 3.4.1 World map of correlations between model predictions and GFED estimations of carbon emissions from wildfires, from 1997 to 2006, in temperate and sub-polar evergreen rainforests, with humidity during the fire season as the predictor. Red pixels have the best models (correlations with observations above 75%), followed by orange and yellow pixels with correlations between 50% and 75%, and between 25% and 50%, respectively. Green pixels do not have reliable models with this predictor. Blue pixels do not show significant fire activity at 1ºx1º resolution.

3.5 Temperate Evergreen Seasonal Broad-Leaved Forests

Temperate evergreen seasonal broad-leaved forests are present mainly in South East Asia, Japan, South East Australia and Tasmania.

After a humid winter, fires in these ecosystems moderately increased near the coast in South East Asia and in Southern Australia, but decreased in Japan, the interior of South East Asia and in Eastern Australia (correlation maps and plots not shown).

Humid summers tended to have more fires in Japan, Southern Australia and Tasmania, but less in South East Asia and South East Australia. Humidity had no discernible influence in fires after 6 months (correlation maps and plots not shown).

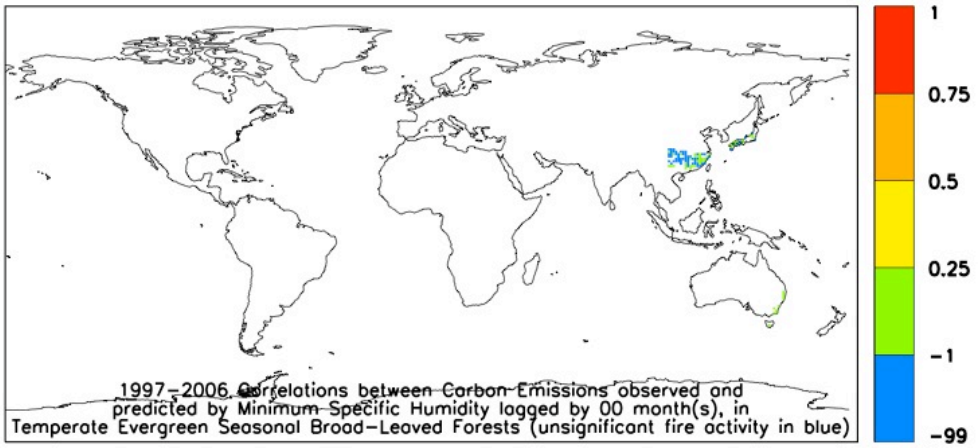

Figure 3.5.1 World map of correlations between model predictions and GFED estimates of carbon emissions from wildfires, from 1997 to 2006, in temperate evergreen seasonal broad-leaved forests, with humidity during the fire season as the predictor. Red pixels have the best models (correlations with observations above 75%), followed by orange and yellow pixels with correlations between 50% and 75%, and between 25% and 50%, respectively. Green pixels do not have reliable models with this predictor. Blue pixels do not show significant fire activity at 1ºx1º resolution.

Burnt areas tended to increase with snow depth 3, 4 and 5 months before, but it is unclear if this effect was only due to the seasonal cycle, or if it was also influenced by the drying effect of snow, as described by Pearce (2000).

Biomass burning during the 10 years of data was not enough to obtain significant statistical results in individual pixels (figure 3.4.1).

3.6 Evergreen Broad-Leaved Sclerophyllous Forests

In the evergreen broad-leaved sclerophyllous forests of Iberia, Mediterranean, West Asia and South Australia, fires slightly increased with snow depth 3, 4, 5 and 6 months before (correlation

maps and plots not shown), which maybe related to the drying effect of snow [Pearce, 2000]. In other ecosystems, this positive correlation between snow and fires could derive from water availability during the growing season, but, in this case, there was also a negative correlation between biomass burning and rainfall lagged up to 6 months before (correlation maps and plots not shown).

During the fire season, both temperature and humidity were positively correlated to larger burnt areas (correlation maps and plots not shown), possibly because warmer weather is also more humid [Gentemann & al., 2008].

Although burnt areas were well correlated with temperature and humidity, there were not enough fires, during 10 years of data, to obtain reliable models in individual pixels (figure 3.6.1).

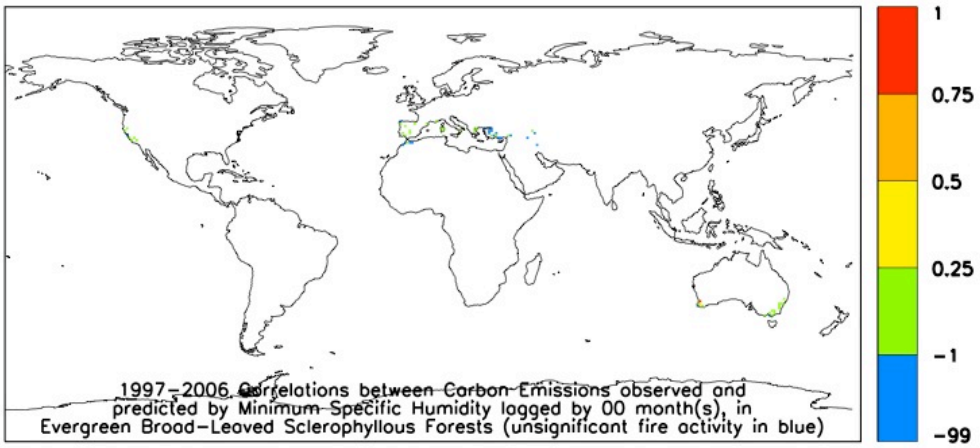

Figure 3.6.1 World map of correlations between model predictions and GFED estimations of carbon emissions from wildfires, from 1997 to 2006, in evergreen broad-leaved sclerophyllous forests, with humidity during the fire season as the predictor. Red pixels have the best models (correlations with observations above 75%), followed by orange and yellow pixels with correlations between 50% and 75%, and between 25% and 50%, respectively. Green pixels do not have reliable models with this predictor. Blue pixels do not show significant fire activity at 1ºx1º resolution.

3.7 (Sub-) Tropical Evergreen Needle-Leaved Forests

Tropical and sub-tropical evergreen needle-leaved forests occupy a small world area in South East Asia and in Central America.

After humid winters, fires tended to increase in South East Asia and Central America; in Central Asia, fires also tended to increase after a snowy winter (correlation maps and plots not shown).

During humid summers, fires decreased in Central Asia, continental South East Asia and Central America, and larger burnt areas tended to occur during warmer weather (correlation maps and plots not shown). Humidity and temperature had no discernible influence after 7 months.

Biomass burning is generally positively correlated with temperature and negatively with humidity, in this ecosystem, but there were not enough fires, during 10 years of data, to obtain reliable models for individual pixels (figure 3.7.1).

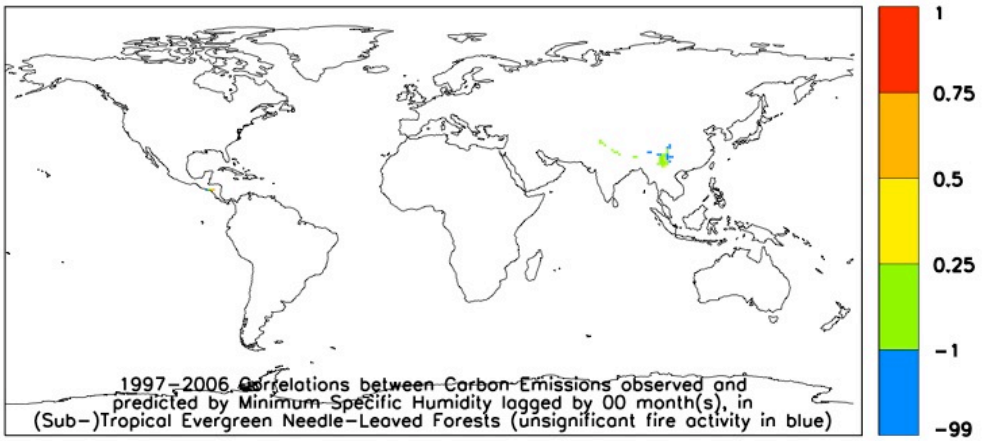

Figure 3.7.1 World map of correlations between model predictions and GFED estimations of carbon emissions from wildfires, from 1997 to 2006, in tropical and sub-tropical evergreen needle-leaved forests, with humidity during the fire season as the predictor. Red pixels have the best models (correlations with observations above 75%), followed by orange and yellow pixels with correlations between 50% and 75%, and between 25% and 50%, respectively. Green pixels do not have reliable models with this predictor. Blue pixels do not show significant fire activity at 1ºx1º resolution.

3.8 Temperate/ Sub-Polar Evergreen Needle-Leaved Forests

After rainy winters in temperate and sub-polar evergreen needle-leaved forests, fires decreased in the interior of North America and in Russia, but increased in the coast of North America (correlation maps and plots not shown). No influence of humidity was discernible after 7 months. Wildfires tended to increase after snowy winters, possibly because of the drying effect of snow [Pearce, 2000].

a)

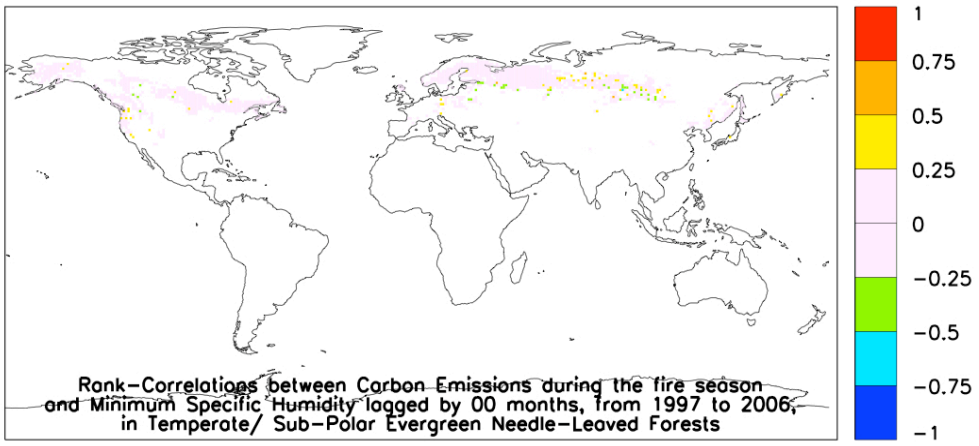

b)

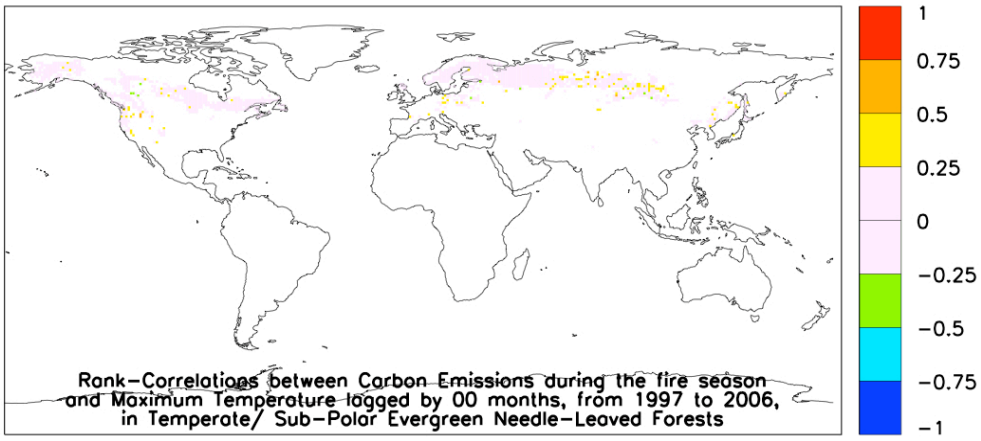

Figure 3.8.1 World maps of rank-correlations between wildfires and a) air humidity and b) air temperature, during the fire season, from 1997 to 2006, in temperate and sub-polar evergreen needle-leaved forests. Pixels in green and blue show areas where fires increase during a) drier or b) colder weather, whereas yellow, orange and red pixels show areas where fires increase with a) more humid or b) warmer weather.

During humid summers, fires increased in Northern Siberia and in the west coast of Northern North America, but decreased in West Russia, Southern Siberia and continental North America (figure 3.8.1 a).

In the summer, both temperature and humidity were higher in these forests. Air temperature is probably the main concurrent factor influencing fire behaviour here, because summers in boreal ecosystems are quite dry, so even a relatively high increase in humidity would not decrease the probability of ignition nor of fire spread during warm weather (figures 3.8.2 and 3.8.3).

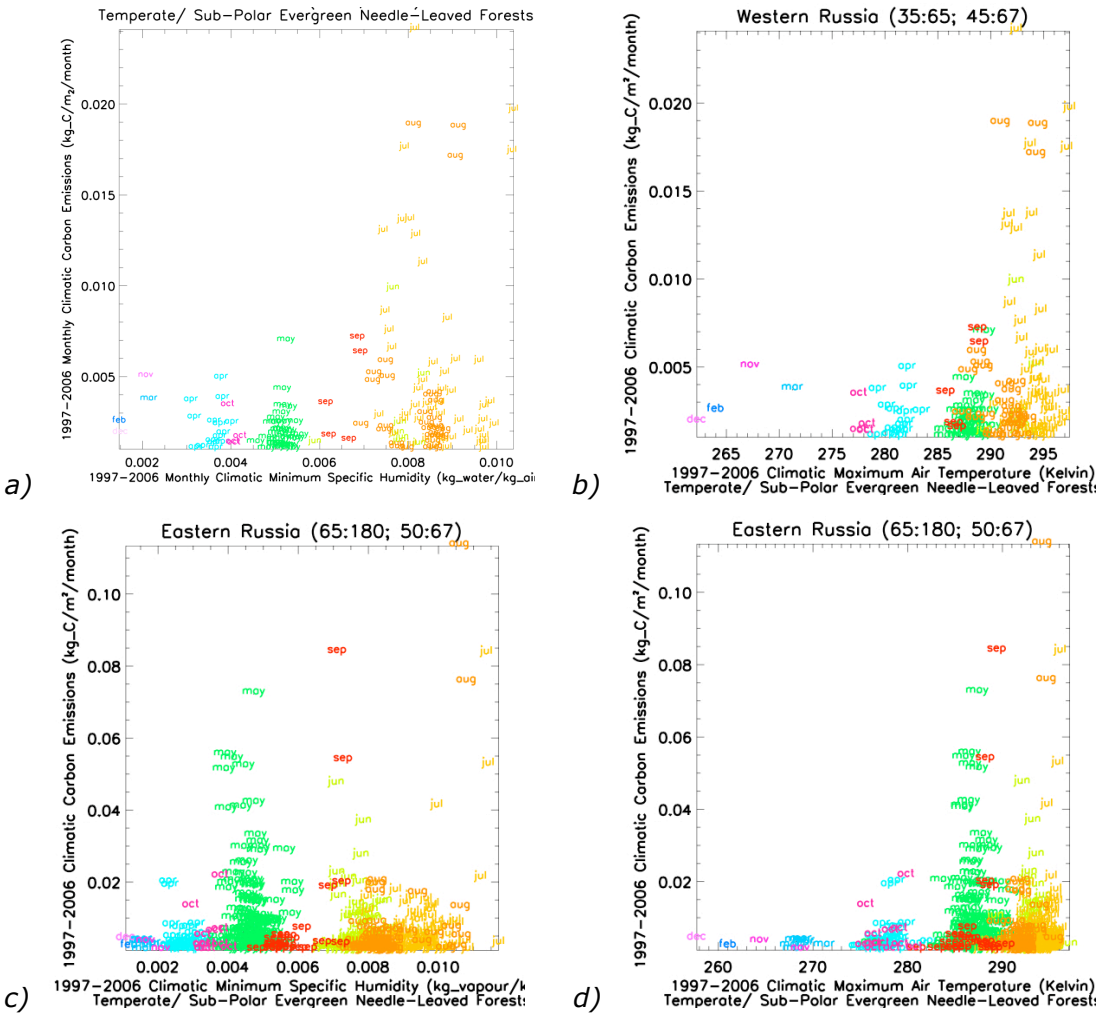

Figure 3.8.2 Scatterplots of carbon emissions from wildfires versus a) minimum air humidity and b) maximum air temperature, in the temperate and sub-polar evergreen needle forests of West Russia, and versus c) minimum air humidity and d) maximum air temperature, in East Russia. Each point corresponds to a pixel of 1ºx1º resolution, with values averaged over 10 homonymous months, from 1997 to 2006.

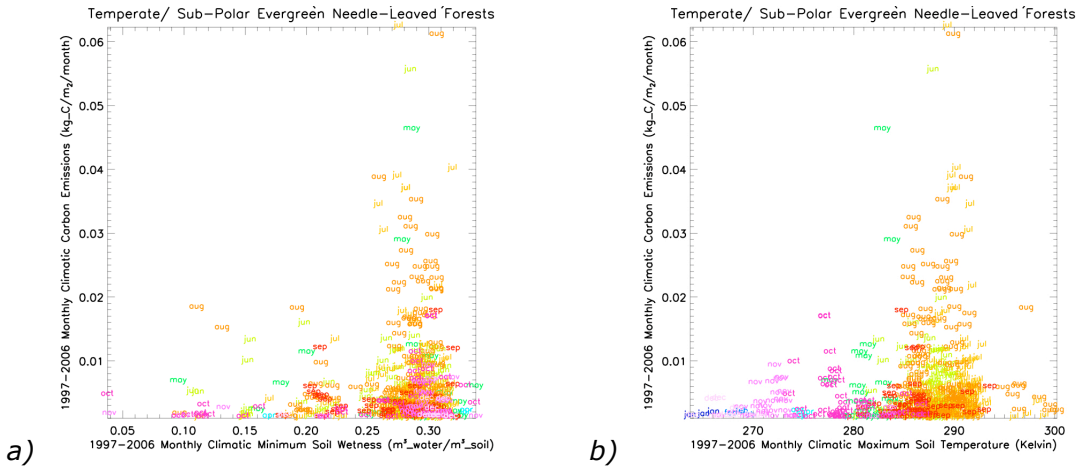

a) b)

Figure 3.8.3 Scatterplots of carbon emissions from wildfires versus a) minimum soil wetness and b) maximum soil temperature, in the temperate and sub-polar evergreen needle-leaved forests of Northern North America. Each point corresponds to a pixel of 1ºx1º resolution, with values averaged over 10 homonymous months, from 1997 to 2006.

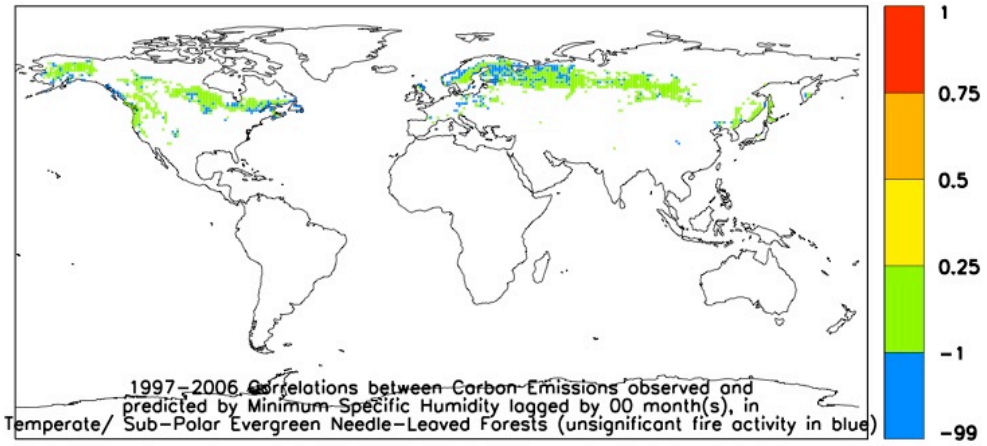

Figure 3.8.4 World map of correlations between model predictions and GFED estimations of carbon emissions from wildfires, from 1997 to 2006, in temperate and sub-polar evergreen needle-leaved forests, with humidity during the fire season as the predictor. Green pixels do not have reliable models with this predictor. Blue pixels do not show significant fire activity at 1ºx1º resolution.

Some pixels in Northern North America and Northern Asia (figure 3.8.1 b and 3.8.3 b) show an increase of carbon emissions with temperature, in agreement with former research in Canada [Gillett &

al., 2004] and in Siberia [Balzter & al., 2005], but fire return periods in individual pixels were too large to get reliable fire models with just 10 years of data (figure 3.8.4).

3.9 (Sub-)Tropical Drought-Deciduous Forests

After humid winters, fires increase in the tropical and sub-tropical drought-deciduous forests of Africa, Madagascar, India, South East Asia, Equatorial Asia, Central America, Caribbean and South America. Fires also increase after a snowy winter (correlation maps and plots not shown).

During humid summers, there are fewer fires in South Southern Africa, Madagascar, India, South East Asia, Equatorial Asia, Central America and Southern South America, but more in North Southern America and south of the Himalayas (figure 3.9.1 a). Wildfires are positively correlated with warmer temperatures during the fire season (figure 3.9.1 b).

The best fire models (figure 3.9.3) were obtained for pixels in small areas of Africa, Madagascar (also figure 3.9.2), South East Asia and Central South America.

a)

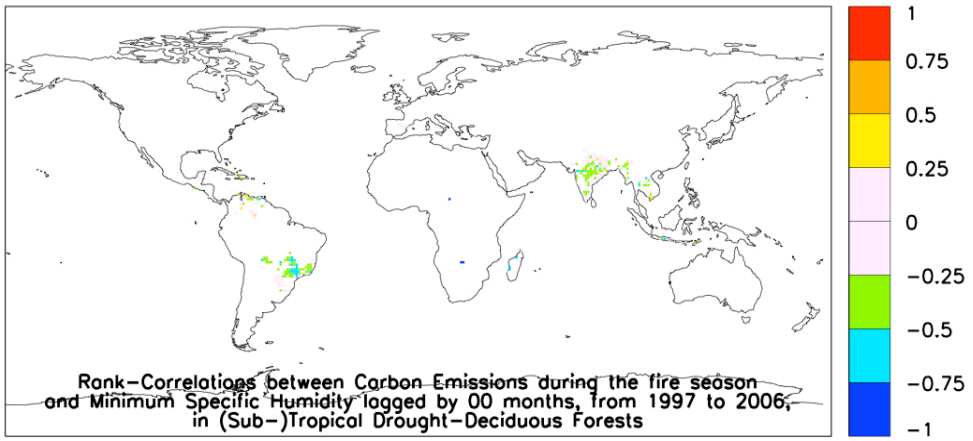

b)

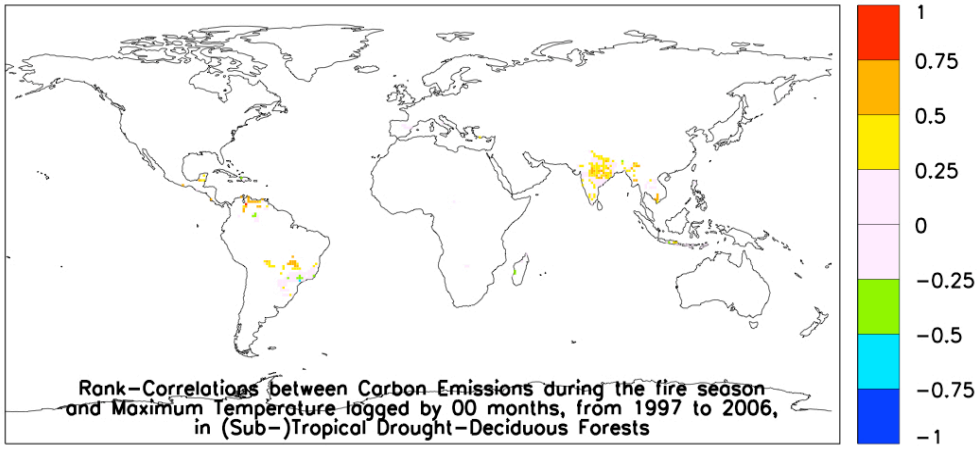

Figure 3.9.1 World maps of rank-correlations between wildfires and a) air humidity and b) air temperature, during the fire season, from 1997 to 2006, in tropical and sub-tropical drought-deciduous forests. Pixels in green and blue show areas where fires increase during a) drier or b) colder weather, whereas yellow, orange and red pixels show areas where fires increase with a) more humid or b) warmer weather.

Figure 3.9.2 Time series of carbon emissions, from 1997 to 2006, for an individual pixel in the tropical and sub-tropical drought-deciduous forests of Madagascar, in yellow. A fire model, with monthly averages of minimum daily air humidity used as a predictor, is superposed in black.

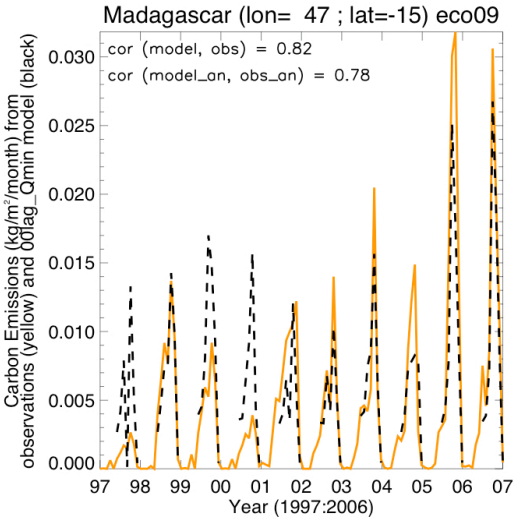

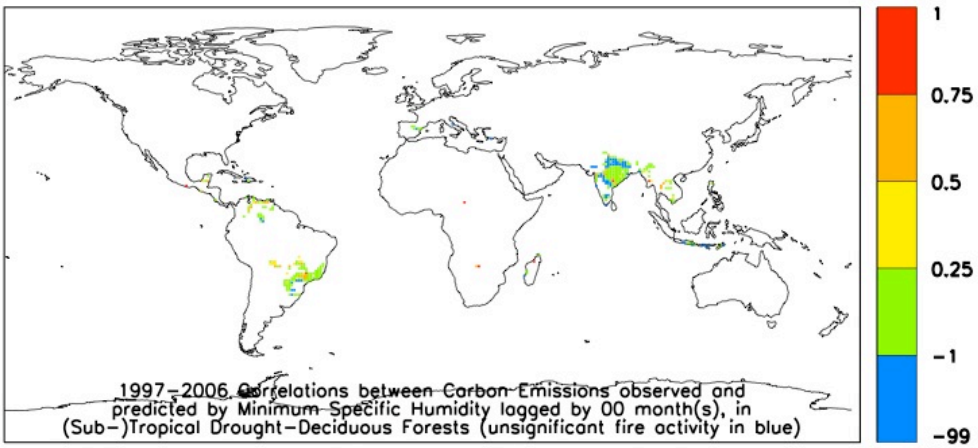

Figure 3.9.3 World map of correlations between model predictions and GFED estimations of carbon emissions from wildfires, from 1997 to 2006, in tropical and sub-tropical drought-deciduous forests, with humidity during the fire season as the predictor. Red pixels have the best models (correlations with observations above 75%), followed by orange and yellow pixels with correlations between 50% and 75%, and between 25% and 50%, respectively. Green pixels do not have reliable models with this predictor. Blue pixels do not show significant fire activity at 1ºx1º resolution.

3.10 Cold-Deciduous Forests with Evergreens

After wet and humid winters, fires decreased in the cold-deciduous forests with evergreens of Iberia, Mediterranean, Central Europe, Russia, South East Asia, Japan and North America (correlation maps and plots not shown).

During warmer and more humid summers, burnt areas increased in Central Europe, Iberia, Mediterranean, Northern Asia, South East Asia, Japan and South East North America, but decreased in Central Asia and Central Eastern Russia (figures 3.10.1).

Both temperature and humidity were positively correlated to biomass burning in the summer, possibly because higher humidity occurs during warmer weather [Gentemann & al., 2008]. Summers in these ecosystems are quite dry, therefore even air humidity higher than usual is not enough to hinder fire ignition or spread.

Although fires were well correlated with temperature and humidity during the fire season, there were not enough fires, during 10 years of data, to obtain reliable models in individual pixels (figure 3.10.2).

a)

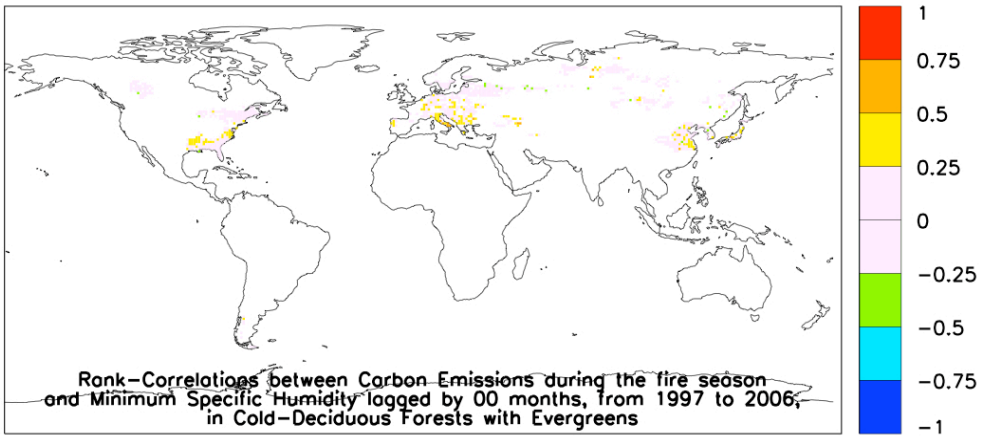

b)

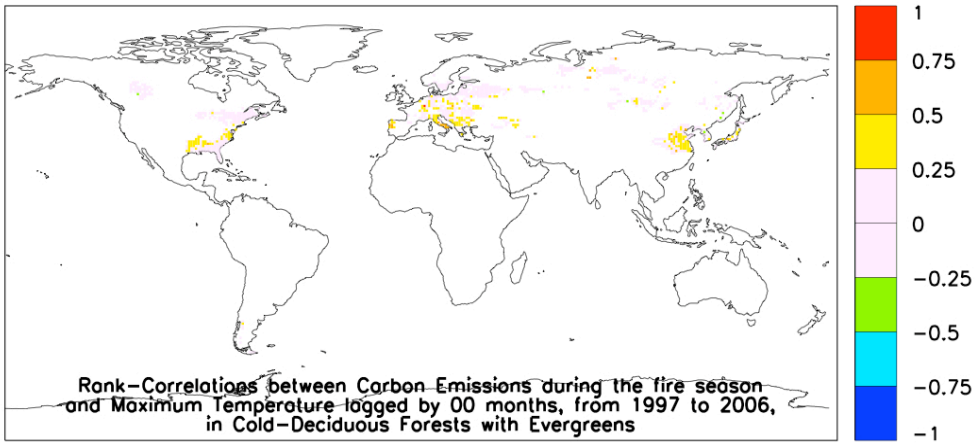

Figure 3.10.1 World maps of rank-correlations between wildfires and a) air humidity and b) air temperature, during the fire season, from 1997 to 2006, in cold-deciduous forests with evergreens. Pixels in green and blue show areas where fires increase during a) drier or b) colder weather, whereas yellow, orange and red pixels show areas where fires increase with a) more humid or b) warmer weather.

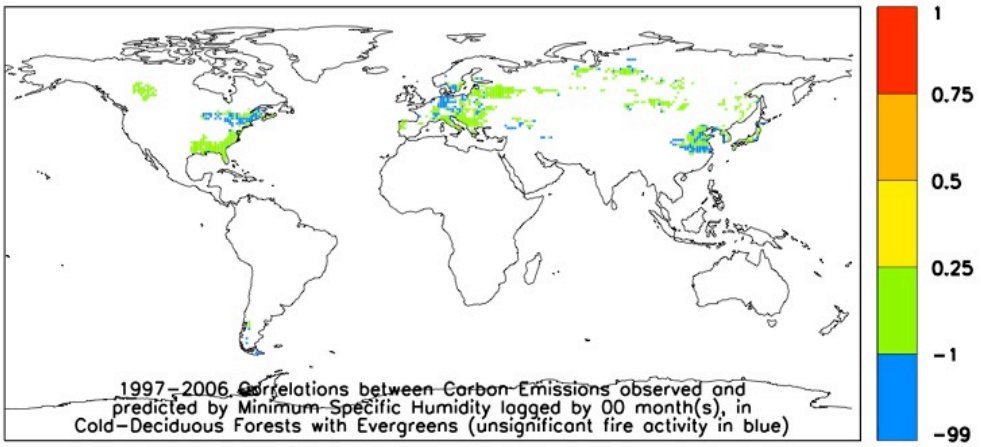

Figure 3.10.2 World map of correlations between model predictions and GFED estimations of carbon emissions from wildfires, from 1997 to 2006, in cold-deciduous forests with evergreens, with humidity during the fire season as the predictor. Green pixels do not have reliable models with this predictor. Blue pixels do not show significant fire activity at 1ºx1º resolution.

3.11 Cold-Deciduous Forests without Evergreens

Cold-deciduous forests without evergreens occupy a large global area, mainly in Europe, West and East Russia and South-Eastern North America.

After a humid winter, fires decreased in Central Europe and North America, but increased in Russia, India, Central and South America. Fires also increased after a snowy winter (correlation maps and plots not shown).

Humid summers had fewer fires in Eastern Russia, Central Asia and in the continental climate of Southern North America, but more in Central Europe and in the maritime climate of South-Eastern North America (figure 3.11.1 a).

Air temperature is probably the main concurrent factor influencing burnt areas in this ecosystem: warmer summers tend to have more fires in these forests (figure 3.11.1 b), and even air humidity

higher than usual is not enough to hinder fire ignition or spread in many areas (figure 3.11.1 a).

Even though consistent correlations were found between biomass burning and concurrent humidity and temperature, in this ecosystem, individual pixels of 1°x1°resolution did not have enough fires, from 1997 to 2006, for any reliable fire models to be obtained (figure 3.11.2).

a)

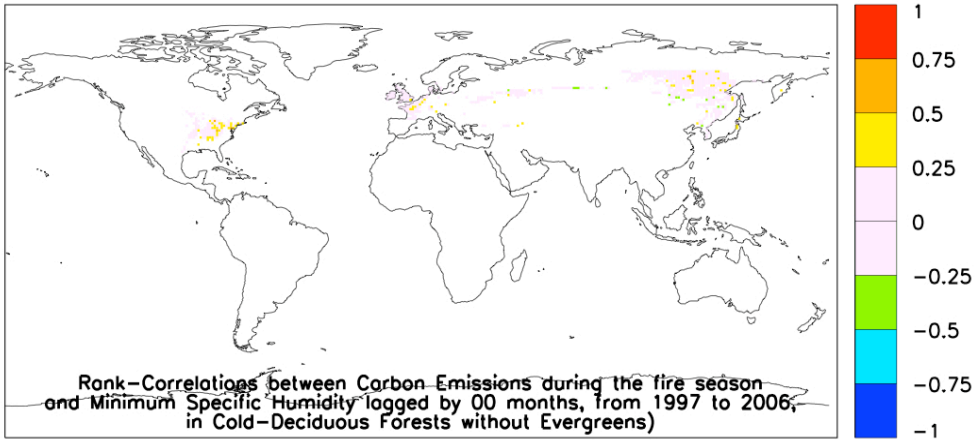

b)

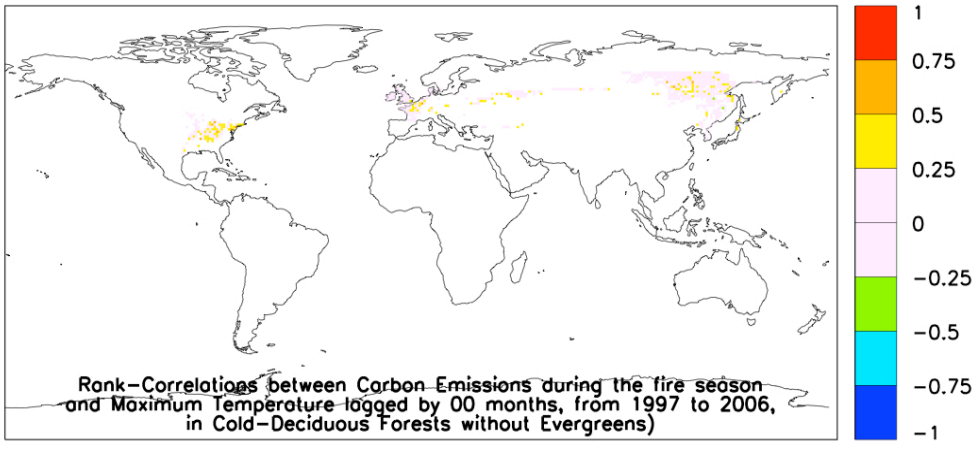

Figure 3.11.1 World maps of rank-correlations between wildfires and a) air humidity and b) air temperature, during the fire season, from 1997 to 2006, in cold-deciduous forests without evergreens. Pixels in green and blue show areas where fires increase during a) drier or b) colder weather, whereas yellow, orange and red pixels show areas where fires increase with a) more humid or b) warmer weather.

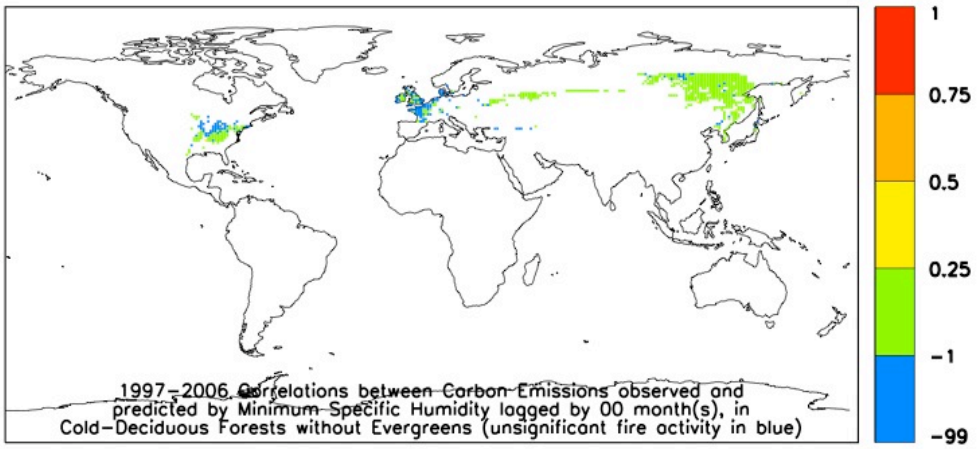

Figure 3.11.2 World map of correlations between model predictions and GFED estimations of carbon emissions from wildfires, from 1997 to 2006, in cold-deciduous forests without evergreens, with humidity during the fire season as the predictor. Green pixels have some fire activity, but do not have reliable models with this predictor. Blue pixels do not show significant fire activity at 1ºx1º resolution.

3.12 Xeromorphic Woodlands

Xeromorphic woodlands are present mainly in Southern North America, Central America, South America and India, with small areas in Equatorial Africa.

After rainy and humid winters, there were larger burnt areas during the following fire season in Equatorial Africa, India, Central America and Northern South America. After 7 months, there was no discernible influence of humidity (correlation maps and plots not shown).

During humid fire seasons, wildfires moderately decreased in India, Central America, Central and Southern South America, except in the western coast (figure 3.12.1 a). Burnt areas tended to be smaller when the soil was wetter (figure 3.12.2). In the western coast of South America, fires had a different behaviour: they increased during humid fire seasons, but decreased after humid winters (figure

3.12.1 a). Burnt areas increased with warm weather during the fire season (figure 3.12.1 b).

In a few isolated pixels of South America (figure 3.12.3), the decrease in biomass burning with air humidity and soil wetness in this ecosystem was regular enough (figure 3.12.2) to obtain some good correlations (superior to 75%) between models and observations, but these models were poor predictors of anomalies.

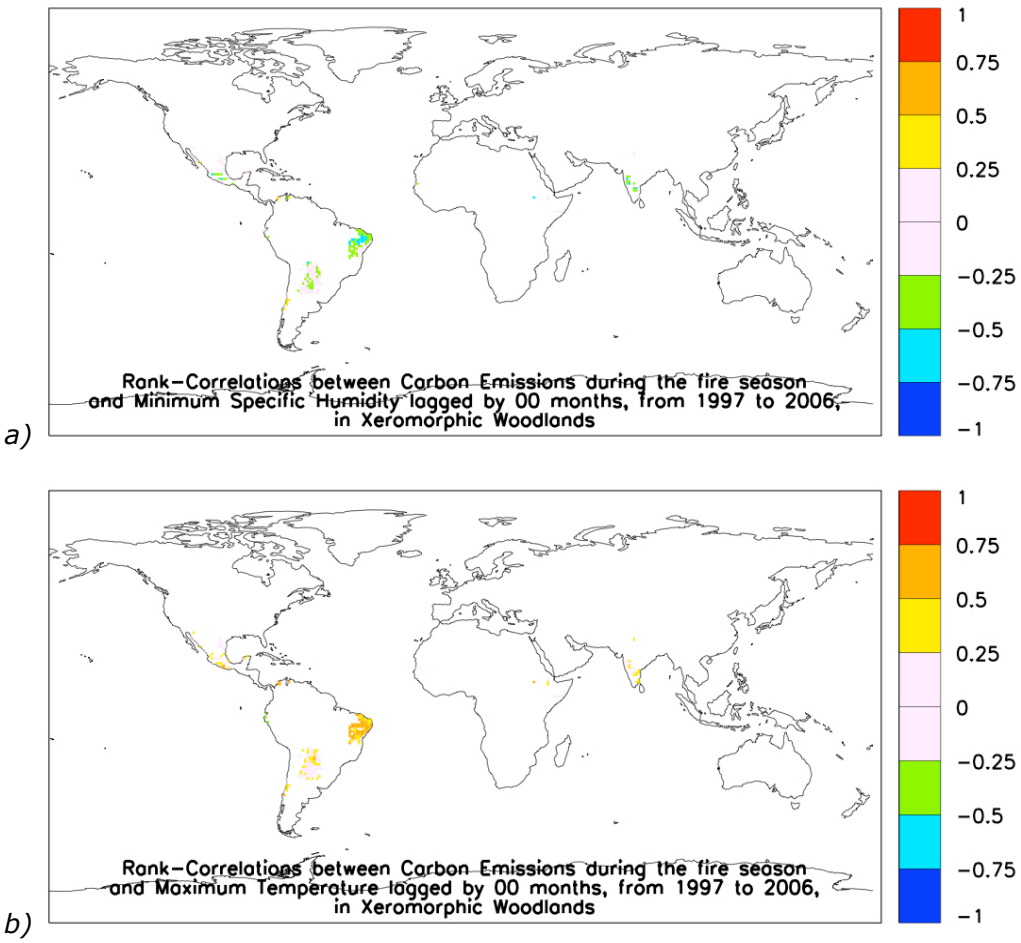

Figure 3.12.1 World maps of rank-correlations between wildfires and a) air humidity and b) air temperature, during the fire season, from 1997 to 2006, in xeromorphic woodlands. Pixels in green and blue show areas where fires increase during a) drier or b) colder weather, whereas yellow, orange and red pixels show areas where fires increase with a) more humid or b) warmer weather.

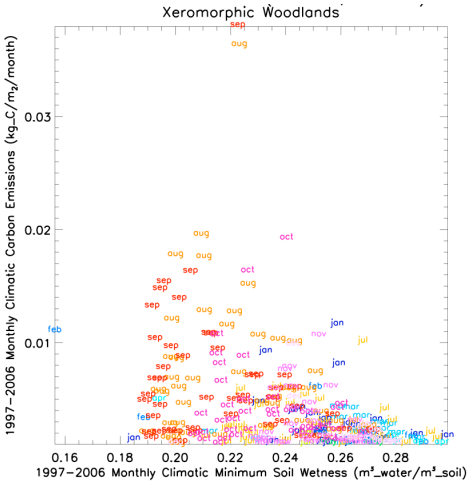

Figure 3.12.2 Scatterplot of carbon emissions from wildfires versus minimum soil wetness, in the xeromorphic woodlands of Southern South America. Each point corresponds to a pixel of 1ºx1º resolution, with values averaged over homonymous months, from 1997 to 2006. Fires tend to decrease with soil wetness.

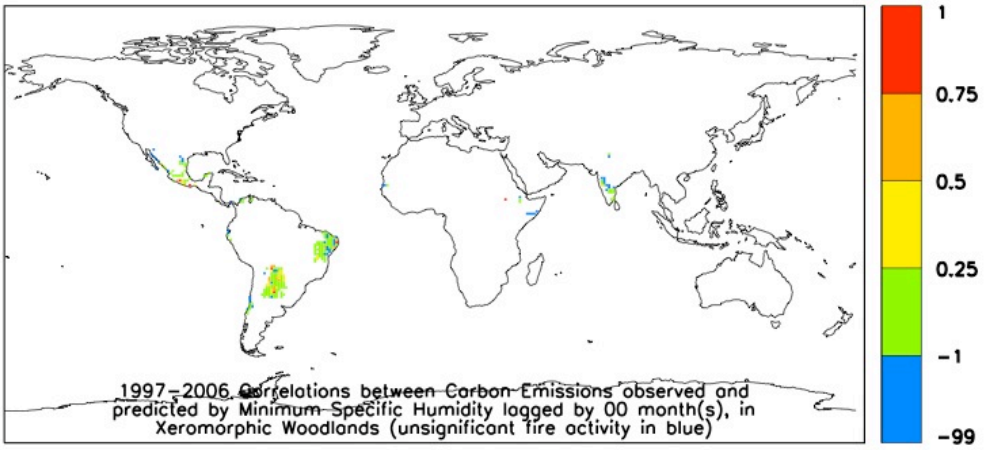

Figure 3.12.3 World map of correlations between model predictions and GFED estimations of carbon emissions from wildfires, from 1997 to 2006, in xeromorphic woodlands, with humidity during the fire season as the predictor. Red pixels have the best models (correlations with observations above 75%), followed by orange and yellow pixels with correlations between 50% and 75%, and between 25% and 50%, respectively. Green pixels do not have reliable models with this predictor. Blue pixels do not show significant fire activity at 1ºx1º resolution.

3.13 Evergreen Broad-Leaved Sclerophyllous Woodlands

Fires in the evergreen broad-leaved sclerophyllous woodlands of Iberia, Mediterranean, Southern Africa and some regions of Eastern and Northern Australia, decreased after a humid winter (figure 3.13.1), but increased in Equatorial Africa and in certain regions of Northern and Southern Australia. After a snowy winter, fires tended to increase (correlation maps and plots not shown).

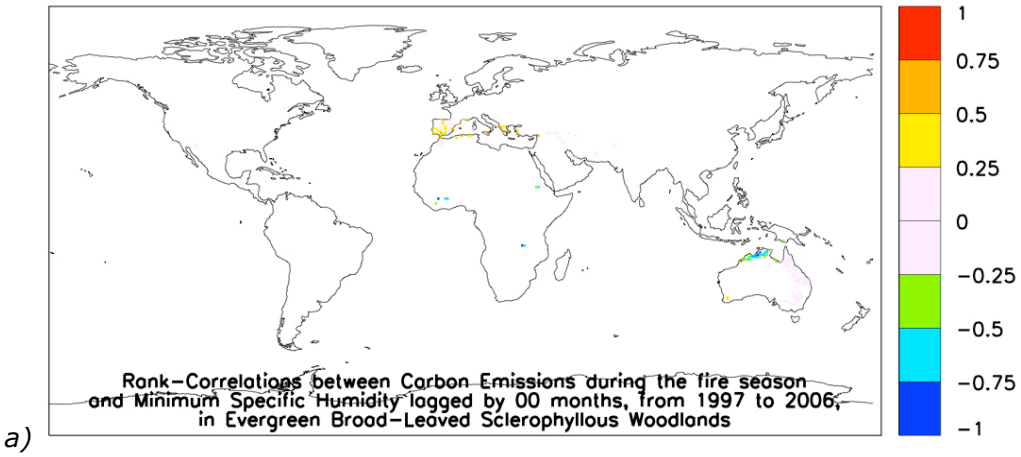

a)

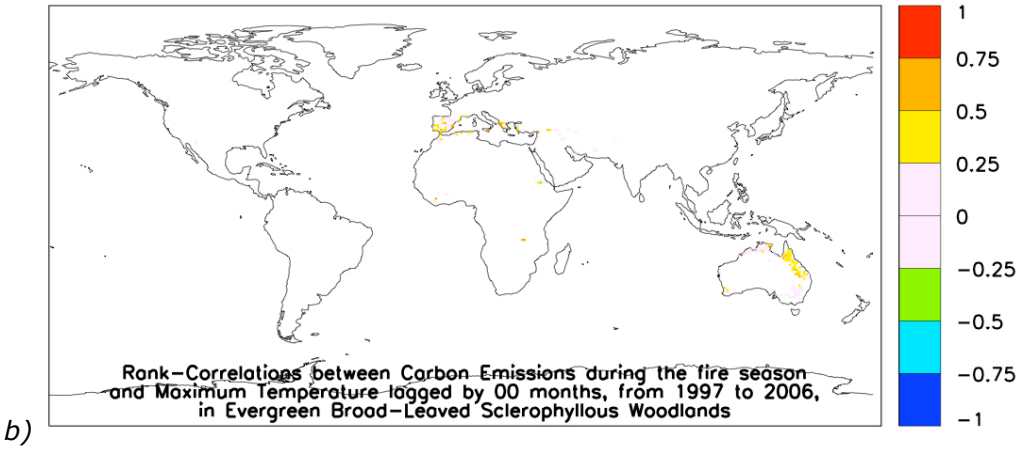

b)

Figure 3.13.1 World maps of rank-correlations between wildfires and a) air humidity and b) air temperature, during the fire season, from 1997 to 2006, in evergreen broad-leaved sclerophyllous woodlands. Pixels in green and blue show areas where fires increase during a) drier or b) colder weather, whereas yellow, orange and red pixels show areas where fires increase with a) more humid or b) warmer weather.

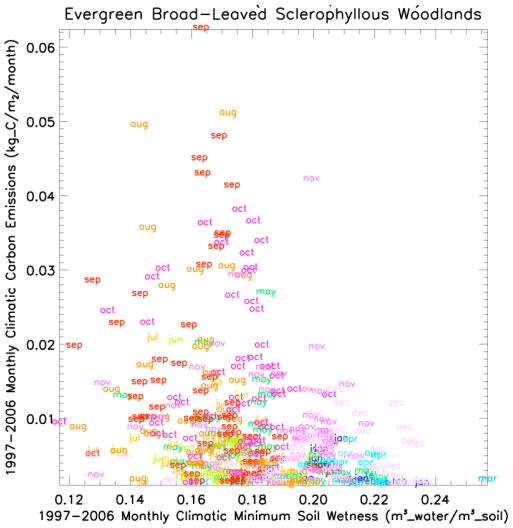

Figure 3.13.2 Scatterplot of carbon emissions from wildfires versus minimum soil wetness, in the evergreen broad-leaved sclerophyllous woodlands of Northern Australia. Each point corresponds to a pixel of 1ºx1º resolution, with values averaged over homonymous months, from 1997 to 2006. Biomass burning tends to decrease with soil wetness.

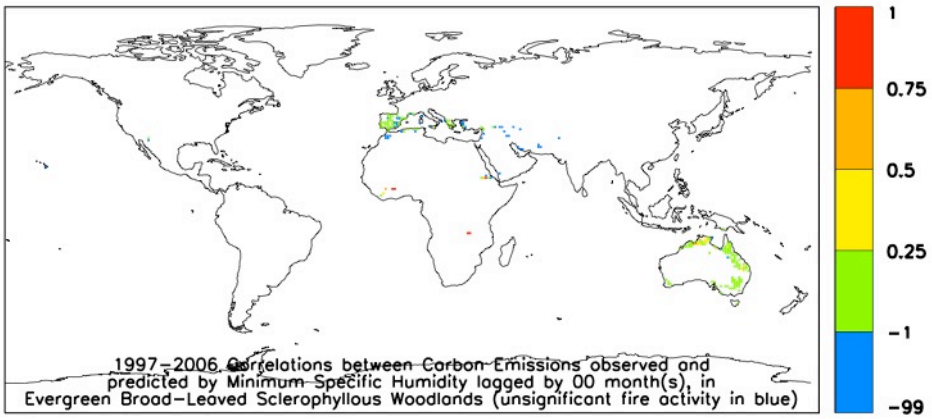

Figure 3.13.3 World map of correlations between model predictions and GFED estimations of carbon emissions from wildfires, from 1997 to 2006, in evergreen broad-leaved sclerophyllous woodlands, with humidity during the fire season as the predictor. Red pixels have the best models (correlations with observations above 75%), followed by orange and yellow pixels with correlations between 50% and 75%, and between 25% and 50%, respectively. Green pixels do not have reliable models with this predictor. Blue pixels do not show significant fire activity at 1ºx1º resolution.

During more humid summers, fires decreased in Africa and Northern Australia, but increased in Iberia, Mediterranean and South West

Australia (figure 3.13.1). Biomass burning decreased with soil wetness in Northern Australia (figure 3.13.2).

Fires in this ecosystem were too irregular to obtain good predictive models, though some isolated pixels in Africa show a more consistent behaviour (figure 3.13.3).

3.14 Evergreen Needle-Leaved Woodlands

Evergreen needle-leaved woodlands occupy a large area in North America, and smaller areas in West Russia, West Asia and South East Asia.

After a wet and humid winter, fires decreased in North America, but increased in Central America. More humid summers had fewer fires in West Asia, South East Asia and Central America, but more in North America (figure 3.14.2). This effect of humidity was not so much evident in individual pixels as in scatterplots of carbon emissions versus air and soil humidity, in a whole eco-region: these show an increase of burnt areas during more humid summers in Northern North America (figure 3.14.2), possibly because of higher temperatures being associated with higher humidity at sub-polar latitudes (figure 3.14.1). This is corroborated by the fact that larger burnt areas in South East Asia, North America (figure 3.14.2) and Central America tend to occur during warmer summers (figure 3.14.1), with higher humidity (figure 3.14.3).

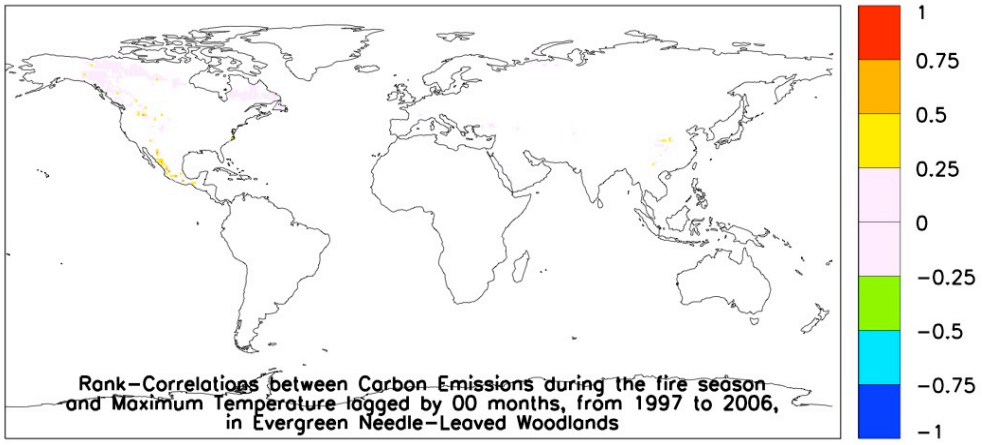

Figure 3.14.1 World maps of rank-correlations between wildfires and air temperature, during the fire season, from 1997 to 2006, in evergreen needle-leaved woodlands. Pixels in green and blue show areas where fires increase during colder weather, whereas yellow, orange and red pixels show areas where fires increase with warmer weather.

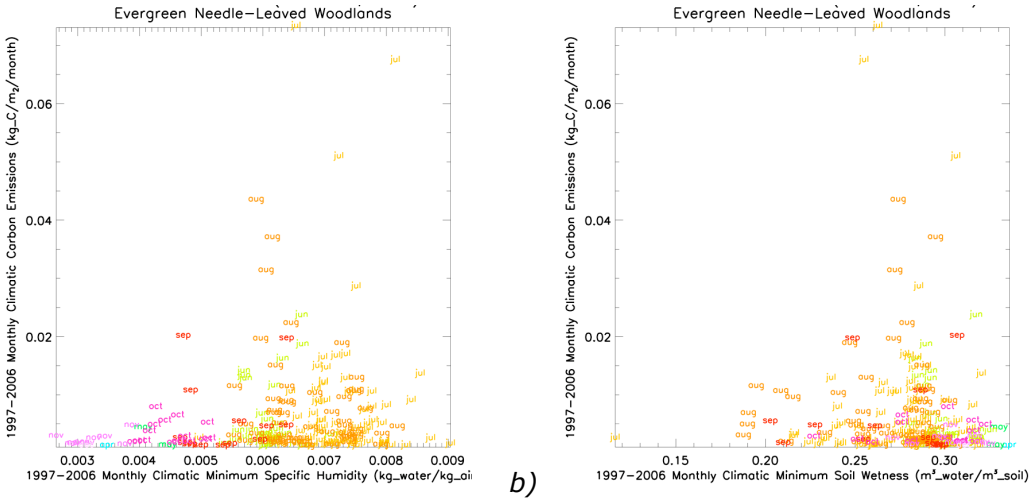

Figure 3.14.2 Scatterplot of carbon emissions from wildfires versus minimum specific humidity (a) and versus minimum soil wetness (b), in the evergreen needle-leaved woodlands of Northern North America. Each point corresponds to a pixel of 1ºx1º resolution, with values averaged over homonymous months, from 1997 to 2006. Fires increase during periods of higher humidity, which occur during the summer.

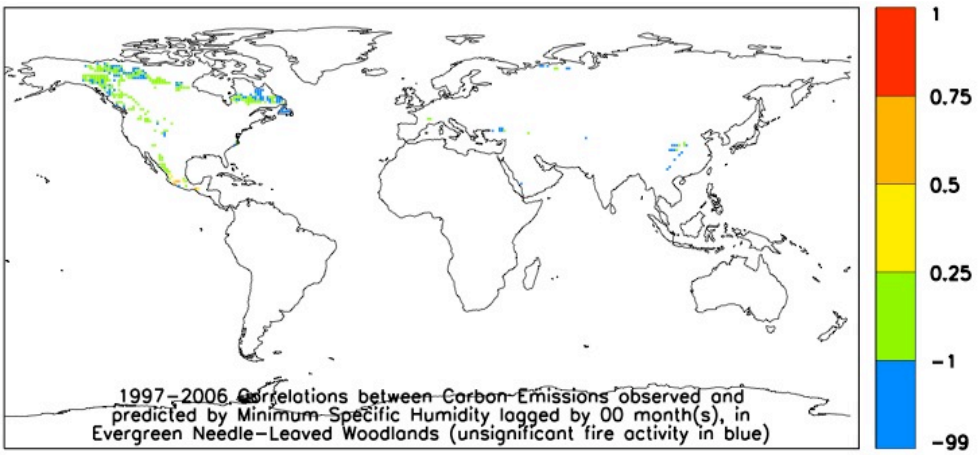

Figure 3.14.3 World map of correlations between model predictions and GFED estimations of carbon emissions from wildfires, from 1997 to 2006, in evergreen needle-leaved woodlands, with humidity during the fire season as the predictor. Red pixels have the best models (correlations with observations above 75%), followed by orange and yellow pixels with correlations between 50% and 75%, and between 25% and 50%, respectively. Green pixels do not have reliable models with this predictor. Blue pixels do not show significant fire activity at 1ºx1º resolution.

3.15 (Sub-)Tropical Drought-Deciduous Woodlands

Drought-deciduous woodlands occupy a large area in tropical and sub-tropical zones of Africa and smaller areas in India and South East Asia. They are generally absent from the equatorial zone, except in the very windy area of Eastern Equatorial Africa.

After a rainy and humid winter, fires increased in Africa (except in monsoon West Africa), India and South East Asia (figures 3.15.2).

During dry seasons more humid than average, fires decreased in North Africa, Southern Africa, India and South East Asia (figures 3.15.1 a, 3.15.3-5). The seasonal cycle was quite strong (figures 3.15.2), with well-defined dry and wet seasons, but there was also some interannual variability. For a few individual pixels (figure

3.15.5), this variability can be approximately reproduced, in models with air humidity as the predictor.

The positive correlations with rainfall at longer lags are probably indicative of an increase in short time-scale biomass, like understory vegetation, in forests, or grass, in grasslands, giving more fuel load to burn during the next fire season. This suggests that rain during the growing season contributes to more bio-fuel being available to burn during the following fire season, resulting in larger burnt areas, whereas recent rainfall tends to prevent fires (figures 3.15.3).

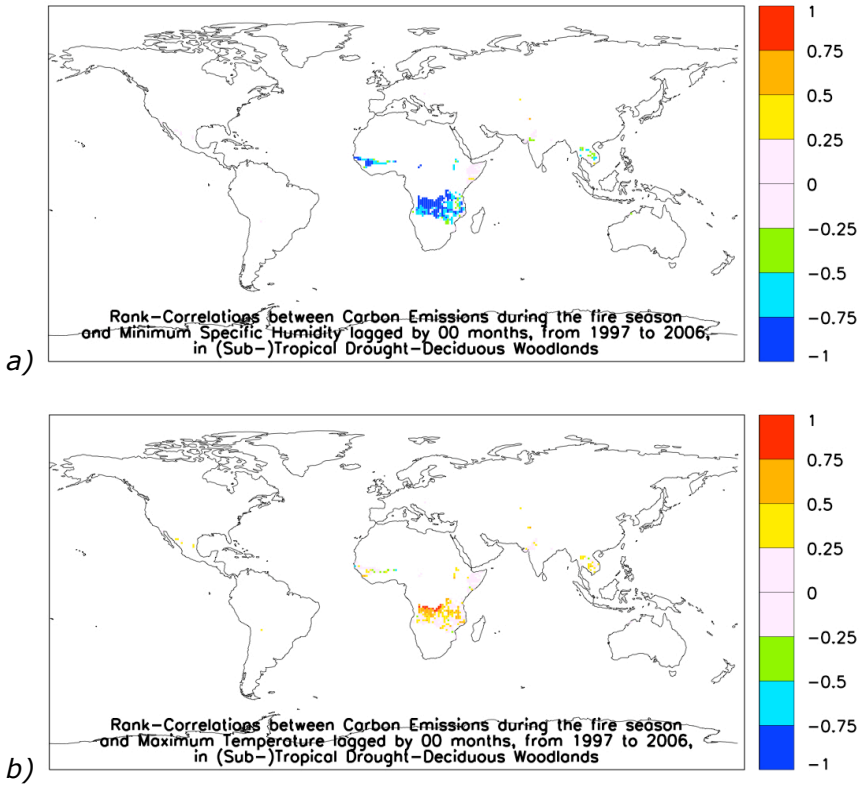

Figure 3.15.1 World maps of rank-correlations between wildfires and a) air humidity and b) air temperature, during the fire season, from 1997 to 2006, in tropical and sub-tropical drought-deciduous woodlands. Pixels in green and blue show areas where fires increase during a) drier or b) colder weather, whereas yellow, orange and red pixels show areas where fires increase with a) more humid or b) warmer weather.

High temperatures during the fire season were correlated with increased carbon emissions, except in the West African monsoon region, where convective rainfall occurred during the warmest weather (figure 3.15.1 b).

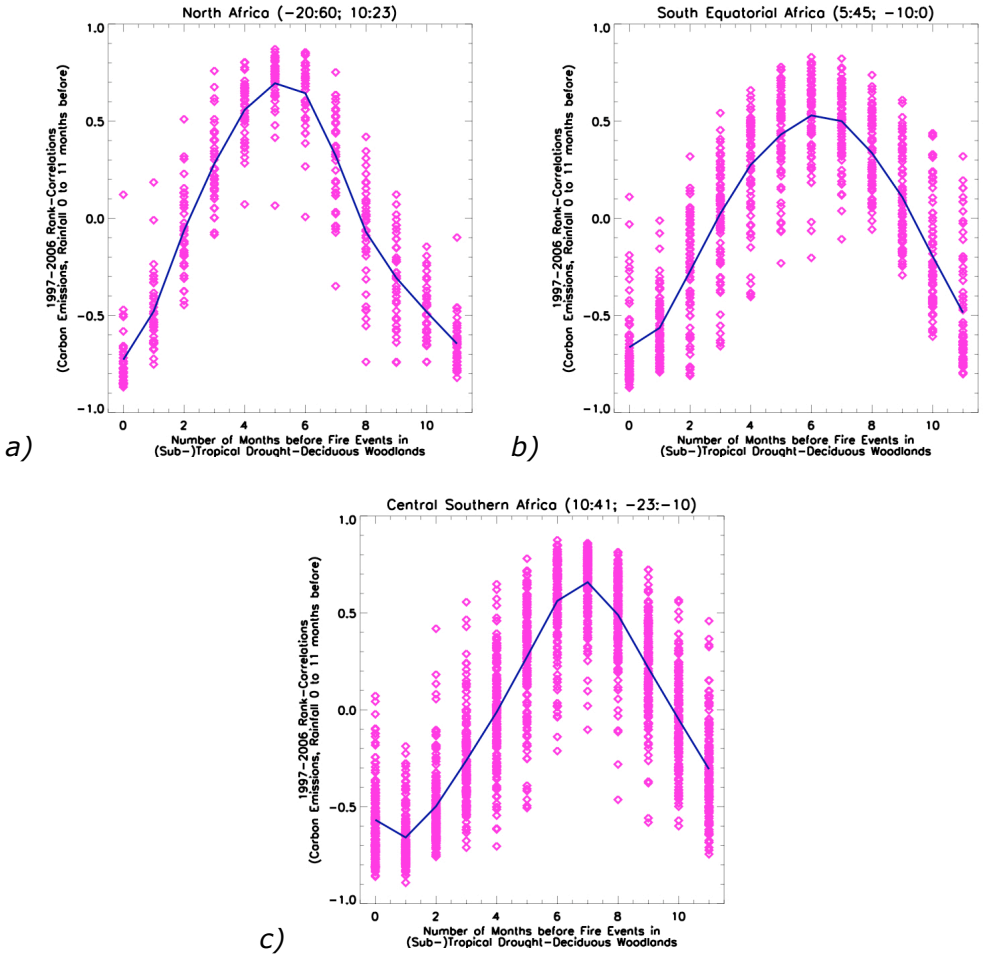

Figure 3.15.2 Scatterplot of rank-correlations between monthly carbon emissions during the fire season and monthly rainfall, contemporary and up to 11 months before, versus the lags, i.e., the number of months by which the rain preceded the fire, in all the 1ºx1º resolution pixels with significant fire activity of the tropical and sub-tropical drought-deciduous woodlands of North Africa (a), South Equatorial Africa (b) and Central Southern Africa (c), from 1997 to 2006. Different pixels of an eco-region show different rank-correlations between fires and rainfall, but there are mainly negative correlations for lags up to 2 months, and positive for lags of 4 to 7 (a), 3 to 9 (b) and 5 to 9 months (c). This pattern is repeated for larger lags, showing the dominance of the seasonal cycle in these eco-regions.

Lightning was usually associated with convective rainfall, so wildfires decrease when lightning concurrently increases, but increase with lightning during the previous growing season. In the monsoon area of West Africa, lightning can be used as a proxy for rainfall (3.15.8).

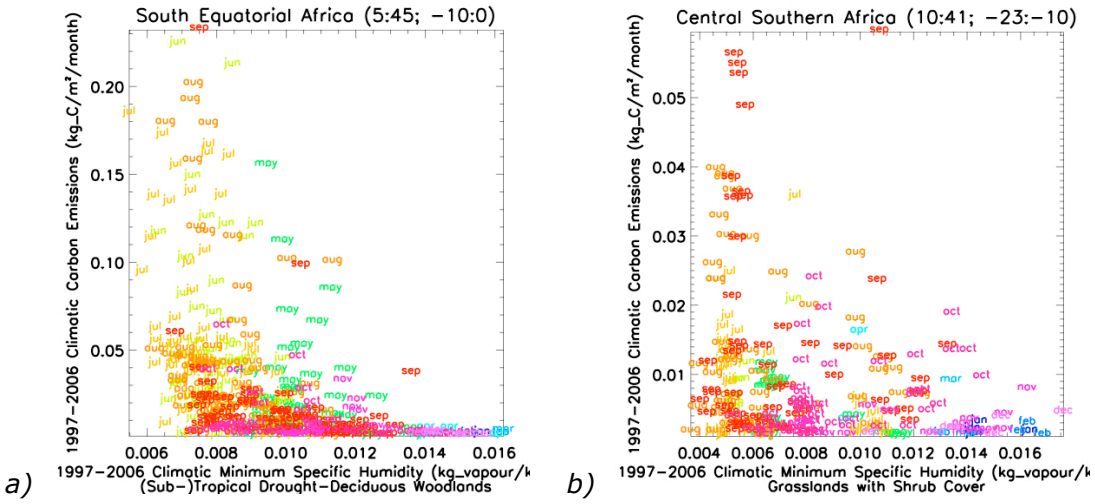

a) b)

Figure 3.15.3 Scatterplot of carbon emissions versus minimum specific humidity in the tropical and subtropical drought-deciduous woodlands of South Equatorial Africa (a) and Central Southern Africa (b). Each point corresponds to a pixel of 1ºx1º resolution, with values averaged over homonymous months, from 1997 to 2006.

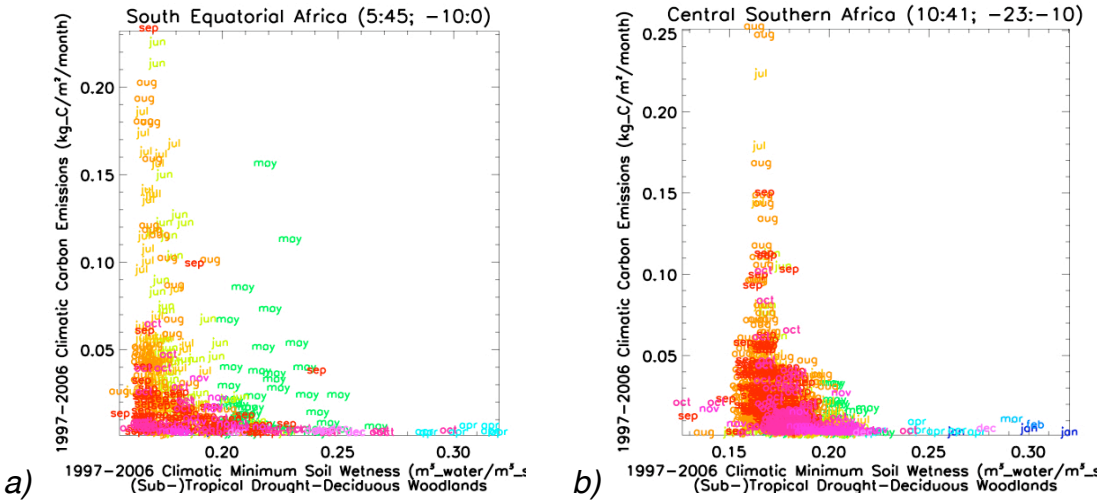

a) b)

Figure 3.15.4 Scatterplot of carbon emissions versus minimum soil wetness in the tropical and subtropical drought-deciduous woodlands of South Equatorial Africa (a) and Central Southern Africa (b). Each point corresponds to a pixel of 1ºx1º resolution, with values averaged over homonymous months, from 1997 to 2006.

Drought-deciduous woodlands are one of the ecosystems with more fires and where fire behaviour is more predictable. Good fire models (correlation with observations superior to 75%) were obtained for all sub-tropical Africa and South East Asia. The best predictors are lagged rainfall, as a proxy for fuel load during the dry season, soil and air temperature, soil wetness and air humidity (figures 3.15.5-8).

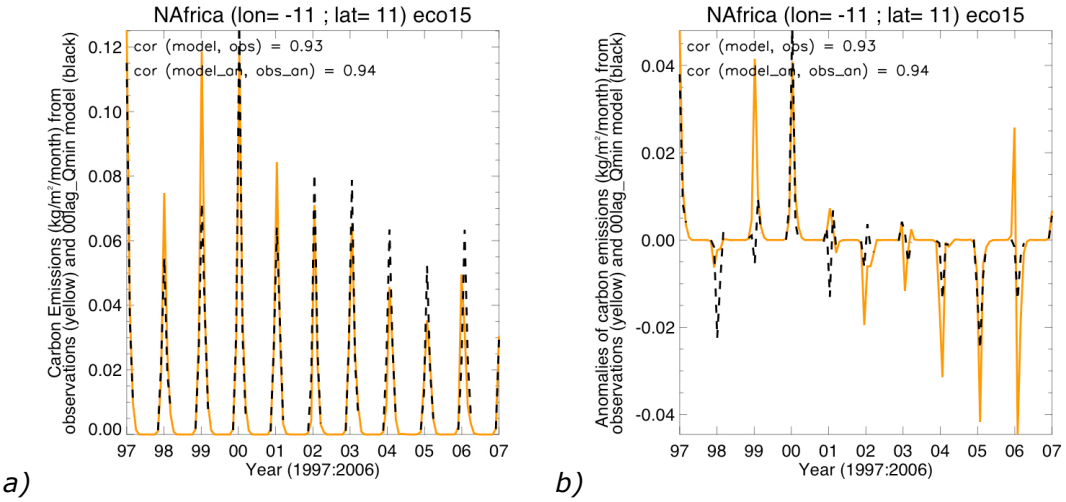

a) b)

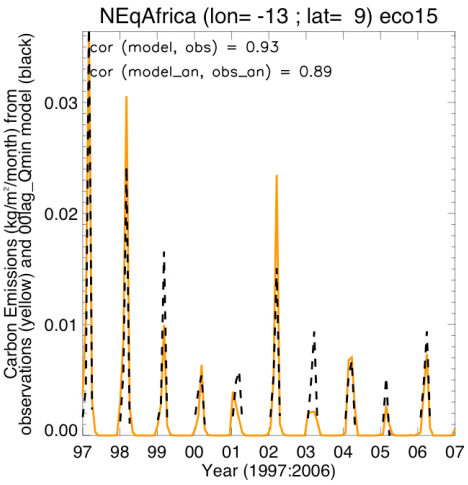
NEqAfrica (lon= -13 ; lat= 9) eco15
cor (model, obs) = 0.93
cor (model_an, obs_an) = 0.89
Carbon Emissions (kg/m²/month) from observations (yellow) and 00lag_Qmin model (black)
0.00
0.01
0.02
0.03
97 98 99 00 01 02 03 04 05 06 07
Year (1997:2006)

c)

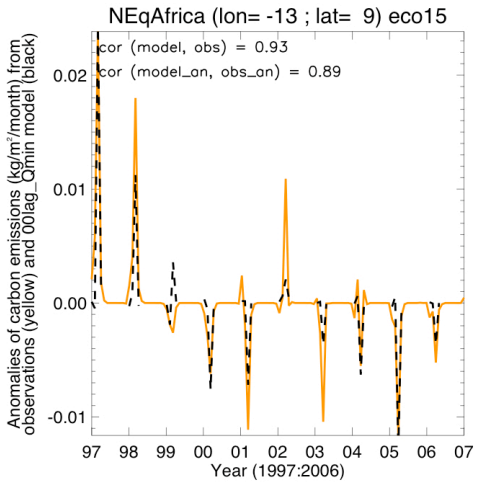
NEqAfrica (lon= -13 ; lat= 9) eco15
cor (model, obs) = 0.93
cor (model_an, obs_an) = 0.89
Anomalies of carbon emissions (kg/m²/month) from observations (yellow) and 00lag_Qmin model (black)
-0.01
0.00
0.01
0.02
97 98 99 00 01 02 03 04 05 06 07
Year (1997:2006)

d)

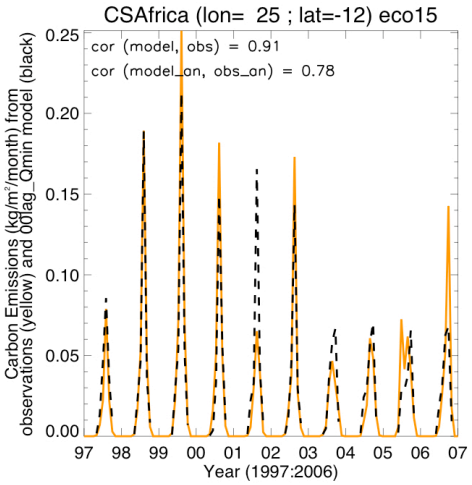
CSAfrica (lon= 25 ; lat=-12) eco15
cor (model, obs) = 0.91
cor (model_an, obs_an) = 0.78
Carbon Emissions (kg/m²/month) from observations (yellow) and 00lag_Qmin model (black)
0.00
0.05
0.10
0.15
0.20
0.25
97 98 99 00 01 02 03 04 05 06 07
Year (1997:2006)

e)

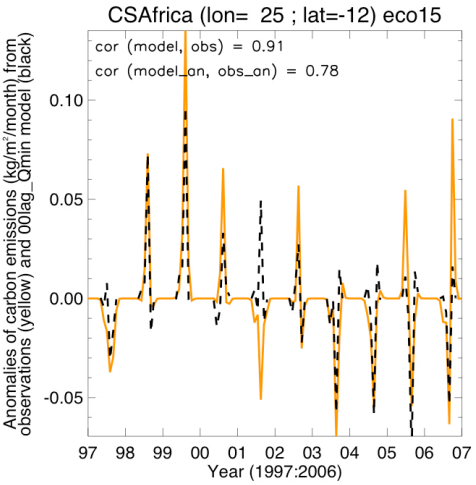
CSAfrica (lon= 25 ; lat=-12) eco15
cor (model, obs) = 0.91
cor (model_an, obs_an) = 0.78
Anomalies of carbon emissions (kg/m²/month) from observations (yellow) and 00lag_Qmin model (black)
-0.05
0.00
0.05
0.10
97 98 99 00 01 02 03 04 05 06 07
Year (1997:2006)

f)

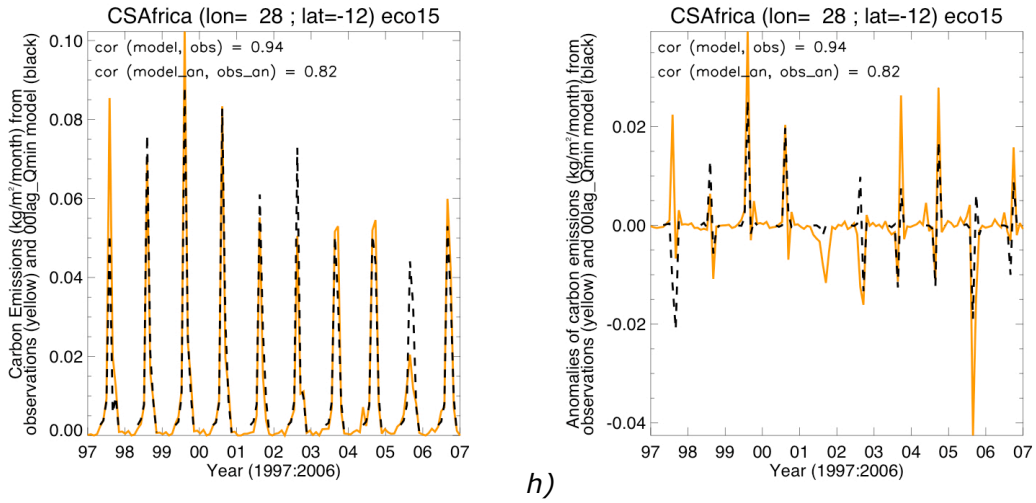

g) *h)*

Figure 3.15.5 Time series of biomass burning (expressed as carbon emissions) and anomalies, from 1997 to 2006, given by GFED estimates, in four individual pixels of the tropical and sub-tropical drought-deciduous woodlands of North Africa (a-b), North Equatorial Africa (c-d) and Central Southern Africa (e-h). Over-plotted in black is a model based on monthly averages of minimum specific humidity. Good correlations (above 75%) between models and GFED estimates show that these models capture a considerable part of the interannual variability in carbon emissions.

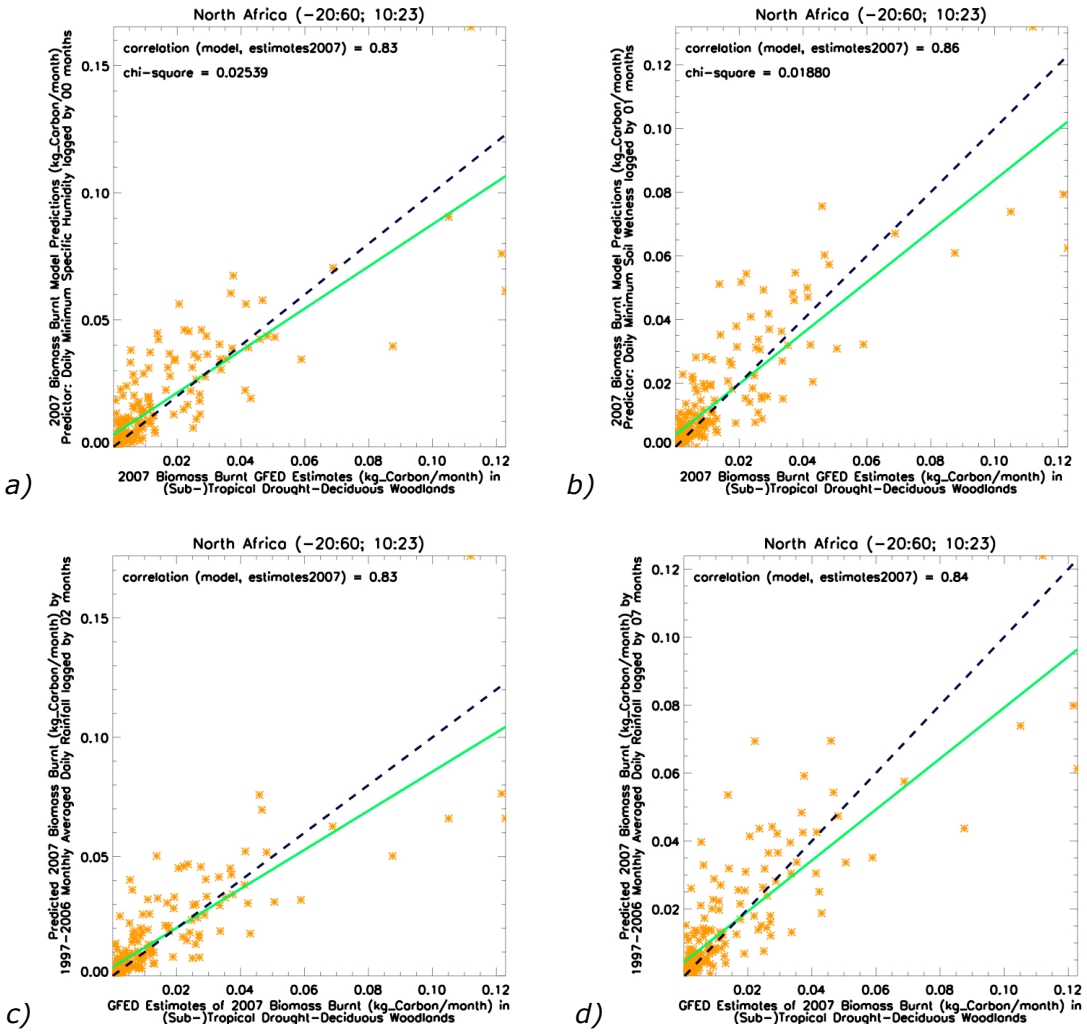

Figure 3.15.6 Scatterplots of predicted biomass burnt for the year of 2007 versus the correspondent GFED estimates, expressed in kilograms of carbon emissions per month, in the tropical and sub-tropical drought-deciduous woodlands of North Africa. The green line shows the linear fit through the points, whereas the black dashed line marks where the 1:1 ideal slope would be. Models are based on monthly averaged daily minimum humidity (a), soil wetness lagged by 1 month (b), and on monthly averaged daily rainfall lagged by 2 (c) and 7 months (d). Only eco-regions where models are correlated by more than 75% with observations are presented.

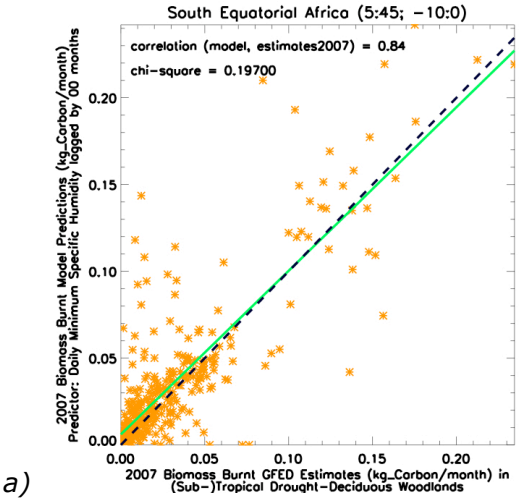
South Equatorial Africa (5:45; −10:0)
correlation (model, estimates2007) = 0.84
chi-square = 0.19700
2007 Biomass Burnt Model Predictions (kg_Carbon/month)
Predictor: Daily Minimum Specific Humidity lagged by 00 months
2007 Biomass Burnt GFED Estimates (kg_Carbon/month) in
(Sub-)Tropical Drought-Deciduous Woodlands
0.00
0.05
0.10
0.15
0.20

a)

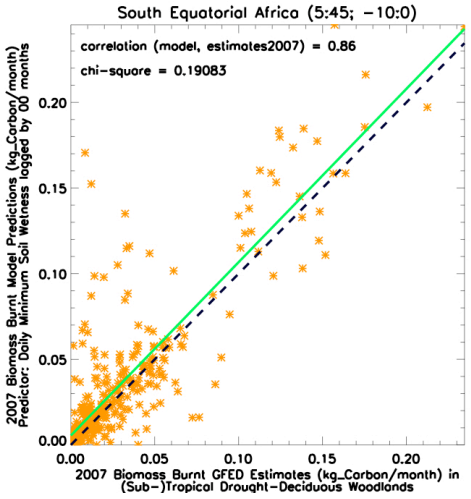
South Equatorial Africa (5:45; −10:0)
correlation (model, estimates2007) = 0.86
chi-square = 0.19083
2007 Biomass Burnt Model Predictions (kg_Carbon/month)
Predictor: Daily Minimum Soil Wetness lagged by 00 months
2007 Biomass Burnt GFED Estimates (kg_Carbon/month) in
(Sub-)Tropical Drought-Deciduous Woodlands
0.00
0.05
0.10
0.15
0.20

b)

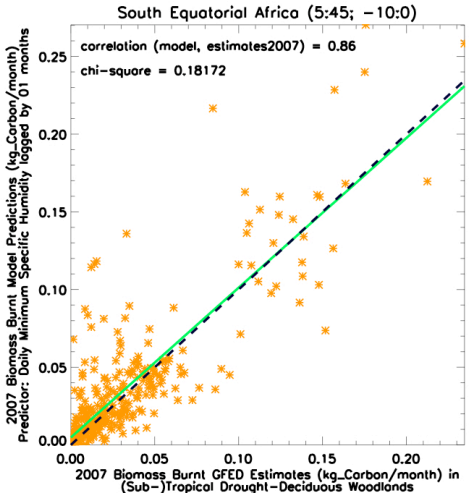
South Equatorial Africa (5:45; −10:0)
correlation (model, estimates2007) = 0.86
chi-square = 0.18172
2007 Biomass Burnt Model Predictions (kg_Carbon/month)
Predictor: Daily Minimum Specific Humidity lagged by 01 months
2007 Biomass Burnt GFED Estimates (kg_Carbon/month) in
(Sub-)Tropical Drought-Deciduous Woodlands
0.00
0.05
0.10
0.15
0.20
0.25

c)

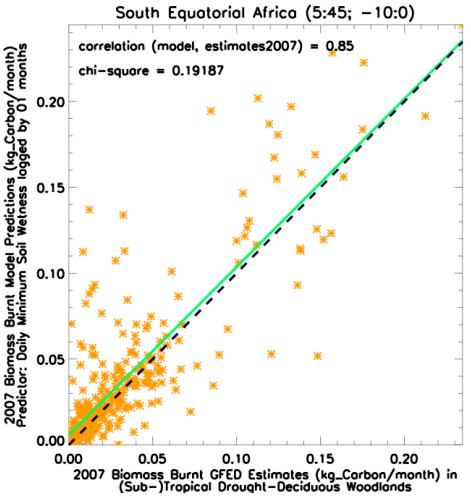
South Equatorial Africa (5:45; −10:0)
correlation (model, estimates2007) = 0.85
chi-square = 0.19187
2007 Biomass Burnt Model Predictions (kg_Carbon/month)
Predictor: Daily Minimum Soil Wetness lagged by 01 months
2007 Biomass Burnt GFED Estimates (kg_Carbon/month) in
(Sub-)Tropical Drought-Deciduous Woodlands
0.00
0.05
0.10
0.15
0.20

d)

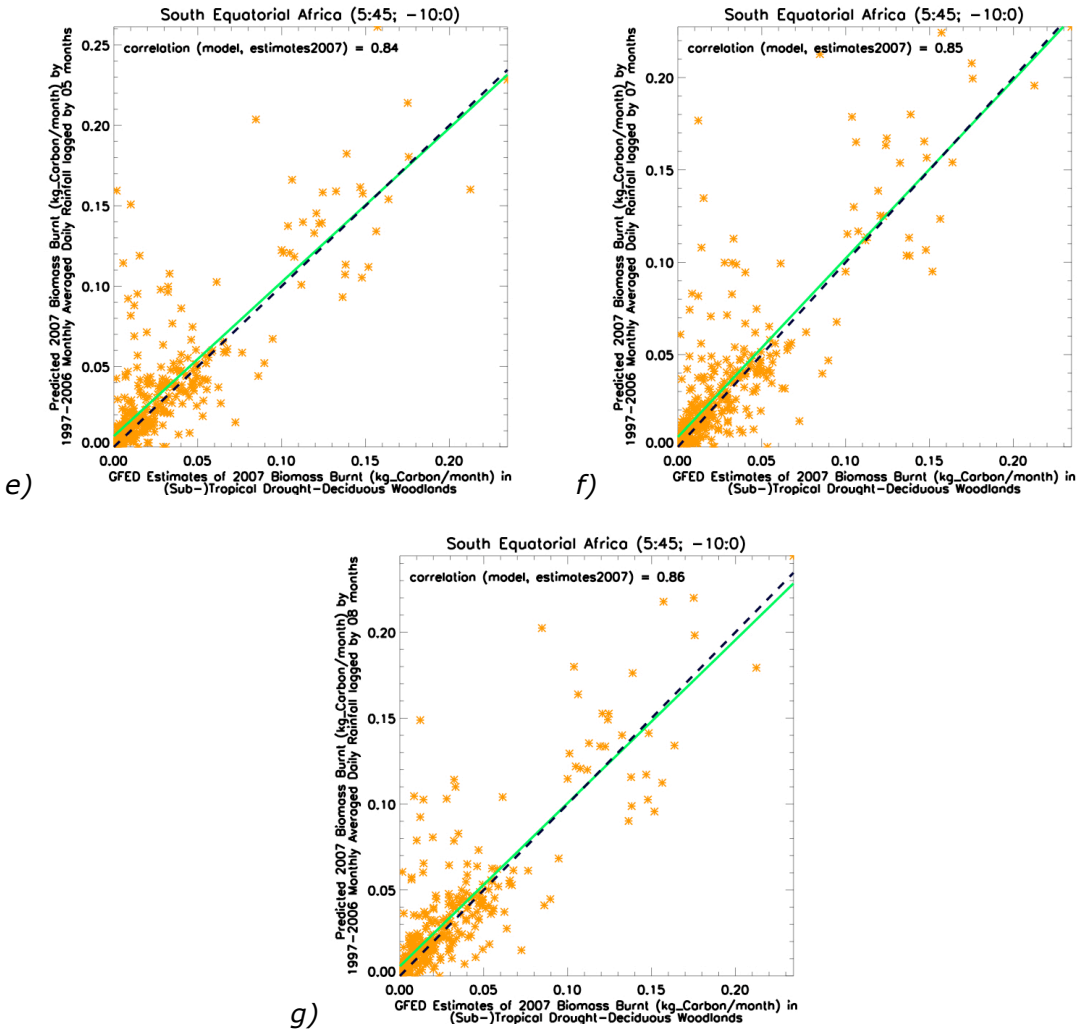

Figure 3.15.7 Scatterplots of predicted biomass burnt for the year of 2007 versus the correspondent GFED estimates, expressed in kilograms of carbon emissions per month, in the tropical and sub-tropical drought-deciduous woodlands of South Equatorial Africa. Models based on monthly averaged daily minimum specific humidity (a) and soil wetness (b), contemporary to the fire events; minimum air humidity (c) and soil wetness (d), lagged by 1 month; and rainfall lagged by 5 (e), 7 (f) and 8 months (g). Only eco-regions where models are correlated by more than 75% with observations are presented.

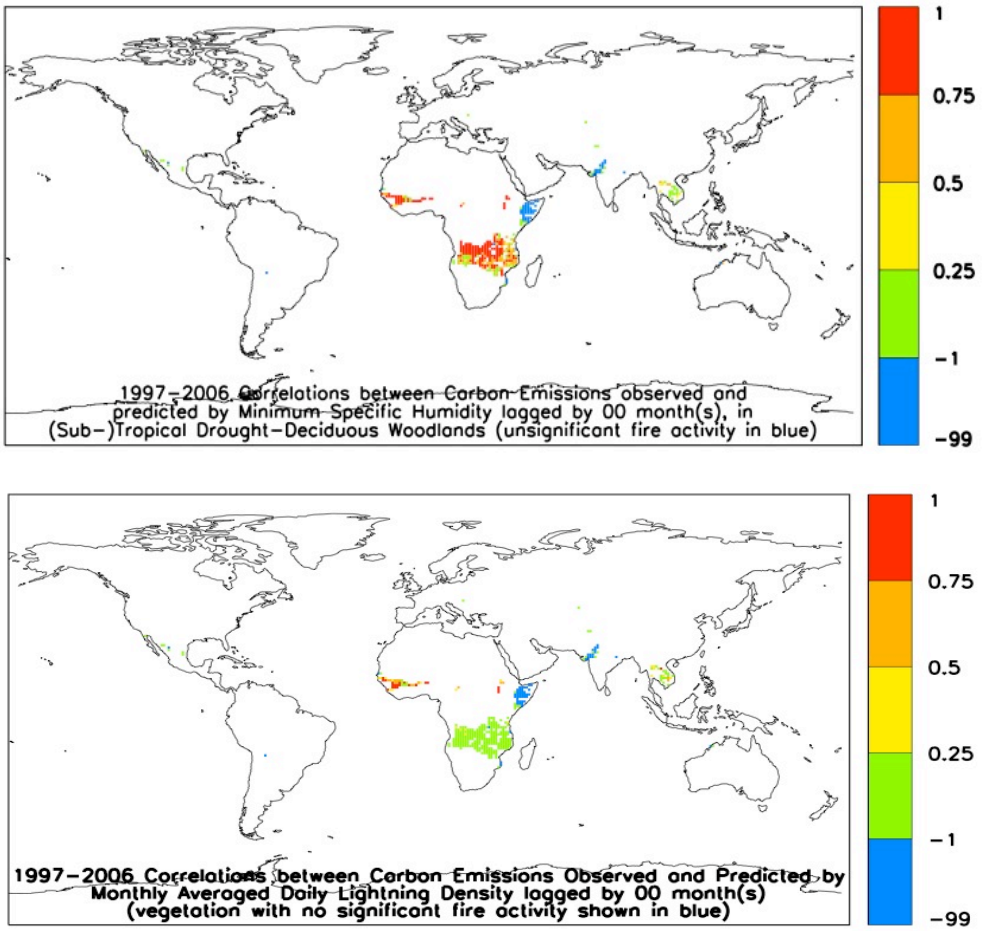

Figure 3.15.8 World map of correlations between model predictions and GFED estimations of carbon emissions from wildfires, from 1997 to 2006, in tropical and sub-tropical drought-deciduous woodlands, with a) specific humidity and b) lightning density during the fire season as the predictor. Red pixels have the best models (correlations with observations above 75%), followed by orange and yellow pixels with correlations between 50% and 75%, and between 25% and 50%, respectively. Green pixels do not have reliable models with these predictors. Blue pixels do not show significant fire activity at 1ºx1º resolution.

3.16 Cold Deciduous Woodlands

Cold-deciduous woodlands occupy large areas in Northern East Russia and Canada. Fires in this ecosystem are infrequent, possibly because of the low temperatures throughout the year.

During the fire season, in the summer, air temperature was positively correlated (between 25% and 50%) with biomass burning. Likewise, air humidity was positively correlated (also between 25% and 75%) to larger burnt areas, possibly because, in high latitudes, warmer weather is also more humid, but not as much as to hinder ignition and fire spread (correlation maps and plots not shown).

Fires have a large returning period in this ecosystem, so there were not enough fires, in 10 years of data, to get reliable models for individual pixels (figure 3.16.1).

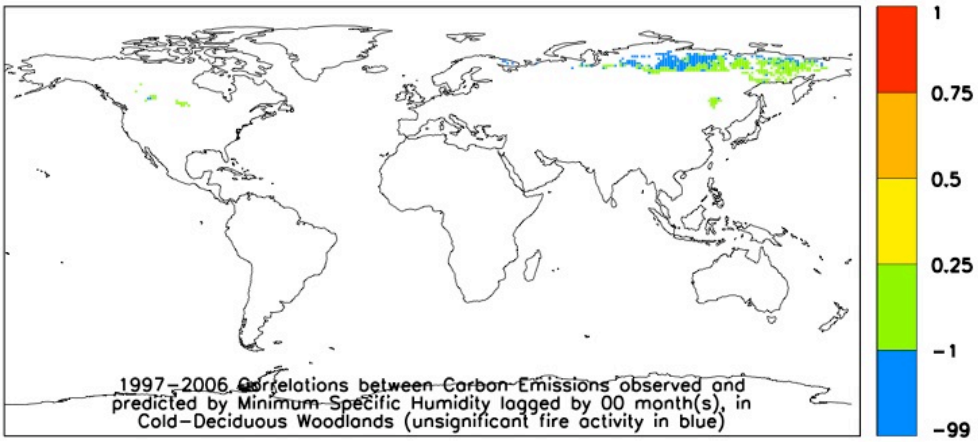

Figure 3.16.1 World map of correlations between model predictions and GFED estimations of carbon emissions from wildfires, from 1997 to 2006, in cold-deciduous woodlands, with humidity during the fire season as the predictor. Red pixels have the best models (correlations with observations above 75%), followed by orange and yellow pixels with correlations between 50% and 75%, and between 25% and 50%, respectively. Green pixels do not have reliable models with this predictor. Blue pixels do not show significant fire activity at 1ºx1º resolution.

3.17 Evergreen Broad-Leaved/ Dwarf Shrublands

Evergreen broad-leaved shrublands are present mainly in the Mediterranean, West Asia, South Southern Africa and western Australia.

After humid winters, there were fewer fires in South Southern Africa and West Asia, but more in Equatorial Africa and South East Asia. Humidity prior to 6 months before the fire season had no discernible influence in fire behaviour (correlation maps and plots not shown).

a)

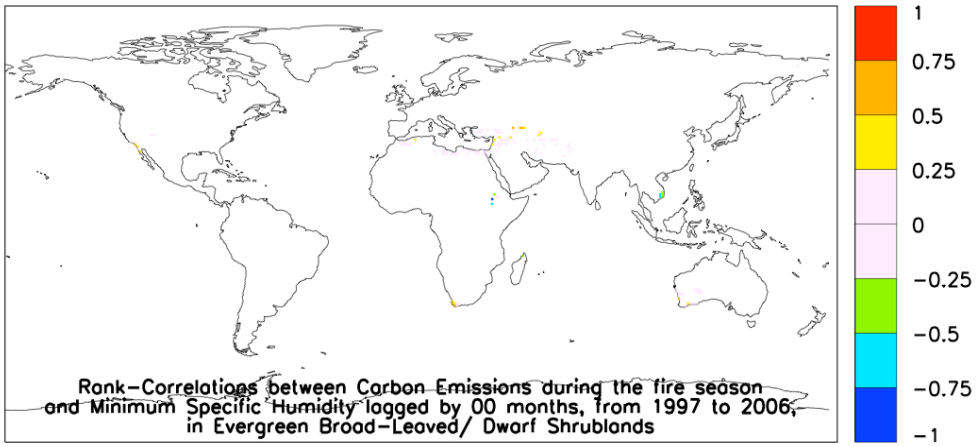

b)

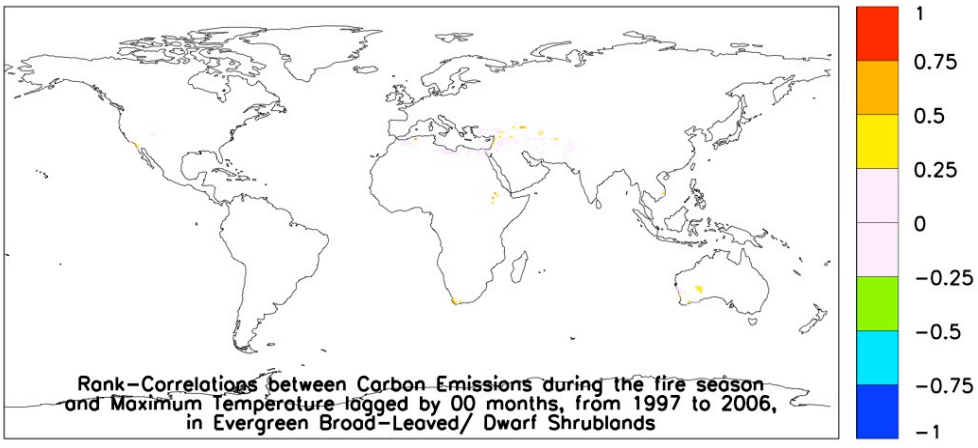

Figure 3.17.1 World maps of rank-correlations between wildfires and air humidity, during the fire season, from 1997 to 2006, in evergreen broad-leaved and dwarf shrublands. Pixels in green and blue show areas where fires increase during drier periods, whereas yellow, orange and red pixels show areas where fires increase with more humid weather.

Again, like in other ecosystems previously presented, humidity in eco-regions of mid-latitudes, namely South Southern Africa, West Asia and South West Australia, had a positive correlation with biomass burning, possibly because higher humidity occurs during the warmest periods (figures 3.17.1). On the equatorial zone, however, namely Equatorial Africa and Asia, burnt areas were negatively correlated with humidity (between 25% and 75%).

Only a few isolated pixels in Equatorial Africa (figure 3.17.2) had models significantly correlated (by more than 75%) with observations, but even those did not accurately describe the variability in biomass burning.

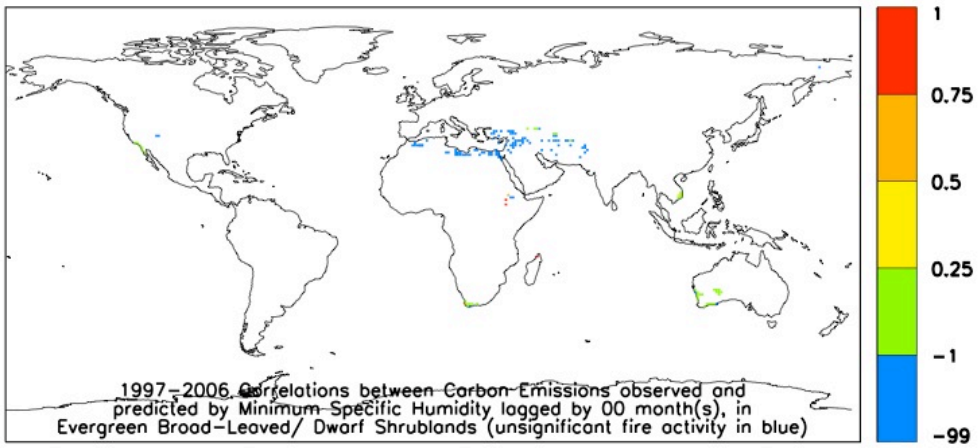

Figure 3.17.2 World map of correlations between model predictions and GFED estimations of carbon emissions from wildfires, from 1997 to 2006, in evergreen broad-leaved and dwarf shrublands, with humidity during the fire season as the predictor. Red pixels have the best models (correlations with observations above 75%), followed by orange and yellow pixels with correlations between 50% and 75%, and between 25% and 50%, respectively. Green pixels do not have reliable models with this predictor. Blue pixels do not show significant fire activity at 1ºx1º resolution.

3.18 Evergreen Needle-Leaved/ Microphyllous Shrublands

Fires occurred mainly during the warmer and more humid periods of the summer season, in the evergreen shrublands of the Mediterranean, Northern Asia, Eastern Russia and Southern North America. Humidity was positively correlated with biomass burning, like in other boreal ecosystems, possibly because fire behaviour varies mainly with temperature in these regions, and humidity is higher during warmer weather.

Not enough fires were detected in pixels of 1°×1°resolution to obtain statistically significant results (figure 3.18.1).

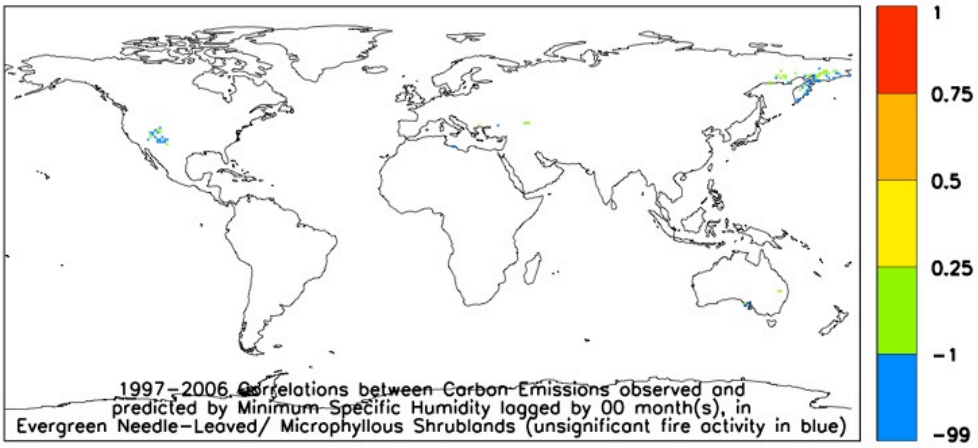

Figure 3.18.1 World map of correlations between model predictions and GFED estimations of carbon emissions from wildfires, from 1997 to 2006, in evergreen needle-leaved and microphyllous shrublands, with humidity during the fire season as the predictor. Red pixels have the best models (correlations with observations above 75%), followed by orange and yellow pixels with correlations between 50% and 75%, and between 25% and 50%, respectively. Green pixels do not have reliable models with this predictor. Blue pixels do not show significant fire activity at 1º×1º resolution.

3.19 Drought-Deciduous Shrublands

Drought-deciduous woodlands occupy small regions in Central Asia, North Southern Africa, Southern North America and the Caribbean.

After a winter more humid than average, fires tended to decrease in Central Asia, but to increase in Southern Africa and in the Caribbean. Fires also tended to increase after a winter with higher snow depth than average, but there was not enough data to conclude if it is just an effect of the seasonal cycle, or if this is due to a drying effect of snow, as described by Pearce (2000), favouring ignition during the following summer season.

Humid summers had fewer fires in this ecosystem (correlation maps and plots not shown). Temperature is negatively correlated with biomass burning in the Caribbean, possibly because warmer weather is associated to convective rainfall.

No reliable predictive fire models were found in drought-deciduous shrublands (figure 3.19.1).

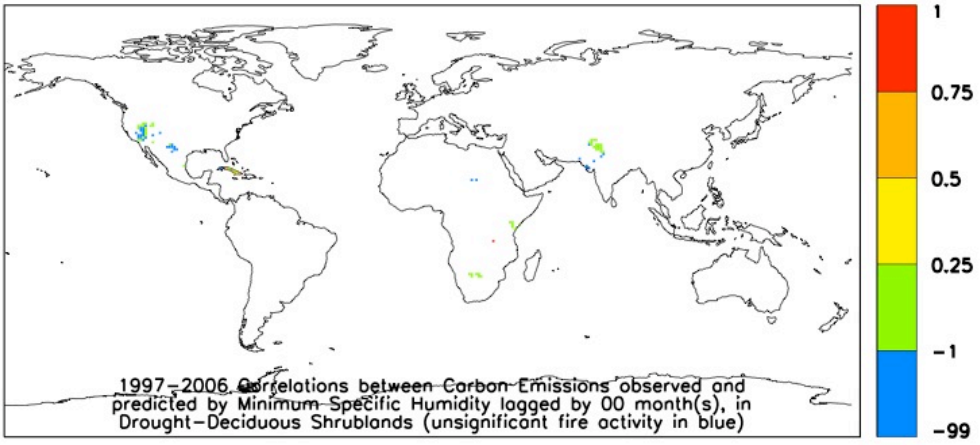

Figure 3.19.1 World map of correlations between model predictions and GFED estimations of carbon emissions from wildfires, from 1997 to 2006, in drought-deciduous shrublands, with air humidity during the fire season as the predictor. Red pixels have the best models (correlations with observations above 75%), followed by orange and yellow pixels with correlations between 50% and 75%, and between 25% and 50%, respectively. Green pixels do not have reliable models with this predictor. Blue pixels do not show significant fire activity at 1ºx1º resolution.

3.20 Cold-Deciduous Sub-Alpine and Sub-Polar Shrublands

Cold-deciduous shrublands are present only in the sub-polar regions of North Northern Asia and Northern Europe.

During the 10 years analyzed, from 1997 to 2006, most pixels did not show any significant fire activity at 1° x 1°resolution, and the others did not have enough regular fires to establish any reliable statistical relationship with climate variability (figure 3.20.1).

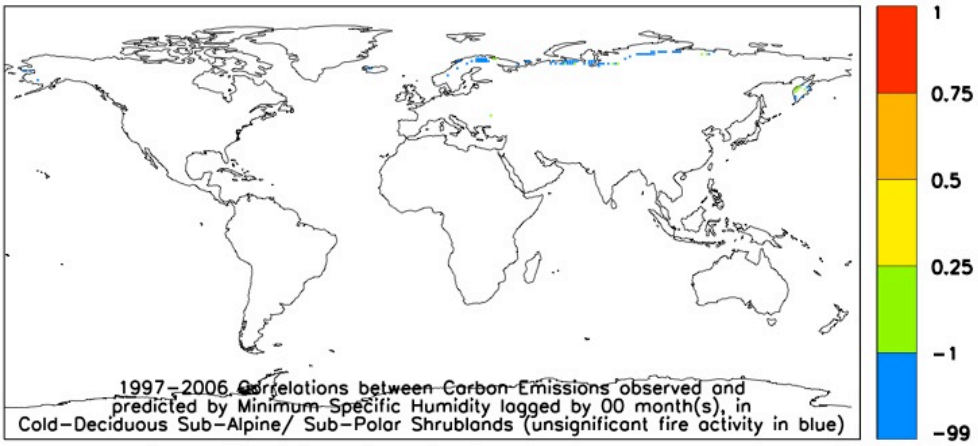

Figure 3.20.1 World map of correlations between model predictions and GFED estimations of carbon emissions from wildfires, from 1997 to 2006, in cold-deciduous sub-alpine and sub-polar shrublands, with humidity during the fire season as the predictor. Pixels in blue do not show significant fire activity at 1ºx1º resolution. Pixels in green have some fire activity, but not enough to provide any reliable models.

3.21 Xeromorphic and Dwarf Shrublands

Xeromorphic shrublands occupy a large global area, mainly in West Asia, Central Asia, Africa, South Australia, west coast of North America and Southern South America.

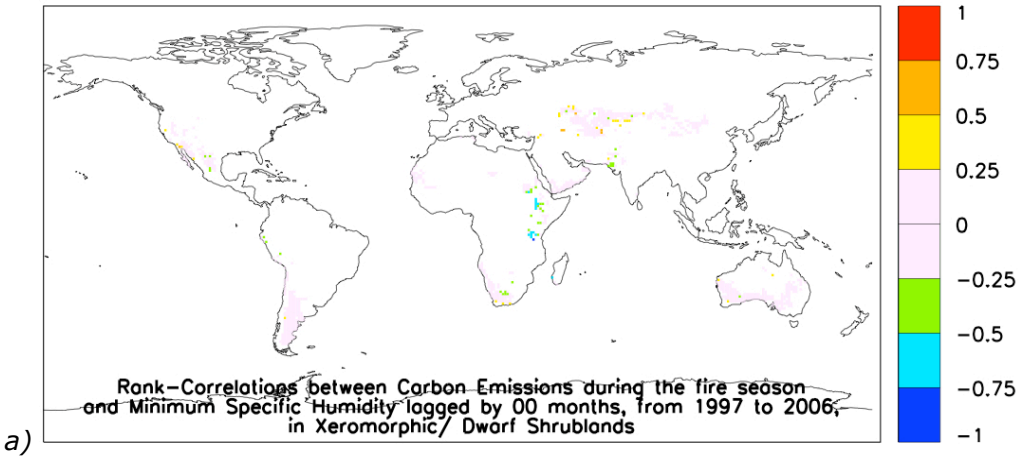

a)

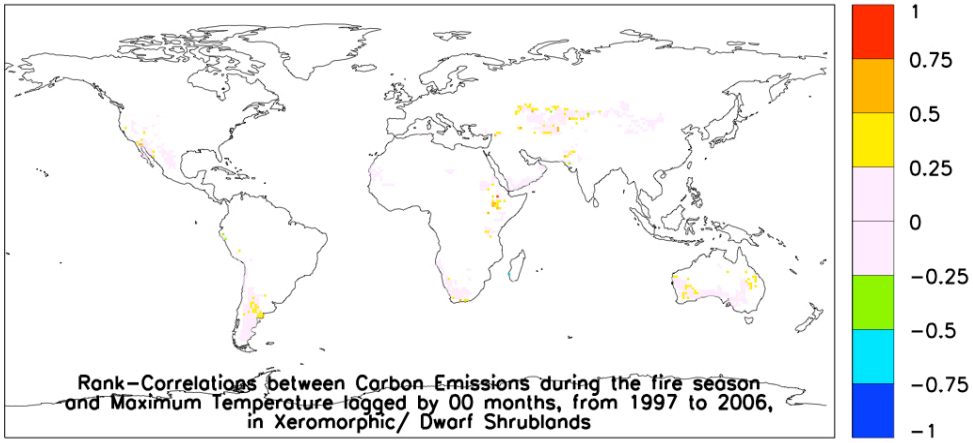

b)

Figure 3.21.1 World maps of rank-correlations between wildfires and a) air humidity and b) air temperature, during the fire season, from 1997 to 2006, in xeromorphic and dwarf shrublands. Pixels in green and blue show areas where fires increase during a) drier or b) colder weather, whereas yellow, orange and red pixels show areas where fires increase with a) more humid or b) warmer weather.

After a rainy winter, fires decreased in Central Asia, South Australia and in Southern South America, but increased in the Mediterranean, Equatorial Africa and Northern India (correlation maps and plots not shown).

Fires also tended to increase after a snowy winter, possibly due to the drying effect of ice [Pearce, 2000], but decrease with snow depth during the fire season.

During humid summers, fires decreased in West Asia, Russia, Equatorial Africa, North Southern Africa, West Asia, India, Eastern Australia, Central America and Southern South America, but increased in South Southern Africa, Central Asia, South West Australia, South Northern America and in the Andes (figure 3.21.1 a). This positive correlation between humidity and biomass burning maybe due to the fact that, in high latitudes, higher humidity occurs during warmer weather, but it is still low enough to allow for ignition and fire spread. This is corroborated by a positive correlation between burnt areas and temperature in these eco-regions (figure 3.21.1 b).

There were not enough regular fires in xeromorphic shrublands to obtain fire models, except in a few isolated pixels in Equatorial Africa (figure 3.21.2).

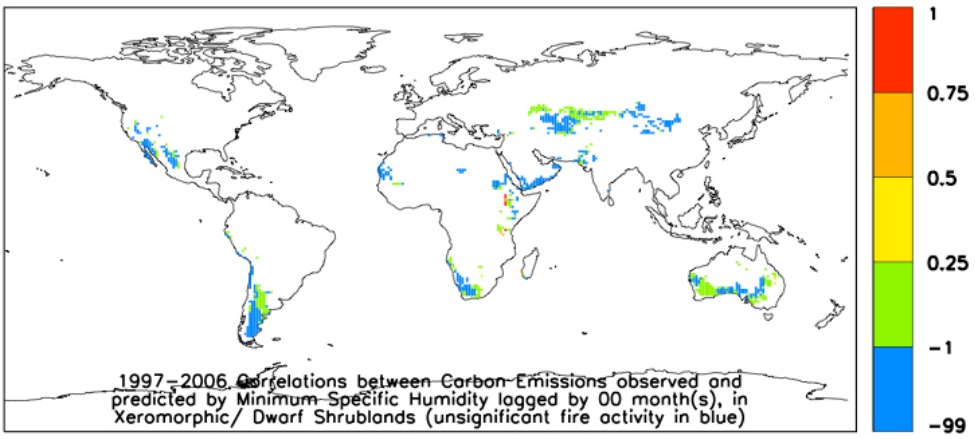

Figure 3.21.2 World map of correlations between model predictions and GFED estimations of carbon emissions from wildfires, from 1997 to 2006, in xeromorphic and dwarf shrublands, with humidity during the fire season as the predictor. Red pixels have the best models (correlations with observations above 75%), followed by orange and yellow pixels with correlations between 50% and 75%, and between 25% and 50%, respectively. Green pixels do not have reliable models with this predictor. Blue pixels do not show significant fire activity at 1ºx1º resolution.

3.22 Arctic/ Alpine Tundra, Mossy Bogs

This ecosystem occupies a large area in Northern North America, Greenland, Iceland, North Northern Europe and North Northern Asia.

Rainfall is scarce, and does not seem to influence fires, neither during the fire season nor during the growing season (correlation maps not shown).

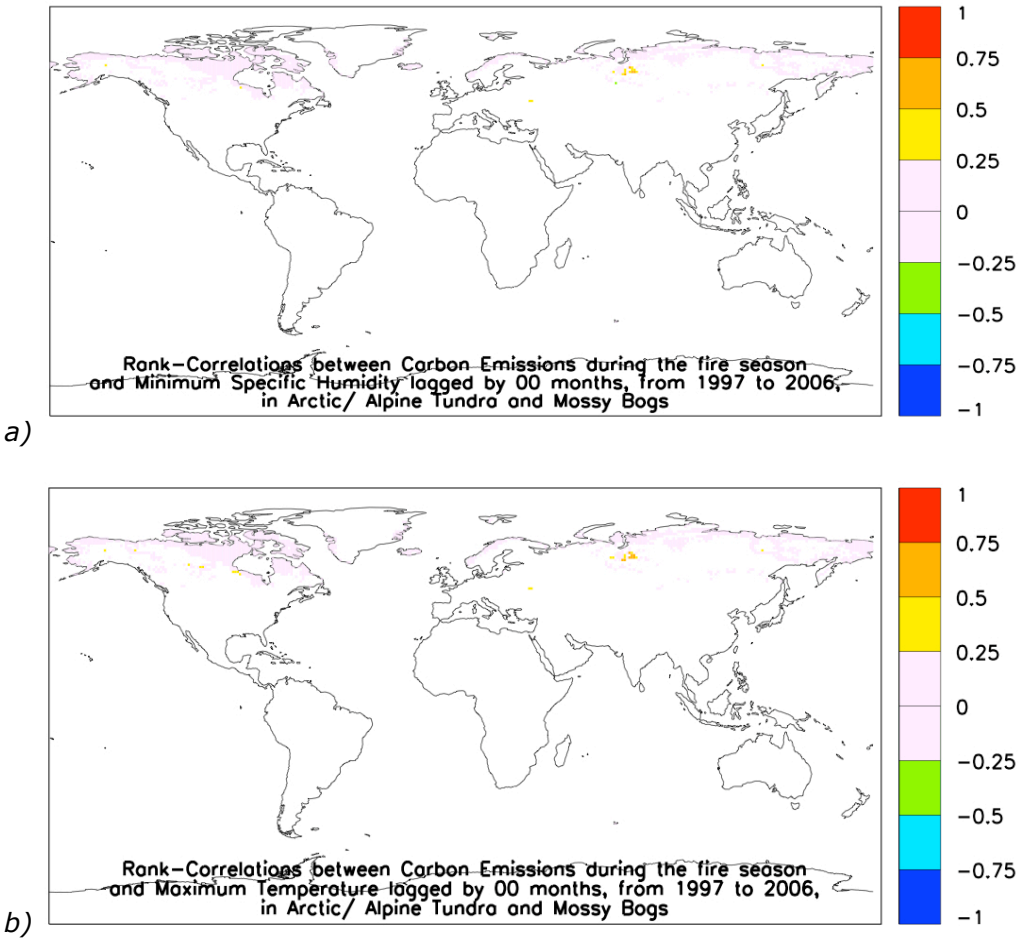

Figure 3.22.1 World maps of rank-correlations between wildfires and a) air humidity and b) air temperature, during the fire season, from 1997 to 2006, in arctic and alpine tundra and mossy bogs. Pixels in green and blue show areas where fires increase during a) drier or b) colder weather, whereas yellow, orange and red pixels show areas where fires increase with a) more humid or b) warmer weather.

Both temperature and humidity are positively correlated with biomass burning (figures 3.22.1), possibly because temperature is the main influence on the variability of fire behaviour in boreal ecosystems, and higher humidity is associated to higher temperatures. In Northern North America, larger burnt areas occur during periods of higher air humidity (figure 3.22.2 a) and soil wetness (figure 3.22.2 b).

Individual pixels did not have enough fires in 10 years to establish a statistical relationship between climate variables and fire activity (figure 3.22.3).

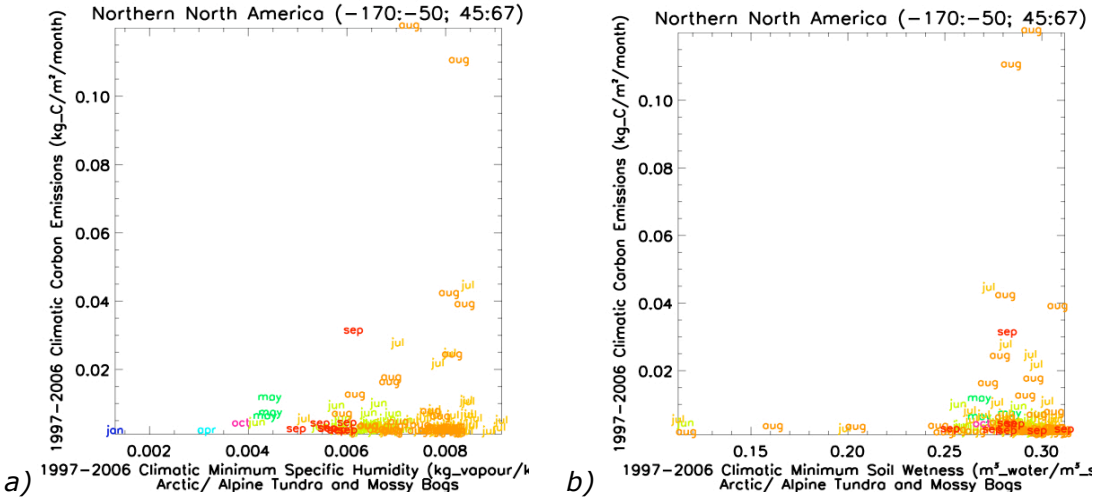

Figure 3.22.2 Scatterplot of carbon emissions from wildfires versus a) minimum specific humidity and b) minimum soil wetness, in the tundra and mossy bogs of Northern North America. Each point corresponds to a pixel of 1ºx1º resolution, with values averaged over homonymous months, from 1997 to 2006.

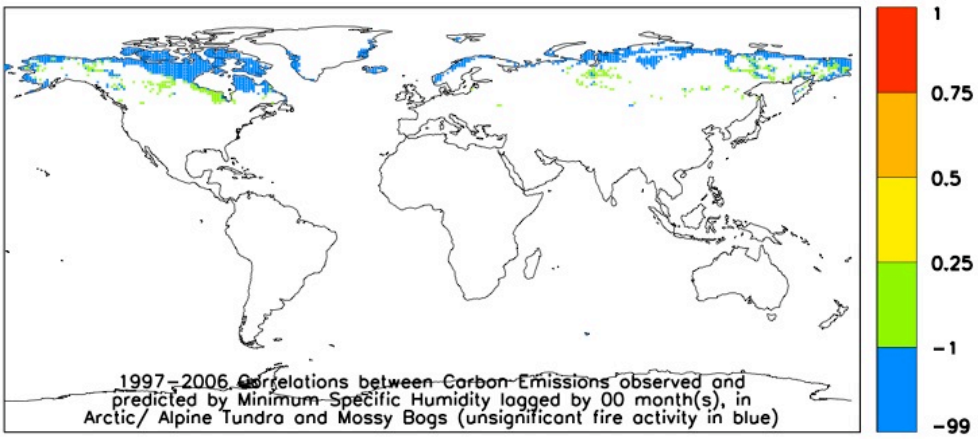

Figure 3.22.3 World map of correlations between model predictions and GFED estimations of carbon emissions from wildfires, from 1997 to 2006, in arctic and alpine tundra and mossy bogs, with humidity during the fire season as the predictor. Red pixels have the best models (correlations with observations above 75%), followed by orange and yellow pixels with correlations between 50% and 75%, and between 25% and 50%, respectively. Green pixels do not have reliable models with this predictor. Blue pixels do not show significant fire activity at 1ºx1º resolution.

3.23 Grassland, 10-40% Woody Cover

Grasslands with 10 to 40% woody cover occupy a large world area in North America, Russia, West Asia, Africa and Central South America, and also in small areas of South East Asia and North Australia. It is one of the ecosystems with more regular fires in tropical and sub-tropical latitudes.

After rainy and humid winters, fires increased in Africa (except the monsoon area), South East Asia, Northern Australia and Central South America (figures 3.23.2), but decreased in West Asia and North America. Rainfall and high humidity were strongly negatively correlated with temperature during the wet season in Africa and South America (correlation maps and plots not shown), so temperature

6 months before the fire season can also be used as a fire predictor.

Humid summers had fewer fires in Southern Africa, Eastern Russia, South East Asia, Northern Australia, North America, Central South America and Southern South America (figure 3.23.1 a).

Fires were well correlated with high temperatures during the fire season, except in certain coastal areas of Africa, where convective rainfall occurs during the warmest weather (figure 3.23.1 b). Fires also increased in Africa with increasing fuel load 1 month before.

Contemporary humidity and soil wetness, and rainfall prior to the fire season, are good predictors of biomass burning (figures 3.23.4-8).

The best fire models, some correlated by more than 90% with observations, were found in South America and in Africa, with lagged rainfall and contemporary air and soil humidity as predictors (figures 3.23.4-8). Concurrent air and soil temperature were also good predictors (figures 3.23.4-8).

Rainfall during the growing season in these tropical grasslands contributes to large burnt areas during the following fire season (figure 3.23.2); therefore, lagged previous rainfall is a good predictor of carbon emissions as a proxy for fuel load (figures 3.23.2, 3.23.4 c-d, 3.23.5 e-m, 3.23.6 e-k and 3.23.7 c-h). Rainfall and high humidity during the fire season strongly hinder fires, especially in the more pluvious zones near the equator (figure 3.23.1 a), where lightning density can also be used as a proxy for rainfall in fire models (figure 3.23.8 b).

a)

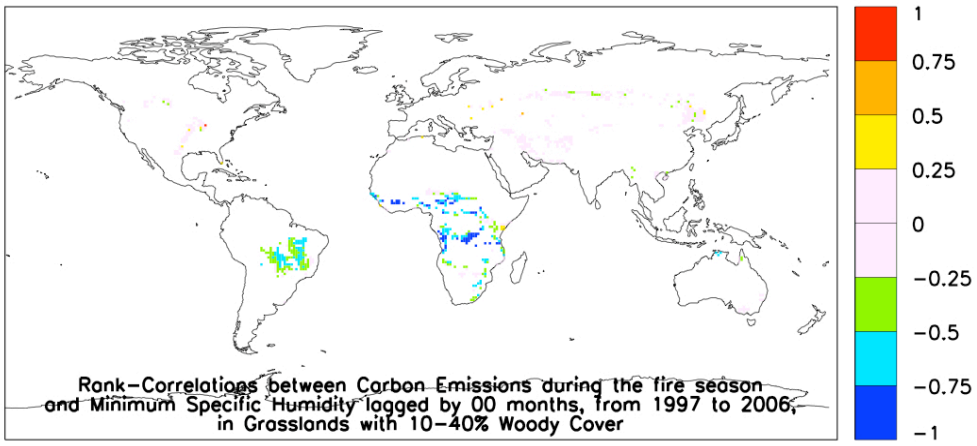

b)

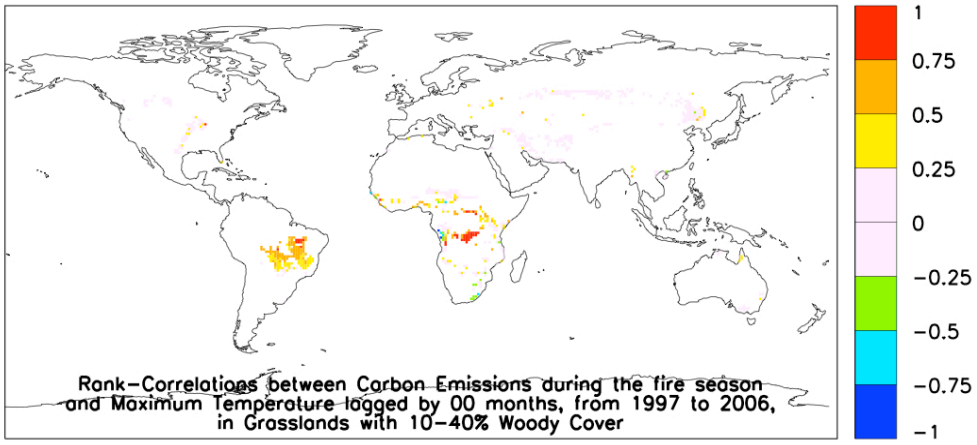

Figure 3.23.1 World maps of rank-correlations between wildfires and a) air humidity and b) air temperature, during the fire season, from 1997 to 2006, in grasslands with 10 to 40% woody cover. Pixels in green and blue show areas where fires increase during a) drier or b) colder weather, whereas yellow, orange and red pixels show areas where fires increase with a) more humid or b) warmer weather.

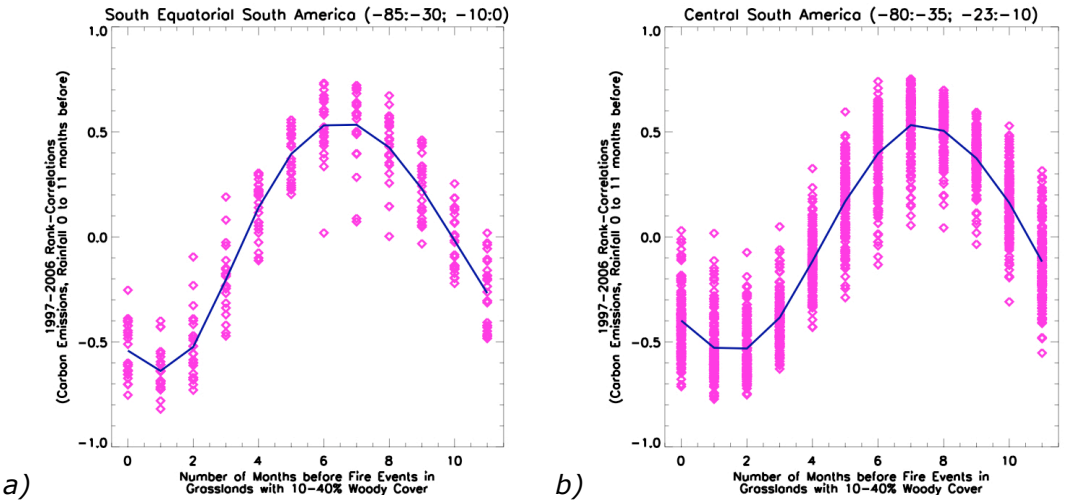

a) b)

Figure 3.23.2 Scatterplot of rank-correlations between monthly carbon emissions during the fire season and monthly rainfall, contemporary and up to 11 months before, versus the lags, i.e., the number of months by which the rain preceded the fire, in all 1ºx1º resolution pixels with significant fire activity, in the grasslands with 10-40% woody cover of a) South Equatorial South America and b) Central South America, from 1997 to 2006. Different pixels of an eco-region show different rank-correlations between fires and rainfall, but they are mainly negative for lags up to 2 months, and positive for lags of 4 to 9 months in Equatorial South America (a) and of 5 to 10 months in Central South America (b). This pattern is repeated for longer time lags, indicating the strong influence of the seasonal cycle.

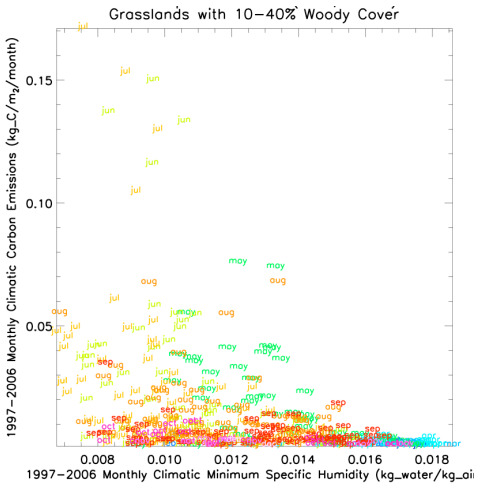

Figure 3.23.3 Scatterplot of carbon emissions from wildfires versus minimum specific humidity in the grasslands with 10 to 40% woody cover of South Equatorial Africa. Each point corresponds to a pixel of 1ºx1º resolution, with values averaged over homonymous months, from 1997 to 2006.

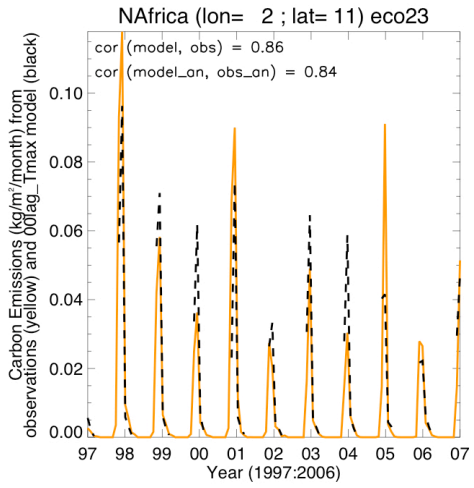
NAfrica (lon= 2 ; lat= 11) eco23
cor (model, obs) = 0.86
cor (model_an, obs_an) = 0.84
Carbon Emissions (kg/m²/month) from observations (yellow) and 00lag_Tmax model (black)
0.00
0.02
0.04
0.06
0.08
0.10
97 98 99 00 01 02 03 04 05 06 07
Year (1997:2006)

a)

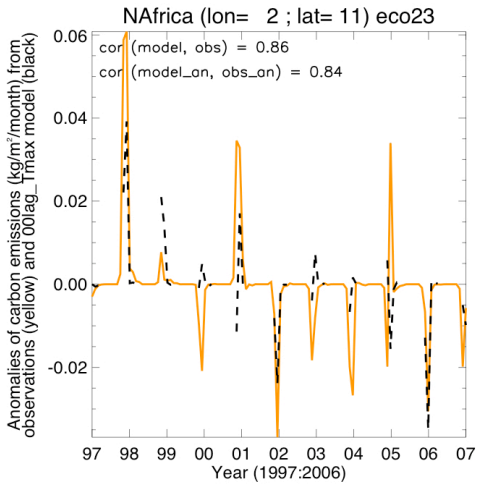
NAfrica (lon= 2 ; lat= 11) eco23
cor (model, obs) = 0.86
cor (model_an, obs_an) = 0.84
Anomalies of carbon emissions (kg/m²/month) from observations (yellow) and 00lag_Tmax model (black)
-0.02
0.00
0.02
0.04
0.06
97 98 99 00 01 02 03 04 05 06 07
Year (1997:2006)

b)

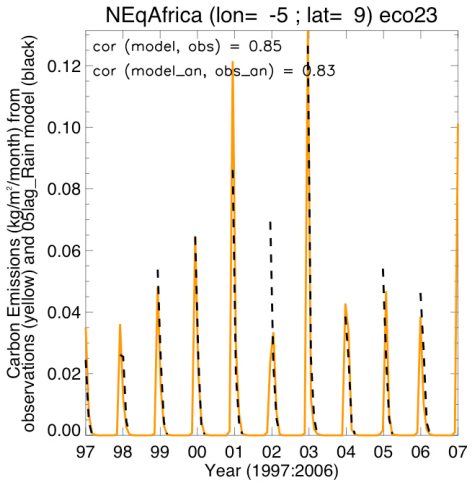
NEqAfrica (lon= -5 ; lat= 9) eco23
cor (model, obs) = 0.85
cor (model_an, obs_an) = 0.83
Carbon Emissions (kg/m²/month) from observations (yellow) and 05lag_Rain model (black)
0.00
0.02
0.04
0.06
0.08
0.10
0.12
97 98 99 00 01 02 03 04 05 06 07
Year (1997:2006)

c)

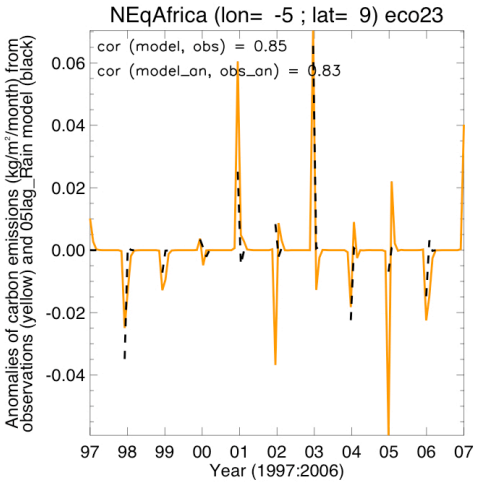
NEqAfrica (lon= -5 ; lat= 9) eco23
cor (model, obs) = 0.85
cor (model_an, obs_an) = 0.83
Anomalies of carbon emissions (kg/m²/month) from observations (yellow) and 05lag_Rain model (black)
-0.04
-0.02
0.00
0.02
0.04
0.06
97 98 99 00 01 02 03 04 05 06 07
Year (1997:2006)

d)

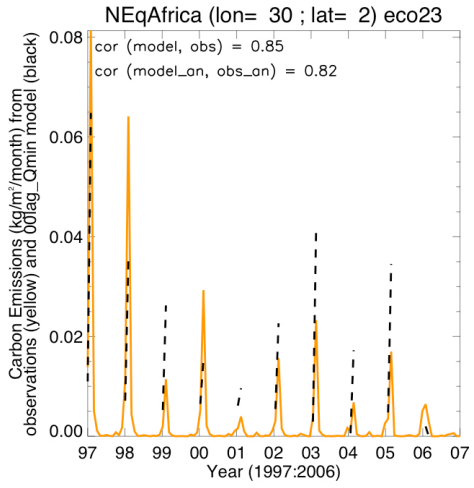
NEqAfrica (lon= 30 ; lat= 2) eco23
cor (model, obs) = 0.85
cor (model_an, obs_an) = 0.82
Carbon Emissions (kg/m²/month) from observations (yellow) and 00lag_Qmin model (black)
0.00
0.02
0.04
0.06
0.08
97 98 99 00 01 02 03 04 05 06 07
Year (1997:2006)

e)

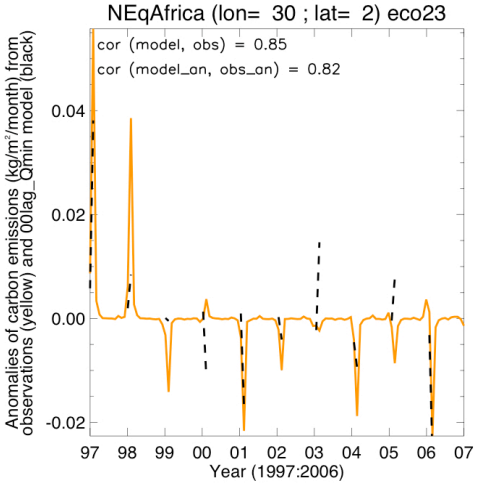
NEqAfrica (lon= 30 ; lat= 2) eco23
cor (model, obs) = 0.85
cor (model_an, obs_an) = 0.82
Anomalies of carbon emissions (kg/m²/month) from observations (yellow) and 00lag_Qmin model (black)
-0.02
0.00
0.02
0.04
97 98 99 00 01 02 03 04 05 06 07
Year (1997:2006)

f)

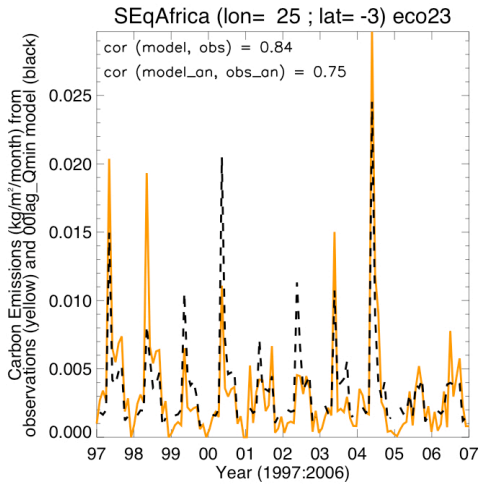
SEqAfrica (lon= 25 ; lat= -3) eco23
cor (model, obs) = 0.84
cor (model_an, obs_an) = 0.75
Carbon Emissions (kg/m²/month) from observations (yellow) and 00lag_Qmin model (black)
Year (1997:2006)

g)

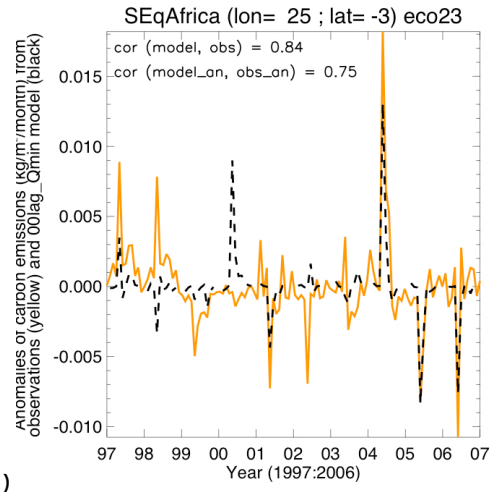
SEqAfrica (lon= 25 ; lat= -3) eco23
cor (model, obs) = 0.84
cor (model_an, obs_an) = 0.75
Anomalies of carbon emissions (kg/m²/month) from observations (yellow) and 00lag_Qmin model (black)
Year (1997:2006)

h)

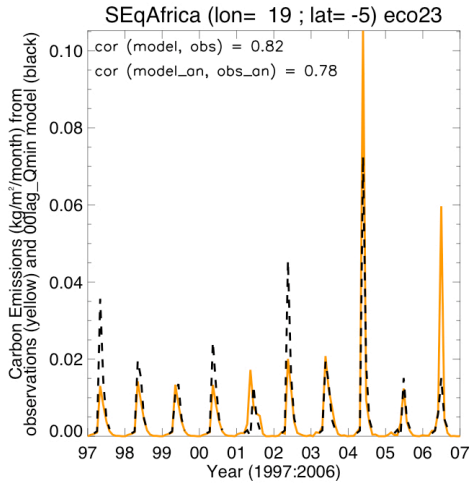
SEqAfrica (lon= 19 ; lat= -5) eco23
cor (model, obs) = 0.82
cor (model_an, obs_an) = 0.78
Carbon Emissions (kg/m²/month) from observations (yellow) and 00lag_Qmin model (black)
Year (1997:2006)

i)

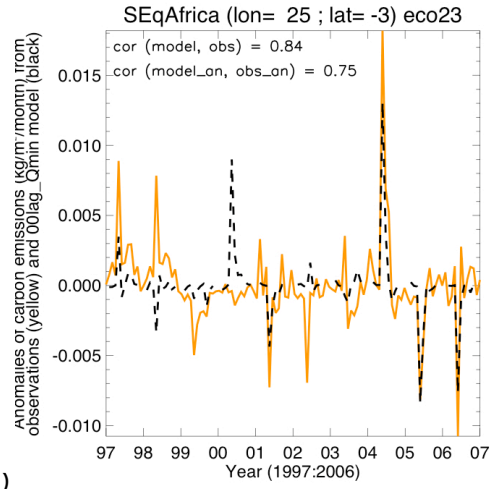
SEqAfrica (lon= 25 ; lat= -3) eco23
cor (model, obs) = 0.84
cor (model_an, obs_an) = 0.75
Anomalies of carbon emissions (kg/m²/month) from observations (yellow) and 00lag_Qmin model (black)
Year (1997:2006)

j)

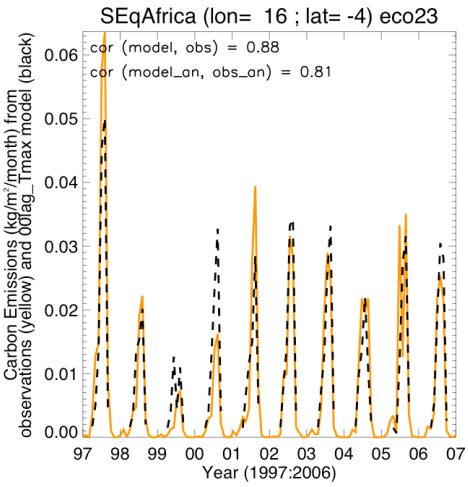
SEqAfrica (lon= 16 ; lat= -4) eco23
cor (model, obs) = 0.88
cor (model_an, obs_an) = 0.81
Carbon Emissions (kg/m²/month) from observations (yellow) and 00lag_Tmax model (black)
Year (1997:2006)

k)

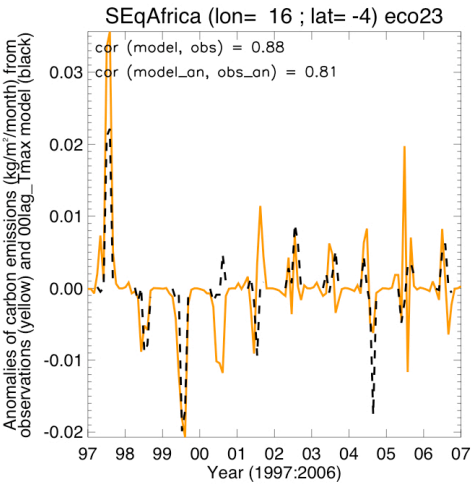
SEqAfrica (lon= 16 ; lat= -4) eco23
cor (model, obs) = 0.88
cor (model_an, obs_an) = 0.81
Anomalies of carbon emissions (kg/m²/month) from observations (yellow) and 00lag_Tmax model (black)
Year (1997:2006)

l)

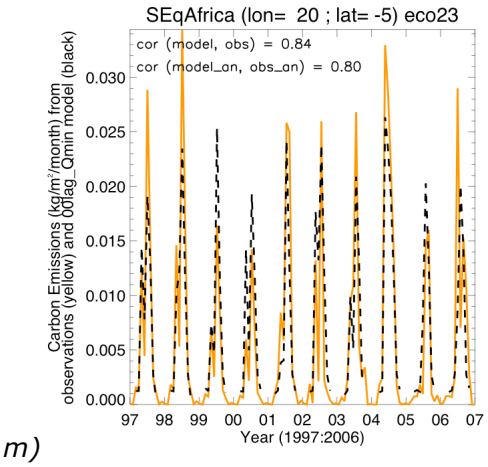

m)

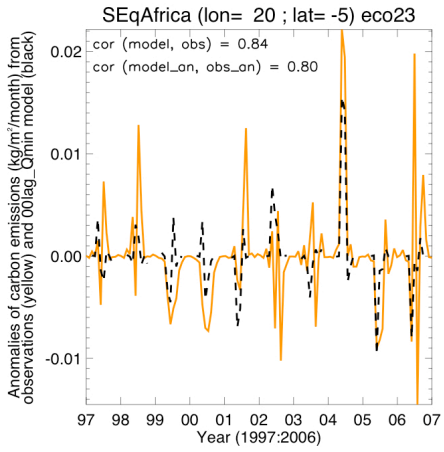

n)

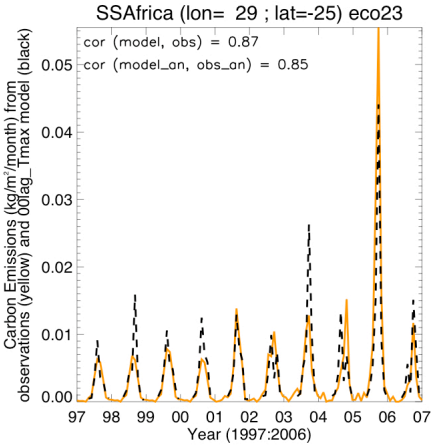

o)

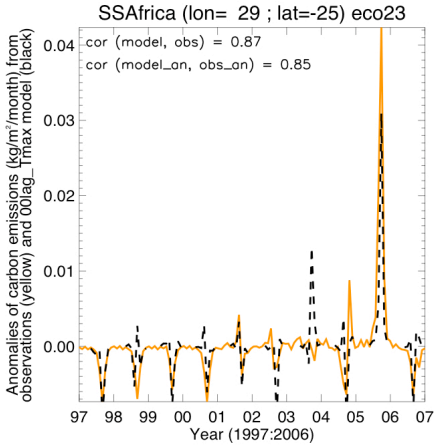

p)

Figure 3.23.4 Time series of biomass burning (expressed as carbon emissions) and anomalies, from 1997 to 2006, given by GFED estimates, in eight individual pixels of the grasslands with 10% to 40% woody cover of North Africa (a-b), North Equatorial Africa (c-f), South Equatorial Africa (g-n) and South Southern Africa (o-p). Over-plotted in black is a model based on 1 predictor: monthly averages of minimum air humidity (e-j, m-n) or of maximum air temperature (a-b, k-l, o-p), contemporary with the fire events, or rainfall 5 months before (c-d). High correlations (above 75%) between modelled anomalies and the correspondent anomalies of GFED estimates show that these models capture a considerable part of the interannual variability in carbon emissions.

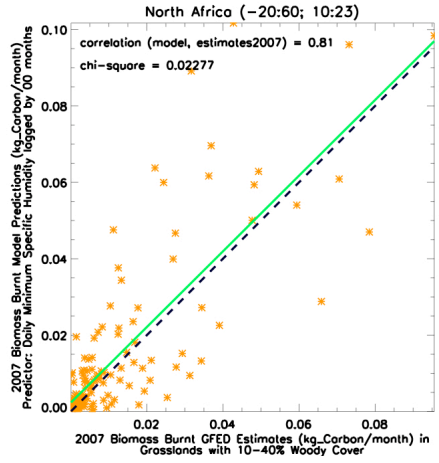
North Africa (-20:60; 10:23)
correlation (model, estimates2007) = 0.81
chi-square = 0.02277
2007 Biomass Burnt Model Predictions (kg_Carbon/month)
Predictor: Daily Minimum Specific Humidity lagged by 00 months
2007 Biomass Burnt GFED Estimates (kg_Carbon/month) in
Grasslands with 10-40% Woody Cover

a)

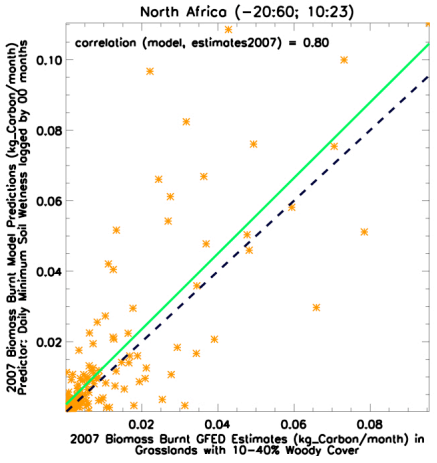
North Africa (-20:60; 10:23)
correlation (model, estimates2007) = 0.80
2007 Biomass Burnt Model Predictions (kg_Carbon/month)
Predictor: Daily Minimum Soil Wetness lagged by 00 months
2007 Biomass Burnt GFED Estimates (kg_Carbon/month) in
Grasslands with 10-40% Woody Cover

b)

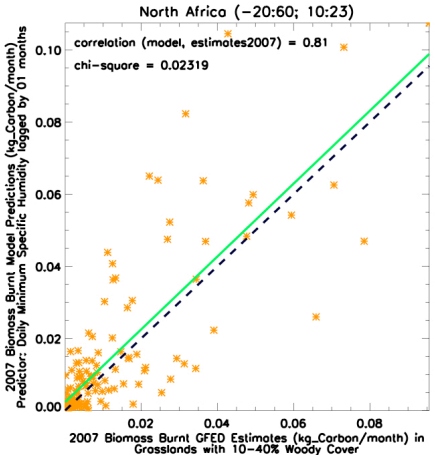
North Africa (-20:60; 10:23)
correlation (model, estimates2007) = 0.81
chi-square = 0.02319
2007 Biomass Burnt Model Predictions (kg_Carbon/month)
Predictor: Daily Minimum Specific Humidity lagged by 01 months
2007 Biomass Burnt GFED Estimates (kg_Carbon/month) in
Grasslands with 10-40% Woody Cover

c)

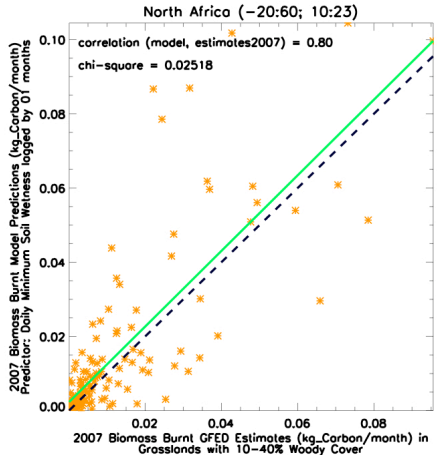
North Africa (-20:60; 10:23)
correlation (model, estimates2007) = 0.80
chi-square = 0.02518
2007 Biomass Burnt Model Predictions (kg_Carbon/month)
Predictor: Daily Minimum Soil Wetness lagged by 01 months
2007 Biomass Burnt GFED Estimates (kg_Carbon/month) in
Grasslands with 10-40% Woody Cover

d)

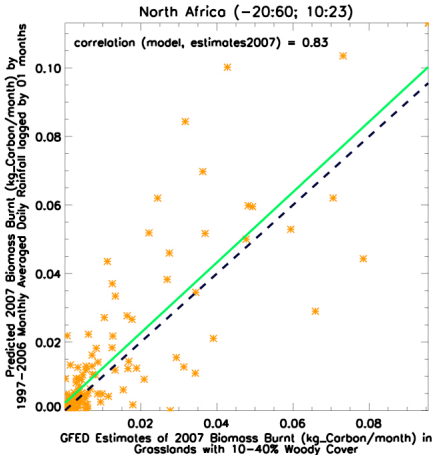
North Africa (-20:60; 10:23)
correlation (model, estimates2007) = 0.83
Predicted 2007 Biomass Burnt (kg_Carbon/month) by
1997-2006 Monthly Averaged Daily Rainfall lagged by 01 months
GFED Estimates of 2007 Biomass Burnt (kg_Carbon/month) in
Grasslands with 10-40% Woody Cover

e)

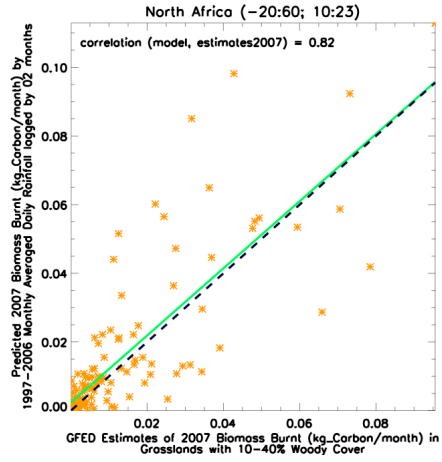
North Africa (-20:60; 10:23)
correlation (model, estimates2007) = 0.82
Predicted 2007 Biomass Burnt (kg_Carbon/month) by
1997-2006 Monthly Averaged Daily Rainfall lagged by 02 months
GFED Estimates of 2007 Biomass Burnt (kg_Carbon/month) in
Grasslands with 10-40% Woody Cover

f)

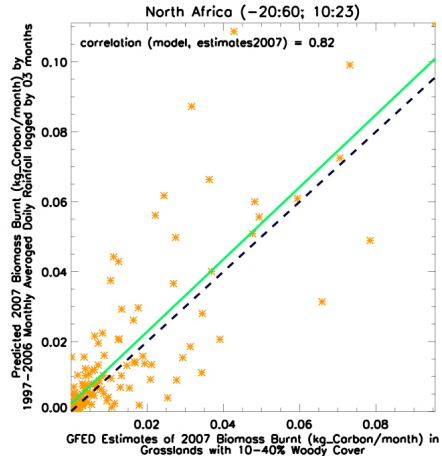
North Africa (-20:60; 10:23)
correlation (model, estimates2007) = 0.82
Predicted 2007 Biomass Burnt (kg_Carbon/month) by 1997-2006 Monthly Averaged Daily Rainfall lagged by 03 months
GFED Estimates of 2007 Biomass Burnt (kg_Carbon/month) in Grasslands with 10-40% Woody Cover

g)

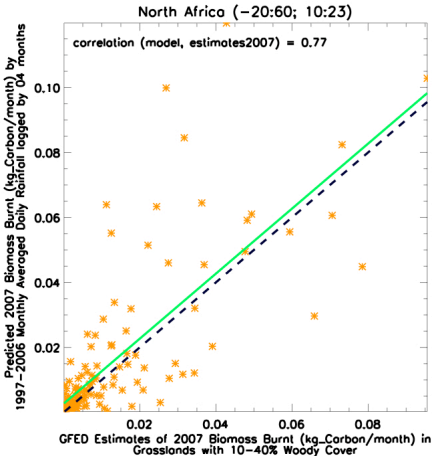
North Africa (-20:60; 10:23)
correlation (model, estimates2007) = 0.77
Predicted 2007 Biomass Burnt (kg_Carbon/month) by 1997-2006 Monthly Averaged Daily Rainfall lagged by 04 months
GFED Estimates of 2007 Biomass Burnt (kg_Carbon/month) in Grasslands with 10-40% Woody Cover

h)

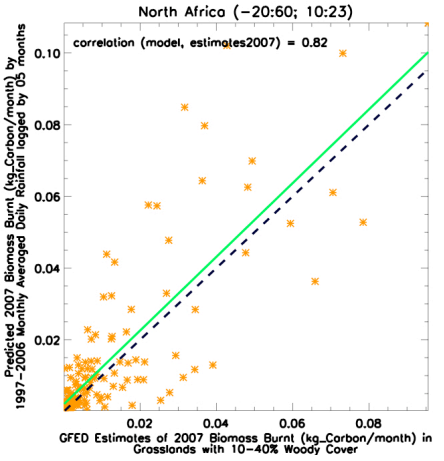
North Africa (-20:60; 10:23)
correlation (model, estimates2007) = 0.82
Predicted 2007 Biomass Burnt (kg_Carbon/month) by 1997-2006 Monthly Averaged Daily Rainfall lagged by 05 months
GFED Estimates of 2007 Biomass Burnt (kg_Carbon/month) in Grasslands with 10-40% Woody Cover

i)

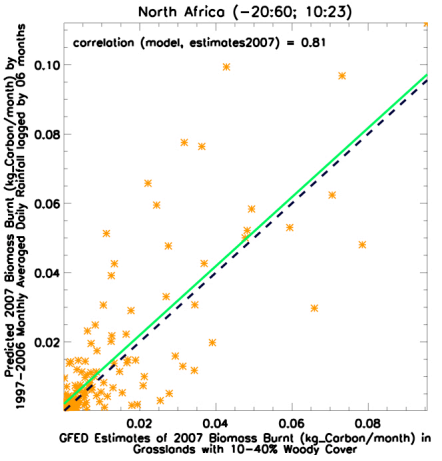
North Africa (-20:60; 10:23)
correlation (model, estimates2007) = 0.81
Predicted 2007 Biomass Burnt (kg_Carbon/month) by 1997-2006 Monthly Averaged Daily Rainfall lagged by 06 months
GFED Estimates of 2007 Biomass Burnt (kg_Carbon/month) in Grasslands with 10-40% Woody Cover

j)

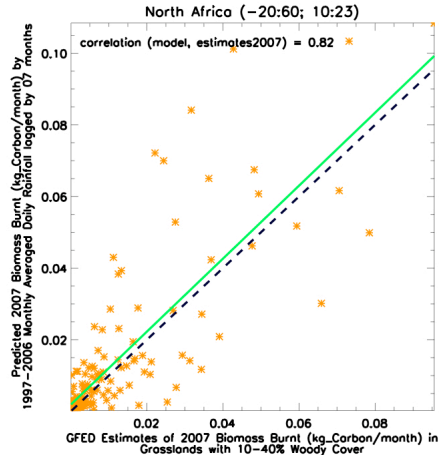
North Africa (-20:60; 10:23)
correlation (model, estimates2007) = 0.82
Predicted 2007 Biomass Burnt (kg_Carbon/month) by 1997-2006 Monthly Averaged Daily Rainfall lagged by 07 months
GFED Estimates of 2007 Biomass Burnt (kg_Carbon/month) in Grasslands with 10-40% Woody Cover

k)

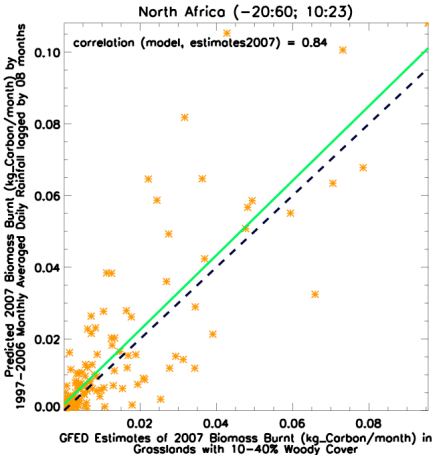
North Africa (-20:60; 10:23)
correlation (model, estimates2007) = 0.84
Predicted 2007 Biomass Burnt (kg_Carbon/month) by 1997-2006 Monthly Averaged Daily Rainfall lagged by 08 months
GFED Estimates of 2007 Biomass Burnt (kg_Carbon/month) in Grasslands with 10-40% Woody Cover

l)

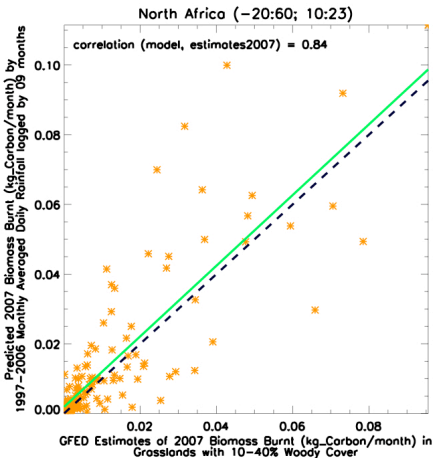

m)

Figure 3.23.5 Scatterplot of predicted biomass burnt for the year of 2007 versus the correspondent GFED estimates, expressed in kilograms of carbon emissions per month, in the grasslands with 10 to 40% woody cover of North Africa. The green line shows the linear fit through the points, whereas the black dashed line marks where the 1:1 ideal slope would be. Models are based on monthly averaged daily minimum specific humidity, contemporary with the fire events (a) and lagged by 1 month (c), minimum soil wetness, contemporary (b) and lagged by 1 month (d), and rainfall lagged by 1 (e), 2 (f), 3 (g), 4 (h), 5 (i), 6 (j), 7 (k), 8 (l) and 9 months (m). Only eco-regions where models are correlated by more than 75% with observations are presented.

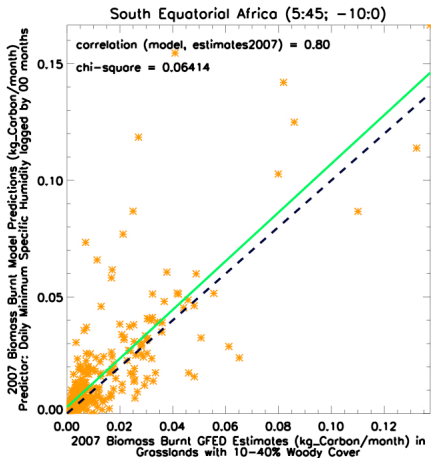

a)

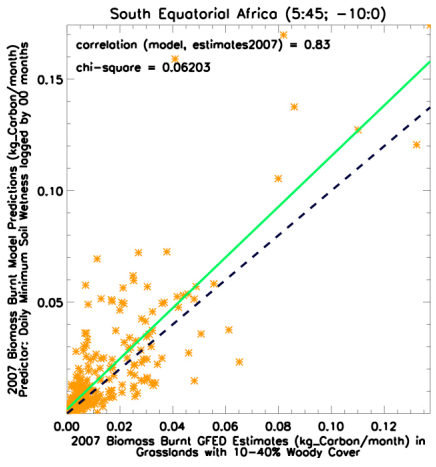

b)

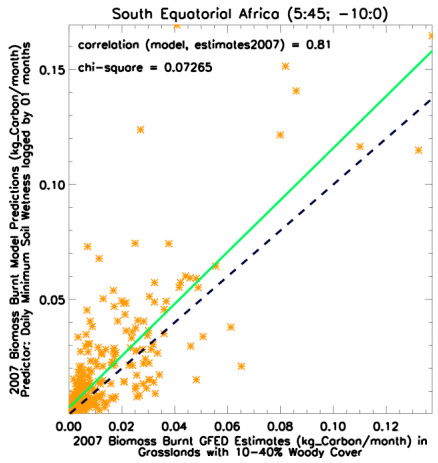
South Equatorial Africa (5:45; −10:0)
correlation (model, estimates2007) = 0.81
chi-square = 0.07265
2007 Biomass Burnt Model Predictions (kg_Carbon/month)
Predictor: Daily Minimum Soil Wetness lagged by 01 months
0.15
0.10
0.05
0.00
0.02
0.04
0.06
0.08
0.10
0.12
2007 Biomass Burnt GFED Estimates (kg_Carbon/month) in
Grasslands with 10−40% Woody Cover

c)

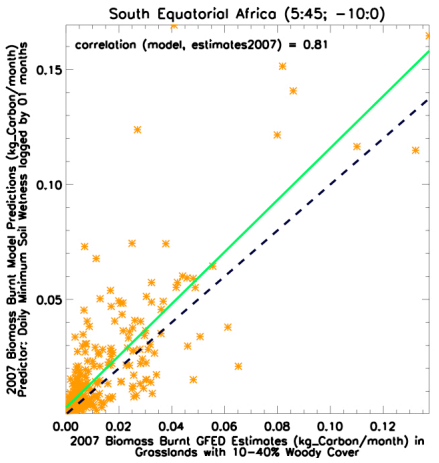
South Equatorial Africa (5:45; −10:0)
correlation (model, estimates2007) = 0.81
2007 Biomass Burnt Model Predictions (kg_Carbon/month)
Predictor: Daily Minimum Soil Wetness lagged by 01 months
0.15
0.10
0.05
0.00
0.02
0.04
0.06
0.08
0.10
0.12
2007 Biomass Burnt GFED Estimates (kg_Carbon/month) in
Grasslands with 10−40% Woody Cover

d)

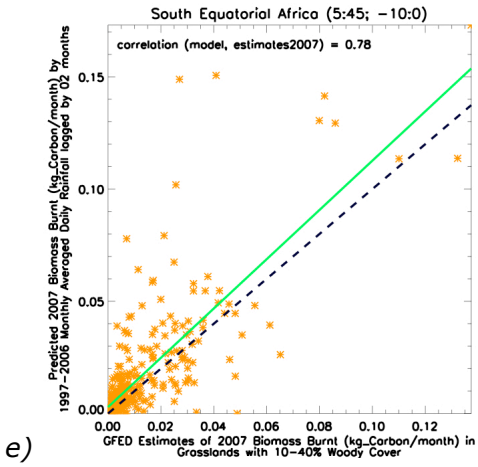
South Equatorial Africa (5:45; −10:0)
correlation (model, estimates2007) = 0.78
Predicted 2007 Biomass Burnt (kg_Carbon/month) by 1997–2006 Monthly Averaged Daily Rainfall lagged by 02 months
GFED Estimates of 2007 Biomass Burnt (kg_Carbon/month) in Grasslands with 10–40% Woody Cover

e)

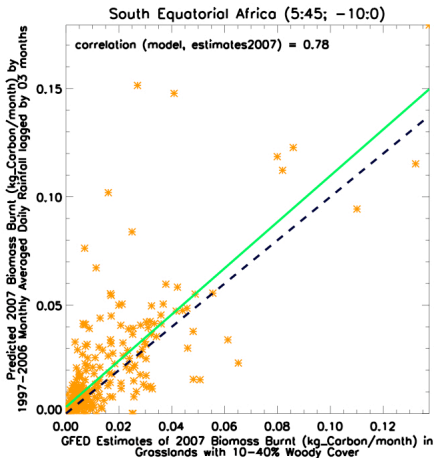
South Equatorial Africa (5:45; −10:0)
correlation (model, estimates2007) = 0.78
Predicted 2007 Biomass Burnt (kg_Carbon/month) by 1997–2006 Monthly Averaged Daily Rainfall lagged by 03 months
GFED Estimates of 2007 Biomass Burnt (kg_Carbon/month) in Grasslands with 10–40% Woody Cover

f)

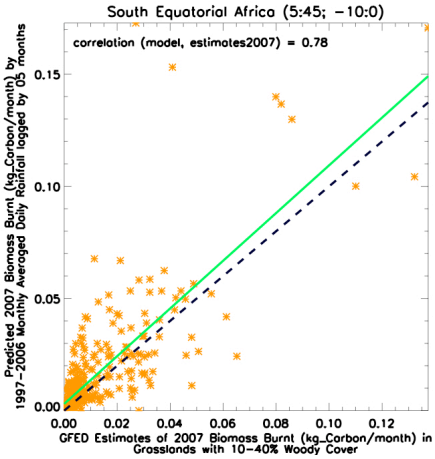
South Equatorial Africa (5:45; −10:0)
correlation (model, estimates2007) = 0.78
Predicted 2007 Biomass Burnt (kg_Carbon/month) by 1997–2006 Monthly Averaged Daily Rainfall lagged by 05 months
GFED Estimates of 2007 Biomass Burnt (kg_Carbon/month) in Grasslands with 10–40% Woody Cover

g)

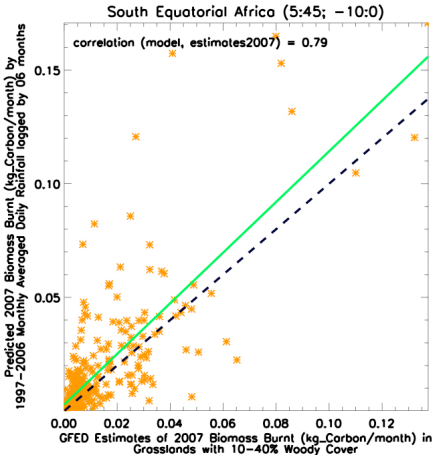
South Equatorial Africa (5:45; −10:0)
correlation (model, estimates2007) = 0.79
Predicted 2007 Biomass Burnt (kg_Carbon/month) by 1997–2006 Monthly Averaged Daily Rainfall lagged by 06 months
GFED Estimates of 2007 Biomass Burnt (kg_Carbon/month) in Grasslands with 10–40% Woody Cover

h)

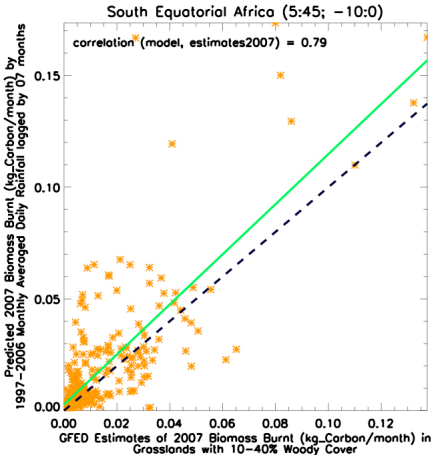
South Equatorial Africa (5:45; −10:0)
correlation (model, estimates2007) = 0.79
Predicted 2007 Biomass Burnt (kg_Carbon/month) by 1997–2006 Monthly Averaged Daily Rainfall lagged by 07 months
GFED Estimates of 2007 Biomass Burnt (kg_Carbon/month) in Grasslands with 10–40% Woody Cover

i)

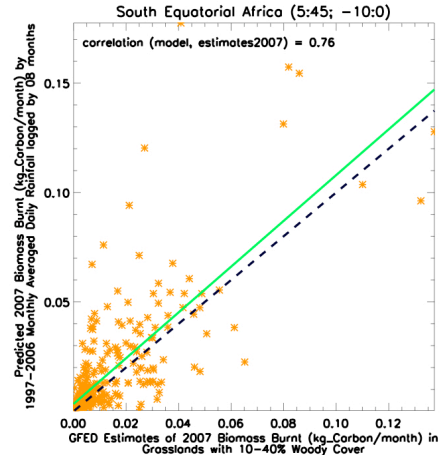
South Equatorial Africa (5:45; −10:0)
correlation (model, estimates2007) = 0.76
Predicted 2007 Biomass Burnt (kg_Carbon/month) by 1997–2006 Monthly Averaged Daily Rainfall lagged by 08 months
GFED Estimates of 2007 Biomass Burnt (kg_Carbon/month) in Grasslands with 10–40% Woody Cover

j)

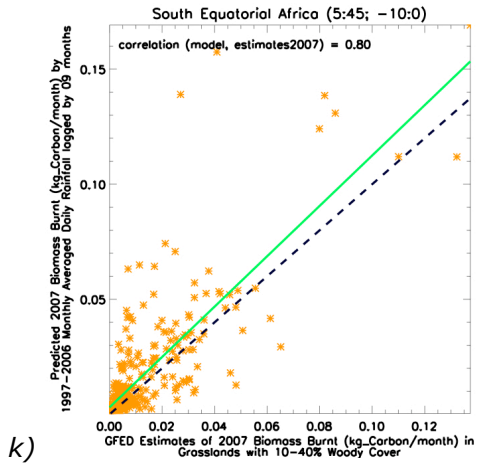

k)

Figure 3.23.6 Scatterplot of predicted biomass burnt for the year of 2007 versus the correspondent GFED estimates, expressed in kilograms of carbon emissions per month, in the grasslands with 10 to 40% woody cover of South Equatorial Africa. The green line shows the linear fit through the points, whereas the black dashed line marks where the 1:1 ideal slope would be. Models are based on monthly averaged daily minimum specific humidity, contemporary with the fire events (a), minimum soil wetness contemporary (b) and lagged by 1 month (c), and rainfall, lagged by 2 (b), 3 (c), 5 (d), 6 (e), 7 (f), 8 (g) and 9 months (h). Only models correlated by more than 75% with observations are presented.

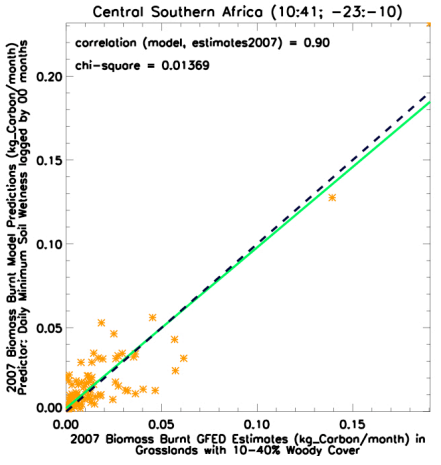

a)

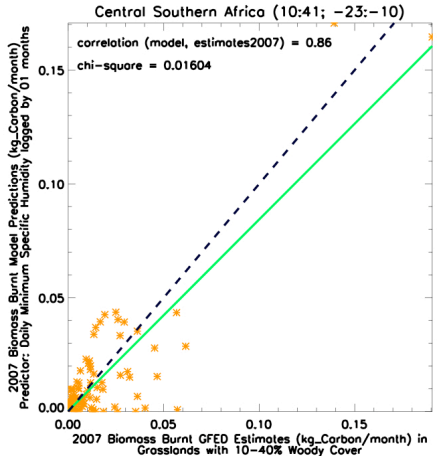
Central Southern Africa (10:41; −23:−10)
correlation (model, estimates2007) = 0.86
chi−squore = 0.01604
2007 Biomass Burnt Model Predictions (kg_Carbon/month)
Predictor: Daily Minimum Specific Humidity lagged by 01 months
2007 Biomass Burnt GFED Estimates (kg_Carbon/month) in
Grasslands with 10−40% Woody Cover

b)

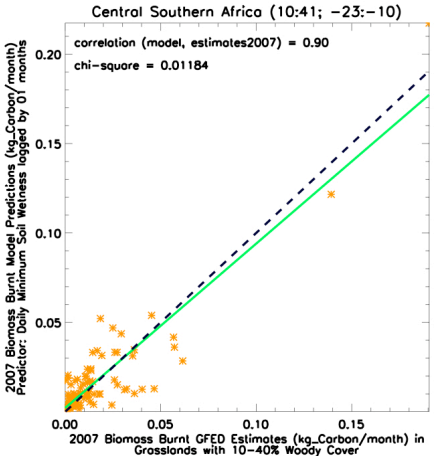
Central Southern Africa (10:41; −23:−10)
correlation (model, estimates2007) = 0.90
chi−squore = 0.01184
2007 Biomass Burnt Model Predictions (kg_Carbon/month)
Predictor: Daily Minimum Soil Weiness lagged by 01 months
2007 Biomass Burnt GFED Estimates (kg_Carbon/month) in
Grasslands with 10−40% Woody Cover

c)

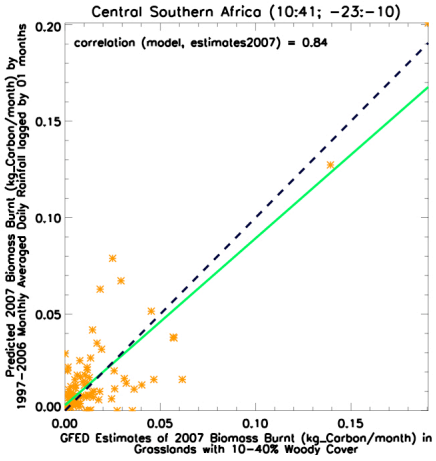
Central Southern Africa (10:41; −23:−10)
correlation (model, estimates2007) = 0.84
Predicted 2007 Biomass Burnt (kg_Carbon/month) by
1997−2006 Monthly Averaged Daily Rainfall lagged by 01 months
GFED Estimates of 2007 Biomass Burnt (kg_Carbon/month) in
Grasslands with 10−40% Woody Cover

c)

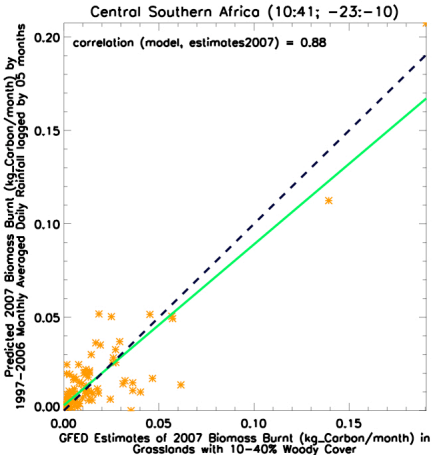
Central Southern Africa (10:41; −23:−10)
correlation (model, estimates2007) = 0.88
Predicted 2007 Biomass Burnt (kg_Carbon/month) by
1997−2006 Monthly Averaged Daily Rainfall lagged by 05 months
GFED Estimates of 2007 Biomass Burnt (kg_Carbon/month) in
Grasslands with 10−40% Woody Cover

d)

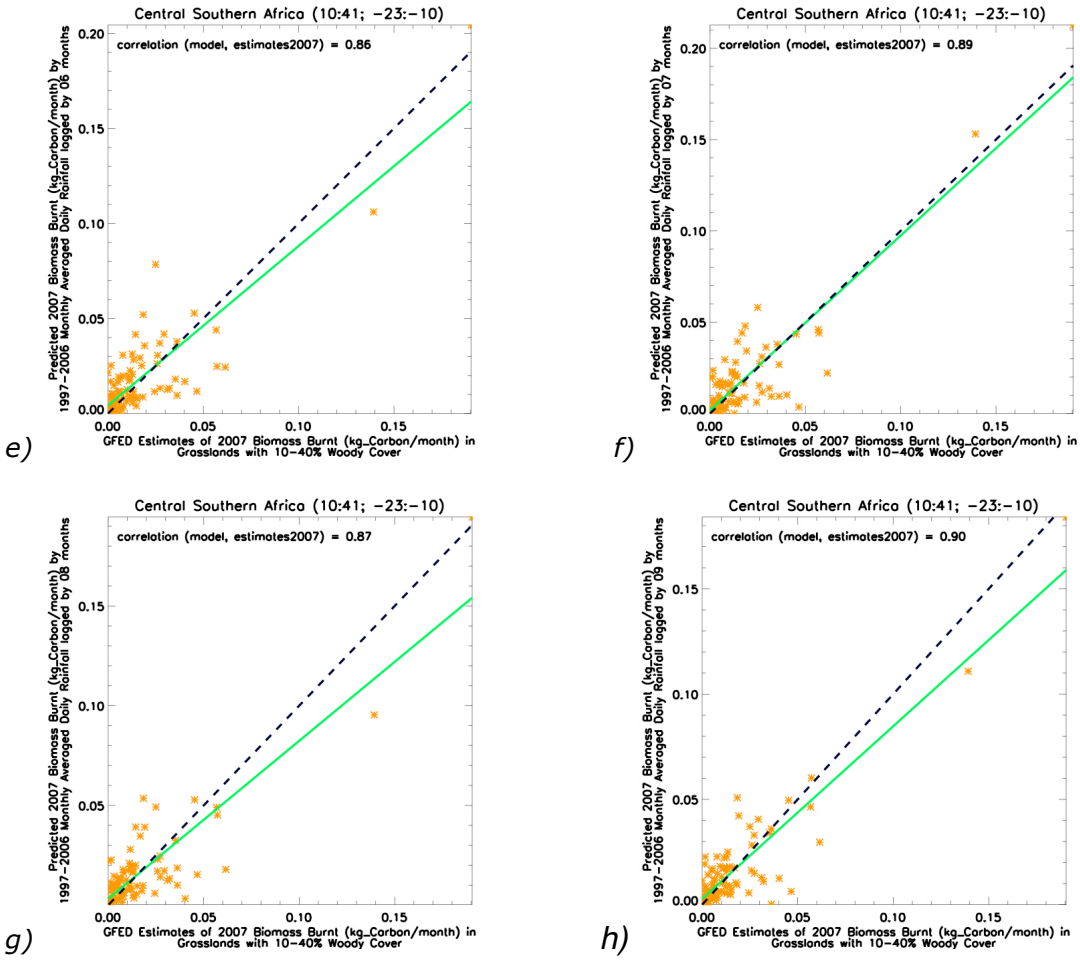

Figure 3.23.7 Scatterplots of predicted biomass burnt for the year of 2007 versus the correspondent GFED estimates, expressed in kilograms of carbon emissions per month, in the grasslands with 10 to 40% woody cover of Central Southern Africa. The green line shows the linear fit through the points, whereas the black dashed line marks where the 1:1 ideal slope would be. Models are based on monthly averaged daily minimum soil wetness, contemporary (a) and lagged by 1 month (b), and on daily rainfall lagged by 1 (c), 5 (d), 6 (e), 7 (f), 8 (g) and 9 (h) months. Although the correlation between the predictions and the observations is very high (up to 90%), the values are more spread for larger carbon emissions, so this model is likely to considerably improve with more data. Only eco-regions where models are correlated by more than 75% with observations are presented.

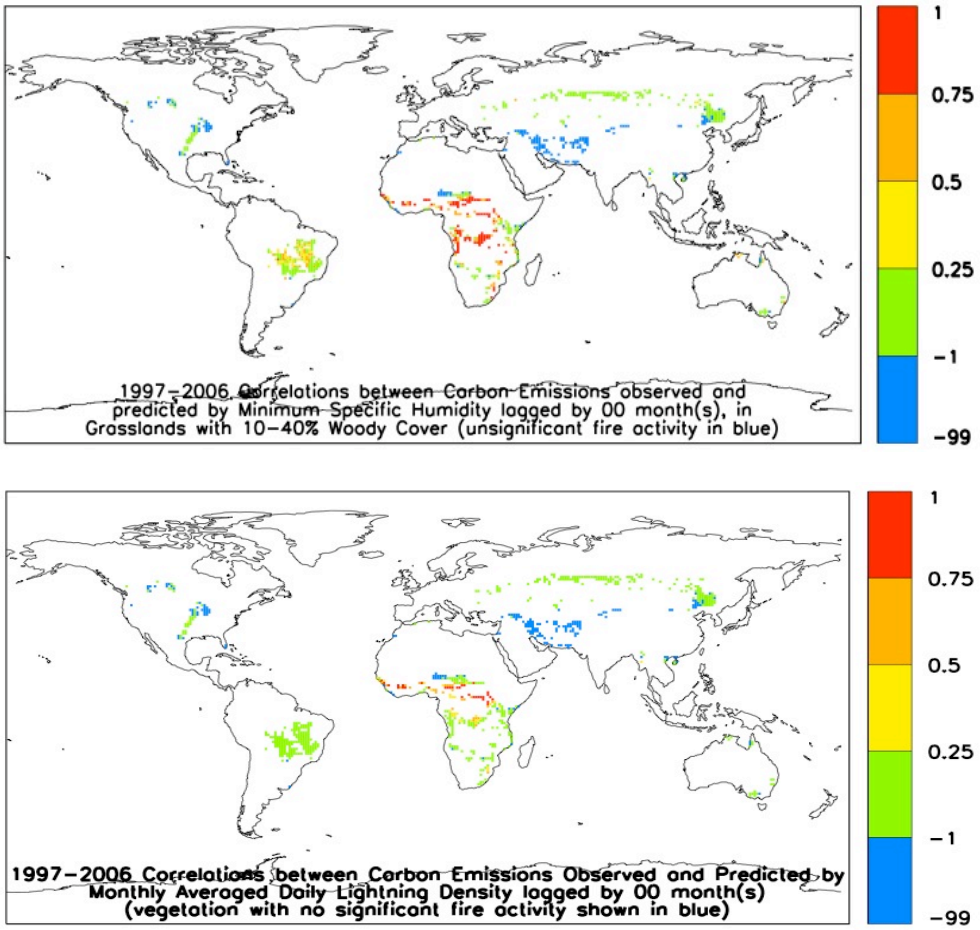

Figure 3.23.8 World map of correlations between model predictions and GFED estimations of carbon emissions from wildfires, from 1997 to 2006, in grasslands with 10 to 40% woody cover, with a) specific humidity and b) lightning density during the fire season as the predictor. Red pixels have the best models (correlations with observations above 75%), followed by orange and yellow pixels with correlations between 50% and 75%, and between 25% and 50%, respectively. Green pixels do not have reliable models with this predictor. Blue pixels do not show significant fire activity at 1ºx1º resolution.

3.24 Grassland, less than 10% Woody Cover

Grasslands with less than 10% of woody cover occupy a large world area, mainly in Northern South America, Equatorial Africa and Northern Australia.

After a humid and rainy wet season in these grasslands, fires increased in Africa (except in the monsoon area), North Australia and South America. 4, 5 and 6 months after heavy rainfall, wildfires strongly increased (rank-correlations superior to 75%) in Equatorial Africa (figure 3.24.4), so this could be used for predictive models (figures 3.24.5 g-j).

Humid fire seasons had fewer fires in Equatorial Africa, Northern South America, Eastern Brazil, the Amazon borders and Northern Australia (figure 3.24.1a).

High temperatures during the fire season favoured wildfires, except in the western coastal area of North Southern Africa and immediately south of the Sahel, where convective rainfall occurred during the warmest weather (figure 3.24.1 b).

Rainfall prior to the fire season and contemporary humidity and soil wetness were good predictors of biomass burning in North and Equatorial Africa (figures 3.24.2, 3.24.3, 3.24.5 and 3.24.6a), together with contemporary temperature (figure 3.24.6 b).

a)

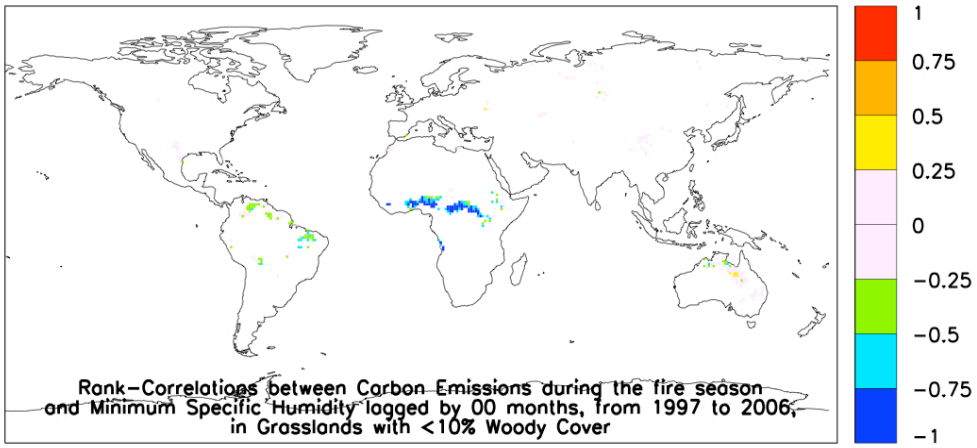

b)

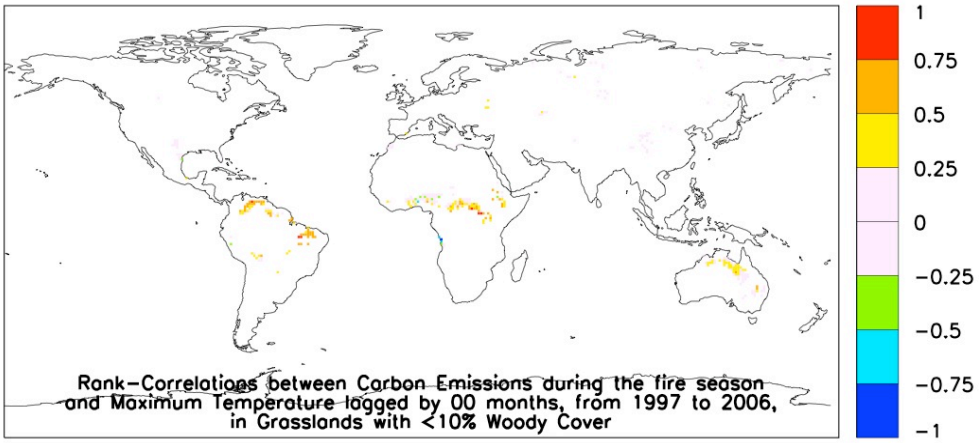

Figure 3.24.1 World maps of rank-correlations between wildfires and a) air humidity and b) air temperature, during the fire season, from 1997 to 2006, in grasslands with less than 10% woody cover. Pixels in green and blue show areas where fires increase during a) drier or b) colder weather, whereas yellow, orange and red pixels show areas where fires increase with a) more humid or b) warmer weather.

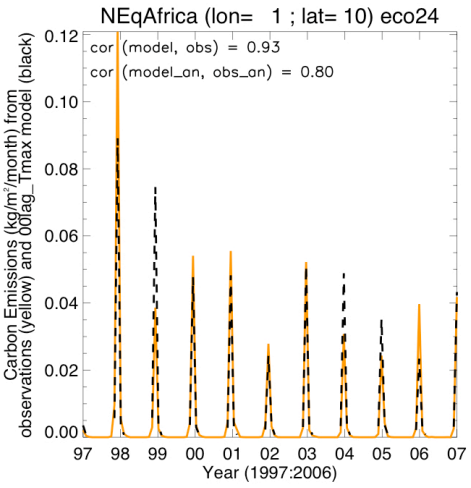
NEqAfrica (lon= 1 ; lat= 10) eco24
cor (model, obs) = 0.93
cor (model_an, obs_an) = 0.80
Carbon Emissions (kg/m²/month) from observations (yellow) and 00lag_Tmax model (black)
Year (1997:2006)

a)

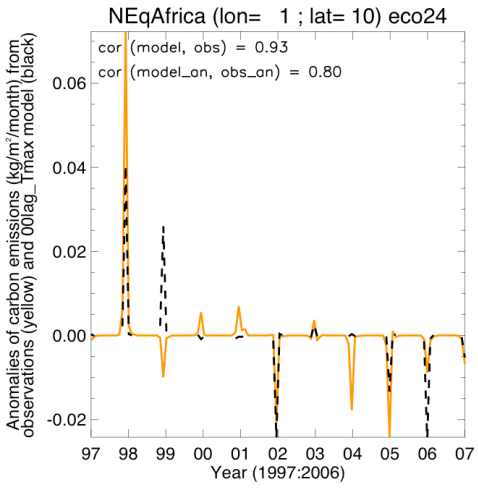
NEqAfrica (lon= 1 ; lat= 10) eco24
cor (model, obs) = 0.93
cor (model_an, obs_an) = 0.80
Anomalies of carbon emissions (kg/m²/month) from observations (yellow) and 00lag_Tmax model (black)
Year (1997:2006)

b)

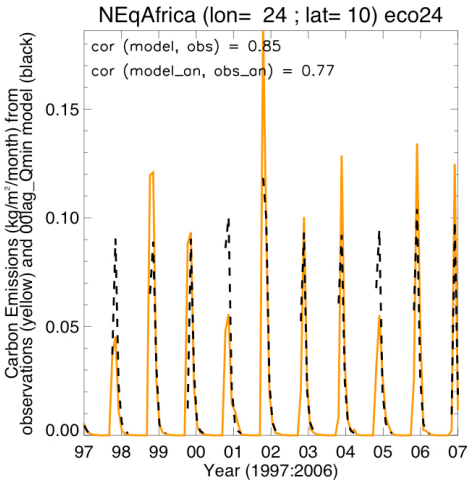
NEqAfrica (lon= 24 ; lat= 10) eco24
cor (model, obs) = 0.85
cor (model_an, obs_an) = 0.77
Carbon Emissions (kg/m²/month) from observations (yellow) and 00lag_Qmin model (black)
Year (1997:2006)

c)

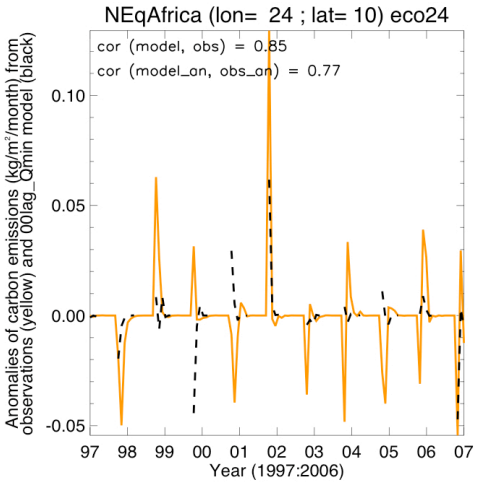
NEqAfrica (lon= 24 ; lat= 10) eco24
cor (model, obs) = 0.85
cor (model_an, obs_an) = 0.77
Anomalies of carbon emissions (kg/m²/month) from observations (yellow) and 00lag_Qmin model (black)
Year (1997:2006)

d)

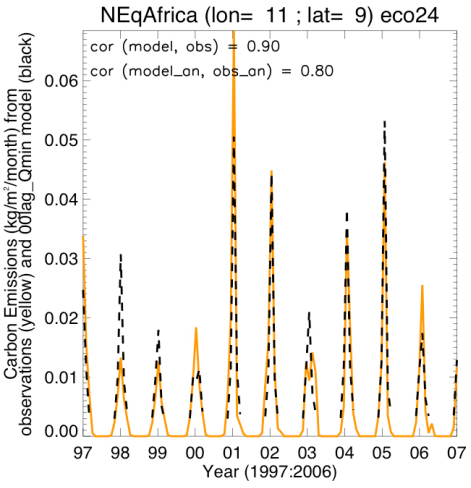
NEqAfrica (lon= 11 ; lat= 9) eco24
cor (model, obs) = 0.90
cor (model_an, obs_an) = 0.80
Carbon Emissions (kg/m²/month) from observations (yellow) and 00lag_Qmin model (black)
Year (1997:2006)

e)

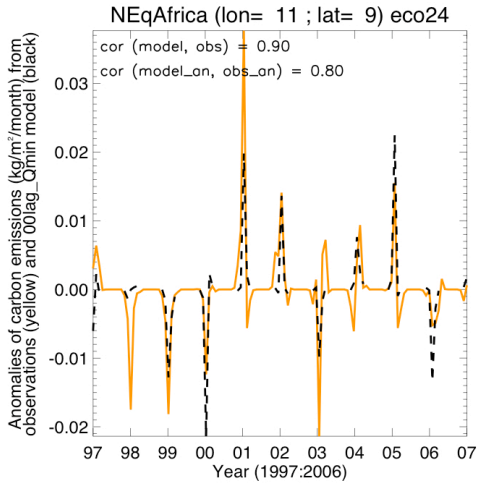
NEqAfrica (lon= 11 ; lat= 9) eco24
cor (model, obs) = 0.90
cor (model_an, obs_an) = 0.80
Anomalies of carbon emissions (kg/m²/month) from observations (yellow) and 00lag_Qmin model (black)
Year (1997:2006)

f)

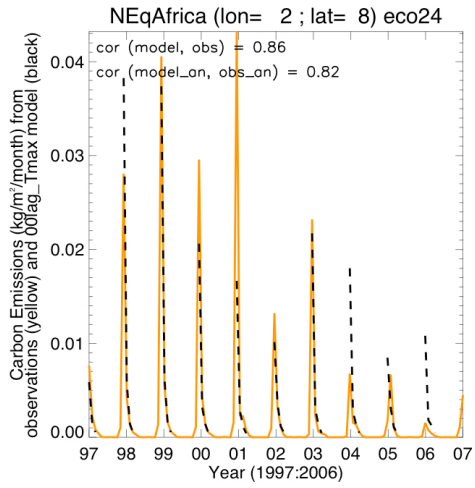

g)

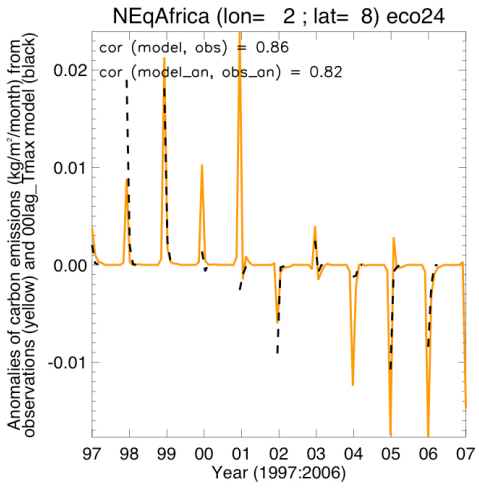

h)

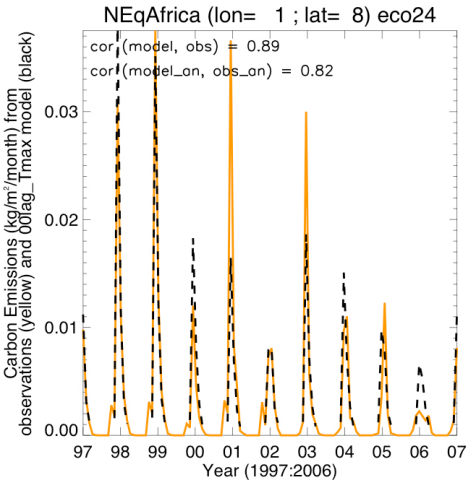

i)

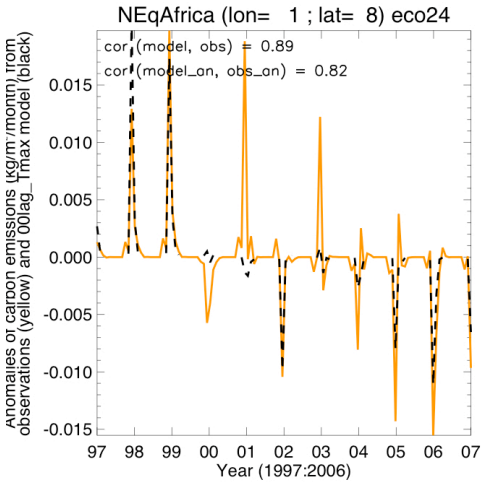

j)

Figure 3.24.2 Time series of biomass burning (expressed as carbon emissions) and anomalies, from 1997 to 2006, given by GFED estimates, in five individual pixels of the grasslands with less than 10% woody cover of North Equatorial Africa (a-j). Over-plotted in black is a model based on monthly averages of maximum air temperature (a-b, g-h, i-j) or minimum specific humidity (c-d, e-f). High correlations (above 75%) between models and GFED estimates show that these models capture a considerable part of the interannual variability in carbon emissions.

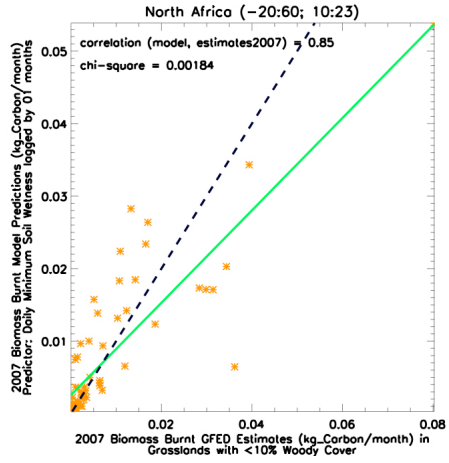
North Africa (−20:60; 10:23)
correlation (model, estimates2007) = 0.85
chi-square = 0.00184
2007 Biomass Burnt Model Predictions (kg_Carbon/month)
Predictor: Daily Minimum Soil Weiness lagged by 01 months
2007 Biomass Burnt GFED Estimates (kg_Carbon/month) in
Grasslands with <10% Woody Cover

a)

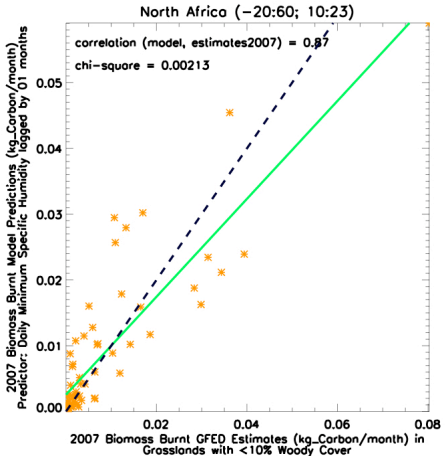
North Africa (−20:60; 10:23)
correlation (model, estimates2007) = 0.87
chi-square = 0.00213
2007 Biomass Burnt Model Predictions (kg_Carbon/month)
Predictor: Daily Minimum Specific Humidity lagged by 01 months
2007 Biomass Burnt GFED Estimates (kg_Carbon/month) in
Grasslands with <10% Woody Cover

b)

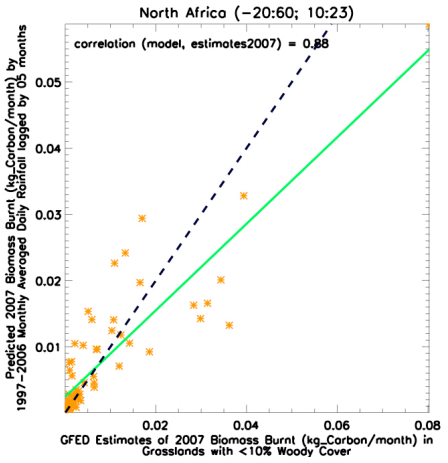
North Africa (−20:60; 10:23)
correlation (model, estimates2007) = 0.88
Predicted 2007 Biomass Burnt (kg_Carbon/month) by
1997-2006 Monthly Averaged Daily Rainfall lagged by 05 months
GFED Estimates of 2007 Biomass Burnt (kg_Carbon/month) in
Grasslands with <10% Woody Cover

c)

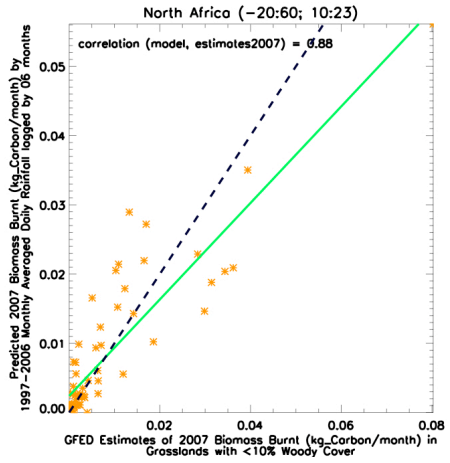
North Africa (−20:60; 10:23)
correlation (model, estimates2007) = 0.88
Predicted 2007 Biomass Burnt (kg_Carbon/month) by
1997-2006 Monthly Averaged Daily Rainfall lagged by 06 months
GFED Estimates of 2007 Biomass Burnt (kg_Carbon/month) in
Grasslands with <10% Woody Cover

d)

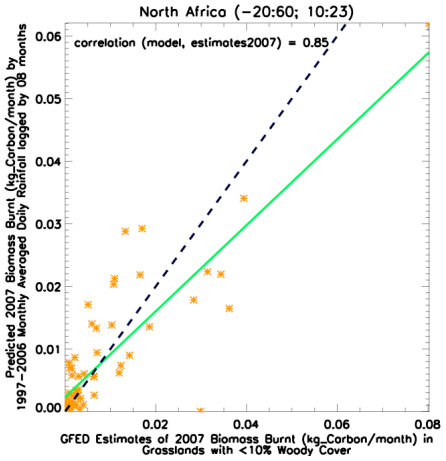

e)

Figure 3.24.3 Scatterplot of predicted biomass burnt for the year of 2007 versus the correspondent GFED estimates, expressed in kilograms of carbon emissions per month, in the grasslands with less than 10% woody cover of North Equatorial Africa. The green line shows the linear fit through the points, whereas the black dashed line marks where the 1:1 ideal slope would be. Model based on monthly averaged daily lagged by 1 (a), 5 (b), 6 (c) and 8 months (d). Only eco-regions where models are correlated to observations by more than 75% are shown. Carbon emissions from large fires, for which data is scarce, are under-predicted, but the model is likely to improve with more data.

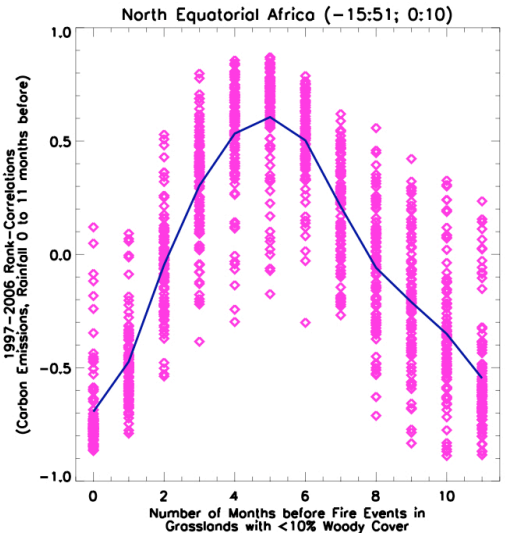

Figure 3.24.4 Scatterplot of rank-correlations between monthly carbon emissions during the fire season and monthly rainfall, contemporary and up to 11 months before, versus the lags, i.e., the number of months by which the rain preceded the fire, in all the 1ºx1º resolution pixels with significant fire activity in the grasslands with less than 10% woody cover of North Equatorial Africa, from 1997 to 2006. Different pixels of an eco-region show different rank-correlations between fires and rainfall, but they are mainly negative for lags up to 2 months, and positive for lags of 3 to 7 months.

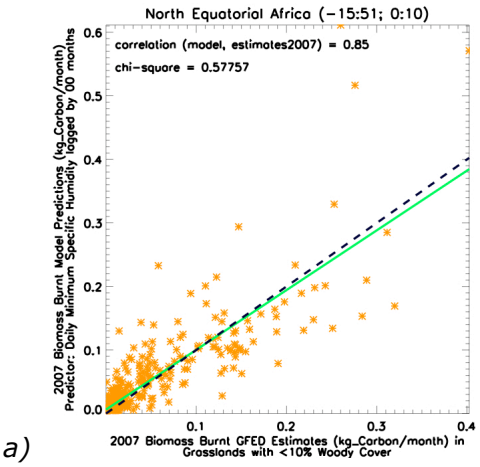
North Equatorial Africa (−15:51; 0:10)
correlation (model, estimates2007) = 0.85
chi-square = 0.57757
2007 Biomass Burnt Model Predictions (kg_Carbon/month)
Predictor: Daily Minimum Specific Humidity lagged by 00 months
2007 Biomass Burnt GFED Estimates (kg_Carbon/month) in
Grasslands with <10% Woody Cover

a)

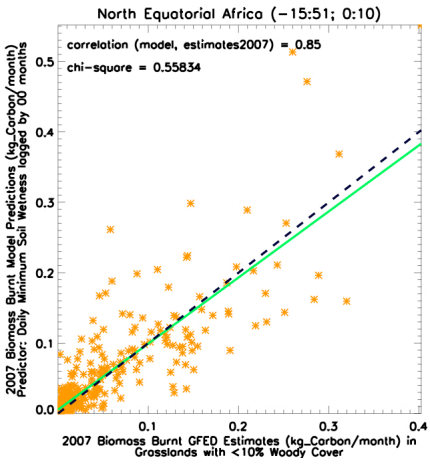
North Equatorial Africa (−15:51; 0:10)
correlation (model, estimates2007) = 0.85
chi-square = 0.55834
2007 Biomass Burnt Model Predictions (kg_Carbon/month)
Predictor: Daily Minimum Soil Wetness lagged by 00 months
2007 Biomass Burnt GFED Estimates (kg_Carbon/month) in
Grasslands with <10% Woody Cover

b)

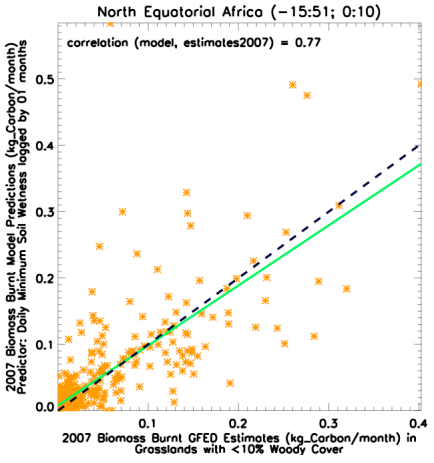
North Equatorial Africa (−15:51; 0:10)
correlation (model, estimates2007) = 0.77
2007 Biomass Burnt Model Predictions (kg_Carbon/month)
Predictor: Daily Minimum Soil Wetness lagged by 01 months
2007 Biomass Burnt GFED Estimates (kg_Carbon/month) in
Grasslands with <10% Woody Cover

c)

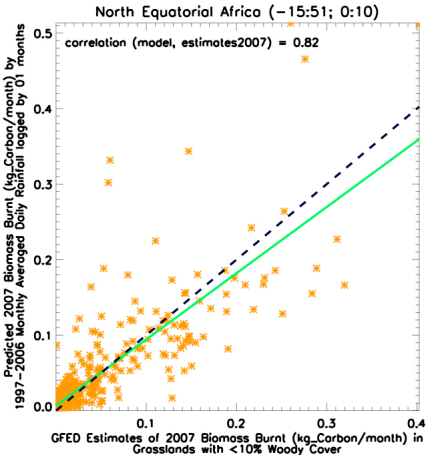
North Equatorial Africa (−15:51; 0:10)
correlation (model, estimates2007) = 0.82
Predicted 2007 Biomass Burnt (kg_Carbon/month) by
1997-2006 Monthly Averaged Daily Rainfall lagged by 01 months
GFED Estimates of 2007 Biomass Burnt (kg_Carbon/month) in
Grasslands with <10% Woody Cover

d)

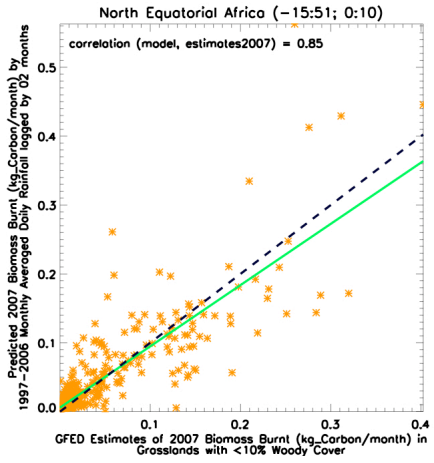
North Equatorial Africa (−15:51; 0:10)
correlation (model, estimates2007) = 0.85
Predicted 2007 Biomass Burnt (kg_Carbon/month) by
1997-2006 Monthly Averaged Daily Rainfall lagged by 02 months
GFED Estimates of 2007 Biomass Burnt (kg_Carbon/month) in
Grasslands with <10% Woody Cover

e)

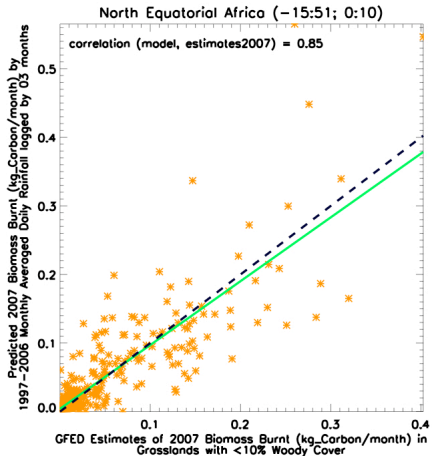
North Equatorial Africa (−15:51; 0:10)
correlation (model, estimates2007) = 0.85
Predicted 2007 Biomass Burnt (kg_Carbon/month) by
1997-2006 Monthly Averaged Daily Rainfall lagged by 03 months
GFED Estimates of 2007 Biomass Burnt (kg_Carbon/month) in
Grasslands with <10% Woody Cover

f)

g)

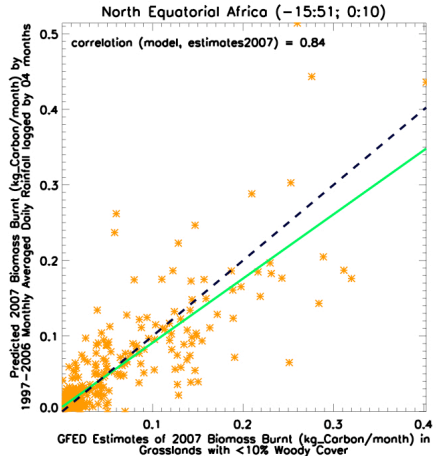
North Equatorial Africa (−15:51; 0:10)
correlation (model, estimates2007) = 0.84
Predicted 2007 Biomass Burnt (kg_Carbon/month) by 1997–2006 Monthly Averaged Daily Rainfall lagged by 04 months
GFED Estimates of 2007 Biomass Burnt (kg_Carbon/month) in Grasslands with <10% Woody Cover

h)

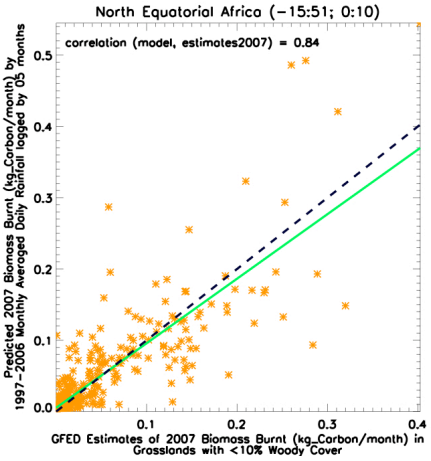
North Equatorial Africa (−15:51; 0:10)
correlation (model, estimates2007) = 0.84
Predicted 2007 Biomass Burnt (kg_Carbon/month) by 1997–2006 Monthly Averaged Daily Rainfall lagged by 05 months
GFED Estimates of 2007 Biomass Burnt (kg_Carbon/month) in Grasslands with <10% Woody Cover

i)

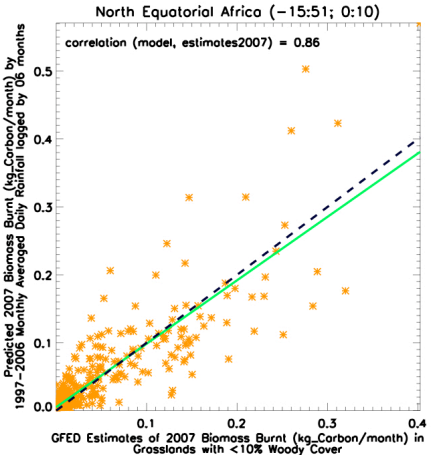
North Equatorial Africa (−15:51; 0:10)
correlation (model, estimates2007) = 0.86
Predicted 2007 Biomass Burnt (kg_Carbon/month) by 1997–2006 Monthly Averaged Daily Rainfall lagged by 06 months
GFED Estimates of 2007 Biomass Burnt (kg_Carbon/month) in Grasslands with <10% Woody Cover

j)

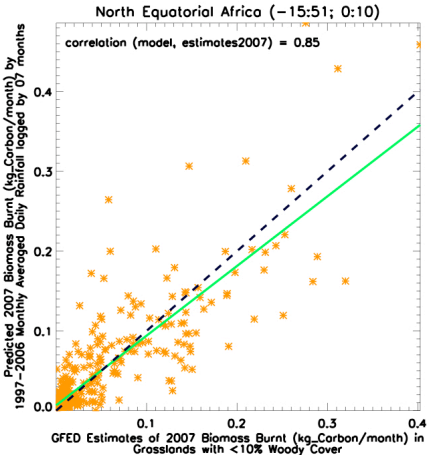
North Equatorial Africa (−15:51; 0:10)
correlation (model, estimates2007) = 0.85
Predicted 2007 Biomass Burnt (kg_Carbon/month) by 1997–2006 Monthly Averaged Daily Rainfall lagged by 07 months
GFED Estimates of 2007 Biomass Burnt (kg_Carbon/month) in Grasslands with <10% Woody Cover

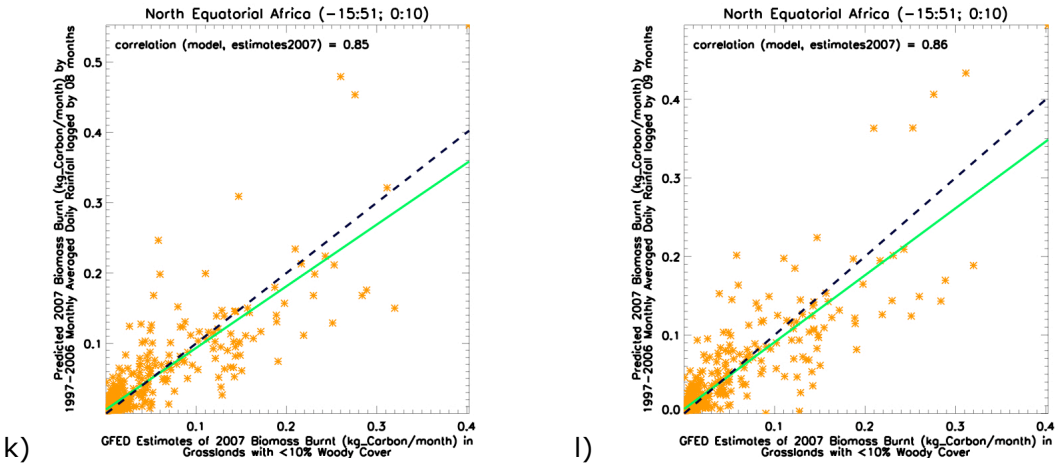

Figure 3.24.5 Scatterplots of predicted biomass burnt for the year of 2007 versus the correspondent GFED estimates, expressed in kilograms of carbon emissions per month, in the grasslands with less than 10% woody cover of North Equatorial Africa. Model based on monthly averaged daily minimum specific humidity, contemporary with fire events (a), minimum soil wetness, contemporary (b) and lagged by 1 month (c), and rainfall lagged by 1 (d), 2 (e), 3 (f), 4 (g), 5 (h), 6 (i), 7 (j), 8 (k) and 9 months (l). Only eco-regions where models are correlated to observations by more than 75% are shown.

a)

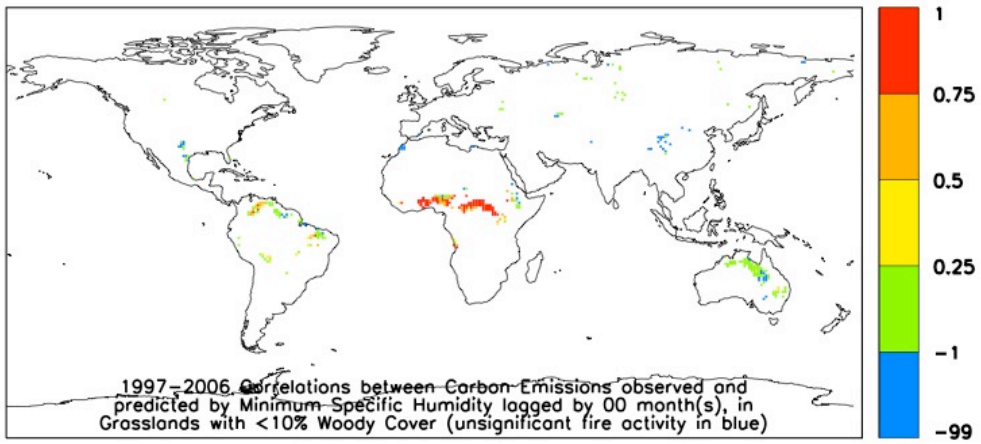

b)

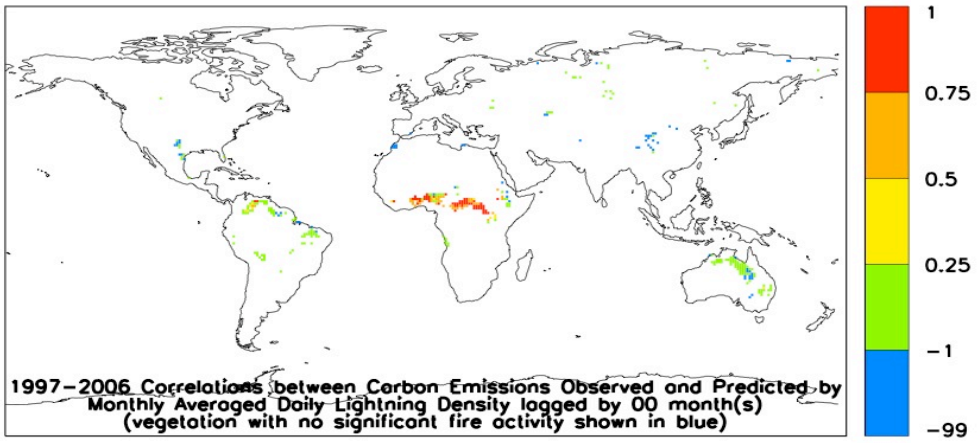

Figure 3.24.6 World map of correlations between model predictions and GFED estimations of carbon emissions from wildfires, from 1997 to 2006, in grasslands with less than 10% woody cover, with a) specific humidity and b) lightning density during the fire season as the predictor. Red pixels have the best models (correlations with observations above 75%), followed by orange and yellow pixels with correlations between 50% and 75%, and between 25% and 50%, respectively. Green pixels do not have reliable models with this predictor. Blue pixels do not show significant fire activity at 1ºx1º resolution.

3.25 Grassland, Shrub Cover

Fires in grasslands with shrub cover seem to be more fuel-driven in tropical regions, but more weather-driven in temperate regions:

after a rainy and humid winter, there were fewer fires in Western Russia, West Asia and in the monsoon area in West Africa, but more in North Africa, Equatorial Africa, South Southern Africa, Madagascar and Central America (correlation maps and plots not shown).

During humid fire seasons, wildfires decreased in North Africa, South Southern Africa, Madagascar, South East Asia and Australia (figure 3.25.1-3).

In Central Europe and Russia, individual pixels showed an increase of fires with humidity (figure 3.25.1), possibly because summers are more humid than winters; however, scatterplots of carbon emissions versus humidity in West Russian grasslands with shrubs showed that, overall, more humid places had less fires than drier places (figure 3.25.3 a). This is another example of the importance of analyzing both individual pixels (changes in monthly carbon emissions with weather), and all the pixels of a whole eco-region (climatic averages of carbon emissions versus climatic averages of weather variables).

Fast winds during the summer in grasslands with shrub cover were correlated to larger burnt areas, but this may be caused by high-pressure systems bringing dry weather, not by wind spreading fire.

Contemporary air humidity, soil wetness and temperature, together with rainfall prior to the fire season, were good predictors of biomass burning in Equatorial and Southern Africa (figures 3.25.4-5).

a)

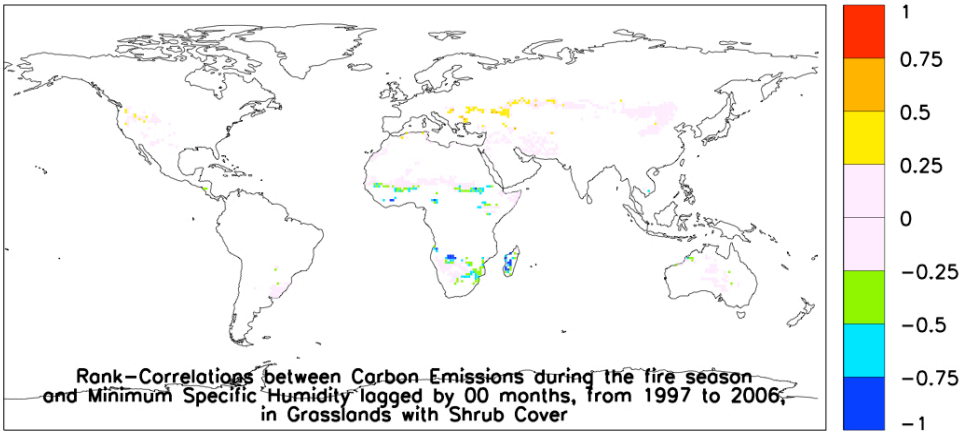

b)

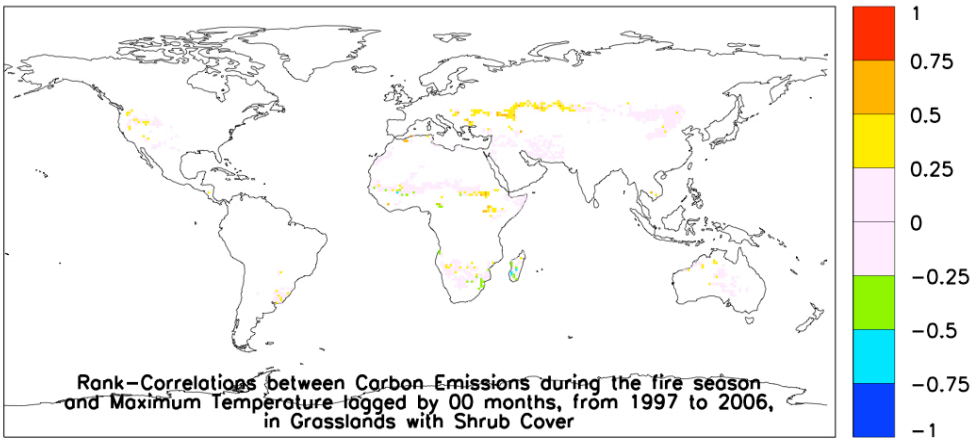

Figure 3.25.1 World maps of rank-correlations between wildfires and a) air humidity and b) air temperature, during the fire season, from 1997 to 2006, in grasslands with shrub cover. Pixels in green and blue show areas where fires increase during a) drier or b) colder weather, whereas yellow, orange and red pixels show areas where fires increase with a) more humid or b) warmer weather.

Figure 3.25.2 Scatterplot of rank-correlations between monthly carbon emissions during the fire season and monthly rainfall, contemporary and up to 11 months before, versus the lags, i.e., the number of months by which the rain preceded the fire, in all the 1ºx1º resolution pixels with significant fire activity in the grasslands with shrub cover of Madagascar, from 1997 to 2006. Different pixels of an eco-region show different rank-correlations between fires and rainfall, but they are mainly negative for lags up to 2 months, and positive for lags of 4 to 9 months.

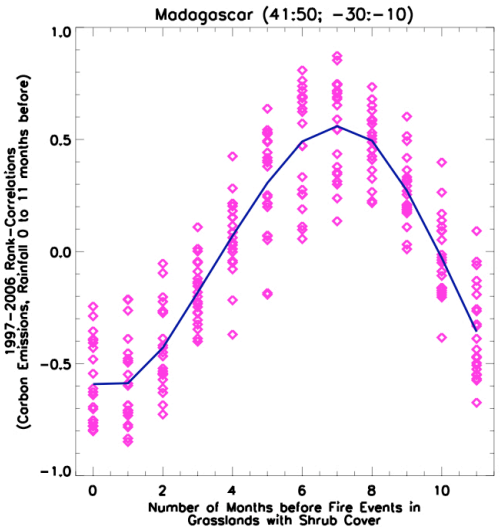

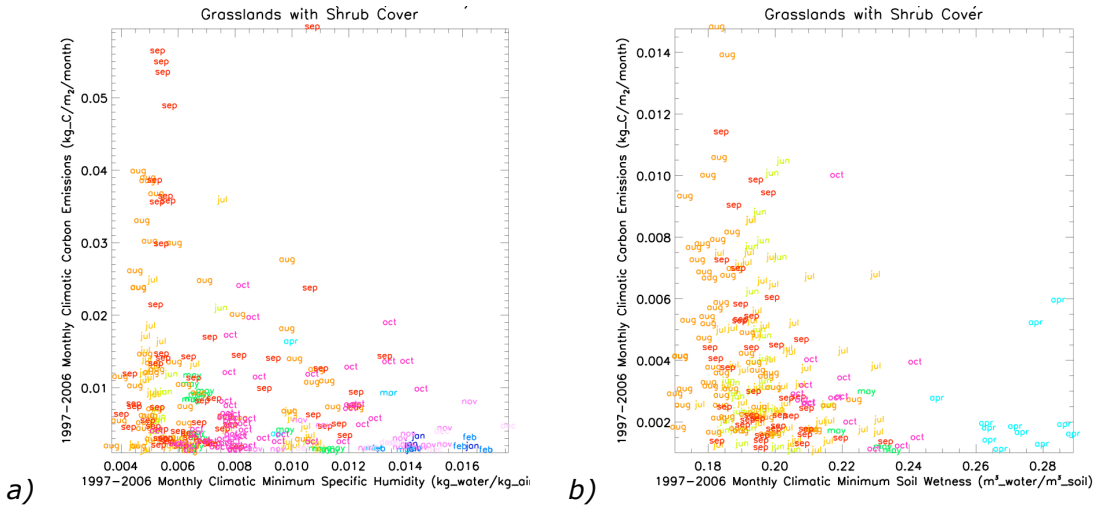

a) b)

Figure 3.25.3 Scatterplot of carbon emissions from wildfires versus minimum air humidity in the grasslands with shrub cover of Central Southern Africa (a), and versus minimum soil wetness in Western Russia (b). Each point corresponds to a pixel of 1ºx1º resolution, with values averaged over homonymous months, from 1997 to 2006.

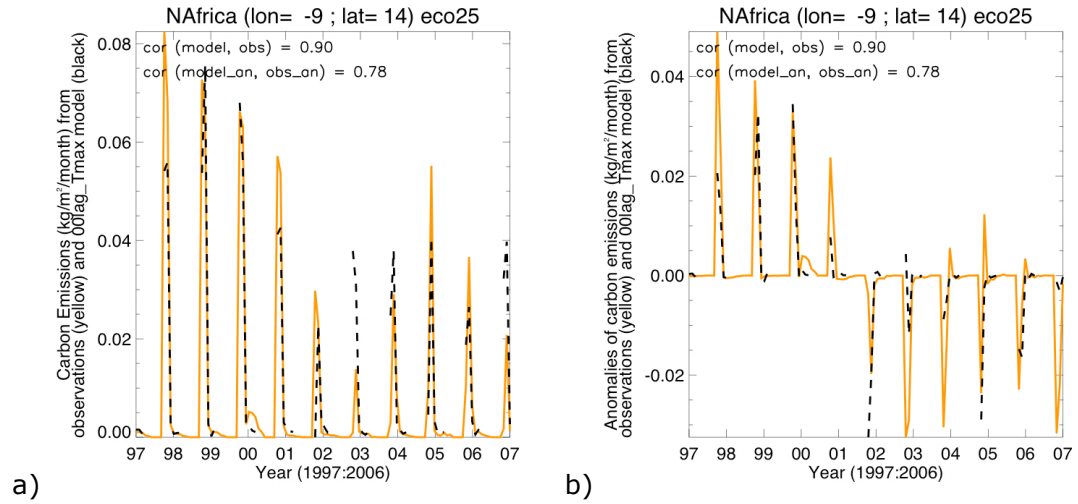

Figure 3.25.4 Time series of biomass burning (expressed as carbon emissions) and anomalies, from 1997 to 2006, given by GFED estimates, for one individual pixel in the grasslands with shrub cover of North Africa (a-b). Over-plotted in black is a model based on monthly averages of minimum specific humidity. High correlations (above 75%) between predictions and GFED estimates of anomalies show that these models capture a considerable part of the interannual variability in carbon emissions.

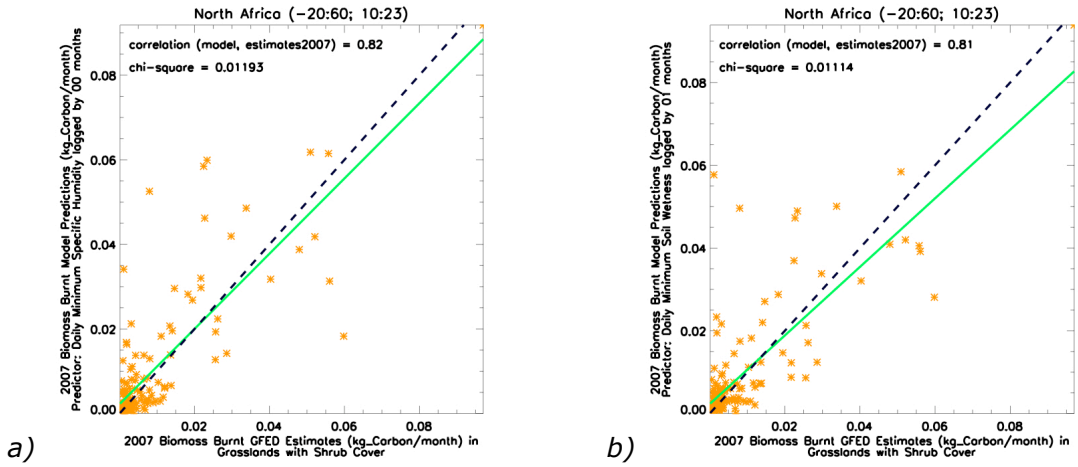

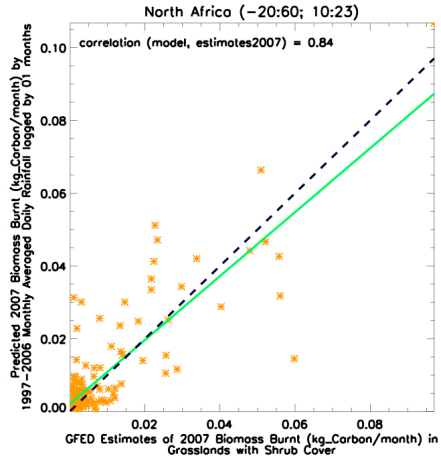
North Africa (-20:60; 10:23)
correlation (model, estimates2007) = 0.84
Predicted 2007 Biomass Burnt (kg_Carbon/month) by 1997-2006 Monthly Averaged Daily Rainfall lagged by 01 months
GFED Estimates of 2007 Biomass Burnt (kg_Carbon/month) in Grasslands with Shrub Cover

c)

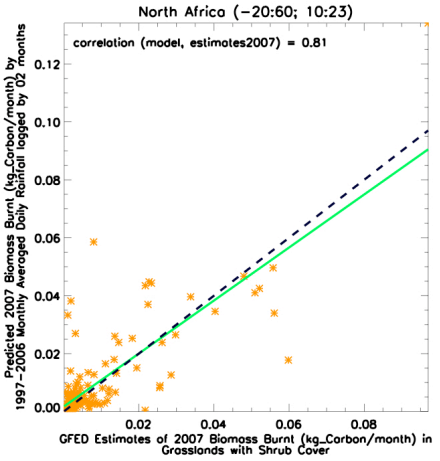
North Africa (-20:60; 10:23)
correlation (model, estimates2007) = 0.81
Predicted 2007 Biomass Burnt (kg_Carbon/month) by 1997-2006 Monthly Averaged Daily Rainfall lagged by 02 months
GFED Estimates of 2007 Biomass Burnt (kg_Carbon/month) in Grasslands with Shrub Cover

d)

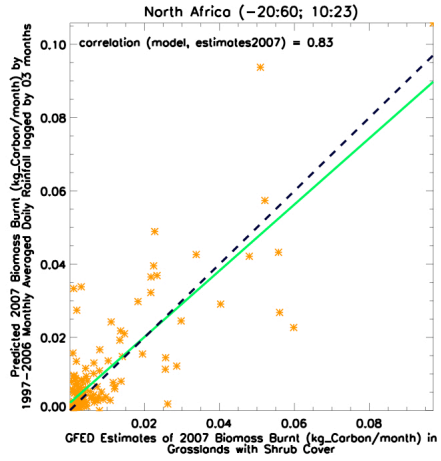
North Africa (-20:60; 10:23)
correlation (model, estimates2007) = 0.83
Predicted 2007 Biomass Burnt (kg_Carbon/month) by 1997-2006 Monthly Averaged Daily Rainfall lagged by 03 months
GFED Estimates of 2007 Biomass Burnt (kg_Carbon/month) in Grasslands with Shrub Cover

e)

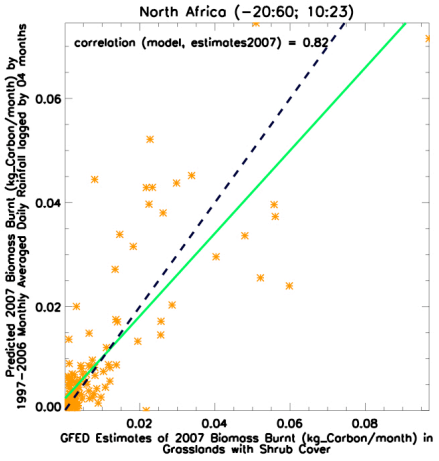
North Africa (-20:60; 10:23)
correlation (model, estimates2007) = 0.82
Predicted 2007 Biomass Burnt (kg_Carbon/month) by 1997-2006 Monthly Averaged Daily Rainfall lagged by 04 months
GFED Estimates of 2007 Biomass Burnt (kg_Carbon/month) in Grasslands with Shrub Cover

f)

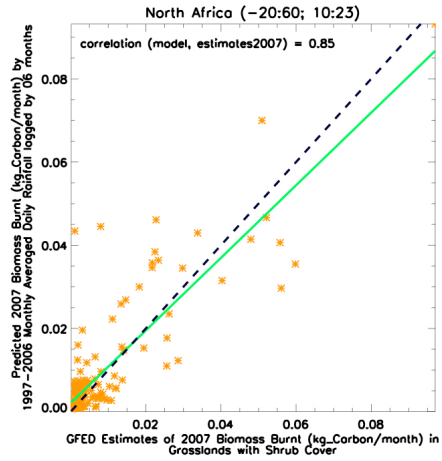
North Africa (-20:60; 10:23)
correlation (model, estimates2007) = 0.85
Predicted 2007 Biomass Burnt (kg_Carbon/month) by 1997-2006 Monthly Averaged Daily Rainfall lagged by 06 months
GFED Estimates of 2007 Biomass Burnt (kg_Carbon/month) in Grasslands with Shrub Cover

g)

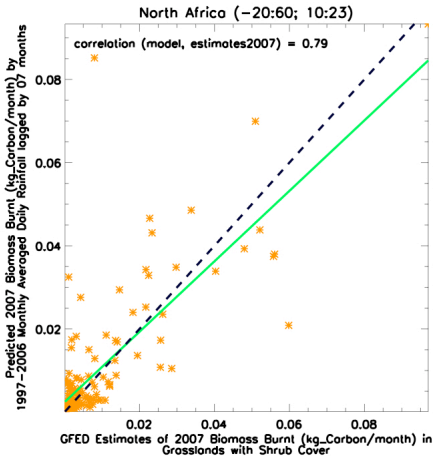
North Africa (-20:60; 10:23)
correlation (model, estimates2007) = 0.79
Predicted 2007 Biomass Burnt (kg_Carbon/month) by 1997-2006 Monthly Averaged Daily Rainfall lagged by 07 months
GFED Estimates of 2007 Biomass Burnt (kg_Carbon/month) in Grasslands with Shrub Cover

h)

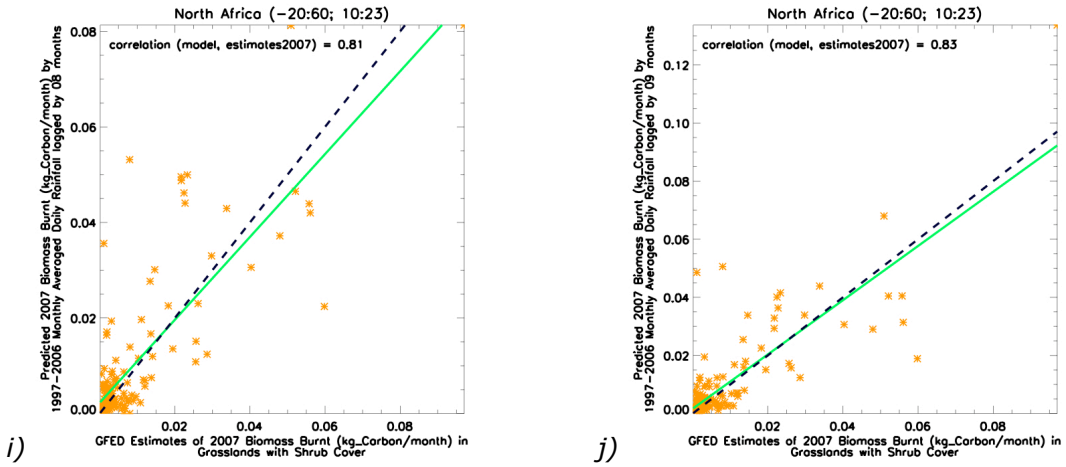

Figure 3.25.4 Scatterplot of predicted biomass burnt for the year of 2007 versus the correspondent GFED estimates, expressed in kilograms of carbon emissions per month, in the grasslands with shrub cover of North Africa. Linear fit through the points shown in green; ideal 1:1 slope shown as a dashed black line. Models based on monthly averaged daily rainfall lagged by 4 (a), 6 (b), 7 (c), 8 (d) and 9 months (e), and on monthly averaged daily minimum specific humidity contemporary with fire events (f). Only eco-regions where models are correlated to observations by more than 75% are shown.

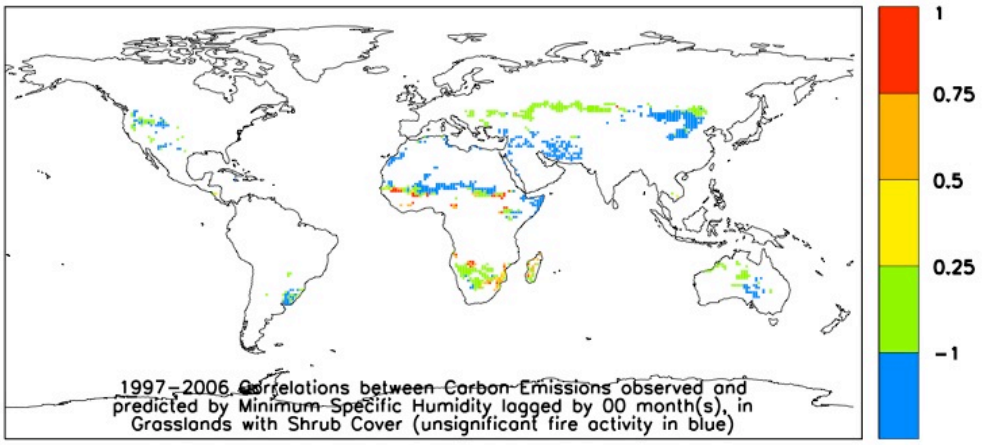

Figure 3.25.5 World map of correlations between model predictions and GFED estimations of carbon emissions from wildfires, from 1997 to 2006, in grasslands with shrub cover, with humidity during the fire season as the predictor. Red pixels have the best models (correlations with observations above 75%), followed by orange (between 50% and 75%) and yellow pixels (between 25% and 50%). Green pixels do not have reliable models with this predictor. Blue pixels do not show significant fire activity at 1ºx1º resolution.

3.26 Tall Grassland, No Woody Cover

Tall grasslands are present mainly in Equatorial Africa, Southern Africa, continental North America and Southern South America.

After a rainy wet season, there were fewer fires in Southern South America, but more in Equatorial Africa (figure 3.26.2) and South Southern Africa. Rainfall up to 8 months before was followed by large carbon emissions, maybe because it contributed to the growth of fuel load during the wet season.

Equatorial Africa had a small fire season, and rain just up to 2 months before was strongly correlated with fires during the following dry season (figure 3.26.2).

During wet and humid summers, there were fewer fires in Equatorial Africa, West Africa, South Southern Africa, Equatorial Asia and North America, but more in Southern South America (figure 3.26.1 a). Warmer summers tended to have more fires (figure 3.26.1 b).

Tall grasslands in Equatorial Africa were one of the eco-regions with more predictable fire behaviour, and where some of the most reliable models were obtained (figures 3.26.3). Contemporary temperature, soil wetness and air humidity, and also rainfall prior to the fire season, were all good predictors of biomass burning in this eco-region.

a)

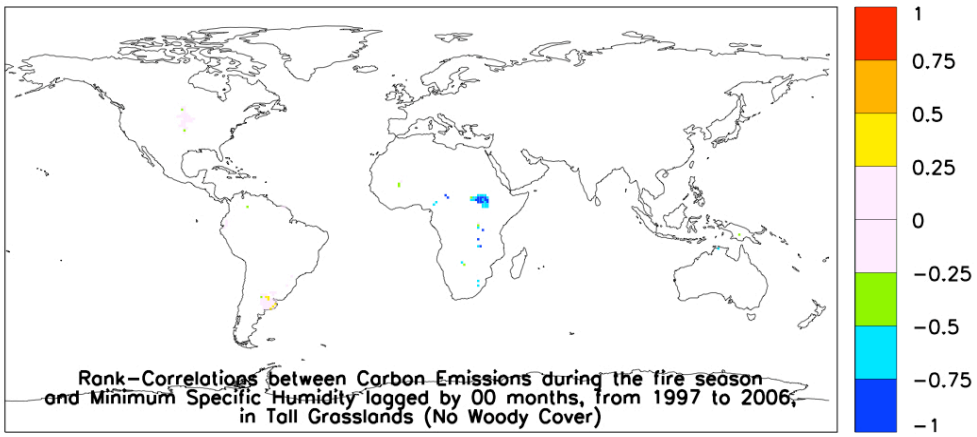

b)

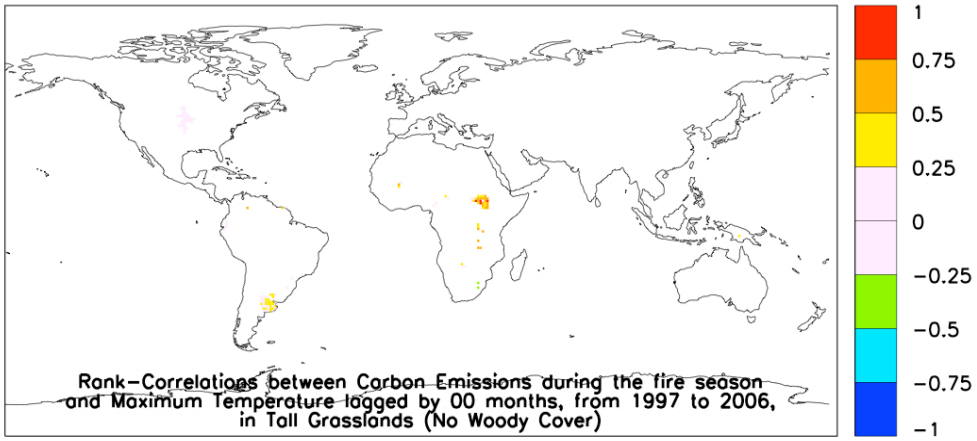

Figure 3.26.1 World maps of rank-correlations between wildfires and a) air humidity and b) air temperature, during the fire season, from 1997 to 2006, in tall grasslands. Pixels in green and blue show areas where fires increase during a) drier or b) colder weather, whereas yellow, orange and red pixels show areas where fires increase with a) more humid or b) warmer weather.

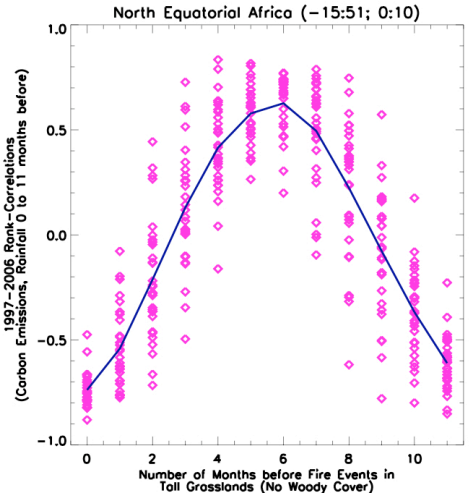

Figure 3.26.2 Scatterplot of rank-correlations between monthly carbon emissions during the fire season and monthly rainfall, contemporary and up to 11 months before, versus the lags, i.e., the number of months by which the rain preceded the fire, in all the 1ºx1º resolution pixels with significant fire activity in the tall grasslands of North Equatorial Africa, from 1997 to 2006. Different pixels of an eco-region show different rank-correlations between fires and rainfall, but they are mainly negative for lags up to 2 months, and positive for lags of 3 to 8 months.

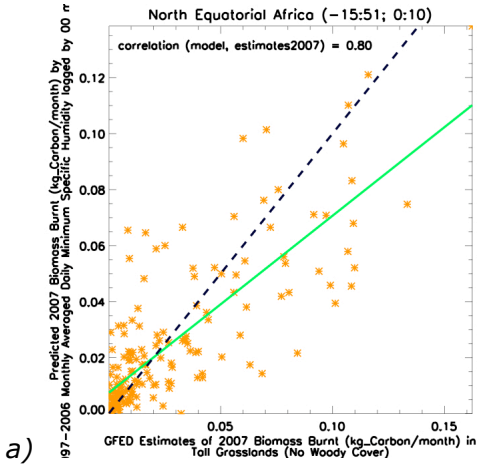

a)

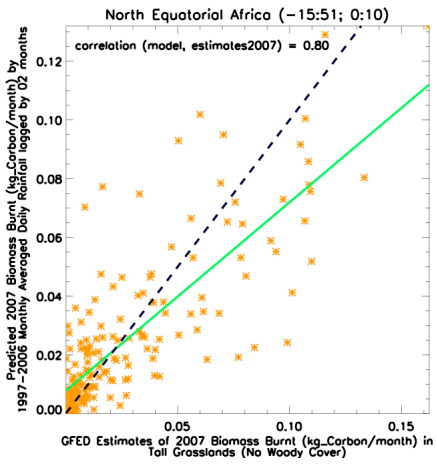

b)

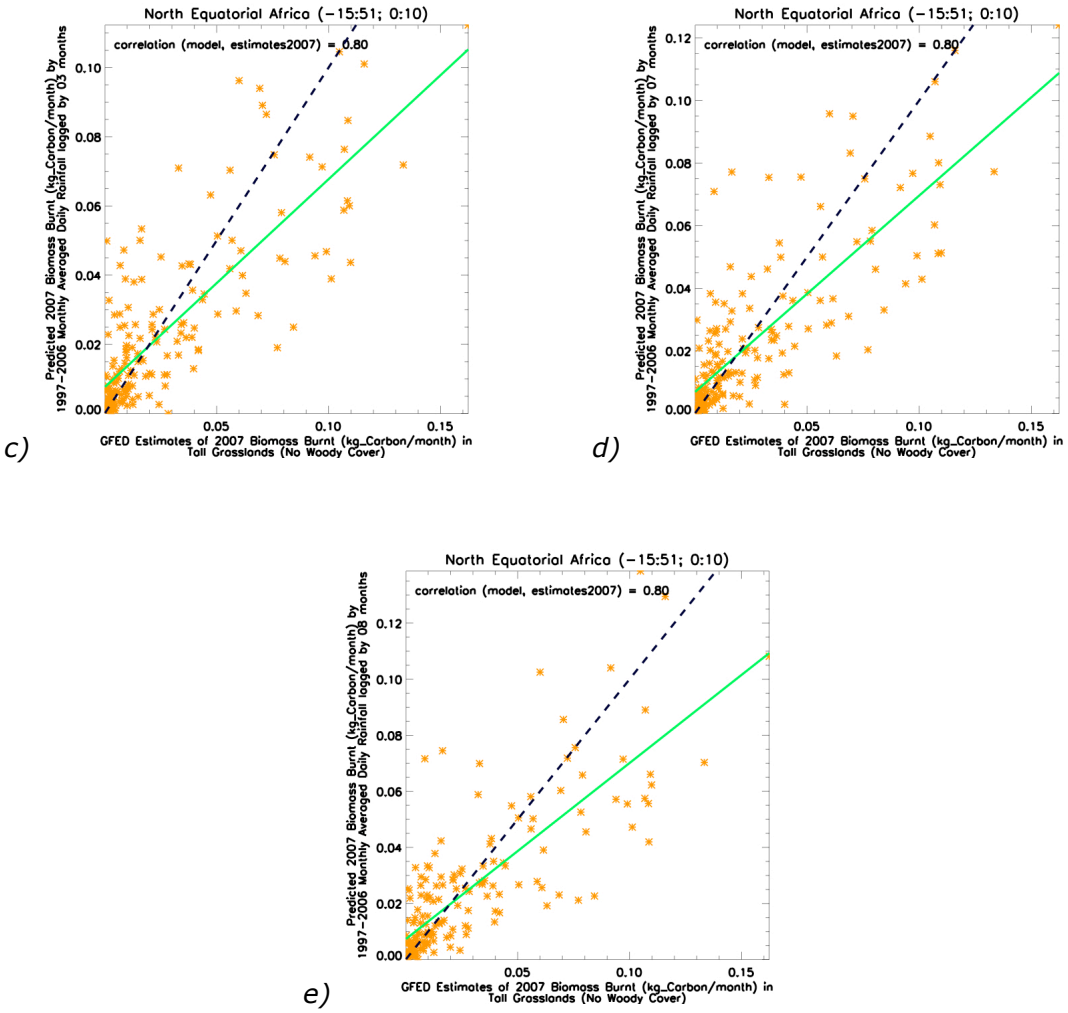

Figure 3.26.3 Scatterplot of predicted biomass burnt for the year of 2007 versus the correspondent GFED estimates, expressed in kilograms of carbon emissions per month, in the tall grasslands of North Equatorial Africa. Model based on monthly averaged daily a) minimum specific humidity contemporary with fire events, and on rainfall lagged by b) 2, c) 3, d) 7 and e) 8 months. Only eco-regions where, overall, models are correlated to observations by more than 75% are shown. Carbon emissions from large fires, for which data is scarce, are under-predicted, but the model can greatly improve with more data.

a)

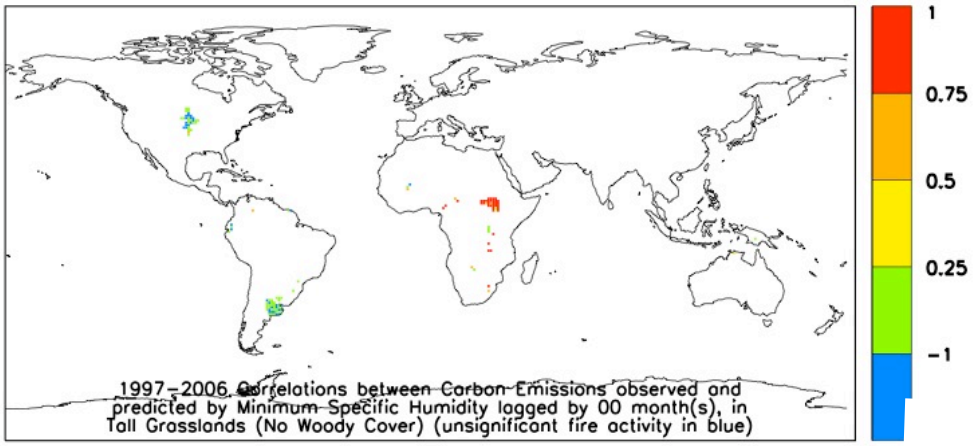

b)

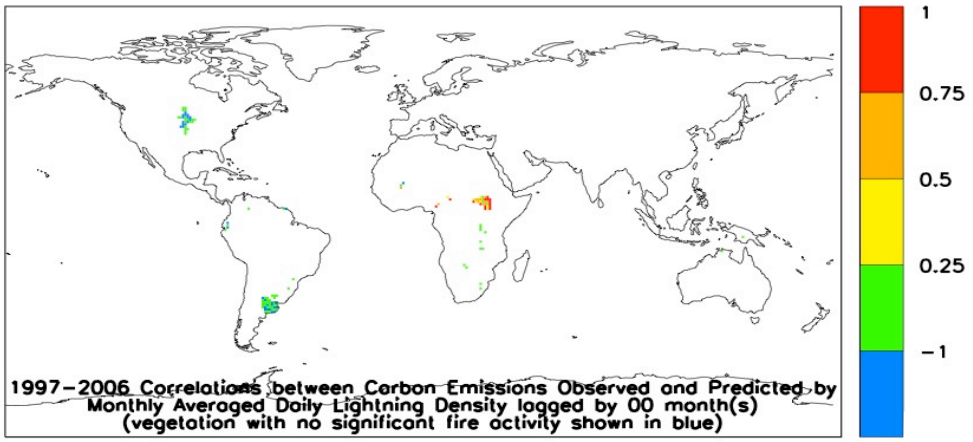

Figure 3.26.4 World map of correlations between model predictions and GFED estimations of carbon emissions from wildfires, from 1997 to 2006, in tall grasslands, with humidity (a) and lightning density (b) during the fire season as the predictor. Red pixels have the best models (correlations with observations above 75%), followed by orange (between 50% and 75%) and yellow pixels (between 25% and 50%). Green pixels do not have reliable models with these predictors. Blue pixels do not show significant fire activity at 1ºx1º resolution.

3.27 Medium Grassland, No Woody Cover

After a rainy and humid winter, there were fewer fires in the medium grasslands of North America, but more in those of Africa and Madagascar (correlation maps and plots not shown).

Humid summers tended to have smaller burnt areas in Southern Africa, Madagascar, Northern Australia, North America and the Caribbean (figure 3.27.1 a).

Fires tended to increase during warmer weather (figure 3.27.1 b). Good models with temperature as a predictor were found in Africa and Madagascar (figure 3.27.3).

In Africa, burnt areas in medium grasslands increased with wind speed, but this is not necessarily connected to easier fire spread by fast winds; it may be related to high correlations between wind and high-pressure systems, thus making wind a proxy for dry weather.

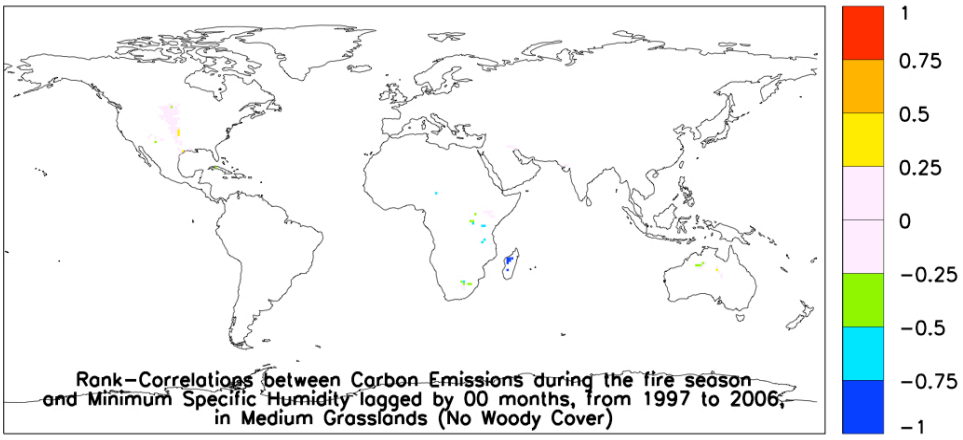

a)

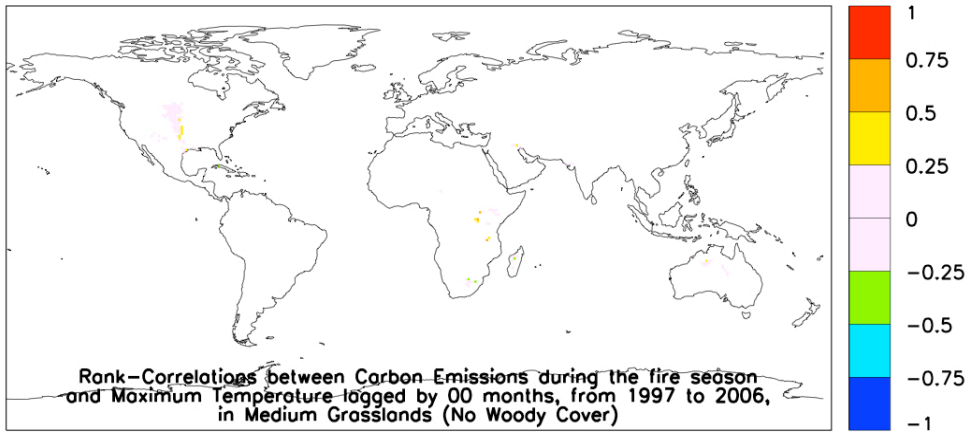

b)

Figure 3.27.1 World maps of rank-correlations between wildfires and a) air humidity and b) air temperature, during the fire season, from 1997 to 2006, in medium grasslands. Pixels in green and blue show areas where fires increase during a) drier or b) colder weather, whereas yellow, orange and red pixels show areas where fires increase with a) more humid or b) warmer weather.

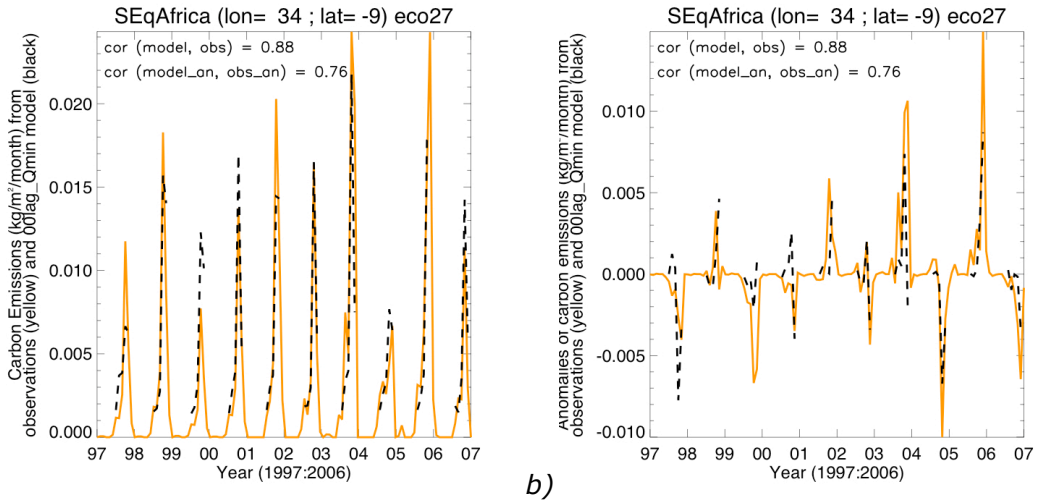

a) b)

Figure 3.27.2 Time series of a) biomass burning (expressed as carbon emissions) and b) anomalies, from 1997 to 2006, given by GFED estimates, for one individual pixel in the medium grasslands of South Equatorial Africa. Over-plotted in black is a model based on monthly averages of minimum specific humidity. High correlations (above 75%) between predictions and GFED estimates show that these models capture a considerable part of the interannual variability in carbon emissions.

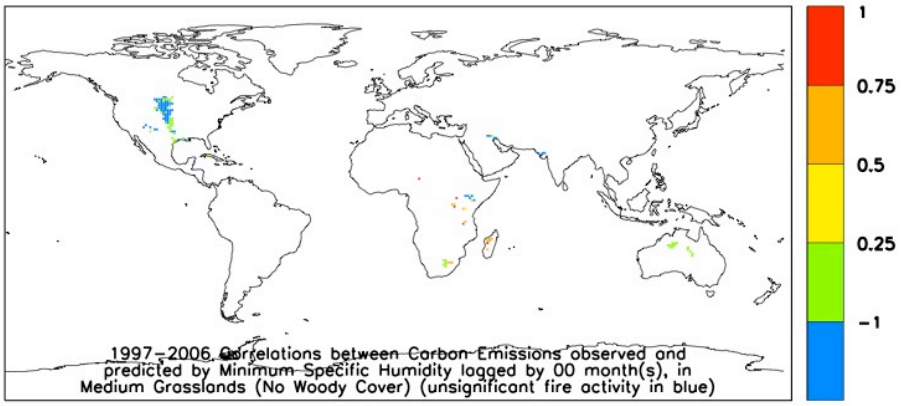

Figure 3.27.2 World map of correlations between model predictions and GFED estimations of carbon emissions from wildfires, from 1997 to 2006, in medium grasslands, with humidity during the fire season as the predictor. Red pixels have the best models (correlations with observations above 75%), followed by orange (between 50% and 75%) and yellow pixels (between 25% and 50%). Green pixels do not have reliable models with this predictor. Blue pixels do not show significant fire activity at 1ºx1º resolution.

3.28 Short Grassland, No Woody Cover

Short grasslands occupy large areas in Eastern Europe, Central Asia, Southern Africa, Madagascar, Australia, New Zealand, North America and the mountains in the west coast of South America. After a humid winter, fires decrease in Australia, North America, Western Russia, but increase in South Southern Africa, Madagascar, Eastern Russia and South America.

Humid summers had fewer fires in Eastern Russia, South Southern Africa, Madagascar, North West Australia, North America and South America, but more in Central Europe, Western Russia and Central Asia (figure 3.28.1 a).

Warmer dry seasons had usually more fires, except in the mountains of the Andes, in South America, and in the south east of Southern Africa and in East Russia (figure 3.28.1 b).

These maps of rank-correlations between carbon emissions and weather variables (figure 3.28.1) are an example of the importance of analyzing individual pixels, and not only whole eco-regions: for example, over West and East Russia, scatterplots of carbon emissions versus air and soil temperature show no visible effect of temperature on fire behaviour (figure 3.28.2).

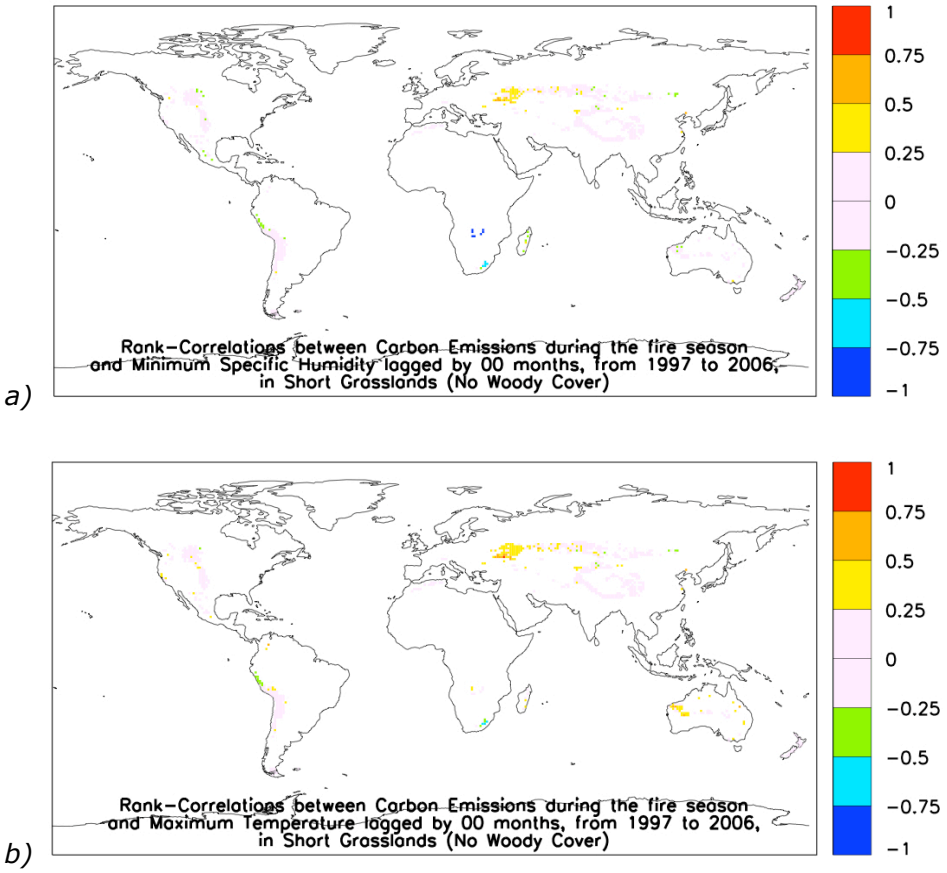

Figure 3.28.1 World maps of rank-correlations between wildfires and a) air humidity and b) air temperature, during the fire season, from 1997 to 2006, in short grasslands. Pixels in green and blue show areas where fires increase during a) drier or b) colder weather, whereas yellow, orange and red pixels show areas where fires increase with a) more humid or b) warmer weather.

For each month, most pixels in these eco-regions had a similar climatic temperature, and the average of carbon emissions from the eco-regions during the fire season did not vary considerably from month to month, regardless of temperature values. In Central Southern Africa, more fires tend to occur during the driest months,

and 5 months after a month of abundant rainfall during the growing season, so it was possible to obtain some good fire models based on concurrent humidity or lagged rainfall in this eco-region (figures 3.28.3 and 3.28.4).

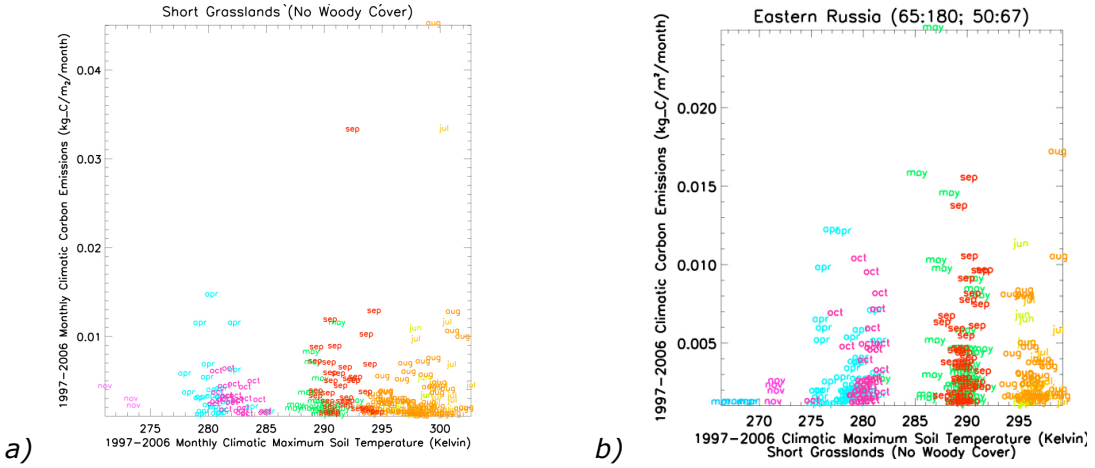

Figure 3.28.2 Scatterplot of carbon emissions from wildfires versus maximum soil temperature in the short grasslands of West Russia (a) and East Russia (b). Each point corresponds to a pixel of 1ºx1º resolution, with values averaged over homonymous months, from 1997 to 2006.

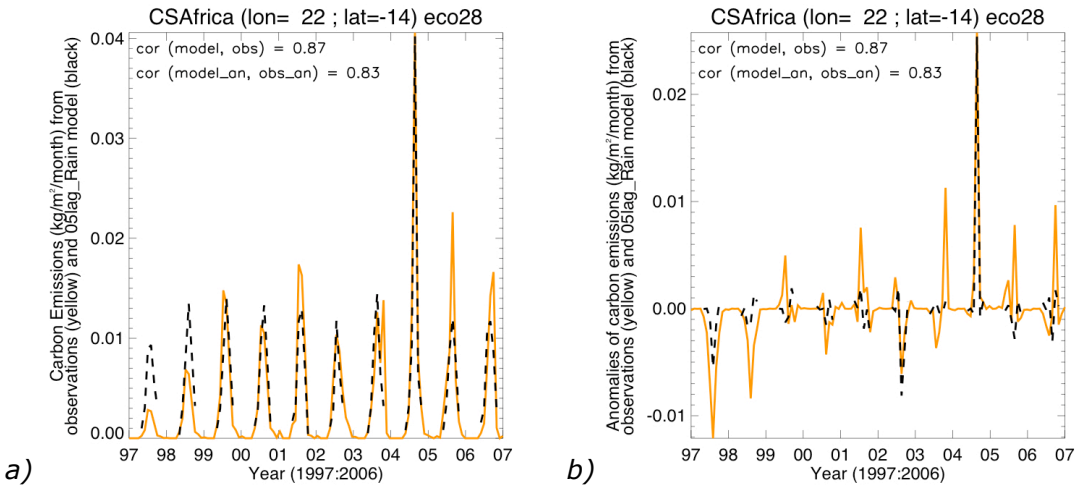

Figure 3.28.3 Time series of a) biomass burning (expressed as carbon emissions) and b) anomalies, from 1997 to 2006, given by GFED estimates, for one individual pixel in the medium grasslands of Central Southern Africa. Over-plotted in black is a model based on rainfall 5 months before fire events. High correlations (above 75%) between predictions and GFED estimates show that these models capture a considerable part of the interannual variability in carbon emissions.

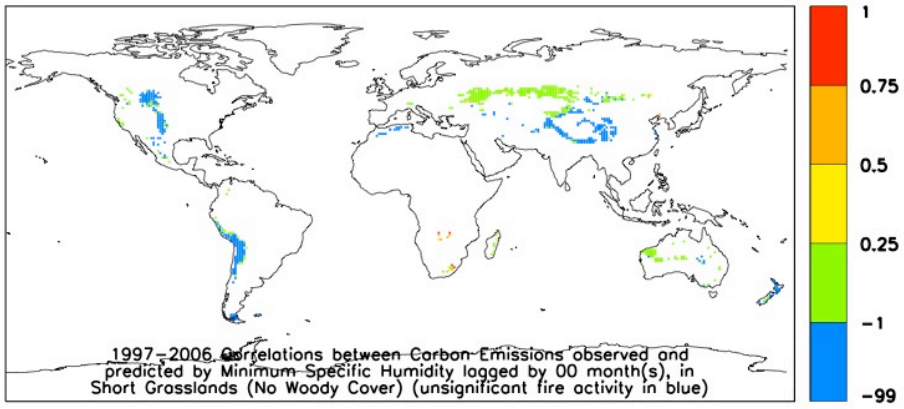

Figure 3.28.4 World map of correlations between model predictions and GFED estimations of carbon emissions from wildfires, from 1997 to 2006, in short grasslands, with humidity during the fire season as the predictor. Red pixels have the best models (correlations with observations above 75%), followed by orange (between 50% and 75%) and yellow pixels (between 25% and 50%). Green pixels do not have reliable models with this predictor. Blue pixels do not show significant fire activity at 1ºx1º resolution.

3.29 Regions

The previous sections described fire behaviour in land ecosystems, according to a given land-cover classification [GISS, 2006]. This section will describe the spatial and temporal distribution of fires over various geographical regions (section 2.2.5). These regions were used previously in the definition of eco-regions, i.e. areas in a limited geographical region, including only one main vegetation-type, where fire behaviour was expected to be relatively homogeneous.

Global maps of monthly burnt area show that wildfires are more frequent during the summers of temperate and sub-polar regions, in both hemispheres (Northern Asia, Europe and North America, in the Northern Hemisphere; Australia and the southern extremes of Africa and South America, in the Southern Hemisphere), and during the dry and warm winter seasons of the African and South American inter-tropical zones, both north and south of the Equator. Besides the predictable seasonal variability, however, there are also considerable year-to-year variations (figure 2.1.2).

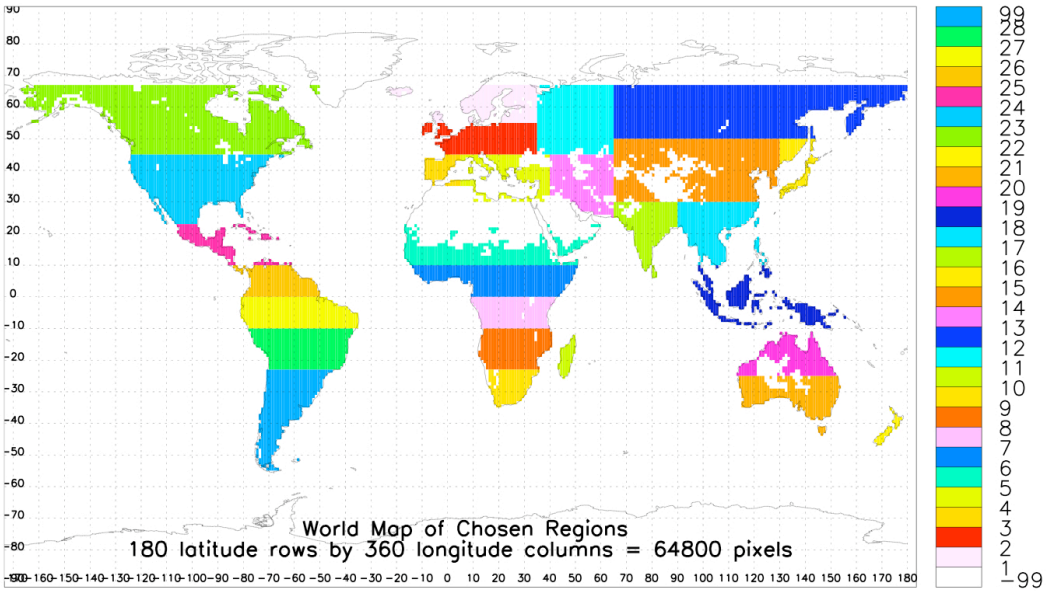

Figure 3.29 World map of the 28 chosen regions (key in table 3.29). Each section belongs exclusively to one main climatic zone: sub-polar, temperate, subtropical or tropical. There are no fire regions within the polar circles.

Table 3.29 shows the distribution of fires in the chosen geographic regions (identified in figure 3.29.6). North Africa, Equatorial Africa and Australia had fires during the whole year. Southern North America, Central America, Equatorial South America and Central South America had a very long fire season, 7 months minimum. Northern Europe, Northern Russia and Canada had small fire seasons of about 3 or 4 months maximum.

North America, Eastern Asia, South East Asia and Australia showed different behaviours in continental and maritime climatic zones. There were marked differences of wildfire behaviour in North American coast and on the prairies of the interior (figures 3.8.1, 3.28.1).

Number	Region	Beginning	Maximum	End
1	Northern Europe	July	August	September
2	Central Europe	June	August	September
3	Iberia	May	August	October
4	Mediterranean	May	August	October
5	North Africa	Increase in October	January	Never, but diminish in June
6	North Equatorial Africa	Increase in May	September	Never, but diminish in December
7	South Equatorial Africa	Increase in May	September	Never, but diminish in December
8	Central Southern Africa	April	August	December
9	South Southern Africa	April	August	December
10	Madagascar	April	August	December
11	West Russia	May	August	September
12	East Russia	April	--	November
13	West Asia	May	--	October
14	Central Asia	February	August	December
15	Japan	May	--	October

16	India	January	April	May
17	South East Asia	December	March	May
18	Equatorial Asia	January	September	November
19	North Australia	Increase in April	September	Never, but diminish in January
20	South Australia	Increase in August	November	Never, but diminish in February
21	New Zealand	August	November	February
22	Northern North America	May	August	November
23	Southern North America	March	August	November
24	Central America	November	April	June
25	North Equatorial South America	May	August	November
26	South Equatorial South America	July	September	March
27	Central South America	July	September	March
28	Southern South America	August	November	February

Table 3.29 Fire seasons in the chosen geographical regions.

The mountains in the western coast of South America, like the Andes, often showed different fire behaviour than the rest of Southern South America (figures 3.12.1, 3.28.1). A possible explanation is that, in the mountains of Andes, plants lack fire adapted traits because of the absence of summer lightning over evolutionary time scales [Bond & van Wilgen, 1996]. Wildfires in the forests surrounding the Himalayas also behaved differently than in India and Central Asia. India had fires mainly up north in the frontier with the Himalayas (figures 3.7.1, 3.9.1, 3.15.1, 3.19.1, 3.21.1).

Chapter IV Conclusions

Summary

This chapter presents the conclusions of this research. It lists the ecosystems with more wildfires, those with more interannual variability and larger fire return periods, the response of different ecosystems to the meteorological variables with more impact on fire behaviour (air and soil temperature, lightning density, wind speed, air humidity, soil wetness and precipitation), and the eco-regions where fire behaviour is more predictable and where the best statistical fire models were found.

4.1 Spatial and Temporal Distribution of Wildfires

The ecosystems with more wildfires were tropical and subtropical grasslands, with or without woody or shrub cover, particularly in Africa, and tropical and subtropical drought-deciduous woodlands and shrublands. Areas of equatorial rainforests and tropical or subtropical drought-deciduous forests undergoing rapid deforestation, in Equatorial South America, Equatorial Africa and Equatorial Asia, have also frequent fires, but they occurred mainly in the borders of the forest, near large roads, sites of land-conversion for agriculture or pasture, or where the population density is higher.

The most extreme cases of inter-annual variability in fire events occurred in equatorial rainforests, during the El Niño of 1997-1998, when even the interior of rainforests burned extensively. These ecosystems rarely burn, on account of daily rainfall; but, when

wildfires do occur, they release a great quantity of carbon to the atmosphere, because of their rich content in fuel loads.

Apart from the extreme 1997-1998 El Niño fire events, the ecosystems with more interannual variability overall were boreal and temperate forests and woodlands: these regions had a large fire return period, with some 1° × 1° resolution pixels registering just one or no fires from 1997 to 2006, so few regular fire patterns were found. Wildfires in these ecosystems usually occur during the warmer months, in the summer, even if they coincide with periods of higher humidity.

Tropical and sub-tropical grasslands and shrublands had the minimum year-to-year variations. These ecosystems have a strong seasonal cycle, with fire events usually occurring during the tropical dry season, even if it coincides with the coolest periods of the tropical winters.

The monsoon region in West Africa shows a different behaviour than the rest of Equatorial Africa, not only in fire occurrence, but also in the influence of humidity some months before the fire season.

Different vegetation types within the same climate may have different fire behaviours. Conversely, the same ecosystem type showed different responses to weather variables in maritime or continental climates.

Vegetation type at approximately the same latitude seems to influence fire behaviour more strongly than climate. For example, equatorial rainforests in Equatorial Asia, Central Africa and northern South America show little sensitivity to positive temperature anomalies, whereas dry tropical semi-deciduous forests, in Brazilian southern coast, and Manaus, in Amazonia, catch fire more often when the weather is hotter than usual; nevertheless, all these regions have the same climate type (Köppen classification Af, with average temperature of the coldest month superior to 18ºC and daily rainfall superior to 60 mm/day in the driest month).

4.2 Temperature

Regions with the same climate type but different vegetation cover had significantly different responses to temperature. Rainforests in Equatorial Asia, Equatorial Africa and Equatorial South America show little sensitivity to temperature anomalies, except in areas subject to deforestation, whereas dry tropical semi-deciduous forests, in the Brazilian southern coast, and Manaus, in Amazonia, although with the same climatic classification, usually have more fires when the weather is hotter than usual.

The best models with temperature as predictor (correlations superior to 75%) were found mainly in tropical and sub-tropical regions, namely Africa, Madagascar, South East Asia and Central and South America, in the deforestation areas of tropical evergreen rainforests, tropical/ sub-tropical seasonal broad-leaved and drought-deciduous forests, in tropical/ sub-tropical evergreen broad-leaved sclerophyllous woodlands, xeromorphic woodlands and drought-deciduous woodlands, and in all grasslands, except mountain tundra. However, there was no whole eco-region with enough good models based on temperature to present consistently good predictions for 2007.

Strong negative rank-correlations (above 75%) between temperature and biomass burning were found in some tropical regions where the hottest weather usually occurs during low-pressure convective systems. High temperatures usually helped trigger fires, but there was one exception: in tropical regions of deep convection, the highest temperatures were associated to convective rainfall, and consequent fire extinction.

In grasslands, temperature and humidity were often significantly correlated (above 75%), so it was unclear if variability in carbon emissions is explained by the effect of temperature or of humidity. In grassland areas where carbon emissions during the fire season were well predicted by the quantity of rainfall during the previous growing season, temperature can be used as predictor, serving as a proxy for rainfall.

4.3 Lightning Density

Lightning density data did not significantly contribute to explain the variability of wildfires in any region, but this may have happened because of months of data missing and coarse resolution.

However, in areas where lightning was often associated to convective thunderstorms followed by rainfall (e.g., North Equatorial Africa, in particular the West-African monsoon regions), it was possible to construct good models based on lightning as a proxy for rainfall. In this case, lightning was highly negatively correlated with wildfires and positively with precipitation.

In boreal and temperate forests, lightning during the summer was positively correlated to fires, but it was not clear if this happened only on account of more sources of ignition or also because lightning was associated to warmer weather.

4.4 Wind Speed

Wind speed was often correlated to other weather variables, and it is unclear, from this research, how it contributes to wildfires.

There were no eco-regions where wind was consistently positively correlated with fires, so extensive burned areas could not be decidedly attributed to a drying effect of the wind on vegetation, or to fire spread by fast winds.

On the contrary, there was a consistent pattern of fire negatively correlated with concurrent wind speed in some regions: tropical and subtropical African grasslands, including savannahs, African drought-deciduous woodlands, and deforestation areas of equatorial rainforests and of tropical seasonal broad-leaved forests. In this cases, strong winds were associated with convective rainfall, so fires decreased with concurrent faster winds or, inversely, increased with previous periods of faster winds during the growing season, possibly because rainfall during that time increased the

quantity of vegetation available to burn during the following fire season.

4.5 Humidity

Most of the best fire models, with correlations above 90% between observations and predictions, were obtained with contemporary humidity as the predictor.

African savannahs, Mediterranean evergreen broad-leaved sclerophyllous woodlands, xeromorphic woodlands in East Brazil, xeromorphic shrublands in East Africa, cold-deciduous forests, drought-deciduous forests and woodlands, the West African monsoon area of tropical seasonal broad-leaved forests and also deforestation areas in equatorial rainforests, all became very prone to fires during periods of low humidity.

Overall, biomass burning tended to occur during the periods of lower values of humidity; exceptions were boreal forests, where specific humidity is usually not high enough to hinder ignition and fire spread, whereas warmer weather, favourable to ignition, is often also more humid.

4.6 Rainfall

Rainfall was strongly anti-correlated with fires during the fire season in all ecosystems with significant fire activity.

In ecosystems of fine fuels, such as grasslands and shrublands, precipitation during the growing season is necessary for vegetation to grow, thus rainfall lagged by 5 or 6 months is positively correlated with biomass burning during the following dry season.

Fires increased with decreasing rainfall in savannahs (grasslands with woody or shrub cover), drought deciduous woodlands and borders of rainforests undergoing deforestation, and also, sometimes, with decreasing temperatures, in regions where the highest temperatures were associated to convective precipitation.

In tropical zones, especially in monsoon regions, the highest temperatures were associated to convective rainfall: the warmest time of the year was the rainy season. Up to a limit, the burnt area increased sharply with temperature, but, beyond that limit, it caused convective rainfall, preventing ignition and fire spread.

Biomass burning was also frequent in the West-African monsoon zone, when the rainy season was less pluvious or arrived later than usual.

4.7 Snow

Moderately good models with snow depth as only predictor (correlations with observations between 70% and 90%) were only found in grasslands of South Southern Africa. Wildfires frequently increase in these eco-regions as snow decreases, but this may be due to the seasonal cycle: vegetation dried in the frozen ground starts burning as soon as snow starts melting.

Some areas in temperate and sub-polar forests, e.g. maritime climate mountain conifer forests in North America, and in the rainforest in the mountains of Andes, show a moderately positive correlation between burnt areas and earlier snowmelt, i.e., fires decrease with recent snow depth, but there were not enough fires in ten years to establish conclusive statistical relationships.

Inversely, there are also extensive areas where fires were positively correlated with recent snow depth, perhaps because of a drying effect of snow: tropical and sub-tropical evergreen seasonal broad-leaved forests, cold-deciduous forests, conifer forests in continental North America and in Asia, Asian steppes, Indian tropical and sub-tropical drought-deciduous forests and shrublands, and African grasslands.

4.8 Mountain Ecosystems

Transition regions between mountain and lowlands seem to be particularly sensitive to fire. Mountain mixed deciduous conifer forests near lowland broad-leaved forests, resinous conifer forests (pines, spruces, larches) mixed with broad-leaved trees, and mountain mixed evergreen needle-leaf and broad-leaf boreal forests near to short grasslands or scrublands, all frequently caught fire during periods of low humidity.

Mountain regions, like the Rocky Mountains and the Andes often exhibit different fire behaviour than other regions of North and South America included in the same climatic or ecosystem type. Biomass burning in the forests surrounding the Himalayas also has different patterns than in the forests of India and Central Asia.

4.9 Rainforests

The interior of rainforests with daily precipitation all year round never had detectable fires from 1997 to 2006, apart from some areas that exceptionally burned during the El Niño of 1997-98.

The borders of the Equatorial South-American, African and Asian rainforests undergoing rapid deforestation, near roads and urban settlements, burned frequently during drier and warmer weather, emitting large quantities of pyrogenic emissions due to their high density in fuel load.

The monsoon region in West Africa shows a different behaviour than the rest of Equatorial Africa, not only in the case of fires occurring during lower temperatures (the dry season), but also in the weaker influence of humidity and rainfall some months before the fire season. High-pressure systems bring drought and a cooler weather, but still hot enough to trigger fires.

4.10 Temperate and Sub-Polar Forests and Woodlands

There were some regions in temperate and sub-polar forests where fire was never detected from 1997 to 2006, possibly because they had not yet recovered from a previous fire, so there was no bio-fuel to burn. Also, regular fires of low intensity might not have been detected by satellite-sensors. Therefore, even if fire were strongly influenced by any weather variable, in these regions, this influence might have gone unnoticed.

Temperate and sub-polar forests usually burn during warmer weather, which can coincide also with higher humidity; low precipitation during the months preceding the summer is often correlated with more carbon emissions during this time.

Fire return periods are large in these ecosystems; many individual pixels had few detectable fire events during the 10 years of data, therefore no significant statistical relationships could be established in those areas.

4.11 Shrublands and Grasslands

In the shrublands and grasslands of the tropical and subtropical zones, fire behaviour is quite regular and tends to repeat the same pattern year after year: during the wet summer season, there is a rapid growth of vegetation, which then burns extensively during the following dry winter season. Therefore, over large eco-regions, the signal of the seasonal cycle is much stronger than interannual variations, so it is unclear how much weather anomalies contribute to increase or decrease biomass burning.

Nevertheless, some interannual variability in biomass burning was also detected in several individual pixels, matching corresponding variations in contemporary humidity, contemporary temperature and rainfall lagged by 5 or 6 months. Lower humidity and rainfall, just

before the dry season, and increased rainfall during the growing season, both lead to larger burnt areas in the following period of fires; anomalies in the models coincide with anomalies in the observed carbon emissions.

Higher precipitation during the growing season in some areas is often followed by abundance of vegetation available to burn and to higher biomass burning during the following fire season. In other places, however, correlations with anomalies are weak, so the high correlations between rainfall lagged by 5 or 6 months with biomass burning might be only due to the seasonal cycle; it is unclear whether or not heavier or lighter rainfall would necessarily lead to significantly more or less quantity of fuel loads, or if this would in turn lead to greater or smaller carbon emissions.

Grasslands in temperate and sub-polar zones also burn during the summer, but there are few data to provide useful statistical relationships.

4.12 Predictive Fire Models

Good models (correlations with observations superior to 75%) were obtained only for individual pixels; scatterplots of weather variables versus carbon emissions over large regions have many points that do not following any detectable pattern; likewise, times series of carbon emissions and weather variables averaged over large regions do not show significant patterns.

Pixels with good models were mainly found with air humidity as predictor, in North Equatorial Africa, North Southern Africa and eastern South Southern Africa. Madagascar, Central America, Central South America and Indochina also have several pixels with good models. Correlations between fire models and observations between 50% and 75% can also be found in the most fire prone regions of Australia, the extreme north and the east-south-east, in Equatorial Asia, in northern India, on the forest south of the Himalayas undergoing deforestation, in the Caribbean, in a national park of

Chile and in Southern Italy. Soil wetness also gives good models in the same places, with similar results to those of air humidity.

Temperature is too much correlated to convective rainfall and with humidity to allow for a model with 2 variables contemporary with the fire season. Added as a second explanatory variable to models where humidity is the first explanatory variable, temperature does not improve them, because its high correlation with humidity and precipitation results in over-fitting. However, contemporary temperature in grasslands slightly improved some fire models with rainfall lagged by 5 or 6 months as first predictor.

The best models were obtained in the regions with more frequent fire events, so they can be used to estimate minimum expected carbon emissions from wildfires.

Weather variables were often well correlated with one another, especially in regions with a strong seasonal cycle, as in tropical grasslands and savannahs, so the inclusion of more than one variable in the model leads to over-fitting. The only case where a second variable improved the model was in cases where there was a good relationship between fire events and rainfall 5 or 6 months before. In these cases, adding contemporary humidity, or temperature, slightly improved the model. There was no over fitting as long as temperature and humidity did not have a strong correlation with lagged rainfall.

Other areas in South America, Australia, South East Asia and Mediterranean also presented conditions where it might be possible to get good models, provided that more data are available, namely strong rank-correlations between meteorological variables and carbon emissions. Still, the data analysed were not enough to get statistically significant models.

Good fire models were only found in ecosystems with frequent large fires, such as woodlands and grasslands in Africa.

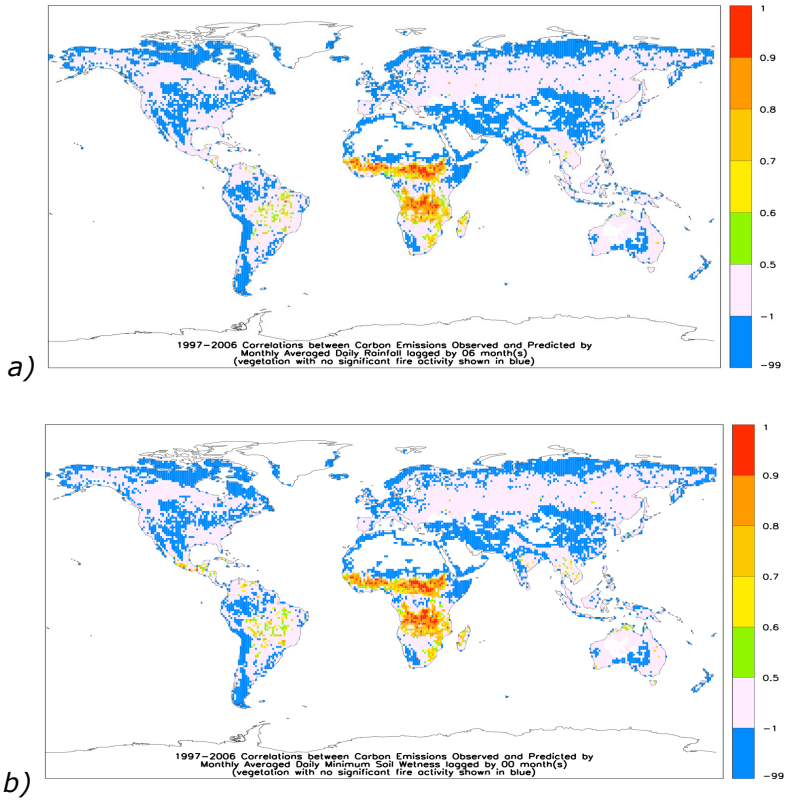

Figure 4.1 World map of correlations between the carbon emissions estimated by GFED and those predicted by the models in this research. Predictors shown are a) rainfall 6 months before the fire events and b) minimum soil wetness during the fire season. Most good models (correlations above 75%) are found in tropical Africa. Blue pixels show areas without noticeable fire activity at 1ºx1º resolution.

4.13 Future Work

These fire models required a considerable amount of data to provide reliable predictions, and no good models were found in ecosystems where fire events were infrequent and irregular.

In boreal and temperate forests and woodlands, statistical results will probably improve with longer time series of data, since these ecosystems have large fire return periods, especially in the regions

that already show a moderate or strong correlation between fire events and one or more weather variables.

Results in this research generally improved as the analyses were done at higher resolutions, e.g., time series and scatterplots for individual pixels show clearer patterns than those for a large region, models for individual pixels are better than those for a whole eco-region, and models for each month of the year give better predictions than those for the whole year. Therefore, in tropical and subtropical zones, models can probably improve with higher resolution data, both spatial and temporal. Many weather data used in this research had a resolution of only 2.5°×2.5°. Biomass burning, land-cover and weather data at 0.5°×0.5° resolution, instead of 1°×1°, for example, would give at least 4 times more spatial information. Time intervals of 1 week or 8 days, instead of 1 month, would give approximately 4 times more temporal information.

The weather variables that provided better predictive fire models were contemporary humidity, rainfall during the growing season and contemporary temperature or humidity plus lagged rainfall. Introducing a second independent weather variable has not considerably improved the fire models, but this may happen with higher resolution data.

The results of this research, particularly the predictive fire models, can be implemented on models of atmospheric chemistry and of environmental and climate change, or used on their own — e.g., to assist in land management, plan fire suppression or prescribed fire, and to estimate future quantities of carbon released to the atmosphere from different eco-regions.

References

Andreae, M. O. & P. Merlet (2001): Emission of trace gases and aerosols from biomass burning. *Global Biogeochemical Cycles, 15, 4*, pp. 955-966.

Baltzer, H., F. F. Gerard, C. T. George, C. S. Rowland, T. E. Jupp, I. McCallum, A. Shvidenko, S. Nilsson, A. Sukhinin, A. Onuchin & C. Schmullius (2005): Impact of the Arctic Oscillation pattern on interannual forest fire variability in Central Siberia. *Geophysical Research Letters, 32, L14709*. DOI: 10.1029/2005GL022526.

Bergeron, Y. (1991): The influence of island and mainland lakeshore landscapes on boreal forest fire regimes. Ecology, 72 (6), 1991, pp. 1980-1992. Ecology Society of America.

Boer, M. M., R. J. Sadler, R. S. Wittkuhn, L. McCaw & P. F. Grierson (2009): Long-term impacts of prescribed burning on regional extent and incidence of wildfires, *Forest Ecology and Management, Volume 259, Issue 1, 5 December 2009, pp. 132-142.*

Bond, W. J. & J. E. Keeley (2005): Fire as a global 'herbivore': the ecology and evolution of flammable ecosystems, *Trends in Ecology & Evolution, Volume 20, Issue 7, July 2005, pp. 387-394*

British Atmospheric Data Centre (2009): online data.

http://badc.nerc.ac.uk

British Geological Survey (2009): Geological Time Table.

http://www.bgs.ac.uk/downloads/browse.cfm?sec=8&cat=42

Broadmeadow, M. S. J., J. Heath & T. J. Randle (1999): Environmental Limitations to O_3 Uptake - Some Key Results from Young Trees Growing

at Elevated CO_2 Concentrations, Water, Air & Soil Pollution, 1999. DOI: 10.1023/A: 1005224823550.

Cachier, H., C. Liousse, M.-H. Pertuisot, A. Gaudichet, F. Echaler & J.-P. Lacaux (1996), African fire particulate emissions and atmospheric influence, in Biomass Burning and Global Change.

Clapham, C. & J. Nicholson (eds) (2005): Concise Dictionary of Mathematics. Oxford University Press. 3rd edition.

Doherty, R. M. & M. Hulme (2002): The relationship between the SOI and extended tropical precipitation in simulations of future climate change. Geophys. Res. Lett. 29, 10, 10.1029/2001GL014601, 2002.

Doherty, R. M, D. S. Stevenson & C. J. Johnson (2006): Tropospheric ozone and El Niño-Southern Oscillation: Influence of atmospheric dynamics, biomass burning emissions, and future climate change. *Journal of Geophysical Research*.

Duncan, B. N., I. Bey, M. Chin, L. J. Mickley, T. D. Fairlie, R. V. Martin & H. Matsueda (2003): Indonesian wildfires of 1997: Impact on tropospheric chemistry. *Journal of Geophysical Research, 108*, D15, 4458. DOI: 10.1029/2002JD003195.

Fearnside, P. M. (1996): Amazonia and global warming: annual balance of greenhouse gas emissions from land use change in Brazil's Amazon region, in Biomass Burning and Global Change, MIT press.

Fernandes, P.M. & H. S. Botelho (2003): A review of prescribed burning effectiveness in fire hazard reduction, *International Journal of Wildland Fire* 12(2), pp. 117 – 128. DOI: 10.1071/WF02042.

Flannigan, M. D., Y. Bergeron, O. Engelmark & B. M. Wotton (1998): Future wildfire in circumboreal forests in relation to global

warming. Journal of Vegetation Science, 9, pp. 469-476, 1998. Opulus Press Uppsala.

Food and Agriculture Organization of the United Nations, Global Forest Resources Assessment 2005: Fires, Wood volume and woody biomass. Web site: http://www.fao.org/forestry/site/fra/en.

Generoso, S., F.-M. Bréon, Y. Balkanski, O. Boucher & M. Schulz (2003): Improving the seasonal cycle and inter-annual variations of biomass burning aerosol sources. *Atmospheric Chemistry and Physics*, 3, pp. 1211-1222.

Gentemann C. L., P. J. Minnett, P. Le Borgne & C. J. Merchant (2008), Multi-satellite measurements of large diurnal warming events, Geophys. Res. Lett, 35, L22602. DOI: 10.1029/2008GL035730.

Giglio, L., G. R. van der Werf, J. T. Randerson, G. J. Collatz & P. Kasibhatla (2006), Global estimation of burned area using MODIS active fire observations. *Atmospheric Chemistry Physics,* 6: 957-974.SRef-ID: 1680-7324/acp/2006-6-957.

Global Precipitation Climatology Centre (GPCC) (2009): online data, http://www.gewex.org/datasets.html

Goddard Institute of Space Studies (GISS): online data at http://www.nasa.gov

Hemming, J. (2008): Tree of Rivers: The Story of the Amazon. Thames & Hudson, London, 2008. ISBN 978-0-500-51401-6.

Hoffman, W. A., W. Schroeder & R. B. Jackson (2003): Regional feedback among fire, climate and tropical deforestation. *Journal of Geophysical Research, 108,* D23, 4721. DOI: 10.1029/2003JD003494.

Immerzeel, W. W., P. Droogers, S. M. de Jong, M. F. P. Bierkens (2009): The water balance as a confirmation of glacial melt in the upper Indus basin. Geophysical Research Abstracts, Vol. 11, EGU2009-12033, EGU General Assembly 2009.

Intergovernmental Panel on Climate Change (IPCC), Working Group I (2007): Fourth Assessment Report (AR4), The Physical Science Basis.

Janetos, A. C., C. O. Justice & R. C. Harris (1996): Mission to planet Earth: land cover/ land use change program, in Biomass Burning and Global Change, MIT press.

Jupp, T. E., C. M. Taylor, H. Balzter & C. T. George (2006): A statistical model linking Siberian forest fire scars with early summer rainfall anomalies. *Geophysical Research Letters*, vol 33, LXXXXX. DOI: 10.1029/2006GLO26679.

Kandel, R. (2002): Le Réchauffement Climatique. *Presses Universitaires de France, 2002. ISBN: 2-13-053155-5*.

Keeley, J.E. (2001): Fire and invasive species in Mediterranean-climate ecosystems of California. Pp. 81–94 *in* K.E.M. Galley and T.P. Wilson (editors). Proceedings of the Invasive Species Workshop: the Role of Fire in the Control and Spread of Invasive Species. *Fire Conference 2000: the First National Congress on Fire Ecology, Prevention and Management*.

Keeley, J. E., C. J. Fotheringham & M. Morais (1999): Reexamining Fire Suppression Impacts on Brushland Fire Regimes. Science, 11 June 1999, 1829. DOI: 10.1126/science.284.5421.1829.

Kuhlbush & Crutzen (1996): Black Carbon and Global Cycle, in Biomass Burning and Global Change, MIT press.

Kürschner, W.M., F. Wagner, E. H. Visscher & H. Visscher (1996): Predicting the response of leaf stomatal frequency to a future CO_2-enriched atmosphere: constraints from historical observations. Geologische Rundschau 86: 512-517.

Laursen, K. K. & L. F. Radke (1996): Biomass burning smoke in the tropics: from sources to sinks, in Biomass Burning and Global Change, MIT press.

Le Page, Y., J. M. C. Pereira, R. Trigo, C. da Camara, D. Oom & B. Mota (2008): Global fire activity patterns and climatic influence: an analysis using the World Fire Atlas. *Atmospheric Chemistry and Physics*.

Liousse, C., J. E. Penner, J. J. Walton, H. Eddleman, C. Chuang & H. Cachier (1996): Modelling biomass burning aerosols, in Biomass Burning and Global Change, MIT press.

Mack, F., J. Hoffstadt, G. Esser & J. G. Goldammer (1996): Modelling the influence of vegetation fires on the global carbon cycle, in Biomass Burning and Global Change, MIT press.

Malingreau, J.-P. & J.-M. Grégoire (1996): Developing a global vegetation fire monitoring system for global change studies, in Biomass Burning and Global Change, MIT press.

Moula, M., J.-M. Broustet, H. D. Eva, J.-P. Lacaux, J.-M. Grégoire & J. Fontan (1996): Contribution of a spread fire model in the study of savanna fires, in Biomass Burning and Global Change, MIT press.

National Research Council Report (1996): Biomass Burning and Global Change, J.S. Levine (editor), MIT press.

National Geospatial Intelligence Agency Technical Report TR8350.2 (1997): "Department of Defense World Geodetic System 1984, Its Definition and Relationships With Local Geodetic Systems".

Nowicki S. M. J. & C. J. Merchant (2004): Observations of diurnal and spatial variability of radiative forcing by equatorial deep convective clouds, *J Geophys Res - Atmos, 109 (D11), art. no. D11202*.

Pearce, *R.S. (2000):* Plant Freezing and Damage. *Annals of Botany* 87: 417-424, 2001.

Piketh, S. J., H. J. Annegarn & M. A. Kneen (1996): Regional scale impacts of biomass burning emissions over Southern Africa, in Biomass Burning and Global Change, MIT press.

Randerson, J. T., G. R. van der Werf, L. Giglio, G. J. Collatz & P. S. Kasibhatla (2007): Global Fire Emissions Database, version 2.1 (GFEDv2.1). *Oak Ridge National Laboratory Distributed Active Archive Center,* Oak Ridge, Tennessee, U.S.A. Online data at: http://daacsti.ornl.gov/VEGETATION/guides/global_fire_emissions_v2.1.html

Robinson, J. M., W. G. Chaloner & T. P. Jones (1997): Pre-Quaternary Records of Wildfire, Sediment Records of Biomass Burning and Global Change. NATO ASI Series, 1997.

Sanderson, M. G., W. J. Collins, D. L. Hemming & R. A. Betts (2007): Stomatal conductance changes due to increasing carbon dioxide levels: Projected impact on surface ozone levels, Tellus B, International Meteorological Institute, Volume 59, Issue 3, pp. 404 – 411.

Shang, Z. B., H. S. He, D. E. Lytle, S. R. Shifley & T. R. Crow (2007): Modeling the long-term effects of fire suppression on

central hardwood forests in Missouri Ozarks, using LANDIS. *Forest Ecology and Management, Volume 242, Issues 2-3, 30 April 2007, pp. 776-790.*

Shoennagel, T., T. T. Veblen, W. H. Romme, J. S. Sibold & E. R. Cook (2005): ENSO and PDO variability affect drought-induced fire occurrence in rocky mountain subalpine forests, *Ecological Applications, 15(6)*, 2000-2014.

Solomon, S., D. Qin, M. Manning, R.B. Alley, T. Berntsen, N.L. Bindoff, Z. Chen, A. Chidthaisong, J.M. Gregory, G.C. Hegerl, M. Heimann, B. Hewitson, B.J. Hoskins, F. Joos, J. Jouzel, V. Kattsov, U. Lohmann, T. Matsuno, M. Molina, N. Nicholls, J. Overpeck, G. Raga, V. Ramaswamy, J. Ren, M. Rusticucci, R. Somerville, T.F. Stocker, P. Whetton, R.A. Wood and D. Wratt, 2007: Technical Summary. In: *Climate Change 2007: The Physical Science Basis. Contribution of Working Group I to the Fourth Assessment Report of the Intergovernmental Panel on Climate Change* [Solomon, S., D. Qin, M. Manning, Z. Chen, M. Marquis, K.B. Averyt, M. Tignor and H.L. Miller (eds.)]. Cambridge University Press, Cambridge, United Kingdom and New York, NY, USA.

Trollope, W. S. W. (1996): Biomass burning in savannas of Southern Africa with particular reference to Kruger National Park, in Biomass Burning and Global Change, MIT press.

Úbeda, X. & J. Mataix-Solera (2008): Fire effects on soil properties: A key issue in forest ecosystems, *CATENA, Volume 74, Issue 3, 15 August 2008, pp. 175-176.*

United Nations Environment Programme (2007): Global Environment Outlook 4th assessment report (GEO-4).

United Nations Environment Programme (2009): Climate Change Science Compendium.

United States Department of Agriculture (2000): Wildland Fire in Ecosystems, Effects of Fire on Flora, Editors: J. K. Brown, J. K. Smith, 2000, USDA General Technical Report RMRS-GTR-42.

United States Geological Survey (2009): online information, website http://www.usgs.gov/

Upton, G., I. Cook (2006): Oxford Dictionary of Statistics, Oxford University Press, 2nd edition, 2006, ISBN: 0-19-861431-4 978-0-19-861431-9.

Van der Werf, G. R., J. T. Randerson, G. J. Collatz, L. Giglio, P. S. Kasibhatla, A. F. Arellano, S. C. Olsen & E. S. Kasischke (2004): Continental-scale partitioning of fire emissions during the 1997 to 2001 El Niño/ La Niña period, *Science*, 303: 73-76.

Van der Werf, G. R., J. T. Randerson, L. Giglio, G. J. Collatz, P.S. Kasibhatla & A. F. Arellano (2006): Interannual variability in global biomass burning emissions from 1997 to 2004. *Atmospheric Chemistry and Physics*, 6, pp. 3423-3441. SRef-ID: 1680-7324/acp/2006-6-3423.

Venevsky, S., K. Thonicke, S. Sitch & W. Cramer (2002): Simulating fire regimes in human-dominated ecosystems: Iberian Peninsula case study, *Global Change Biology* (2002) 8, pp. 984-998.

Viegas, D. X. (1993): Fire Behaviour and Fireline Safety, *Ann. Medit. Burns Club - vol. 6 - n. 3 - September 1993*.

Van Wagtendonk, J. W. (2007): The History and Evolution of Wildland Fire Use, *Fire Ecology, Volume 3, Issue 2*.

Von Storch, H., F. W. Zwiers (1999): Statistical Analysis in Climate Research. Cambridge University Press.

Westerling, A. L., H. G. Hidalgo, D. R. Cayan & T. W. Swetnam (2006): Warming and Earlier Spring Increases Western United States Forest Fire Activity, *SciencExpress*, 10.1126/ science 1128834.

Westerling, A. L. & B. Bryant (2006): Climate Change and Wildfire in and around California: fire modelling and loss modelling, *Report from Climate Change Centre*, CEC-500-2006-190-SF.

Wilks, D. (2005): Statistical Methods in the Atmospheric Sciences, *International Geophysics Series*, Academic Press, 2nd edition, 2005, 648 pp, ISBN: 0127519661.

ANNEX 1 Acronyms

ATSR: Along Track Scanning Radiometer

AVHRR: Advanced Very High Resolution Radiometer

CASA: Carnegie-Ames-Stanford Approach

ECMWF: European Centre of Medium-Range Weather Forecast

FAO: Food and Agriculture Organization of the United Nations

GDEM: Global Digital Elevation Model

GFED: Global Fire Emissions Database

GHRC: Global Hydrology Research Centre

GISS: Goddard Institute of Space Studies

GPCP: Global Precipitation Climatology Project

JPL: Jet Propulsion Laboratory

METI: Japan's Ministry of Economy, Trade and Industry

MODIS: Moderate Resolution Imaging Spectrometer

NASA: United States' National Aeronautics and Space Administration

NGA: United States' National Geospatial Intelligence Agency

NRCS: USDA's Natural Resources Conservation Service

SI: Système International d'Unités

TRMM: Tropical Rainfall Measuring Mission

UN: United Nations

USDA: United States Department of Agriculture

VIRS: Visible and Infra-Red Spectrometer

WGS84: World Geodetic System of 1984

ANNEX 2 Symbols

A_{pixel} = area of a pixel (m^2)

BA = burnt area in a whole pixel (m^2)

BB = biomass burnt, expressed in mass of carbon emitted per month; equivalent to C_emissions (kg_C/ month)

BF = burnt fraction of a pixel (unitless)

C_emissions = total mass of carbon in the biomass burnt (kg_C/month)

CC = combustion completeness (unitless, from 0 to 1)

D_{fire} = mass of carbon in the vegetation killed by previous fires but not burnt (kg_C)

EF_X = emission factor of the chemical X (unitless)

epsilon = parameter for saturated specific humidity ($N^{1/2}\ m^{-1}$)

FL = fuel load available to burn per area (kg_C/m^2)

H = enthalpy or heat of combustion per unit mass (J/kg)

h = heat transfer coefficient

k = coefficient for the rate of pyrolysis (unitless)

ka = thousands of years

lat = latitude (˚)

lon = longitude (˚)

Lv = latent heat necessary to produce volatiles (J/ kg)

m = month of the year, from January to December, in a total of 12

Ma = millions of years

$m\_C_{emissions}$ = mass of carbon emissions from biomass burning (kg_C)

$m\_X_{emissions}$ = mass of chemical X (kg_X)

mm = chronological month, from January 1997 to December 2006, in a total of 120

n = number of years (in this case, n=10, from 1997 to 2006)

p dry = pressure of dry air (Pa)

Q = heat (J)

$R_{authalic}$ = authalic radius (m)

rel σ (m) = relative standard-deviation, for month m of any year

RH = relative humidity (unitless)

S = flux of sensible heat ($J/m^2/s$)

$S_{ellipsoid}$ = surface area of the Earth (m^2)

SH = specific humidity (unitless)

T = surface air temperature (Kelvin)

X(mm) = value of parameter X for month mm of a particular year

X_an (mm) = anomaly of parameter X for month mm of a particular year

WP = weather parameter

χ = factor of combustion completeness (unitless)

ε = error in the model

ϕ = fraction of heat transferred back to the surface (unitless)

$\mu_X(m)$ = climatic mean of parameter X for the month m of any year

ρ = fuel density (kg/m^3)

ρ (WP, C) = linear correlation between a weather parameter (WP) and carbon emissions (C)

σ (m) = standard-deviation, for the month m of any year

σ^2 (m) = variance, for the month m of any year